DANMARKS OG GRØNLANDS GEOLOGISKE UNDERSØGELSE RAPPORT 2017/32

The Cretaceous Petroleum System in the Danish Central Graben (CRETSYS)

Technical notes

N. Skaarup, C. Andersen, M. Bjerager, K. Dybkjær, T. Heijboer, J. R. Ineson, F. Jakobsen, H. Knudsen, L. Kristensen, U. Larsen, L. P. Lauridsen,A. Mathiesen, C. M. Nielsen, F. M. Mørk, H. P. Nytoft, C. B. Pedersen, R. Rasmussen, N. H. Schovsbo, E. Sheldon, E. Thomsen & K. H. Esbensen

GEUS

DANMARKS OG GRØNLANDS GEOLOGISKE UNDERSØGELSE RAPPORT 2017/32

The Cretaceous Petroleum System in the Danish Central Graben (CRETSYS)

Technical notes

N. Skaarup, C. Andersen, M. Bjerager, K. Dybkjær, T. Heijboer, J. R. Ineson, F. Jakobsen, H. Knudsen, L. Kristensen, U. Larsen, L. P. Lauridsen, A. Mathiesen, C. M. Nielsen, F. M. Mørk, H. P. Nytoft, C. B. Pedersen, R. Rasmussen, N. H. Schovsbo, E. Sheldon, E. Thomsen & K. H. Esbensen

Released 01.12.2020

GEOLOGICAL SURVEY OF DENMARK AND GREENLAND
DANISH MINISTRY OF ENERGY, UTILITIES AND CLIMATE

GEUS

The Cretaceous Petroleum System in the Danish Central Graben

CRETSYS

Technical Notes

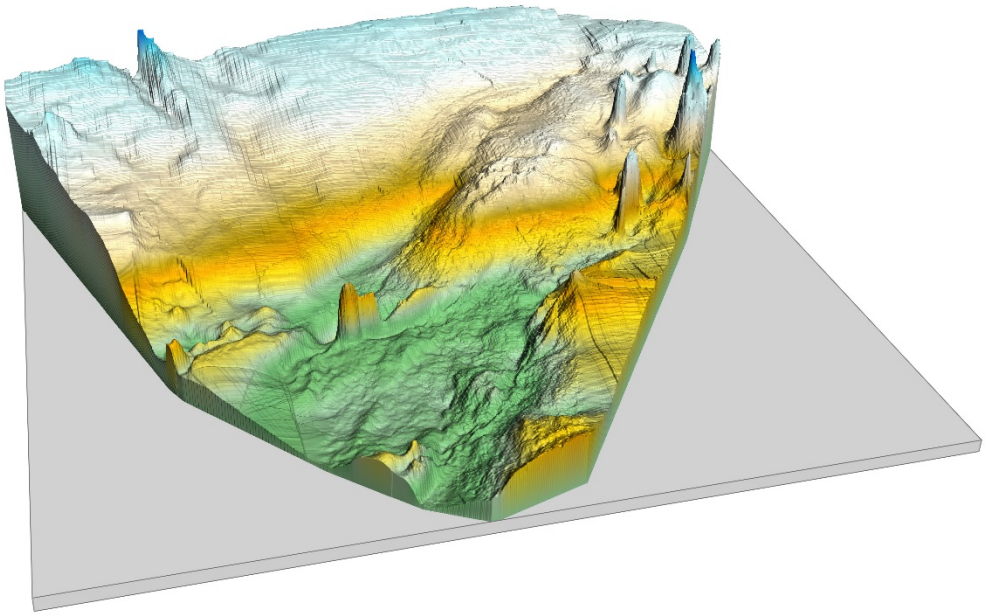

Contents

Chapter 8 Selected topics

1 Introduction

An integrated seismic, stratigraphic, petrophysical and geochemical study of the Cretaceous and Danian succession in the Danish Central Graben has been carried out under the **Cretsys** project at GEUS.

The aim of the project is to establish a consistent, well-constrained seismic-stratigraphic framework for the Cretaceous and Danian in the Danish Central Graben acting as basis for the regional understanding of the basin development, the structural evolution and the depositional environment. A secondary aim is to establish a basis for evaluation of the remaining hydrocarbon potential in the Cretaceous succession.

The **Cretsys** study is a comprehensive study following the Petsys model with a delivery of data and results on a WEB-GIS platform. Following main topics are included on the Cretsys web-site:

A stratigraphic framework and discussion on the regional stratigraphic architecture and depositional setting

3D seismic based interpretation and mapping of both the Lower and the Upper Cretaceous deposits to define basin development

Results from the evaluation on reservoir properties

Shows distribution, implications for migration, modelling of trap filling

The methodology, content and results of the individual topics are described in this technical note.

Selected topics are discussed in more details and included in this paper as separate sections under chapter **8. Selected topics**.

CRETSYS

PARTICIPANTS

A large number of GEUS personal have been involved in the Cretsys project and contributed with valuable input to the project.

These are:

Claus Andersen, Morten Bjerager, Karen Dybkjær, Kim H. Esbensen, Tjerk Heijboer, Jon R. Ineson, Finn Jakobsen, Henrik Knudsen, Lars Kristensen, Uffe Larsen, Louise P. Lauridsen, Anders Mathiesen, Carsten Møller Nielsen, Finn Mørk, Hans Peter Nytoft, Christian Brogaard Pedersen, Rasmus Rasmussen, Niels H. Schovsbo, Emma Sheldon, Nina Skaarup, Erik Thomsen.

In addition the project has received valuable support from Stefan Sølberg, Jette Halskov, Per E. Andersen, Lars Juul Kjærgaard and Carsten Bo Pedersen.

CRETSYS

An important outcome of the **Cretsys** project is establishing a consistent seismic- and stratigraphic framework for the Cretaceous succession. The **Cretsys** stratigraphy and annotations for stratigraphic horizons are indicated in the chronostratigraphic scheme for the Cretaceous and Danian below.

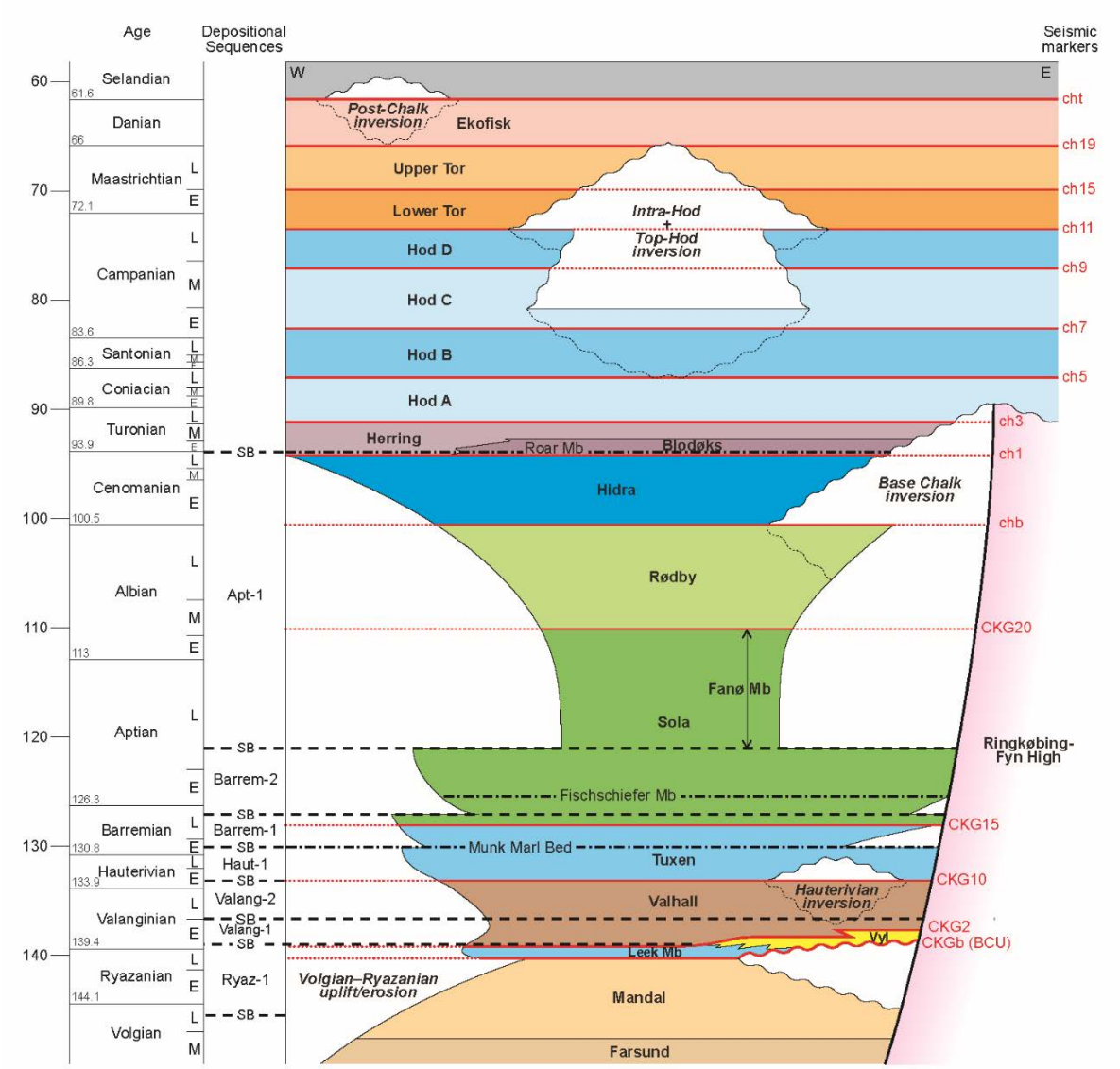

2 Stratigraphy and sedimentology

The integrated stratigraphy presented on the Cretsys website for the entire Cretaceous–Danian succession is a composite framework incorporating classical lithostratigraphy together with sequence stratigraphy where applicable (primarily the Lower Cretaceous) and seismic stratigraphy. The framework is validated with biostratigraphic data based primarily on review and update of existing data, as discussed below. The broad lithostratigraphic subdivision is reviewed below, and particular focus is placed on indicating the parallels with, and minor departures from, the recent revision of the Cretaceous lithostratigraphy in the Danish Central Graben presented by van Buchem *et al.* (2017). The sequence stratigraphic framework for the Cromer Knoll Group follows, to a large extent, the framework presented by Jakobsen *et al.* (2004, 2005); modifications to this scheme are indicated in the following. The stratigraphy of the Upper Cretaceous – Danian Chalk Group is more heavily reliant on the seismic data, integrated as closely as possible with a lithostratigraphic framework from well data (well-logs, cuttings/cores, biostratigraphy). The seismic methodology and subdivision of the Cretaceous–Danian succession is presented here in a separate section. The presentation of representative Cretaceous cored sections relies both on in-house existing core descriptions and on logging undertaken under the Cretsys project (see below).

2.1 Biostratigraphy

Biostratigraphic data from 65 released wells are included in the Cretsys project. The wells were selected based on the completeness or expanded nature of the entire Cretaceous succession, or the Lower or Upper Cretaceous parts of the succession. The wells were also selected in order to cover a wide geographic area of the Danish Sector of the Central Graben including all the major subbasins, and also with respect to the goal of providing seismic ties in key locations. Biostratigraphic data are provided from approximately 50 m above the Balder Formation and into the top of the Late Jurassic succession, where present.

The Cretsys biostratigraphic study was mainly based on microfossils (mostly foraminifera with some Radiolaria (R), diatoms (D) and ostracods (O)) and nannofossils. The data were primarily taken from industrial biostratigraphic consultancy reports. Palynological data were utilised where the other groups were lacking, e.g. in the Upper Jurassic – Lower Valanginian. Palynological data were taken from the Petsys project (Skaarup *et al.* 2015) or from references therein.

The most common industrial sampling method involves ditch cuttings samples, therefore 'first downhole occurrences' (FDOs) of marker (useful) fossils were primarily used in the Cretsys project. Where available, data from conventional core and sidewall core samples were used. Occasionally new nannofossil samples were made from selected core pieces, i.e. to check the age of an uncertain lithostratigraphic boundaries etc.

2.1.1 Selection of biostratigraphic markers and chronostratigraphy

For the biostratigraphic framework, bases (first occurrences) and tops (last occurrences) of boreal microfossils found in Hardenbol *et al.* (1998) were converted to the Gradstein (2012) chronostratigraphy and are shown on Fig 2.1 in **black** if they were also useful in this study, and in **grey** if they were not used in this study. In the Cretsys project, stratigraphically useful marker microfossils and nannofossils - those that persistently occur and can be used to correlate between wells - were selected from industrial consultancy reports, in-house GEUS studies and from relevant published material and are marked on the Fig 2.1 in **red**. Cretsys marker microfossils (**red**), are positioned relative to where they occur compared with established boreal (**black** & **grey**) marker fossils. Their absolute age ranges are not given. Useful references are provided in the figure text for Fig 2.1 and the reference list at the end of this chapter.

Nannofossil first occurrences and last occurrences on Fig 2.1 are from Gradstein (2012) and are marked in **black** if useful in the Cretsys study, and in **grey** if not used. In some instances the absolute age of a nannofossil range has been updated since the study of Gradstein (2012). These species are marked with an asterisk (*) and inserted at the updated position on Fig 2.1. The most up-to-date nannofossil ranges are found on the Nannotax3 website (Young *et al.* 2017). Nannofossils, which as a result of the Cretsys study are found to be useful biostratigraphic markers in the Danish Sector of the North Sea Central Graben are marked in **red**. Fig 2.1 can be downloaded from the Cretsys website ('Biostratigraphy' – 'Biostratigraphic Reference Charts').

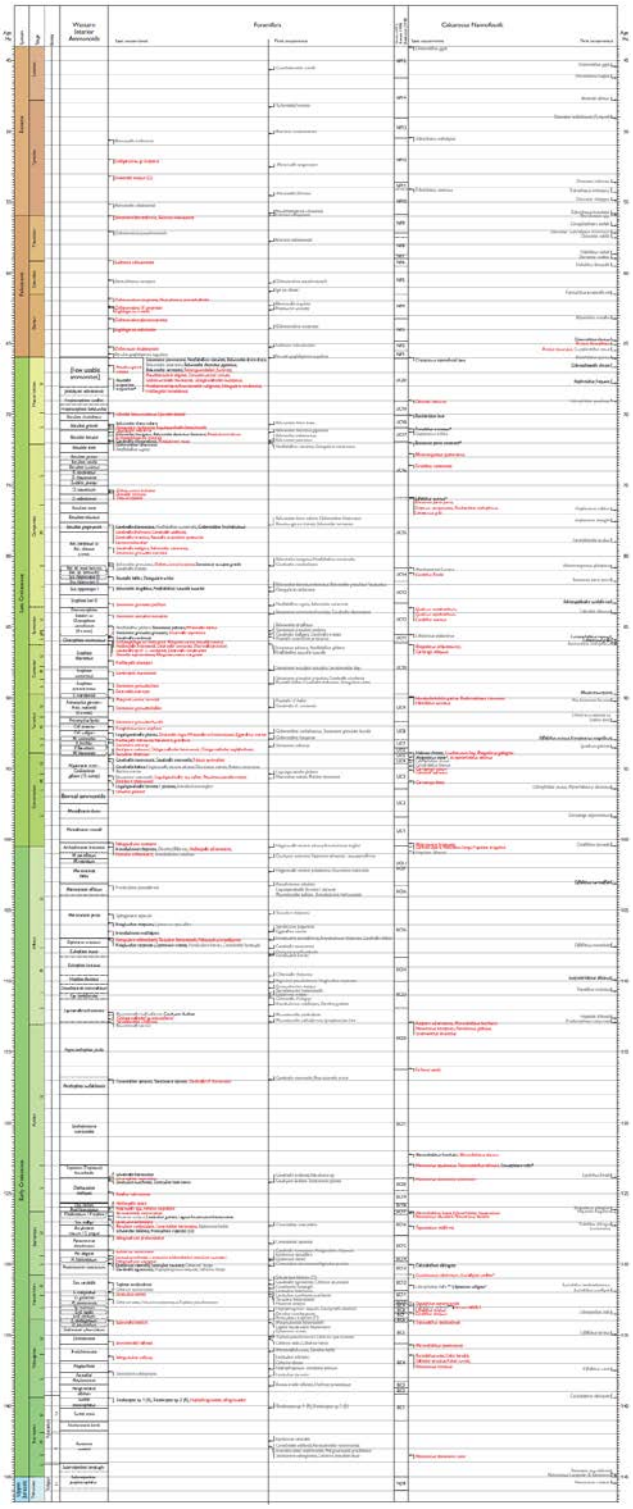

Fig. 2.1. *Chronostratigraphic chart with biostratigraphic marker microfossils and nannofossils. Chronostratigraphic – bioevent correlations are based on Berggren & Norris (1997), Bown et al. (1998), Burnett (1998), Caron (1985), Hart et al. (1989), Kaminski et al. (1995), King (1983), King et al. (1989), Rasmussen & Lassen (2004)* and *Varol (1998).*

2.1.2 Stratigraphic summary charts

A stratigraphic summary chart compiled using the StrataBugs biostratigraphic software is provided for each well. The stratigraphic summary charts include biostratigraphic, lithostratigraphic, sequence stratigraphic and chronostratigraphic information, in addition to geophysical logs, core and casing positions, seismic markers and TWT (see Fig. 2.2 and the description below). The stratigraphic summary charts can be downloaded from the Cretsys website ('Biostratigraphy' – 'Stratigraphic summary charts').

Fig. 2.2. *Example of a stratigraphic summary chart showing litho-, sequence- and chrono- stratigraphy, in addition to core and casing positions, geophysical logs (gamma, sonic, resistivity), TWT, seismic markers and biostratigraphic events.*

The Stratigraphic summary charts contain the following information:

Depth: in feet and metres (the depth column furthest to the left is in the units the well was drilled in). Depths are Measured Depth from the Kelly Bushing MD(KB) or Measured Depth from the Rotary Table MD(RT).

Lithostratigraphy: Formations and Members are given. See chapter 2.2 for brief lithological descriptions. The age range of each lithostratigraphic unit in each individual well as defined in the Cretsys project, is shown on Fig 2.3 which can be downloaded from the CRETSYS website ('Biostratigraphy' – 'Stratigraphic Ranges').

Casing & Cores: casing and core depths are from the exploration company final well report.

Geophysical logs: gamma, sonic and density logs were provided as LAS files and converted by the StrataBugs software.

Sequence Stratigraphy: sequence boundaries are picked from the petrophysical logs and are provided for the Lower Cretaceous succession only, see chapter 2.2.

TWT & Seismic markers: seismic markers are used in conjunction with log stratigraphy and biostratigraphy to quide the lithostratigraphic breakdown. TWT and seismic markers are discussed in chapter 3.

Chronostratigraphy: Period/Epoch and age are given. The chronostratigraphy is assigned based on the microfossil / nannofossil content. Where biostratigraphic data are lacking, lithostratigraphy and seismic information are used to guide the chronostratigraphic assignment.

Events: important biostratigraphic events are noted, including first occurrences (also known as last downhole occurrences; 'LDOs'), last occurrences (also known as first downhole occurrences; 'FDOs'), and single occurrences of marker fossils. The majority of biostratigraphic samples are ditch cuttings samples. Due to potential caving issues with ditch cuttings samples, FDOs are primarily used in this project. Where sidewall core samples or conventional core samples are provided, LDO's are also important. Microfossil and nannofossil species given on the stratigraphic summary charts are those provided in the original biostratigraphic consultancy report. These may not be the currently accepted names. Currently accepted (2017) names are provided on Fig 2.1.

Comments: additional notes relevant to the stratigraphic interpretation may be provided.

			Adda-1	Adda-2	Adda-3	Alma-1	Amalie-1
Horda Fm	H2 Member					Lutetian - Bartonian	
Horda Fm	undifferentiated		Ypresian - Bartonian	Ypresian - Bartonian	Ypresian - Bartonian		
Horda Fm	H1 Member						Ypresian - Lutetian
Balder Fm			early Ypresian	early Ypresian	early Ypresian	early Ypresian	early Ypresian
Sele Fm			Thanetian - Sparnacian	Thanetian - Sparnacian	Thanetian - Sparnacian	Thanetian - Sparnacian	Thanetian - Sparnacian
Lista Fm			Selandian - Thanetian	Selandian - Thanetian	Selandian - Thanetian	Selandian - Thanetian	Selandian - Thanetian
Våle Fm			Selandian	Selandian	Selandian	Selandian	Selandian
Ekofisk Fm			Danian	Danian	Danian	Danian	Danian
Tor Fm	upper member		Late Maastrichtian		Late Maastrichtian	Late Maastrichtian	Late Maastrichtian
	undifferentiated			Late Campanian - Maastrichtian			
Tor Fm	lower member				Late Campanian - Maastrichtian	mid Campanian - Late Maastrichtian	Maastrichtian
Hod Fm	D			?C-D members: Early Santonian - mid Campanian	Late Campanian	combined C-D members: Campanian	Campanian - Early Maastrichtian
Hod Fm	C		combined B & C members: mid Coniacian - mid Campanian	?C-D members: Early Santonian - mid Campanian		combined C-D members: Campanian	Campanian - Late Santonian
Hod Fm	B		combined B & C members: mid Coniacian - mid Campanian	Early Coniacian - mid Santonian		Coniacian - mid Campanian	Coniacian - Late Santonian
Hod Fm	A		Coniacian	Late Turonian - Early Santonian	mid - Late Turonian	Turonian - Santonian	Coniacian - mid Santonian

Fig. 2.3 *Part of the table showing the age ranges of the lithostratigraphic units within each well.*

2.2 Lithostratigraphy

2.2.1 Cromer Knoll Group (latest Ryazanian – earliest Cenomanian)

The lithostratigraphic scheme utilised in the project is shown in Figs 2.4 and 2.5. The Lower Cretaceous Cromer Knoll Group lithostratigraphy is based primarily on Jensen *et al.* (1986) with modifications by Riley *et al.* (1992) and recently by van Buchem *et al.* (2017). The latter changes to the Sola Formation, upgrading the informal Fischschiefer bed to a member (Riley *et al.* 1992) and defining the Fanø Member (van Buchem *et al.* 2017), were within the formational framework, so a brief summary of the main characteristics of the units suffices in these technical notes; more expansive descriptions can be retrieved from the references above. Definition of formation boundaries was also assisted by reference to regional studies, such as those of Crittenden *et al.* (1991), Copestake *et al.* (2003), Surlyk *et al.* (2003) and Jeremiah *et al.* (2010). The Cromer Knoll Group may exceed 800 m in thickness in restricted depocentres, exemplified by the Sten-1 well in the Feda Graben where the group is 765 m thick; the distribution and thickness variation of the Lower Cretaceous is discussed under Seismic Mapping in these notes and documented in detail in the maps accessed in the Cretsys website.

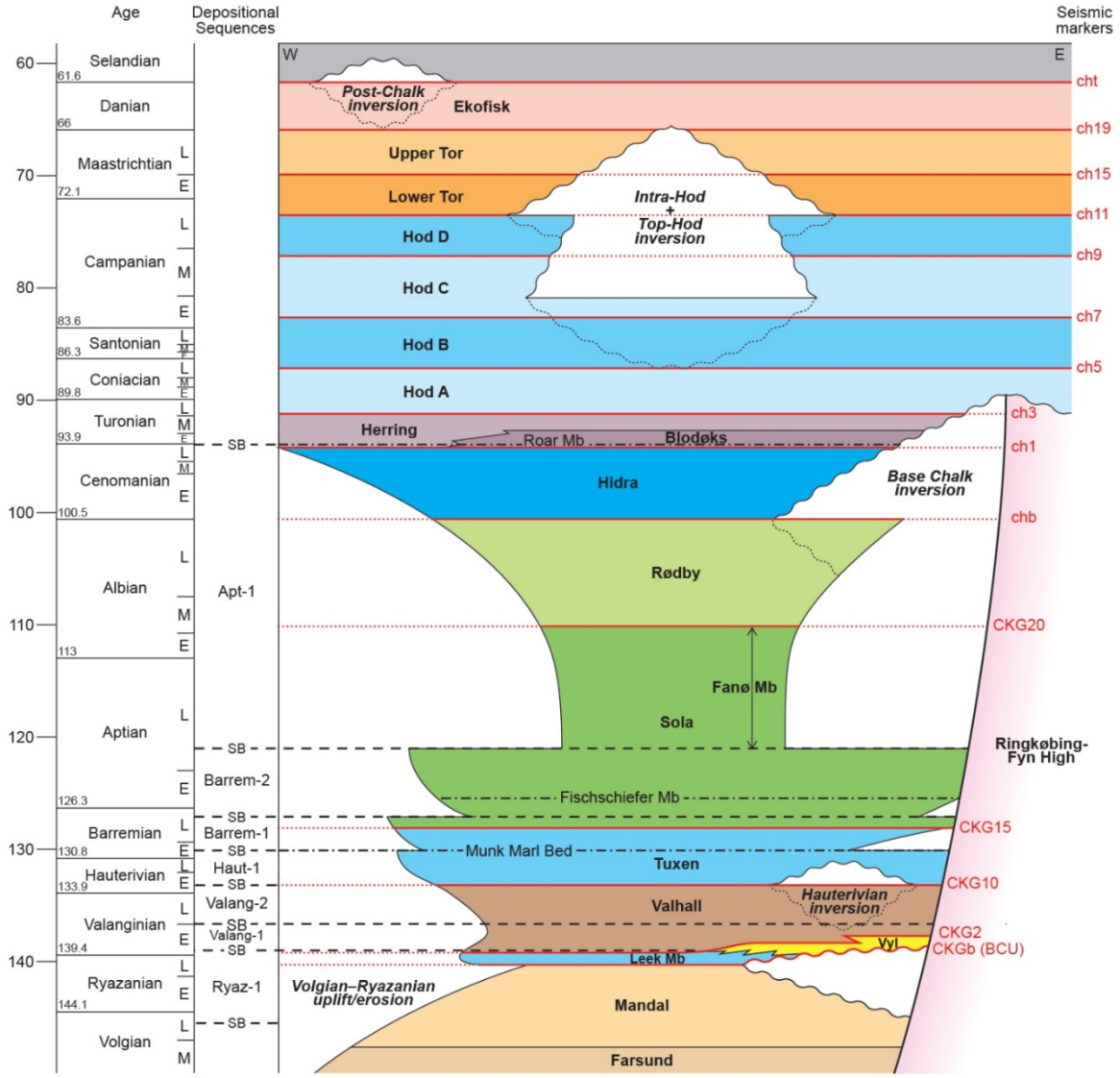

Fig. 2.4. *Cretaceous–Danian stratigraphic framework of the Danish Central Graben utilised in the Cretsys study.*

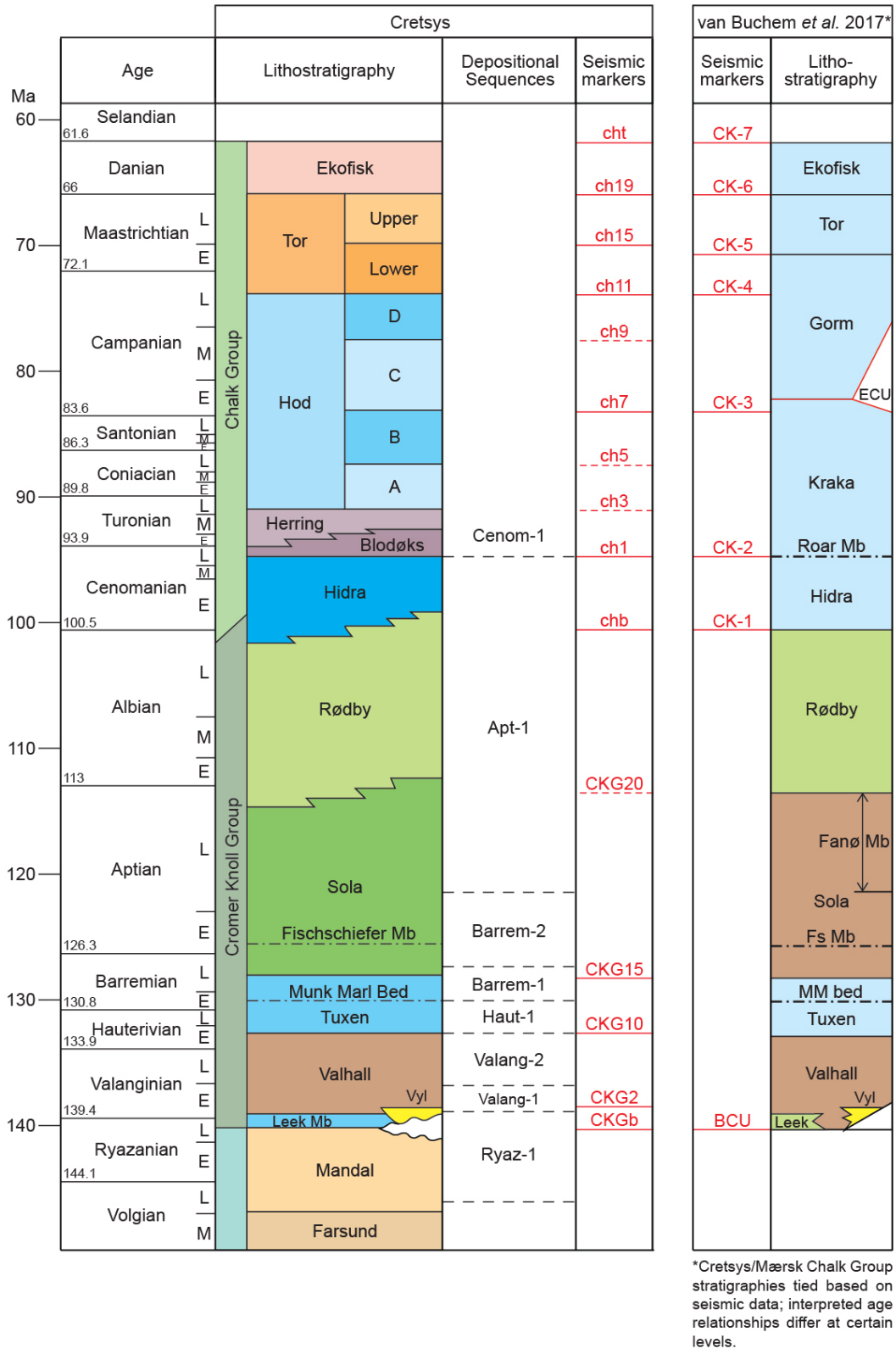

*Cretsys/Mærsk Chalk Group stratigraphies tied based on seismic data; interpreted age relationships differ at certain levels.

Fig. 2.5. *Comparison of the Cretsys stratigraphic framework with the formal stratigraphy defined by van Buchem et al. (2017)*.

Valhall Formation (latest Ryazanian – Early Hauterivian)

The formation can reach over 600 m in thickness in the central depocentres (616 m in Sten-1) but where present is typically 200–400 m thick. In complete sections, it is a uniform, mud-dominated succession, with increasing carbonate content towards the base (the Leek Member, see below) and towards the top; marlstones and thin argillaceous chalks are recorded in the lower and upper levels. The gamma-log patterns reflect this, showing an overall upward increase in values to the middle of the formation reverting to a decrease up to the gradational base of the chalk-dominated Tuxen Formation. The carbonate-rich lowermost unit is referred to the *Leek Member* (< 5 m – *c*. 60 m); in expanded sections (e.g. Sten-1, Iris-1, I-1) the spiky "leek" form of the member in logs reflects the interbedding of discrete thin carbonate beds with calcareous mudstones or marlstones whereas in thinner, more condensed sections the member is commonly carbonate-dominated (e.g. Bo-1). The boundary with the underlying organic-rich dark mudstones of the Mandal/Farsund Formation, typically showing high gamma-ray values, may be abrupt and readily localised but in conformable expanded sections the precise pick may be ambiguous though often guided by palynological markers.

Vyl Formation (Early Valanginian)

This formation is restricted to a narrow zone adjacent to the master fault zone flanking the Ringkøbing-Fyn High, particularly focussed on the breached transfer zone region intersected by the V-1, Deep Adda-1 and Ugle-1 wells. It comprises silty fine-grained sandstones and interbedded siltstones (Jensen *et al.* 1986) although coarser facies have been recorded from the Ugle-1 well. Review of the stratigraphic data of these wells (see Cretsys website Workshop 2) suggested that the Vyl Formation may post-date much of the carbonate-dominated Leek Member (Valhall Formation) and be associated with the interpreted sequence boundary defining the base of the Valang-1 sequence (see Figs 2.4, 2.5).

Tuxen Formation (Early Hauterivian – Late Barremian)

This important reservoir formation in the Danish Central Graben ranges in thickness from < 15 m to nearly 100 m (96 m in Sten-1 in the Feda Graben). The upper two-thirds of the formation comprise a heterogeneous layered succession of bioturbated chalks and marly chalks interbedded with greenish-grey (locally reddish) or dark grey-black marlstones; the lower levels of the formation are generally dominated by marlstones. Log definition of the base of the formation is variable. In expanded sections, the apparently conformable boundary is transitional and picking a significant fall in gamma-ray values (increase in carbonate content) can be subjective; in other cases, for example in the Adda area, the boundary is abrupt and associated with seismic truncation (at seismic marker CKG 10) and a significant biostratigraphic hiatus. The top of the formation is defined at a significant increase in gamma-ray values marking the incoming of the

clay-dominated facies of the Sola Formation above. The formation is subdivided into two discrete reservoir chalk units by the Munk Marl Bed, an interval of dark-grey – black organic-rich laminated marlstones up to 2 m thick; this bed is locally absent on condensed structural highs, such as the Adda Field.

Sola Formation (Late Barremian – Early Albian)

This formation is dominated by fine-grained calcareous siliciclastics – marlstones and variably calcareous claystones – but also includes marly chalk interbeds; a discrete thin reservoir-quality chalk unit (c. 5–8 m thick) of late Early Aptian age is present locally, notably in the Valdemar Field. Two intervals are accorded member status in the Sola Formation. The Lower Aptian *Fischschiefer Member*, an interval of finely laminated organic-rich marlstones (typically *c.* 2 m thick), occurs at the base of the formation in some wells where the top Tuxen Formation is a hiatal surface (e.g. Adda-2) but in conformable sections occurs higher in the Sola Formation (e.g. North Jens-1). This member correlates with the globally-recognised Early Aptian anoxic event, OAE1a (see discussion in van Buchem *et al.* 2017). The uppermost unit in the formation, where preserved, is a succession of early Late Aptian – Early–Middle Albian laminated claystones and calcareous claystones referred to the *Fanø Member* by van Buchem *et al.* (2017). This member is often absent or very thin on mid-Cretaceous structural highs but can reach significant thicknesses in mid-Cretaceous depocentres (e.g. > 80 m in Baron-2). This recently introduced member was incorporated into the Cretsys stratigraphic scheme and features on the Stratigraphic Summary Charts in the website.

Rødby Formation (Early Albian – earliest Cenomanian)

The Rødby Formation represents the upward transition from the clay-rich facies of the Sola Formation to the chalks of the Chalk Group above, as reflected by the overall upward decrease in gamma-ray values. It typically consists of marlstones with subordinate calcareous claystones and chalky limestones (Jensen *et al*. 1986). In many wells it is condensed or absent, but may be over 60 m thick in mid-Cretaceous depocentres. In such expanded sections, where the succeeding chalks of the Hidra Formation are thickly developed and argillaceous (e.g. Roar-2), definition of the boundary can be difficult and the Rødby Formation may extend up into the Lower Cenomanian.

2.2.2 Chalk Group (Cenomanian–Danian)

Definition of the lithostratigraphy of the Chalk Group in the Danish Central Graben (DCG) has been deferred for many years since the informal subdivision presented by Lieberkind *et al.* (1982) into six seismic units (Fig. 2.6). Although many workers and industrial companies utilised terms defined for the UK and Norwegian sectors (Deegan & Scull 1977; Isaksen & Tonstad 1989; Johnson & Lott 1993), the first formal subdivision

was published by van Buchem *et al.* (2017) in the last year of the Cretsys project. These workers proposed the adoption of the Hidra, Tor and Ekofisk Formation from neighbouring areas of the North Sea, and erected two new formations – the Kraka and Gorm Formations, together equivalent to the Hod Formation of previous schemes, and the Roar Member at the base of the Kraka Formation, equivalent (in part) to the Plenus Marl Formation and Black Band Bed of earlier schemes (see description and discussion in van Buchem *et al.* 2017). Given the appearance of this formal stratigraphy at a late stage in the project, and concerns as to the practical applications of the Kraka/Gorm boundary throughout the DCG, it was decided to complete the project using the working stratigraphic scheme (Fig. 2.4) particularly since significant analytical and petrophysical data had already been systemised in this informal scheme. It is fully appreciated, however, that the stratigraphy presented by van Buchem *et al.* (2017) represents the benchmark and formal framework for the foreseeable future and Fig. 2.5 thus presents the correlation between the Cretsys subdivision and that defined by van Buchem *et al.* (2017), based on inspection, comparison and correlation of the important seismic markers presented and illustrated in van Buchem *et al.* (2017) that constrain their formal units. In the following summary of the Cretsys framework for the Chalk Group, the correlative units in the van Buchem *et al.* (2017) scheme are indicated.

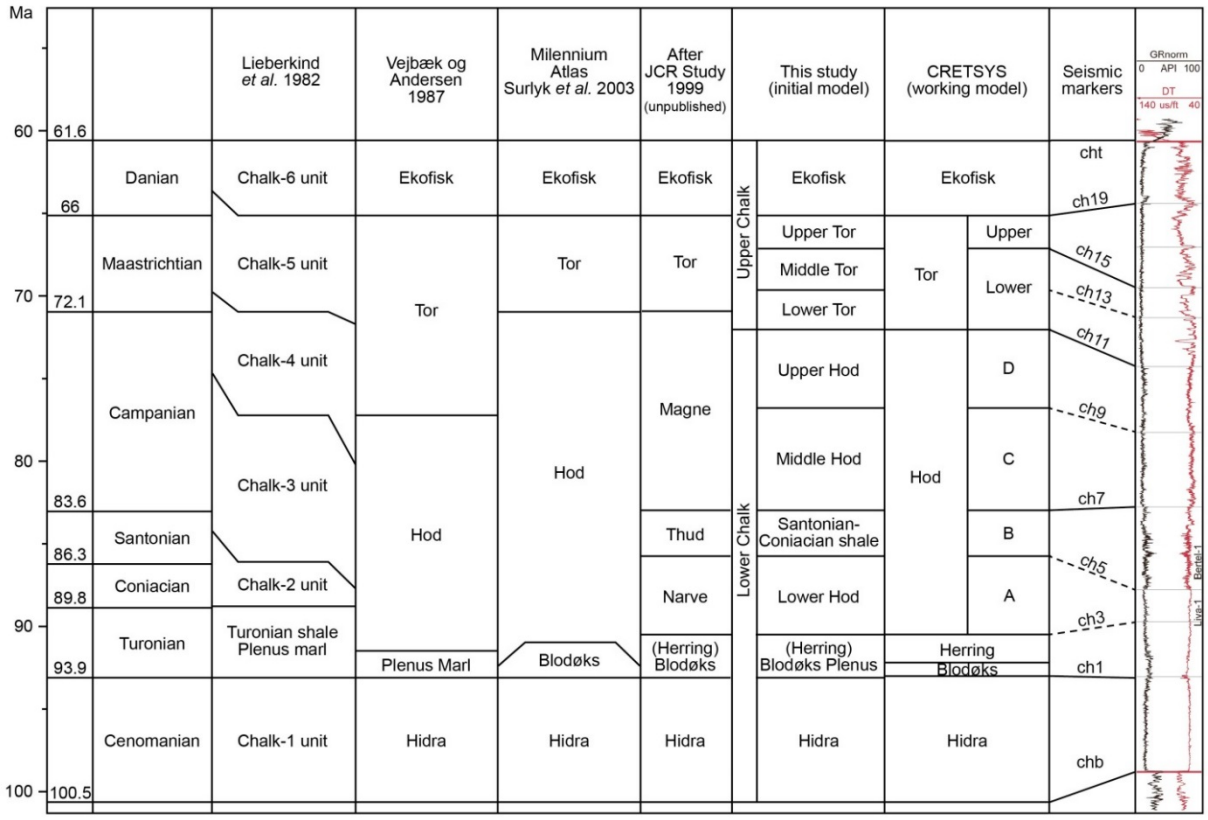

Fig. 2.6. *The Cretsys stratigraphic scheme for the Upper Cretaceous – Danian Chalk Group in relation to previous schemes.*

As illustrated on Figs 2.4–2.6, the formally adopted Hidra, Tor and Ekofisk Formations are used in the Cretsys scheme. The Hidra and Ekofisk Formations are essentially identical to the equivalent units defined by van Buchem *et al.* (2017) – in terms of lithological character, log definition, seismic bounding markers and biostratigraphic age. The Tor Formation as recognised by van Buchem *et al.* (2017) is more restricted in scope (see Fig. 2.5 and discussion under Tor Formation below). The Turonian–Campanian interval represented by the Kraka–Gorm couplet in the van Buchem *et al.* (2017) scheme is informally referred to the Blodøks, Herring and Hod Formations, names borrowed from the adjacent sectors of the North Sea (for comprehensive North Sea-wide lithostratigraphic schemes, see Surlyk *et al.* 2003). The Hod Formation is subdivided into four informal units, A–D. Much of the data on the Cretsys website is referred to a combined Blodøks–Herring unit (also on log correlation panels) but the formations are differentiated in the Stratigraphic Summary Charts, wherever possible.

The distribution of the Chalk Group in the DCG, and the (time) thickness variation of the individual units is documented in the detailed seismic maps on the Cretsys website, and only general comments are given in the summary below. The thickness of the group is highly variable (see under seismic mapping below) but over a kilometre of chalk section is encountered in some drilled depocentres (e.g. Bertel-1 (1117 m), Karl-1 (1121 m)).

Hidra Formation (Cenomanian)

This formation is typically thickly developed in wells showing an expanded upper Cromer Knoll Group section (e.g. Roar-2 (75 m)); some thicker developments referred to this formation (e.g. in the Stork-1 well in the Tail End Graben) probably reflect stacked slumped wedges of Cenomanian chalk. The formation is commonly thin or absent along the flanks of the DCG, particularly in the west on the Heno Plateau and the Mid North Sea High, due to progressive onlap and expansion of Late Cretaceous depocentres in the Cenomanian to Turonian period. The Hidra Formation typically shows a "cleaning-up" profile, marly chalks and interbedded marlstones dominating in the lower levels grading upwards into slightly marly and marl-poor chalks, often locally rich in skeletal grains (wackestone–packstone texture). This upward trend is reflected in the gradual upward decrease in GR values. The base of the formation is gradational in expanded sections whereas the top is an abrupt increase in the gamma-ray values at the base of the dark laminated marlstones that define the base of the Blodøks formation (the Roar Member, correlative of the Plenus Marl/Black Band Bed).

Blodøks and Herring Formations (latest Cenomanian – Turonian)

This combined interval is typically 20–50 m thick but may be as much as 150–200 m thick, typically following thick Hidra Formation developments (e.g. Liva-1); it correlates

with the lower part of the Kraka Formation of van Buchem *et al.* (2017). The log character reflects a gradual upward decrease in the proportion of clay in the chalk succession (similar to the underlying Hidra Formation). The lowermost beds are typically marlstone dominated and form the Roar Member of van Buchem *et al.* (2017); this thin unit (< 1 – 3 m thick) is particularly well-developed in the DCG in the Tyra–Valdemar area. These marlstones grade up into a succession of interbedded marly chalks and marlstones which together with the basal marlstones are included in the Blodøks Formation, as used in Cretsys. This term is borrowed from the Norwegian sector. The Blodøks Formation ranges from a few metres to several tens of metres in thickness and the boundary with the overlying clean chalks of the Herring Formation is clearly transitional and probably diachronous. The Herring Formation, capping the interval, is a succession of clean, clay-poor, well-cemented chalks that are characterised on the logs by low GR values and high sonic velocities; this lithostratigraphic term was borrowed from the UK sector where this hard cemented chalk layer forms a significant marker. The top of the Herring Formation is picked at a shift to a more heterogeneous chalk succession (basal Hod Formation), marly chalk and marlstone interbeds near the base forming discrete GR peaks in some wells (e.g. Adda-3); this surface is correlated with seismic marker ch3 (see Fig. 2.4).

Hod Formation (Late Turonian – Late Campanian)

The Hod Formation in the DCG is a thick chalk succession (over 600 m in some depocentres, e.g. in the Gwen-2, Bertel-1, Per-1 wells) that is lithologically heterogeneous and architecturally complex since it temporally spans the most important period of inversion tectonism in the Cretaceous of the DCG (Fig. 2.4). It has thus proven the main obstacle to lithostratigraphic description of the Chalk Group, as reflected in the varied schemes in the North Sea area (see Fig. 2.6 and Surlyk *et al.* 2003). Van Buchem *et al.* (2017) utilised an integrated dataset, supported particularly by seismic stratigraphy, to define the Kraka and Gorm Formations in this interval, separated by an unconformity. The practical feasibility of this subdivision throughout the DCG remains to be fully tested since though the inversion-related unconformities are widespread, they are focussed on inversion ridges and are not recorded seismically or biostratigraphically in the inactive chalk depocentres. In apparently conformable sections in such settings, the temptation is to position the inferred correlative conformity at a distinctive lithologically created seismic marker (ch7), that very broadly coincides temporally with the onset of significant inversion i.e. the Hod B/Hod C boundary (Late Santonian – Early Campanian). The validity of this correlation remains uncertain, and the combined dataset presented here suggests that the onset of significant inversion tectonism may be better placed in the Early–Middle Campanian (as indicated on Fig. 2.4). Additional complications, as indicated by van Buchem *et al.* (2017), are the variable biostrati-

graphic data quality at this level and the possibility/probability that the Campanian uplift history was not contemporaneous from one inversion axis to another across the DCG.

Subdivision of the Hod Formation in Cretsys has relied on the differentiation of two stratigraphic units, *member B* and *member D*, tied as far as possible to seismic markers, which are characterised by an increased clay component and include marly chalks and slightly marly chalks with thin marlstone interbeds in well-developed sections. This heterogeneous development is reflected in the log patterns (see Fig 2.6) with slight, variable increases in GR values and decreases in sonic velocity, thus allowing log differentiation from the intervening clay-poor chalk units, *member A* and *member C.* As illustrated by the log panels on the Cretsys website, these key lithological units (B, C) are variably developed across the DCG and can be difficult to define in some wells showing uniform Hod Formation sections. At present, no systematic geographic variation in the development of these marly units has been discerned though attention will be focussed on this aspect in future work. The range and uncertainty in chronostratigraphic ages of these units indicated in the reviewed wells in the Cretsys website (see Stratigraphic Ranges spreadsheet, Cretsys website) is probably a combination of highly variable biostratigraphic data quality/abundance and the reworking/caving dilemma inherent in cavings-dominated subsurface biostratigraphy but may also reflect some degree of diachroneity of the boundaries of members A–D. The approximate age ranges of the informal members are shown on Figs 2.4 and 2.5.

Tor Formation (Late Campanian – Late Maastrichtian)

The Tor Formation, the key reservoir level in the Chalk Group, is a succession of relatively pure clay-free chalks that can be thin or absent over crestal inversion structures (e.g. North Jens-1, Baron-2, I-1) or salt structures (e.g. S.E. Igor) but typically ranges up to several hundred metres in thickness (375 m in Karl-1). The facies composition of the formation varies significantly through the DCG from sections dominated by redeposited chalks in the north (e.g. Mona-1, Hejre-2, Karl-1) to rhythmically bedded pelagic chalks in the Salt Dome Province (e.g. Dan, Halfdan, Tyra Fields). The base of the formation is defined at a log break – a shift to slightly lower gamma ray values coinciding with a fall in sonic velocities and density, reflecting the base of cleaner, more porous chalks; this break corresponds to the ch 11 seismic marker, within the Late Campanian. The Tor Formation chalks above are subdivided into an informal *lower member* (Late Campanian – Early Maastrichtian) and an increasingly porous *upper member* (mainly Late Maastrichtian), the boundary being picked primarily on a shift to lower sonic velocities and densities linked to the ch15 seismic marker. It is likely that this boundary is diachronous regionally in the DCG but broadly correlates with the Lower–Upper Maastrichtian boundary.

It is important to stress two points with respect to the formal stratigraphy of van Buchem *et al.* (2017):

1. The seismic pick of the base Tor Formation is clearly different between the two studies – the base-Tor seismic marker of van Buchem *et al.* (2017) termed CK-5 is close to (half a cycle beneath) the ch15 seismic marker of Cretsys (Fig. 2.5). The latter marks the upper–lower Tor boundary in the Cretsys scheme; the Cretsys base-Tor pick (ch11) is equivalent to the CK-4 marker of van Buchem *et al.* (2017) which is within their upper Gorm Formation.
2. Irrespective of the choice of base-Tor pick, there are some presently unexplained differences in the age models presented in Figs 2.4 and 2.5 compared with van Buchem *et al.* (2017). A clear example is the position of the Maastrichtian boundary – the ch15/CK-5 marker is placed at base-Maastrichtian by van Buchem *et al.* (2017) and at the Early/Late Maastrichtian boundary in the Cretsys scheme. The reasons for these inconsistencies are presently unclear, though it is noteworthy that in more detailed figures (e.g. van Buchem *et al.* 2017, fig. 11) the age of the CK-5 marker is indicated with an uncertainty range of late Late Campanian to earliest Late Maastrichtian (mid-range of intra Early Maastrichtian).

Ekofisk Formation (Danian)

The Ekofisk Formation is the most readily recognised lithostratigraphic unit in the Chalk Group of the DCG; it is typically in the order of 30–80 m thick though may exceed 100 m (e.g. 110 m in Alma-1) . It comprises a chalk succession that typically becomes progressively less clay-rich upwards so that the lower marly chalks and marlstones, often siliceous with prominent flint bands ("Danian Tight"), are succeeded by porous, clay-poor chalks ("Danian Porous"). This background facies trend, reflected by the upward-decreasing GR values and densities, is locally interrupted by redeposited clean chalks, sometimes rich in Maastrichtian floras and faunas. The base of the formation is typically picked at a hard sonic spike above the porous Tor Formation chalks; this marks the inferred position of the Top Tor hardground, often confirmed in core sections and typically biostratigraphically distinctive due to the first downhole appearance of Cretaceous fossils. The seismic marker ch19 is commonly referred to as "near Top Tor" since it is tied to the upward shift from porous to cemented chalks which may occur some metres below the top-Tor hardground surface. The base of the Ekofisk Formation can be erroneously placed too high based on biostratigraphic data due to the presence of redeposited Upper Maastrichtian chalks as debrites or slumps within the Danian section. The top of the Ekofisk is defined at a gradual or abrupt upward increase in GR values marking the boundary with Våle Formation or Lista Formation, respectively.

2.3 Lower Cretaceous sequence stratigraphy

The Lower Cretaceous sequence stratigraphic subdivision for the DCG indicated on Fig 2.4 and on the Stratigraphic Summary Charts (Cretsys website) is a modified form of that developed over the last few decades (Ineson 1993; Ineson *et al.* 1997; Jakobsen et al. 2004, 2005; see further mid-Cretaceous adaptations by van Buchem *et al.* 2017). A brief summary is given below. The naming of the sequences follows the system developed under the Petsys project – they are named after the stage (abbreviated) within which the basal sequence boundary falls, and numbered within the category (i.e. Barrem-1, Barrem-2). A drawback with this method is that this can result in much of the sequence falling in the succeeding stage(s), as is the case with the Barrem-2 and Apt-1 sequences (see Fig. 2.4).

Ryaz-1

The basal sequence boundary is defined in the Petsys website within the upper Farsund Formation. The sequence comprises the uppermost Farsund Formation, including the Bo Member and associated sands, and the carbonate-rich Leek Member at the base of the Valhall Formation (and the Cromer Knoll Group). The latter carbonate-rich interval (latest Ryazanian – earliest Valanginian) probably represent the TST and HST of the sequence.

Valang-1

The basal sequence boundary is placed at the base of a clay-rich interval immediately above the Leek Member; the sequence comprises the lower Valhall Formation of Early Valanginian age and is dominated by variably calcareous claystones and subordinate marlstones. The Vyl Formation sandstones in eastern marginal settings are interpreted to occur within the LST of this sequence. It is equivalent to the upper part of the CK1 sequence of Jakobsen *et al.* (2004, 2005).

Valang-2

An intra-Valhall Formation hiatal surface defines the basal sequence boundary, as documented by Dybkjær & Jutson (2003) from the Iris-1 well. This surface typically separates variably calcareous Lower Valanginian claystones from marlstones and calcareous claystones of Hauterivian age; the sequence comprises the upper Valhall formation (Fig 2.4). It is equivalent to the CK2 sequence of Jakobsen *et al.* (2004, 2005).

Haut-1

The basal sequence boundary is defined by the base of the Tuxen Formation chalks and marlstones, a level dated (in North Jens-1, for example) as lying within the Lower Hauterivian. In expanded conformable sections, the boundary is placed within a succession showing a gradual upward increase in carbonate relative to siliciclastic mud and is an inferred "correlative conformity". The equivalent boundary in areas that experienced Hauterivian uplift (e.g. the Adda structure) is an abrupt hiatus and a seismic truncation surface. The sequence spans the lower Tuxen Formation, comprising marlstones and interbedded chalks grading up to marly chalks. It is equivalent to the CK3 sequence of Jakobsen *et al.* (2004, 2005) and to sequences 1 and 2 of van Buchem *et al.* (2017); the distinction between the two sequences of the latter workers is not recognised in this study.

Barrem-1

The base of the Barrem-1 sequence is placed at the base of the Munk Marl Bed (MMB), a distinctive interval up to 2 m thick of black laminated marlstones. The MMB is absent in some wells in the Adda area, probably due to non-deposition/erosion at the sequence boundary and subsequent onlap onto the positive structure (see van Buchem *et al.* 2017); in such situations the boundary is a hiatal surface, uppermost Tuxen chalks onlapping directly onto Lower Tuxen marlstones or marly chalks of the Haut-1 sequence. In complete successions, the sequence includes the chalk-dominated upper Tuxen Formation and the lowermost marly chalks and chalky marls of the Sola Formation. It is equivalent to the combined CK4 and CK5 sequences of Jakobsen *et al.* (2004, 2005); note that subdivision of this interval into two sequences is no longer considered warranted. It equates broadly to sequence 3 of van Buchem *et al.* (2017), although the definition of the upper boundary is not identical (see below).

Barrem-2

In complete expanded sections, the basal sequence boundary is placed in the lower Sola Formation at a marked facies shift from bioturbated marly chalks and chalky marls to dark laminated or locally bioturbated marlstones. This surface is correlated to the top Tuxen Formation boundary in sections that lack the lowermost Sola formation (e.g. Adda-2). The sequence comprise marlstones and marly chalks (in some areas) of the lower Sola Formation; the laminated marlstones of the Fischshiefer Member probably represent the TST of this sequence, succeeded by more carbonate-rich facies (reservoir-quality chalks locally) assigned to the HST. The Barrem-2 sequence is equivalent to the CK6 sequence of Jakobsen *et al.* (2004, 2005) and, broadly, to sequence 4 of van Buchem *et al.* (2017); note that the latter workers define the base of their sequence 4 at the top Tuxen Formation surface in all structural situations.

Apt-1

The basal sequence boundary is placed in the upper Sola Formation at the incoming of non- to weakly calcareous mudstones above the marlstones and marly chalks of the middle Sola Formation. This surface equates to the base of the Fanø Member of van Buchem *et al.* (2017). The claystones of the upper Sola Formation (Late Aptian – mid-Albian) form the lower (LST) part of this sequence; the remainder of the sequence (Rødby and Hidra Formations) is often condensed but describes a gradual increase in carbonate relative to siliciclastic mud, culminating in clean, clay-poor chalks in the uppermost Hidra Formation. Although considered as one, long-lived depositional episode here, it is accepted that this interpretation is probably over-simplified and results from the fragmentary data at this level in the DCG. The Apt-1 sequence is equivalent in part to sequences CK7 and CK8 of Jakobsen *et al.* (2004, 2005); sequences 5 and 6 of the van Buchem *et al.* (2017) scheme make up the upper Sola – Rødby portion of the Apt-1 sequence. The top of the Apt-1 sequence is defined by the sequence boundary at the base of the Roar Member (the Plenus Marl equivalent), the succession immediately above has been loosely termed the Cenom-1 sequence but sequence stratigraphic subdivision has not been attempted above this boundary.

2.4 Core sedimentology

Sedimentological core studies of the Lower Cretaceous and Upper Cretaceous – Danian have been performed in selected wells in the Danish Central Graben and one well on the Ringkøbing Fyn High with the aim of categorizing the cored intervals in terms of general facies assemblages in a stratigraphical and spatial context. A modified JCR terminology has been applied to the lower Cretaceous succession and a general chalk sedimentological terminology has been applied to the Upper Cretaceous – Danian succession and presented in separate chapters below (see also separate report on core sedimentology on the Cretsys website).

2.4.1 Lower Cretaceous core sedimentology

The presented sedimentological logs are mainly based on the logging program conducted under the Priority Project. In logging the Lower Cretaceous cores, particular emphasis was laid on discrimination of basic lithological variants and description of sedimentary/diagenetic structures including trace fossils; a secondary objective was the qualitative description of fractures. The type, abundance and stratigraphic distribution of fractures have been noted.

Cored intervals of the following 15 wells have been included totalling *c.* 500 m of cored section:

- Adda-2 (core 1–4, 7750-7853ft) Sola Fm, Tuxen Fm
- Adda-3 (core 18-23, 7682-7890ft) Rødby Fm, Sola Fm, Tuxen Fm, Valhall Fm
- Baron-2 (core 5, 10121-10153ft) Sola Fm
- Deep Adda-1 (core 2, 8025-8081ft) Tuxen Fm, Valhall Fm
- E-1 (core 7, 8190-8237ft) Sola Fm, Tuxen Fm
- I-1 (core 5, 9493-9541ft) Sola Fm, Tuxen Fm
- Lone-1 (core 1-2, 10891-10929ft) Tuxen Fm
- Mona-1 (core 18-19, 11285-11490ft), Rødby Fm
- N-22 (core 9, 8651-8698ft) Tuxen Fm
- Nora-1 (core 1-2, 10063-10125ft) Tuxen Fm
- North Jens-1 (core 9-11, 7350-7639ft) Sola Fm, Tuxen Fm, Valhall Fm
- Rigs-1 (core 4, 9357-9374ft) Sola Fm
- SE Adda-1 (core 1–3, 7790-7918ft) Sola Fm, Tuxen Fm
- Valdemar-1 (core 1-6, 7350-7680ft) Rødby Fm, Sola Fm, Tuxen Fm
- Valdemar-2H (core 1-3, lengths: 25.3, 44.5, 59 ft) Tuxen Fm
- Valdemar-3H (core 1-2, lengths: 22.5, 60 ft) Tuxen Fm
- Valdemar-4H (core 1-2, lengths: 17.5, 17.2 ft) Tuxen Fm

The terminology of the Lower Cretaceous sedimentological logs is based on the classification of chalk lithotypes, prepared under the auspices of the Joint Chalk Research project (Crabtree *et al.* 1996). The JCR scheme has been modified to incorporate standard facies terms for clay-carbonate mixtures (Fig. 2.7). Thus, within level 2 (Composition-Matrix), the three-fold JCR scheme into clean Chalk (Ch), low Argillaceous (Arl) and high Argillaceous chalk (Arh) is expanded and modified. The 'clean Chalk' (Ch) category, containing less than 10% clay/silica, is retained whereas the low Argillaceous (Arl) and high Argillaceous (Arh) categories are replaced respectively by marly Chalk (Chm; 10-30% clay/silica) and Marlstone (Ml; 30-70% clay/silica). A further category, Claystone (Cs; less than 30% carbonate) is added to complete the facies spectrum.

The four lithotypes – chalk, marly chalk, marlstone and claystone –making up the mid-Cretaceous Valdemar succession are colour-coded on the core logs. In addition, inferred variation in clay content within these broad categories (especially within the marly chalk-marlstone range) is indicated by the log profile (Fig. 2.8).

The vertical and horizontal core logs are presented on two different log frameworks (see Cretsys website).

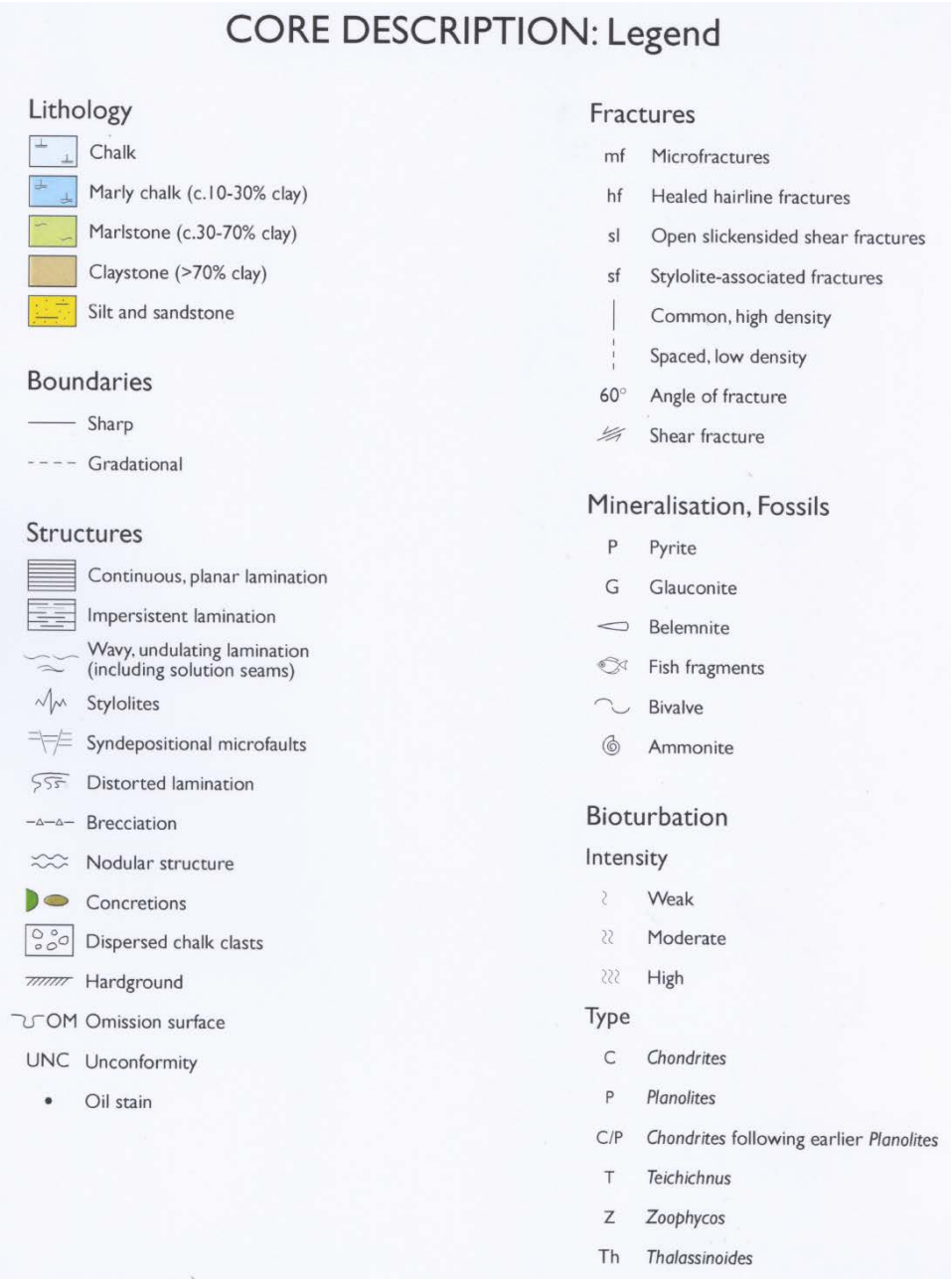

Fig. 2.7. *Legend to core description of the Lower Cretaceous in Deep Adda-1.*

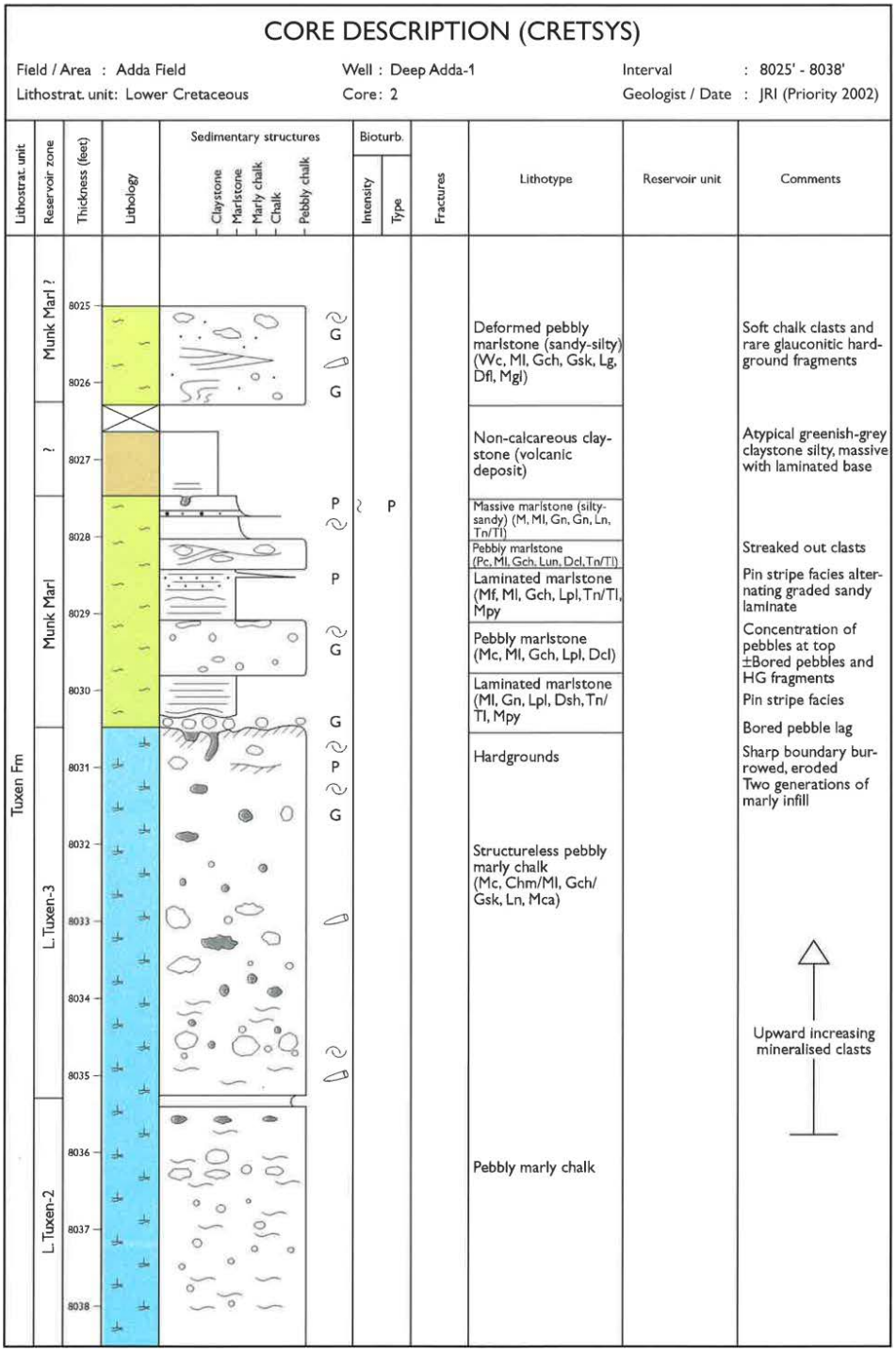

Fig. 2.8. *Example of vertical sedimentological log profile from Deep Adda-1 (Legend in Fig. 2.7)*

2.4.2 Upper Cretaceous – Danian core sedimentology

Sedimentological core studies of the Upper Cretaceous – Danian chalk have been performed in selected wells in the Danish Central Graben and one well on the Ringkøbing Fyn High with the aim of categorizing the cored intervals in terms of facies assemblages (see separate report on core sedimentology in the Cretsys website). Cored intervals of the following wells have been included, totalling 1495 m:

- Adda-3 (110m , 37m, 9m of core), Albian–Danian
- Anne-3 (46m of core), Upper Maastrichtian – Danian
- Baron-2 (106m of core) Coniacian–Santonian – Campanian, Upper Maastrichtian – Danian
- Bo-1 (76m, 55m of core) Albian–Coniacian, Santonian – Upper Campanian, Upper Maastrichtian
- G-2X (18m, 18m of core) Upper Maastrichtian, Danian
- HDN-1X (37m of core), Upper Maastrichtian
- I-1 (27m, 18m of core) Campanian, Upper Maastrichtian, Danian
- Lulu-1 (40m, 27m of core), Danian
- M-10X (113m of core), Upper Maastrichtian – Danian
- Mona-1 (332m of core), Cenomanian–Maastrichtian
- Nana-1XP (101m of core), Upper Maastrichtian – Danian
- P-1 (6m, 3m of core), Upper Maastrichtian – Danian
- Per-1 (14 m, 33m of core), Upper Maastrichtian – Danian
- Rigs-1 (49m of core) Danian–Selandian
- Rigs-2 (49m of core) Barremian–Aptian, Upper Maastrichtian – Danian
- Sif-1X (69m of core), Upper Maastrichtian – Danian
- Spurv-1 (55m of core) Middle Campanian – Lower Maastrichtian
- W. Lulu-1 (34m, 18m of core), Middle Campanian, Danian

The cored sections are subdivided into 7 main facies assemblages; i.e. recurrent groups of facies, typically dominated by one or two characteristic facies. These comprise: Bioturbated pelagic chalk, Skeletal-rich bioturbated chalk, Cyclic chalk (including well developed and weakly developed laminated-bioturbated cyclic chalk and Chalk marl cycles), Marly pelagic chalk (including skeletal-rich marly chalk and cyclic marly chalk), Pelagic/hemipelagic marlstone, Turbiditic chalk, and Mass-transport chalk (including slump/shear deformed chalk, chalk debrites, and structureless chalk (Figs 2.9–2.10)). Associated facies not assigned to a specific facies assemblage comprise Hardground, Condensed nodular chalk, Lag conglomerate and isolated turbidite. This subdivision is based on sedimentological screening of the core sections, incorporating previous in-house detailed core descriptions and polished type slabs where available and published works. Note that metric units are used in general discussion of facies but imperial units are used in reference to well sections to retain the accuracy of initial records.

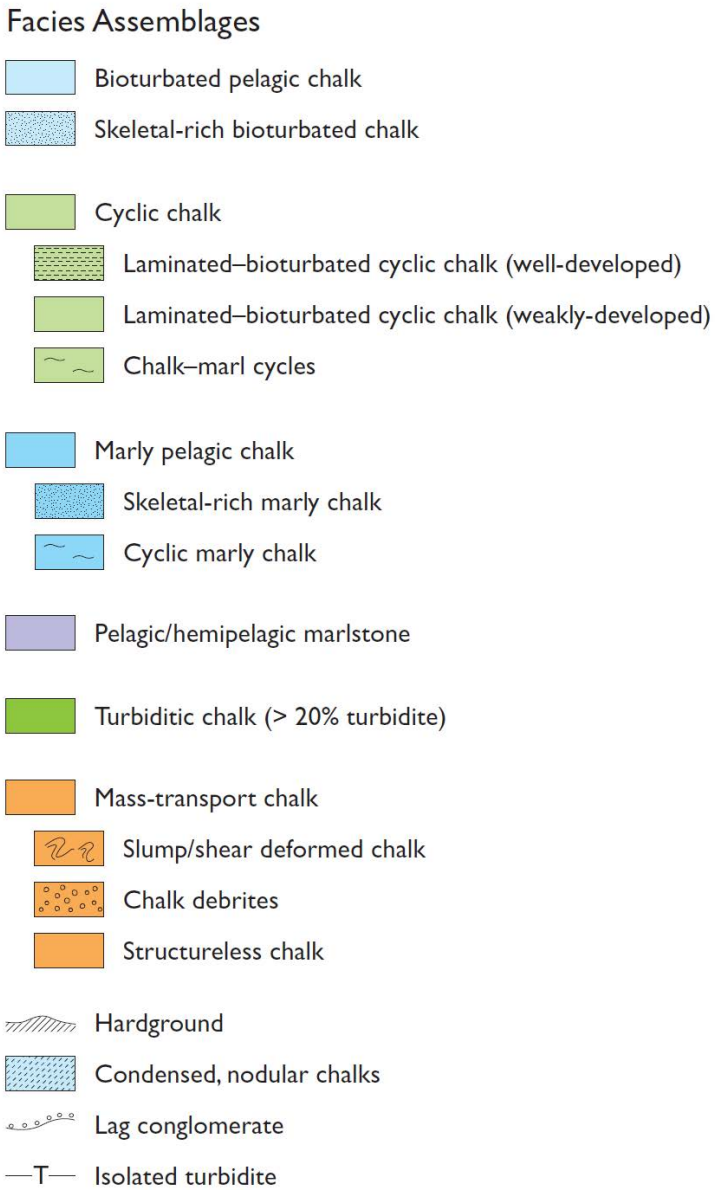

Fig. 2.9. *Legend to generalised core descriptions of the Upper Cretaceous – Danian succession.*

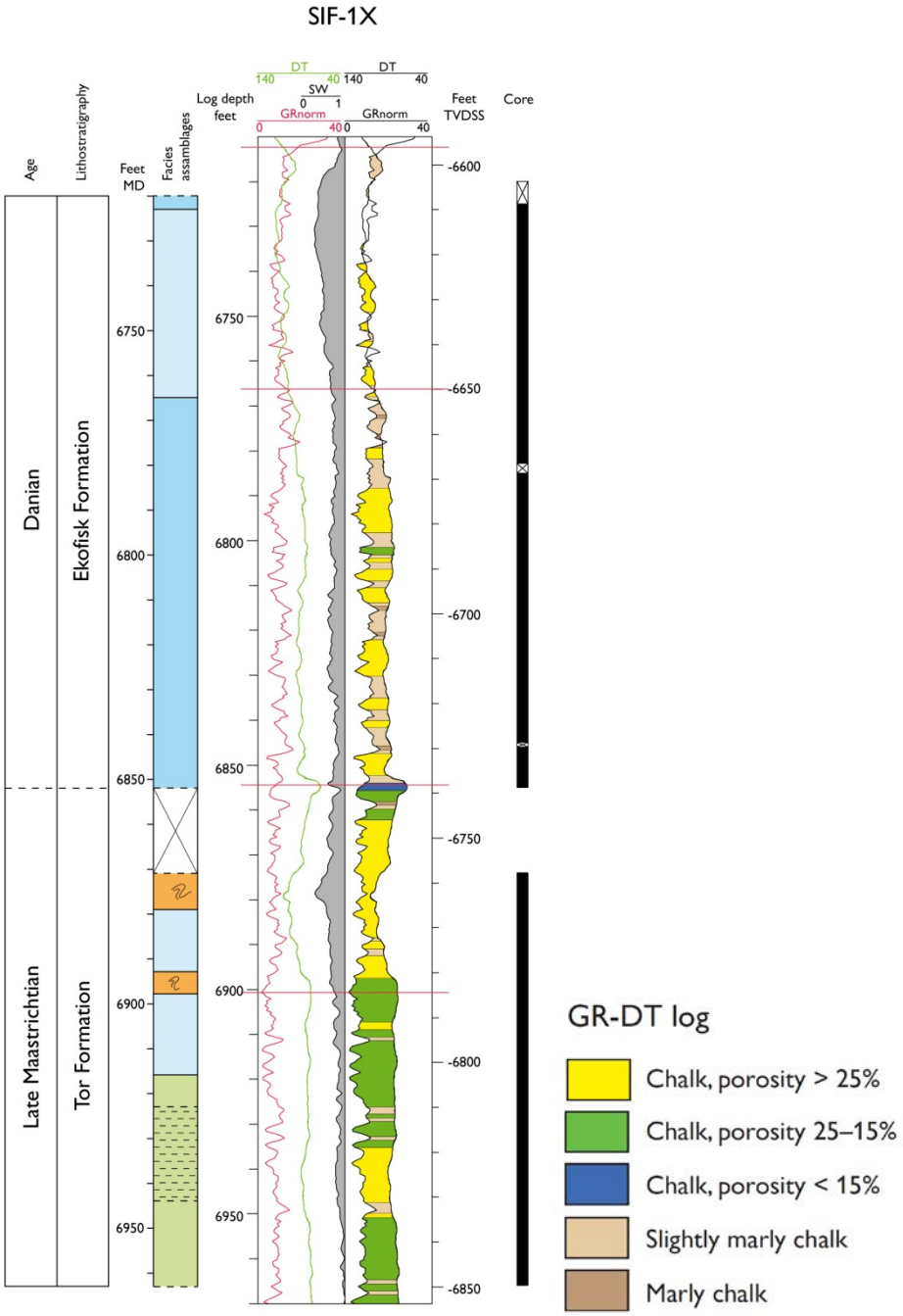

Fig. 2.10. *Example of cored interval with distribution of facies assemblages shown in relation to the GR/DT log of the Upper Maastrichtian – Danian in Sif-1X (legend to facies assemblage in Fig. 2.9).*

References

Anderskouv, K. & Surlyk, F. 2011. Upper Upper Cretaceous chalk facies and depositional history recorded in the Mona-1 core, Mona Ridge. Geological Survey of Denmark and Greenland Bulletin, 25, 1–60.

Berggren, W. A. & Norris R. D. 1997. Biostratigraphy, phylogeny and systematics of Paleocene trochospiral planktic foraminifera. Micropalaeontology 43, 1, 116 pp.

Bown, P. R., Rutledge, Crux, J. A. & Gallagher, L. 1998. Lower Cretaceous. In: Bown, P. R. (ed.): Calcareous Nannofossil Biostratigraphy. British Micropalaeontological Society Series. 86–131. Chapman & Hall/Kluwer Academic.

Burnett, J. A. 1998. Upper Cretaceous. In: Bown, P. R. (ed.), Calcareous Nannofossil Biostratigraphy. British Micropalaeontological Society Series. 132–199, Chapman & Hall/Kluwer Academic.

Caron, M. 1985. Cretaceous planktonic foraminifera. In: Bolli, H. M., Saunders, J. B. & Perch-Nielsen, K. (eds), Plankton Stratigraphy, 1, 17–86.

Copestake, P., Sims, A.P., Crittenden, S., Hamar, G.P., Ineson, J.R., Rose, P.T. & Tringham, M.E. 2003. Lower Cretaceous. In: Evans, D., Graham, C., Armour, A. & Bathurst, P. (eds, coordinators) The Millenium Atlas: Petroleum Geology of the Central and Northern North Sea. Geological Society, London. 191–211.

Crabtree, B., Fritzen, A., Mandzuich, K., Moe, A., Rasmussen, F.O., Siemers, T., Søiland, G. & Tirsgaard, H. 1996. Description and classification of chalks, North Sea region. Joint Chalk Research Phase IV, Norwegian Petroleum Directorate (NPD), 138 pp.

Crittenden, S., Cole, J.M. & Harlow, C. 1991. The Early to ”Middle” Cretaceous lithostratigraphy of the Central North Sea (UK sector). Journal of Petroleum Geology, 14, 387–416.

Deegan, C.E. & Scull, B.J. 1977. A Standard Lithostratigraphic Nomenclature for the Central and Northern North Sea. Report of the Institute of Geological Sciences 77/25; Norwegian Petroleum Directorate Bulletin 1.

Dybkjær, K. & Jutson, D. 2003. Composite biostratigraphy of the Hauterivian–Ryazanian interval in the Iris-1 (5604/30b1) well, Danish Sector, North Sea. Cour. Forsch.-Inst. Senckenberg 244, 1–10.

Fritsen, A. (ed.) 1999. A Joint Chalk Stratigraphic Framework. Volume 1. Joint Chalk Research Program Topic V. Norwegian Petroleum Directorate. 206 pp.

Kaminski, M. A., Neagu, T. & Platon, E. 1995. A revision of the Lower Cretaceous foraminiferal genus Falsogaudryinella from northwest Europe and Romania, and its relationship to Uvigerinammina. In: Kaminski, M. A., Geroch, S. & Gasinski, M. A. (eds), Proceedings of the Fourth International Workshop on Agglutinated Foraminfera. Krakow Poland, Sept 12–19, 1993. Grzybowski Foundation Special Publication, 3, 145–157.

Gradstein, F. M., Ogg, J. G., Schmitz, M. D., and Ogg, G. M., 2012. The geological timescale 2012. Elsevier, Oxford, U.K.

Hardenbol, J., Thierry, J., Farley, M. B., Jacquin, T., de Graciansky, P. C. & Vail, P., 1998. Mesozoic and Cenozoic sequence chronostratigraphic framework of European Basins. In: Graciansky, P. C. et al. (eds), Mesozoic and Cenozoic sequence stratigraphy of European basins: SEPM Special Publication, 60, 3–13, chart 5.

Hart, M. B., Bailey, H. W., Crittenden, S., Fletcher, B. N., Price, R. & Swiecicki, A. 1989. Cretaceous. In: Jenkins, D. G. & Murray, J. W. (eds), Stratigraphic Atlas of Fossil Foraminifera. 273–371. Chichester: Ellis Horwood.

Ineson, J.R. 1993. The Lower Cretaceous chalk play in the Danish Central Trough. In: Parker, J.R. (ed.) Petroleum Geology of Northwest Europe: Proceedings of 4th Conference. Geological Society, London. 175–183.

Ineson, J.R., Jutson, D. & Schiøler, P. 1997. Mid-Cretaceous sequence stratigraphy in the Danish Central Trough. Geological Survey of Denmark and Greenland Report 1997/109.

Isaksen, D. & Tonstad, K. 1989. A revised Cretaceous and Tertiary lithostratigraphic nomenclature for the Norwegian North Sea. NPD Bulletin 5.

Jakobsen, F., Ineson, J.R., Kristensen, L. & Stemmerik, L. 2004. Characterization and zonation of a marly chalk reservoir: the Lower Cretaceous Valdemar Field of the Danish Central Graben. Petroleum Geoscience 10, 21–33.

Jakobsen, F., Ineson, J.R., Kristensen, L., Nytoft, H.P. & Stemmerik, L. 2005. The Valdemar Field, Danish Central Graben: field compartmentalization and regional prospectivity of the Lower Cretaceous chalk play. In: Doré, A.G. & Vining, B.A. (eds) Petroleum Geology: North-West Europe and Global Perspectives – Proceedings of the 6th Petroleum Geology Conference, 177–186. Geological Society, London.

Jensen, T.F., Holm, L., Frandsen, N. & Michelsen, O. 1986. Jurassic – Lower Cretaceous lithostratigraphic nomenclature for the Danish Central Trough. Danmarks Geologiske Undersøgelse, Serie A, 12, 65 pp.

Jeremiah, J.M., Duxbury, S. & Rawson, P. 2010. Lower Cretaceous of the southern North Sea Basins: reservoir distribution within a sequence stratigraphic framework. Netherlands Journal of Geosciences 89, 201–237.

Johnson, H. & Lott, G.K. 1993. Cretaceous of the Central and Northern North Sea. In: Knox, R.W.O'B. & Cordey, R.G. (eds) Lithostratigraphic Nomenclature of the UK North Sea. British Geological Survey, Keyworth, UK.

King, C., 1983. Cainozoic micropalaeontological biostratigraphy of the North Sea. Institute of Geological Sciences Report 82, 7, 1–40.

King, C. 1989. Cenozoic of the North Sea. In: Jenkins, D. G. and Murray, J. W. (eds), Stratigraphical atlas of fossil foraminifera, 418–489. Ellis Horwood.

King, C., Bailey, H. W., Burton, C. A. & King, A. D. 1989. Cretaceous of the North Sea. In: Jenkins, D. G. & Murray, J. W. (eds), Stratigraphic Atlas of Fossil Foraminifera. 372–417. Chichester: Ellis Horwood.

Kristensen, L., Dons, T., Maver, K. G. & Schiøler, P., 1995. A multidisciplinary approach to reservoir subdivision of the Maastrichtian chalk in the Dan Field, Danish North Sea, AAPG Bulletin, 79, 1650-1660.

Lieberkind, K., Bang, I., Mikkelsen, N. & Nygaard, E. 1982. Late Cretaceous and Danian limestone. In: Michelsen, O. (ed.) Geology of the Danish Central Graben. Geological Survey of Denmark, Series B, 8, 49–62.

Martini, E., 1971. Standard Tertiary and Quaternary calcareous nannoplankton zonation. In: Farinacci, A. (ed.), Proceedings of the Second Planktonic Conference Roma. Edizioni Tecnoscienza, Rome, 2, 739–785.

Petsys 2015. Skaarup et al. 2015. The Jurassic Petroleum System in the Danish Central Graben, Technical notes. Danmarks og Grønlands Geologiske Undersøgelse Rapport, 2015/22. Confidential.

Rasmussen, J. A. & Lassen, S. 2004. Foraminiferal palaeoecology of the Upper Maastrichtian, Danish Central Graben. Danmarks og Grønlands Geologiske Undersøgelse Rapport, 2004/88., 32 pp.

Riley, L.A., Harker, S.D. & Green, S.C.H. 1992. Lower Cretaceous palynology and sandstone distribution in the Scapa Field, U.K. North Sea. Journal of Petroleum Geology 15, 97–110.

Schiøler, P., Andsbjerg, J., Clausen, O. R., Dam, G., Dybkjær, K., Hamberg, L., Heilmann-Clausen, C., Johannessen, E. P., Kristensen, L. E., Prince, I., Rasmussen, J. A.,2007. Lithostratigraphy of the Palaeogene – lower Neogene succession of the Danish North Sea. Geological Survey of Denmark and Greenland Bulletin 12, 1–77.

Sheldon, E., Ineson, J. & Bown, P. 2012. Nannofossil biostratigraphy of the N-22X well, Danish Central Graben. Danmarks og Grønlands Geologiske Undersøgelse Rapport 2012/40, 22 pp.

Surlyk, F., Dons, T., Clausen, C.K. & Highham, J. 2003. The Upper Cretaceous. In: Evans, D., Graham, C., Armour, A. & Bathurst, P. (eds, coordinators) The Millenium Atlas: Petroleum Geology of the Central and Northern North Sea. Geological Society, London, 213–233.

van Buchem, F.S.P., Smit, F.W.H., Buijs, G.J.A., Trudgill, B. & Larsen, P.-H. 2017. Tectonostratigraphic framework and depositional history of the Cretaceous–Danian succession of the Danish Central Graben (North Sea) – new light on a mature area. In: Bowman, M. & Levell, B. (eds) Petroleum Geology of NW Europe: 50 years of Learning, Proceedings of the 8th Petroleum Geology Conference. Geological Society, London.

Varol, O., 1998. Palaeogene. In: Bown, P.R. (ed.), Calcareous Nannofossil Biostratigraphy. British Micropalaeontological Society Series, 200–224, Chapman & Hall/Kluwer Academic.

Vejbæk, O.V. & Andersen, C. 1987. Cretaceous – Early Tertiary inversion tectonism in the Danish Central Trough. In: Ziegler, P.A. (ed.) Compressional intra-plate deformations on the Alpine foreland. Tectonophysics 137, 221–238.

Young, J. R., Bown P. R., Lees J. A. (eds) Nannotax3 website. International Nannoplankton Association. 21 Apr. 2017. URL: http://ina.tmsoc.org/Nannotax3

3 Regional seismic interpretation and mapping (methods)

The following chapter gives a brief description of methodology used to perform regional seismic interpretation and mapping of the Cretaceous section in the study area and to facilitate easy use of the results uploaded to the website system. It summarizes information on the 3D seismic database, interpretation approach, selection and definition of regionally mappable markers. Furthermore, the methodology utilized to construct synthetic seismograms, key seismic structural profiles, time-structure and time-isochore maps is described.

A separate paragraph deals with analyses of well-derived acoustic interval velocities.

3.1 Database

Final migration versions from eight (8) separate 3D surveys in the public domain of various vintages form the 3D database. They are from north to south: PAG95, NACS, MC3D-Angelina, PAM-99 South, DUC2005, C99-5505, Kraka-Extension-2000 and ES2002, the latter and part of Angelina being a multi-client survey (Fig. 3.1). The line orientations are SW-NE parallel to the general structural dips apart from the southern surveys in the salt-structure dominated area, DUC2005 and ES2002, where the in-line orientation is E-W. Pertinent details on the individual surveys can be found on the Cretsys website. The link is:

http://data.geus.dk/geusmap/?mapname=oil_and_gas&lang=en

The data quality of the surveys in the Cretaceous section is generally fair to very good; however, it is rather variable in the NACS survey in the north. The available data coverage extends into Norwegian waters (not shown on Fig. 3.1) and it is actually a merge from 2001 by Mærsk Oil and Gas of a number of vintage surveys, which was designed to focus on the Upper Cretaceous section. The resolution of the PAM-99 South survey is rather low compared to neighboring surveys due to lower frequency content. This has been partly overcome by supplementing the interpretation with the reprocessed data from the Mærsk Gita-Maja processing from 2010.

A major problem exists where a thick high-velocity chalk section directly overlies low-velocity Lower Cretaceous sediments. This gives rise to severe ringing and interbed multiples that mask the imaging of the uppermost Lower Cretaceous section. In order to mitigate the multiple problem, a FK-filter with removal of dips up to 1ms/trace was applied post-stack on flattened volumes at Base Chalk to remove parallel events immediately below on the DUC2005 and NACS data. This improved the ability to pick dipping events in the upper part of the Lower Cretaceous although this robust treatment was at the expense of removing some of the subsurface data. Subsequent frequency whitening (10-70 Hz) followed by bandpass filtering 10-20-60-80 Hz improved resolution in the Chalk section. Frequent shifts between the final migration and post-stack filtered data-sets eased the interpretation process.

Apart from the ES2002 data, where a constant shift of 32 msec was applied during loading to tie the DUC2005 data to the north, no time-shifting has taken place. The misfit between the remaining data-sets was either 0 or below 12 msec, which was considered acceptable for regional interpretation. Apart from the PAG95 survey, all data-sets are displayed using the reverse SEG-convention, where a white trough represents an increase in acoustic impedance.

The data-sets have an areal overlap of varying size (Fig. 3.1). A critical area for ties of high confidence between the DUC2005 and PAM-99-South is in the northern part of block 5504/07 north-east of the Valdemar Field, where only a small overlap exists.

There is almost full 3D coverage of the entire DCG, however with minor gaps in block 5603/26 in the Feda Graben and along the Jurassic Lulu Cross-Fault separating the Søgne Basin from the northern Tail End Graben in block 5604/22. More crucial for the structural interpretation is the lack of released 3D data in blocks 5504/ 3&-4, where the Coffee Soil Fault Zone changes direction from NNW-SSE to WNW-ESE north of the NW Adda-1 location. Here the structural interpretation and mapping relies on vintage 2D data.

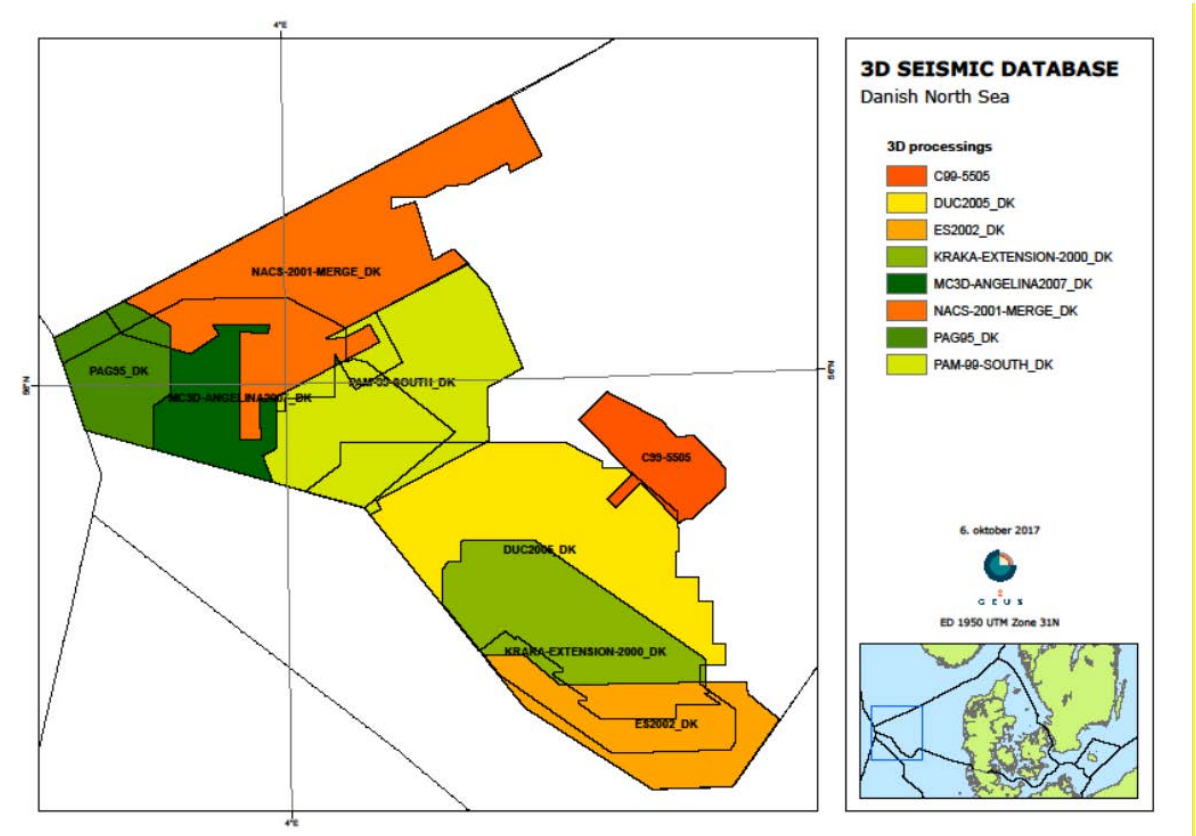

Fig. 3.1. *3D seismic database.*

3.2 Interpretation approach

The seismic interpretation was carried out in Landmark *SeisWorks,* although the Landmark *Decision Space* software was used at a late stage in the project to refine the interpretation of BCU and to map the a pre-BCU seismic marker informally termed *Base Mandal Formation*. As a starting point a large number of distinct reflectors which can be traced over most of the Danish Central Graben (DCG) were tied to well sections using the *Syntool* software (Fig. 3.4) and selected for regional interpretation and mapping. 12 regional markers in total have been interpreted. This gives the opportunity to define 11 seismic units with top and base delimited by the seismic markers. The horizons in the Upper Cretaceous chalk section have been annotated with the prefix *ch* and are numbered from below. The terminology has been adopted from earlier in-house well correlation studies based on distinct log markers. In the Lower Cretaceous Cromer Knoll Group the markers are annotated the prefix CKG and correspond to tops of the formal lithostratigraphic subdivision (Valhall, Tuxen and Sola Formations).

Locally in areas with structural complexity and poor imaging the interpretation has been guided by stratigraphic data from wells established in an interactive process.

The interpretation of the separate surveys is carried out with a distance between lines and traces not exceeding 250 m. The density is higher in the DUC2005 survey (every 10th line and trace) and in areas with survey overlaps. Horizontal fault heaves have been left open in the horizon interpretation. An example of interpretation density is shown on the SeisWorks screen-dump in Fig. 3.2. It is noted that interpretation has been omitted on the structurally complex shallow salt piercements structures with a generally thin chalk cover.

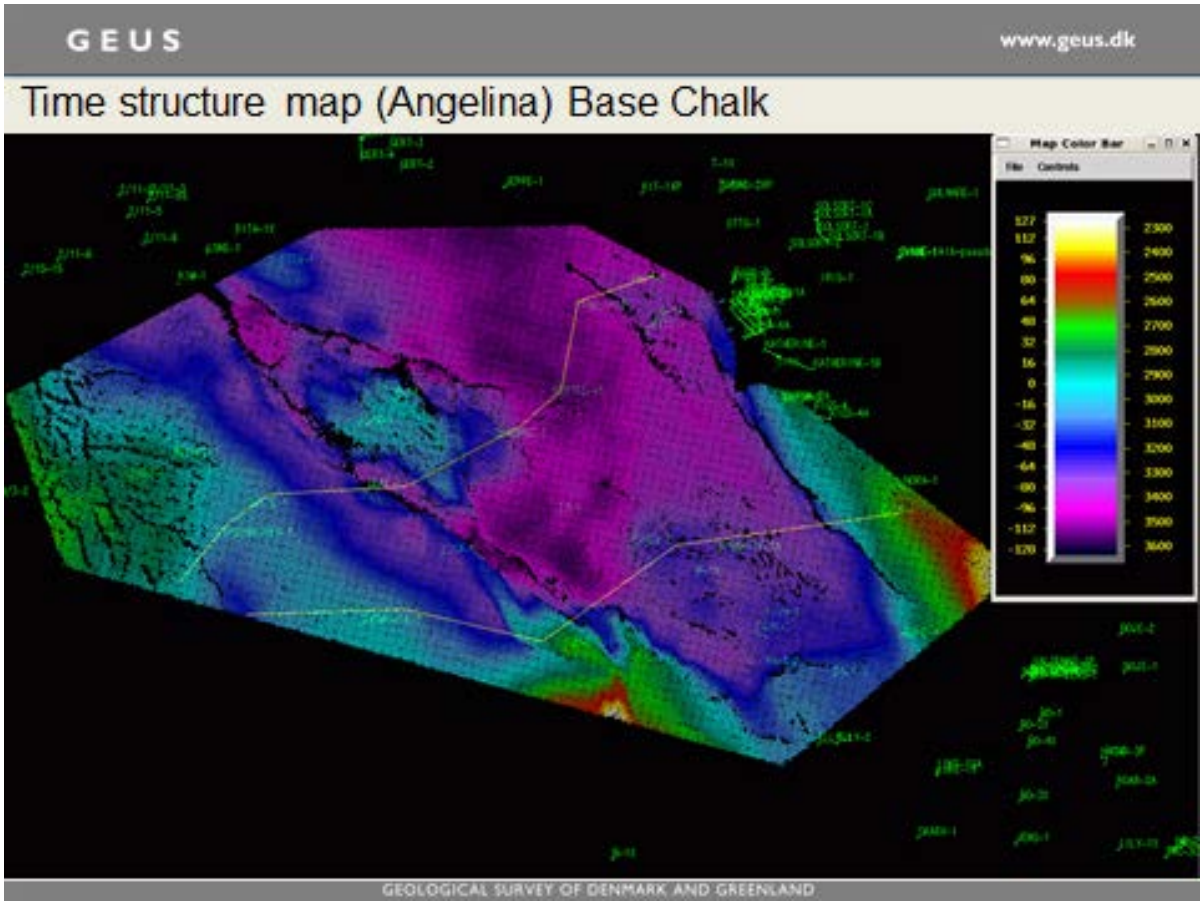

Fig. 3.2. *Screen-dump from Seisworks showing interpretation density and fault traces.*

The relationship of the interpreted seismic markers to the applied lithostratigrapic nomenclature is given in Fig. 3.3. The markers are as follows and briefly described below:

'Base Mandal Formation': This is picked in a weak trough marking a downward increase in acoustic impedance. It is tied into selected wells and marks the base of TOC-rich mudstones of late Volgian and Ryazanian age with elevated GR-readings The interval immediately above includes the Bo- and sandy Poul members.

BCU: The Base Cretaceous Unconformity is an easily recognized seismic event (strong peak) marking the top of the underlying low impedance Mandal/Farsund shales in the basinal areas. At basin margins it represents a hiatus with varying time-stratigraphic gaps to the overlying formations. BCU sub-crop and super-crop map are given in Figs 8C.3 & 8C.4.

CKG10: The top of the claystones of Valhall Formation is picked in a continuous peak overlying a generally rather transparent interval with few continuous internal reflectors. The reflector shows basal onlap to the west, but it is truncated by the Base Chalk *(chb)* reflector towards north in the Søgne Basin and along inversion ridges to the east in the central part of DCG.

CKG15: It is a generally strong trough marking the top of the carbonate-rich Tuxen Formation. It has a more restricted extension than the CKG10 marker towards the Søgne Basin and along inversion ridges to the east, where it is truncated by Base Chalk.

CKG20: This marker is picked in a peak marking the top of the claystones of the Sola Formation. It can only be traced over a restricted area comprising the Outer Rough Basin and the Ål Basin in the north-west, the northern part of the Getrud Graben to the north, and centrally along the Arne-Elin Graben and adjoining areas to the east. In these areas the overlying Rødby Formation is thick, allowing separation of CKG20 from the distinct Base Chalk reflector.

chb: The Base of the Chalk Group is everywhere represented by a distinct strong amplitude peak marking the break from high impedance chalk to lower velocity Lower Cretaceous and older Formations.

ch1: It is picked in a usually continuous peak where the underlying Hidra Formation and marls of the lower Blodøks Formation, equivalent to the Roar Member of van Buchem et al. 2017 are thick. The marker onlaps the Base Chalk (chb) along the basin margins.

ch7: This event is in most areas a distinct high amplitude peak easy to trace and marks the interface between the chalks of Hod C unit above and the lower impedance marly chalks of Hod B unit below. It is with a few exceptions (e.g. Mid North Sea High and Søgne Basin) traced in the entire study area. The horizon is in several places developed as an unconformity surface with truncation of the Hod B unit and is further characterized by several incisions. On the Ringkøbing-Fyn High the stratigraphic data from the Per-1 and Sine-1 wells suggest that the marker instead shall be picked in a trough at the top of a tight chalk succession.

ch11: The seismic marker is picked in a trough of varying amplitude and separates the Tor Formation from the tighter chalk of the Hod Formation. Like *ch7* it represents an unconformity surface with truncations below and onlap above along flanks of intra-chalk inversion zones and is also cut by a number of channel scars. Along the crests of inversion axes the two surfaces (*ch7 and ch11*) locally merge and are characterized by a simple trough-peak relationship.

ch15: It is picked in a trough of variable strength, which in most well sections represents a transition from more upper porous to lower tighter chalk of the Tor Formation. The marker onlaps the *ch11* reflector on the centrally located intra-chalk inversion zone and on the inverted Outer Rough Basin.

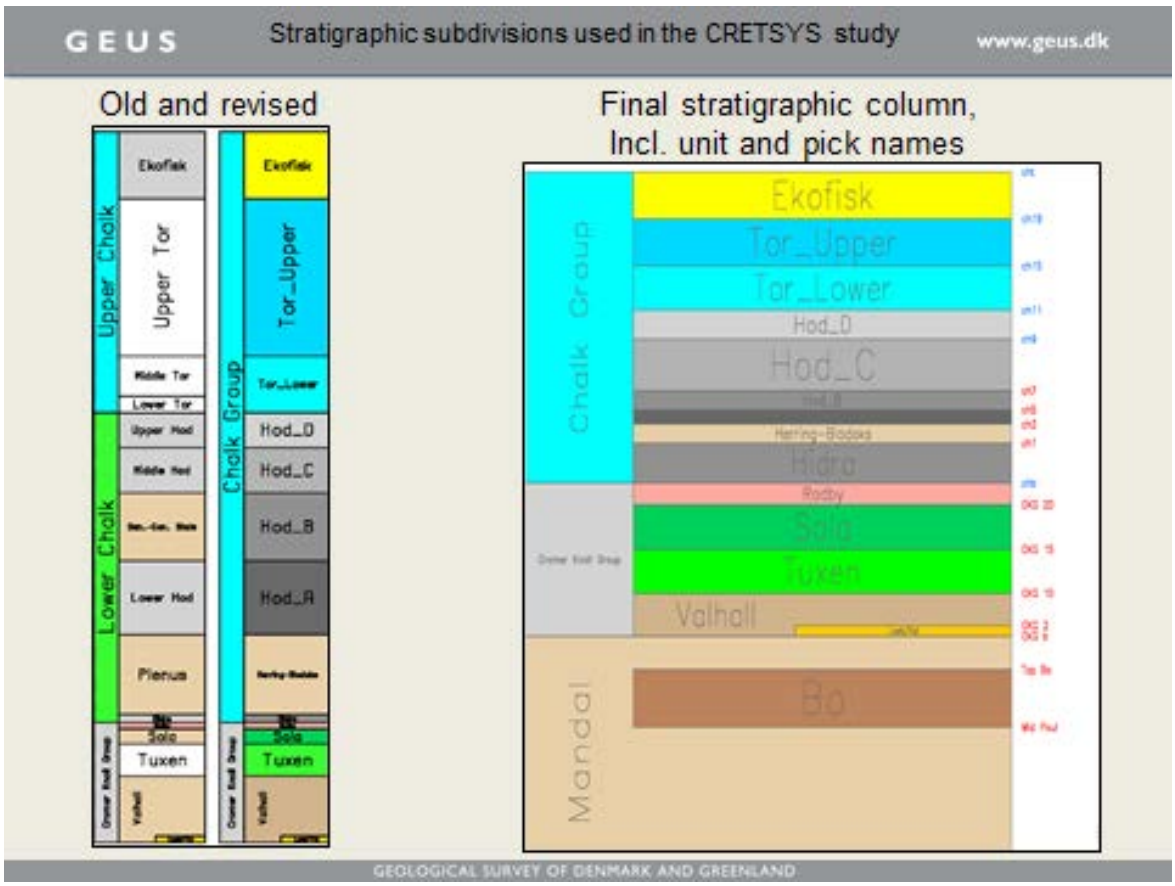

Fig. 3.3. *Relationship between lithostratigraphic subdivision and interpreted seismic markers*

ch19: The marker represents the Near Top Tor Formation and is picked in a generally strong peak generated by the interface of the lower tight member of the Ekofisk Formation and/or the top Mastrichtian hardground and the underlying porous parts of the Tor Formation. It can be traced in the entire DCG apart from the crests of a few inversion ridges, where it merges with the Top Chalk reflector.

cht: The top of the Chalk Group is a distinct high amplitude event which is interpreted over the entire area. However, phase reversals occur on top of the gas accumulations (e.g. Lulu, Boje, Roar, Tyra, Igor, Dan and Kraka fields). The top Chalk reflector represents the top of the Ekofisk Formation when present. On the crestal parts of the inversion ridge in the Valdemar area and further north where the Tor Formation is also thin to absent, the marker may locally represent the top of the Hod Formation. The reflector represents an even deeper cut into the Hod Formation on the crest of the post-chalk Robin Inversion Ridge. The top chalk surface is very irregular east of the Tyra-Igor Ridge with high frequency ‘bumps’ interpreted as slumps and minor slides.

3.3 Synthetic seismograms

Synthetic seismograms have been generated for 120 wells penetrating the Cretaceous succession or with TD in the Cretaceous using the Landmark *Syntool* software and can be accessed using the *seismics* menu on the website. This allows display of time-depth relationships based on velocity surveys and VSP's, GR-Sonic and Density log traces with location of seismic markers and calculated acoustic impedance and reflectivity coefficients, respectively. The location of check shots is shown with small green dots on the time-depth scale to the left. The log-based synthetic trace is further displayed on a line section and the AI- and GR log on a trace section through the well location. A wavelet extraction over a relevant time window was carried out prior to calculation of the synthetic traces. The applied trapezoid frequency spectrum is indicated.

Adjustments to the time-depth curves were necessary in some wells in order to establish a good match to the most distinct reflectors (e.g. Top and Base Chalk and BCU).

The synthetic seismograms were used extensively and proved a valuable tool during the interpretation process to establish well-ties. The time-depths relationships extracted from the synthetics to the marker horizons are posted in a separate excel spread-sheet found under the seismic menu on the website. The TWT values to the marker horizons are further found on a separate column in the stratigraphic summary charts.

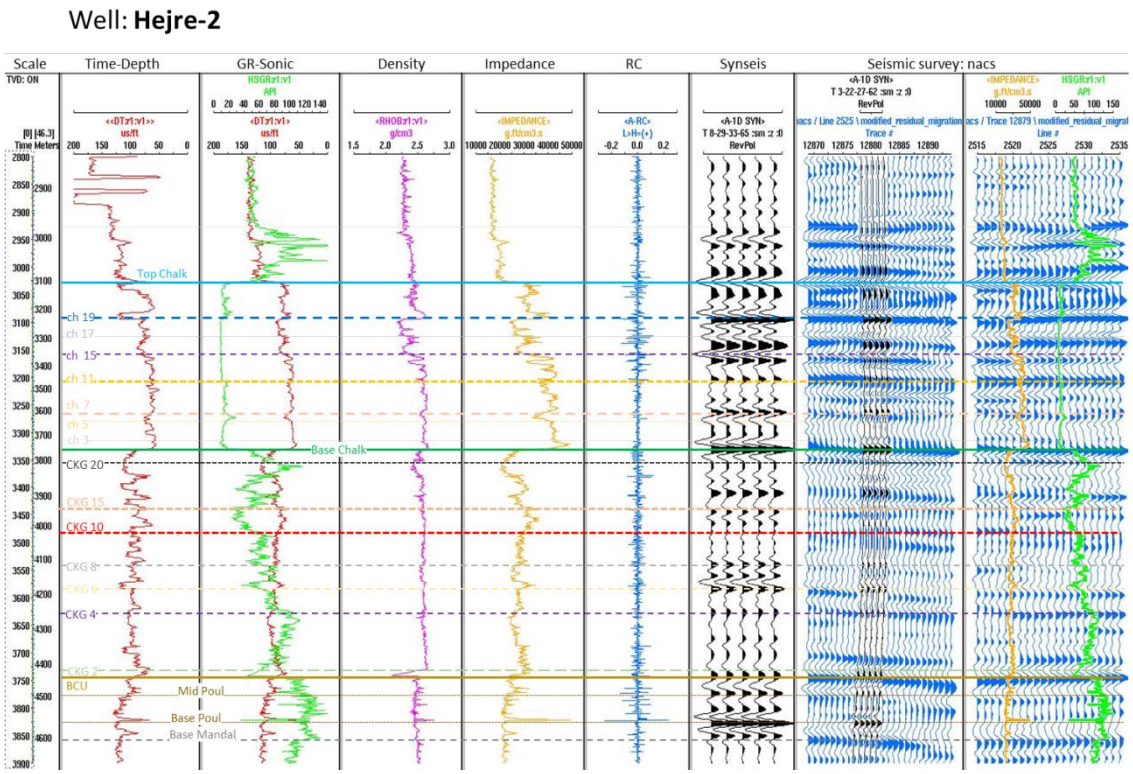

Fig. 3.4. *Example of synthetic seismogram (Syntool) with well ties.*

3.4 Structural profiles

19 interpreted seismic sections are displayed by activating the map menu under the heading *Sections* on the website system. The sections are screen dumps of arbitrary line segments from the individual surveys crossing several well locations. The seismic markers are all annotated with their *ch*- and *CKG* number and the same colour code as for the synthetic seismograms has been applied (Fig. 3.5). In addition to the regionally mapped reflectors described above, more reflectors which can be traced locally are shown on a few sections.

The sections have been chosen with the intention to illustrate the structural style in all Cretaceous sub-basins of DCG and to provide well ties. The profiles show the ties to 79 wells in total.

It is noted that both vertical and horizontal scales may differ from section to section.

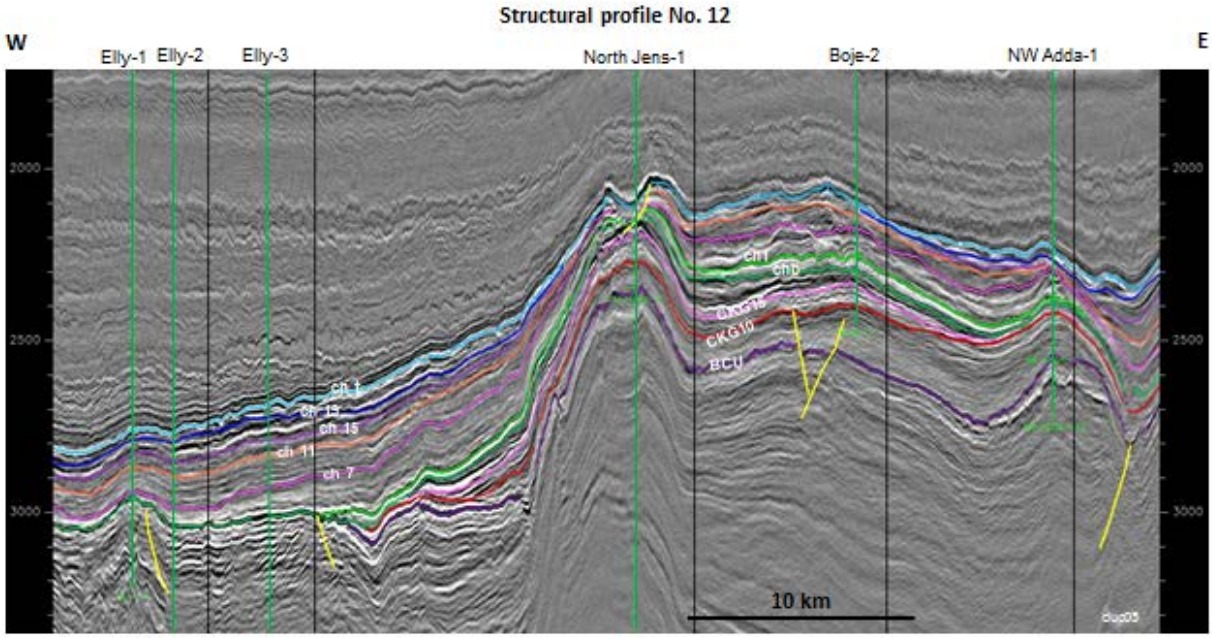

Fig. 3.5. *Example of structural profile*

3.5 Time structure- and time isochore map generation

Time-structure maps of the 12 regionally interpreted horizons and 11 time-isochore maps can be displayed on the website in the map menu. The input files of the latter have been generated by simple subtraction in *SeisWorks* of the relevant horizons survey by survey. For each horizon, the grids, fault lines and contours are placed in separate folders. In addition, separate combined isochore maps of the intervals: *CKG10-chb, chb-ch11* and *ch11-cht* in order to summarize the Cretaceous basin development.

Following quality checking the data were exported survey by survey from Landmark to a gridding process and filtering in *Matlab* resulting in a regular grid with a grid cell density of 100 m. Using the *Safe Software* the final grids were created and exported to ArcGIS. The workflow with further details is illustrated in Figs 3.6, 3.7 & 3.8. It should be noted that the grid size had to be increased in areas only covered with 2D data.

The contour interval on the time-structure maps is 50 msec. and the color coding is kept identical on all maps (apart from the *BCU*) in order to enhance the graphical presentation. The map area of both Top and Base Chalk Group is increased to cover a larger part of the Ringkøbing-Fyn High to the east.

The contour interval on the time-isochore maps is variable, either 10 or 20 msec. The color-coding on each map is designed to optimize the graphical presentation.

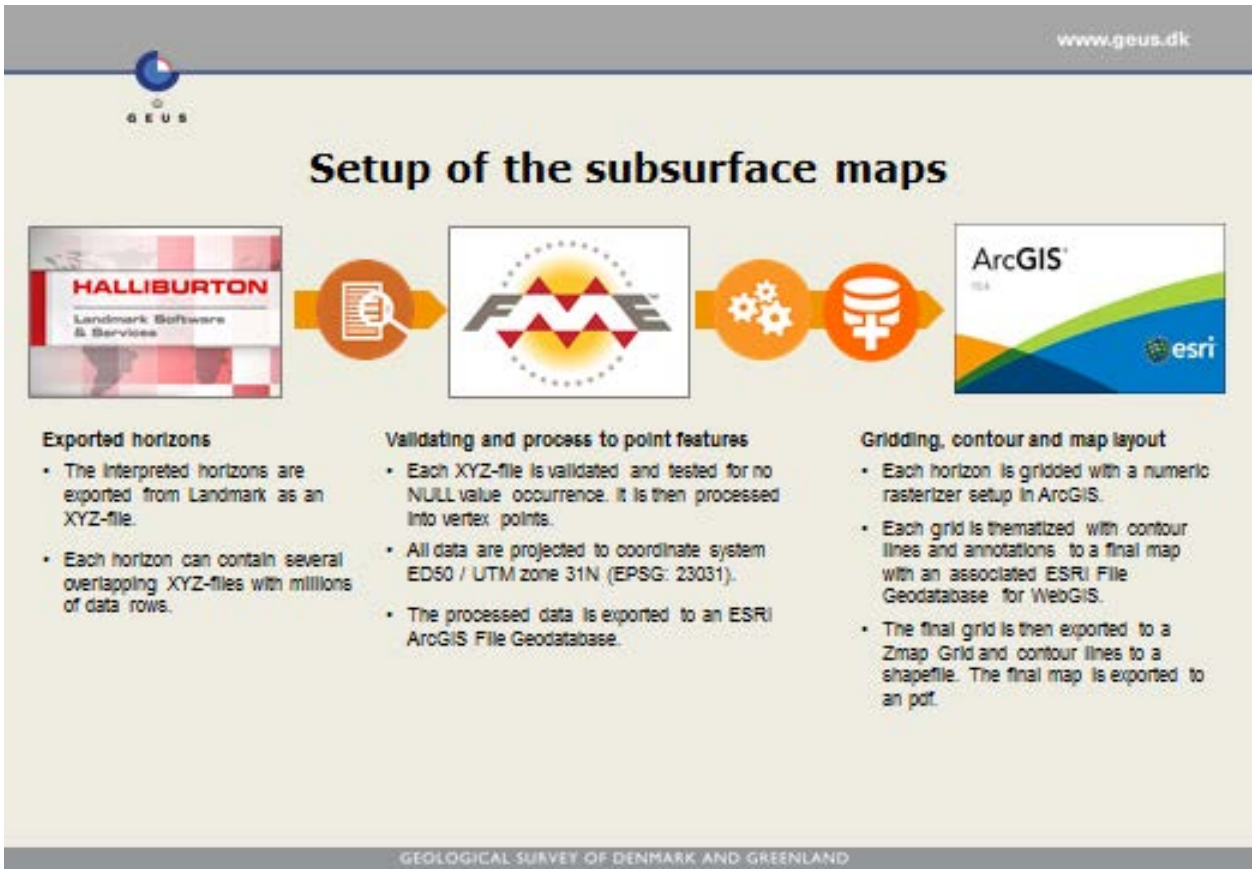

Fig. 3.6. *Work flow for map generation.*

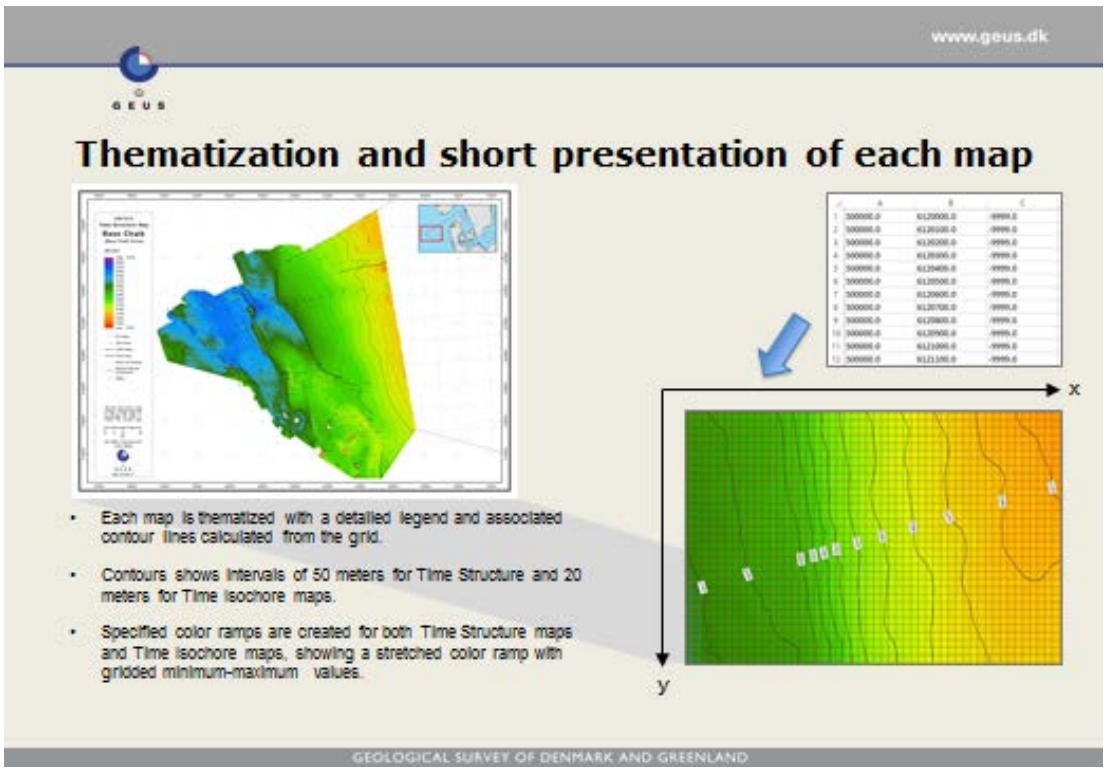

Fig. 3.7. *Workflow for map generation (continued).*

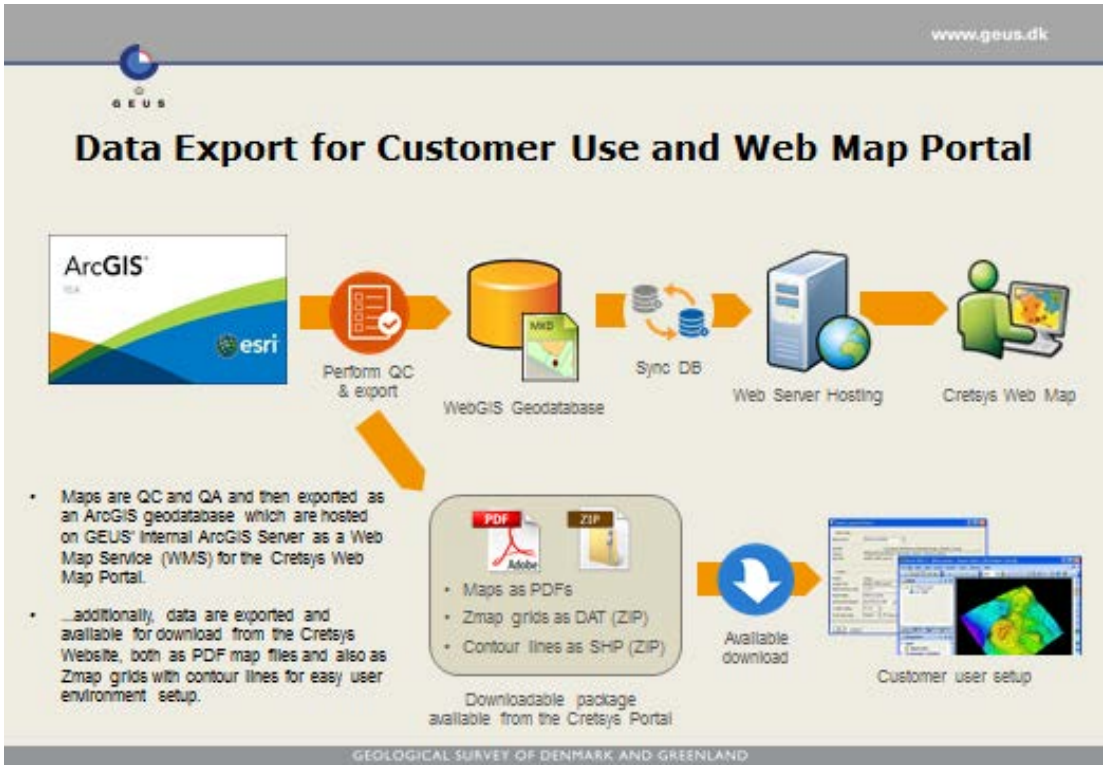

Fig. 3.8. *Work flow for map generation.*

3.6 Seismic feature maps

A set of seismic feature maps related to the five upper seismic units (*chb-ch7* through *ch19-cht*) is presented as separate layers which can be overlaid on the relevant time-isochore maps. The features that are highlighted refer both to the upper surface, such as phase reversals, channel scars and amplitude extractions and Mass Transport Complexes (*MTC's*) internally in the seismic units.

3.7 Well velocities

The Cretaceous velocity structure derived from well sections is analysed with respect to interval velocities of 4 separate intervals bounded by key seismic reflectors. These are in the Lower Cretaceous *BCU – CKG10,* corresponding to the Valhall Formation, and the *CKG10 – chb* interval comprising the mixed carbonate-siliciclastic succession of the Tuxen, Sola and Rødby Formations. The Upper Cretaceous Chalk Group is split into two intervals separated by the *ch11* seismic marker, the lower interval *chb – ch11* corresponding to the Hidra, Blodøks, Herring and Hod Formations and the upper one *ch11 – cht* comprising the Tor and Ekofisk Formations. The data are extracted from the spread-sheet listing depth-picks in wells and the corresponding two-way-time found on the seismic menu on the website. The results are tabulated in a separate spread-sheet showing midpoint depth, thickness, time-thickness and interval velocity in km/s in 91 wells for the four intervals. The interval velocity has been omitted for very thin intervals with poorly defined time-depth relationships. The average velocity to the top of the Chalk Group is also included.

The average velocity to the Top of the Chalk Group in km/s (given with two decimal points) at the well locations is in agreement with the values shown on the Post Chalk Group interval velocity map by Britze et al. (1995a). They vary from 1.98 km/s to 2.11 km/s with the vast majority of values in the range 2.02 – 2.05 km/s as shown on the histogram below (Fig. 3.9). The low velocities below 2.01 km/s are all confined to shallow wells with a depth to Top Chalk Group at about 2000 m and typically with gas saturation in the uppermost chalk section (e.g. Tyra, Roar, Dan and Boje wells). The outliers with high Va value at 2.10 km/s and above are confined to wells located in the NE part of the study, adjacent to the Coffee Soil Fault. This may reflect a difference in overall lithology in the post-chalk section in this area compared to the remaining part of the DCG and/or pressure bleed-off.

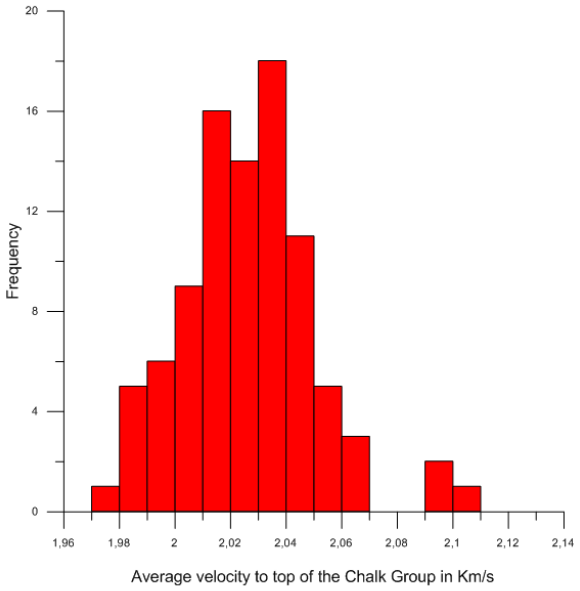

Fig. 3.9. *Histogram showing spread of average velocities to the Top Chalk Group.*

The interval velocities (Vint) are plotted versus midpoint depths of the four Cretaceous intervals in Figs 3.10 & 3.11. There is a clear depth dependency in interval velocity in both chalk intervals (Fig. 3.9) with systematically higher values in the lower *chb – ch11* interval compared to the upper *ch11 – cht* interval in each well. It is noteworthy that the slope of the trend-lines is identical in both intervals. The lower chalk interval is tight and characterized by very high Vint up to more than 5.0 km/s in the deep wells. A Vint of 4.6 km/s and above is found in all wells with an interval midpoint depth above 3500 m TVDSS. This velocity value is roughly equivalent to an average porosity of 10 %. A few marked outliers with low Vint well below the trend-line in Fig. 3.9 are noted. They represent the North Jens-1 and I-1 wells, both located on inversion anticlines.

There is a larger scatter of Vint vs. midpoint depth in the upper chalk interval, *ch11 – cht* comprising the Tor and Ekofisk Formations with a higher proportion of wells with anomalous low Vint below the established trend-line. These wells are typically located on shallow structural closures and with hydrocarbon saturation in the uppermost part of the chalk section. The Middle Rosa Flank-1 well represents an outlier with high Vint.

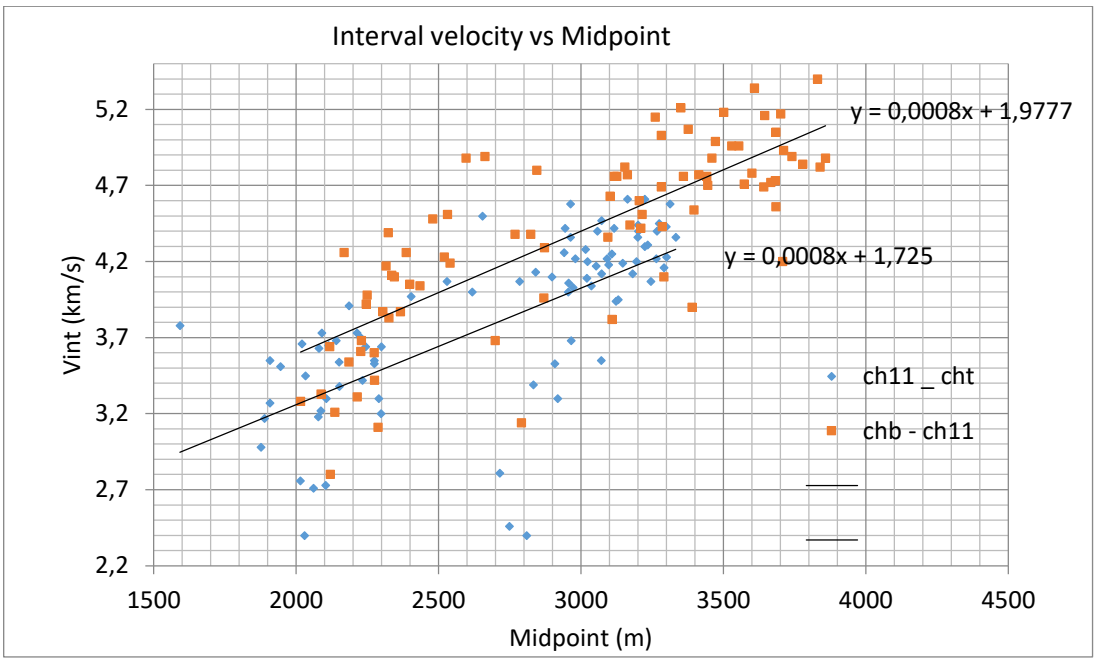

Fig. 3.10. *Vint versus midpoint depth (Upper Cretaceous).*

In contrast to the Chalk Group, the interval velocities of the Lower Cretaceous well sections are markedly lower, generally less than 3.5 km/s. Furthermore, the depth dependency is much weaker as illustrated on Fig. 3.10 which shows that the slopes of the trend-lines of Vint vs. midpoint depths for both the *CKG10 – chb* and the *BCU – CKG10* intervals are much lower, the latter being almost non-existing. The interval velocities of the lower interval, corresponding to the Valhall Formation, cluster around a value of 3.0 km/s, only slightly higher than the underlying upper part of the Farsund Formation. The Vint is independent of the thickness of the interval, as shown in Fig. 3.12, although there is a tendency for Vint to be higher in wells with small thicknesses. A distinct outlier is the V-1 well with a Vint of 4.33 km/s. The high value is attributed to a high content of coarse-grained clastics (Vyl sandstone).

Compared to the Valhall Formation, there is a larger scatter of Vint in the *CKG10 – chb* interval comprising the combined Tuxen, Sola and Rødby Formations. This probably reflects lithological variations with different proportions of carbonate vs. claystone from well to well.

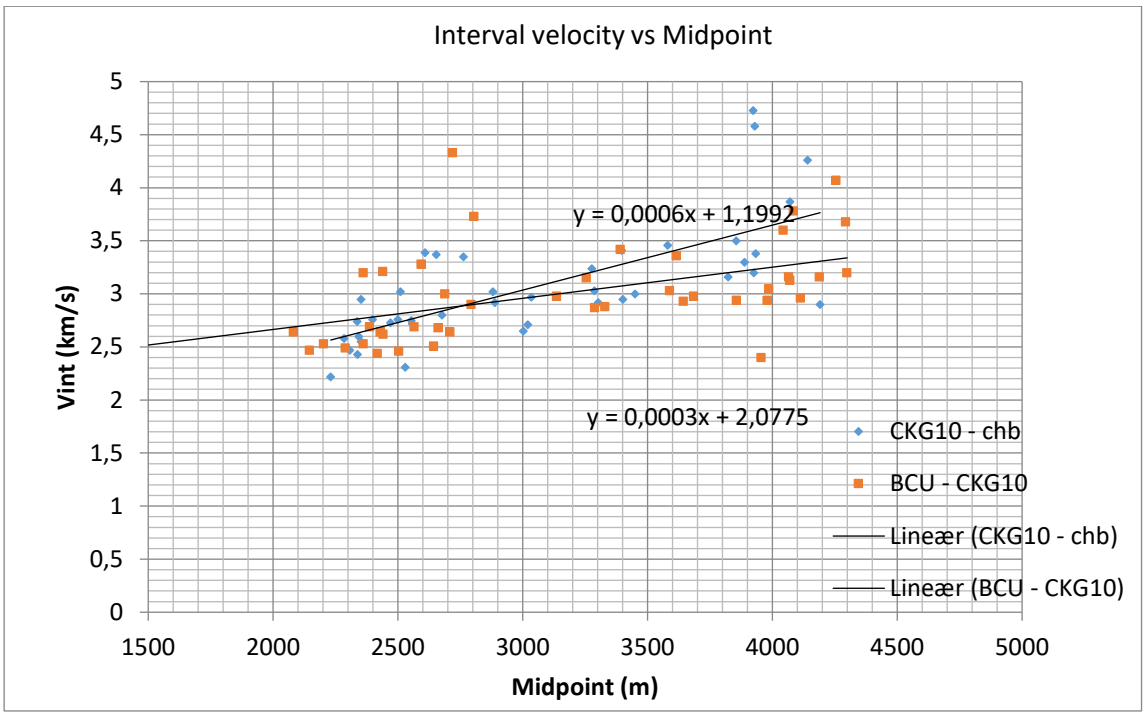

Fig. 3.11. *Vint vs. midpoint depth (Lower Cretaceous).*

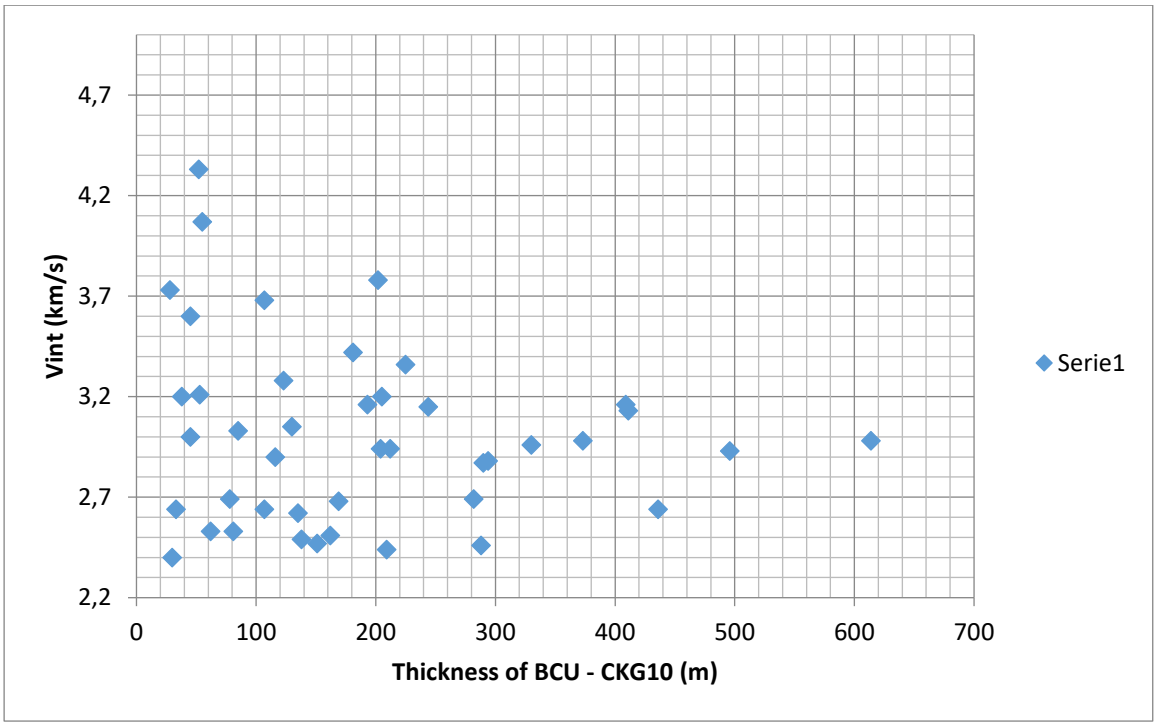

Fig. 3.12. *Vint vs. thickness of the Valhall Formation.*

No depth-converted maps have been produced as part of the project, but published depth structure maps of BCU and Top and Base of the Chalk Group (Britze et al. 1995 a, b and c) is loaded on the website.

References

Britze, P., Japsen. P. & Andersen, C. 1995a: Geological map of Denmark. 1: 200,000: The Danish Central Graben. 'Top Chalk' and the Post Chalk Group (two-way-traveltime, depth and interval velocity) Danm. Geol. Unders., Map Series, 47, 7 pp. and 3 maps.

Britze, P., Japsen, P. & Andersen, C. 1995b: Geological map of Denmark. 1: 200,000: The Danish Cental Graben. 'Base Chalk' and the Chalk Group (two-way-traveltime and depth, thickness and interval velocity). Danm. Geol. Unders. Map Series, 48, 7 pp and 4 maps.

Britze, P., Japsen, P. & Andersen, C. 1995c: Geological map of Denmark. 1: 200,000: The Danish Central Graben. 'Base Cretaceous' and the Cromer Knoll Group (two-way-traveltime and depth, thickness and interval velocity). Danm. Geol. Unders., Map Series 49, 7 pp and 4 maps.

Van Buchem, F.S.P., Smit, F.W.H, Buijs, G.J.A., Trudgill, B. & Larsen, P.-H. 2017: Tectonostratigraphic framework and depositional history of the Cretaceous – Danian succession of the Danish Central Graben (North Sea) – new light on a mature area. In: Bowman, M. & Levell, B. (eds) *Petroleum Geology of NW Europe: 50 Years of Learning – Proceedings of the 8th Petroleum Geology Conference.*

4 Results of log interpretation, including the methodology used for preparing CPI plots, calculating reservoir parameters and analysing GR/DT log facies of the Cretaceous succession

The petrophysical evaluation is based on wireline log data and core analysis data from selected Danish wells using a standard approach for interpreting the log data. The results of the petro-physical evaluations are listed as LAS files including depth columns, effective porosity (PHIE), total porosity (PHIT), shale volume (Vshale) and hydrocarbon saturation (Sh). The current log analysis focuses on chalk and limestone layers within the Cretaceous succession, i.e. potential reservoir units, and the Cretsys website includes CPI plots from 129 wells (press 'Wells' – 'CPI plots'). Corresponding Reservoir parameters are also computed and uploaded: Net thicknesses and belonging average porosities are calculated on the basis of 10% porosity and 30% Vshale cut-offs. Maps with point data showing the variation in reservoir parameters throughout the Danish Central Graben can be plotted interactively from the Cretsys website (press 'Map Data' – 'Reservoir parameters'). The methodology used for preparing GR/DT logs (log facies) is described in detail below.

4.1 Petrophysical evaluation (screening procedure):

- **Generally, the shale volume (Vshale)** is calculated from the gamma-ray log using a linear model.

- **The porosity (PHIE)** is determined from density log, calculated shale volume (Vshale) and various fluid densities.
    - It has been assumed that the chalk matrix density is 2.71 g/cc.
    - Grain density measurements, combined with cross-plots of neutron-density log responses, have been used for lithology determination, if needed.
    - Various fluid densities were applied: *Water-Based Mud systems*: 1.05 -1.10g/cc for oil and water, 0.90g/cc for gas. *Oil-Based Mud systems*: 0.95g/cc for oil and water, 0.80g/cc for gas.
    - The porosity interpretation was calibrated to core porosity data, when available. The core data have been depth-shifted.

- **The hydrocarbon saturation (Sh) was calculated from resistivity logs and various petro-physical parameters:**
  - Petrophysical parameters *a, m, n* and *Rw* were extracted from Well Completion Reports.
  - Otherwise *a* =1, *m* = 2, *n* = 2 and *Rw* from Pickett Plots; i.e. standard approach.
  - The calculation of the water saturation (Sw) is based on the Indonesian Equation.
  - The hydrocarbon saturation (Sh) is then calculated as Sh = 1–Sw.

4.2 CPI Plots

The generated CPI plots, or petrophysical result displays, deal primarily with the reservoir sections of the Upper and Lower Cretaceous deposits. Sand-rich formations of the Lower Cretaceous and Upper Jurassic successions are also considered. CPI plots of the wells are uploaded onto the Cretsys website. An example is shown in Fig. 4.1. Each CPI plot includes the following information, if available:

- Lithostratigraphic subdivision of the succession.
- GR/DT log facies.
- Porosity; log-derived porosities and core porosity data. The core data have been used for calibrating the log-derived porosities.
- Hydrocarbon Saturation.
- Cored intervals.
- Tested interval(s), casing shoes.

4.3 LAS files

Apart from CPI plots, the result of the log interpretation is presented as LAS files, which list log-derived porosity, hydrocarbon saturation and shale volume for each ½ ft; i.e. MD, TVD, TVDss, PHIE, PHIT, Sh and Vshale. The LAS files have been uploaded onto the Cretsys website (press 'Wells' – 'LAS files'). The LAS files can fairly easily be downloaded from the website and then uploaded into a company database.

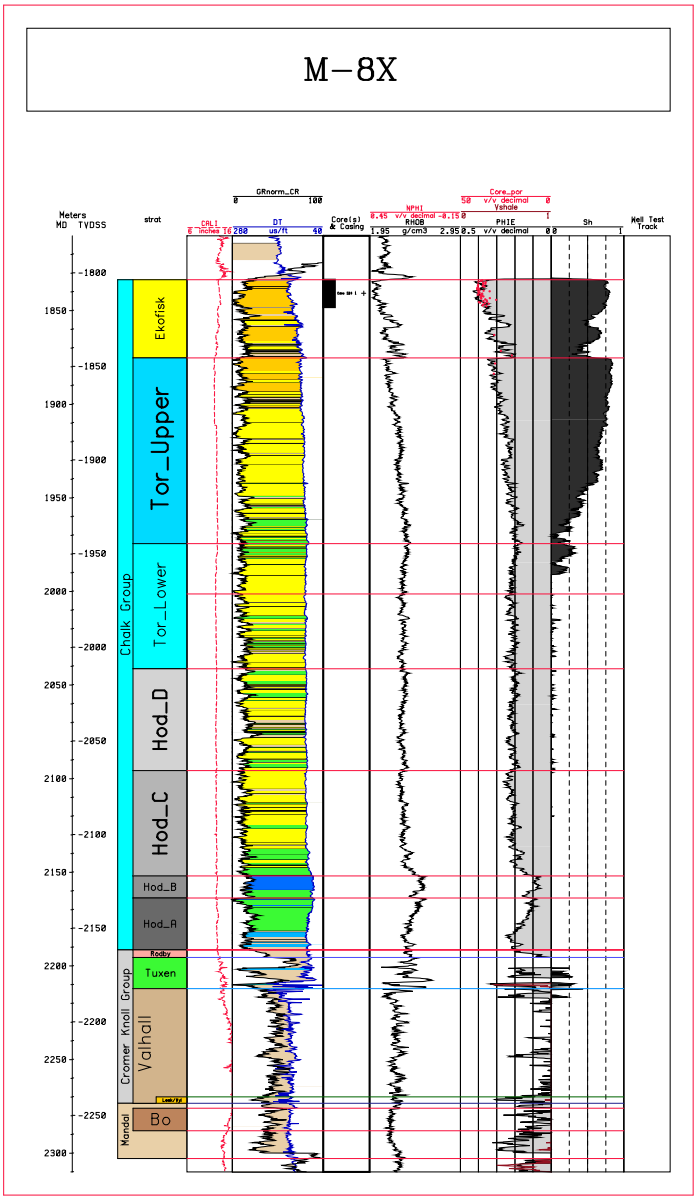

Fig. 4.1. *Example of an extended CPI plot prepared for this study. Stratigraphy, lithology, raw log curves, interpreted curves. Cored intervals are shown by black bars. The GR/DT log facies are plotted in between the gamma-ray and sonic logs*.

4.4 Reservoir parameters

The interpreted log data form the basis for calculating reservoir parameters for each litho-stragraphic unit, i.e. tops, unit thickness, gross interval thickness, net thickness, and average porosity. These parameters are included in the database and are accessible from the Cretsys website. For calculating net thicknesses, GEUS applied 30% Vshale cut-off and 10% porosity cut-off. The basic unit for calculating these parameters in each well is the lithostratigraphic unit sub-division, which was updated and revised

during the study period as a consequence of the establishment of a new seismic-stratigraphic framework. When accessing the Cretsys website, reservoir parameters can be plotted interactively as point data on base maps. All tables and maps are related to the lithostratigraphic units set up for the Cretsys study (cf. Fig. 4.2). The column to the left corresponds to a preliminary version; the final version is plotted to the right:

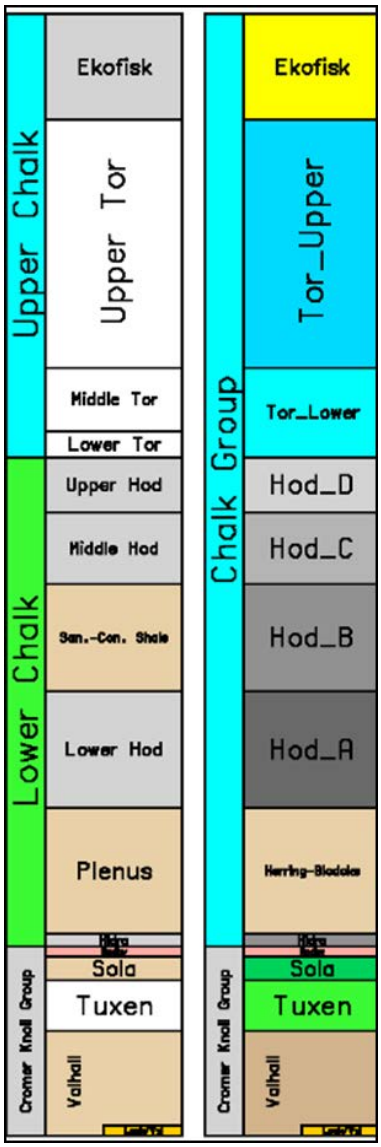

Fig. 4.2. *Lithostratigraphic columns used in the Cretsys Study. Preliminary version to the left; the right column represents the final version.*

4.5 GR/DT log facies

The GR/DT log facies illustrates the distribution of carbonates and shales/clays within a particular unit. In the Chalk Group (Upper Cretaceous), the chalk facies were subdivided into 5 classes or GR/DT log facies:

Class	Porosity range PHIE	DT range (micro-sec/ft)	Colour code
Very porous chalk	> 30%	> 93	Orange
Porous chalk	20 – 30%	79 – 93	Yellow
Low porosity chalk	10 – 20%	66 – 79	Green
Tight chalk	< 10%	< 66	Blue
Chalk with elevated GR		Independent of DT	Brown

The classification of the **Upper Cretaceous chalks** is primarily based on porosities derived from the sonic log, and it should be noted that the sonic porosities may deviate slightly from porosities derived from a conventional petrophysical evaluation based on neutron-density logs (PHIE).

For a particular well, the GR/DT logs (log facies) were prepared on the basis of sonic and gamma-ray log responses. Firstly, a normalized GR log (GRnorm) is generated by subtracting an assumed background radiation from the raw GR log data. Secondly, a suitable GRnorm baseline is introduced; this baseline separates rather clean chalk from more shaly intervals (the latter corresponds to 'chalk with elevated GR response' together with shales and clays). As described above, the chalk layers defined by the GRnorm baseline are considered to be rather clean, meaning almost shale-free. Thirdly, the chalk section is subdivided into 4 porosity classes on the basis of sonic log responses: very porous chalk, porous chalk, low porosity chalk and tight chalk.

The classification of the **Lower Cretaceous limestones** is primarily based on sonic log response. Only two classes are considered, and a DT baseline of 100 micro-sec/ft is used for distinguishing 'high porosity limestone' from 'low porosity limestone'. A sonic/DT baseline of 100 micro-sec/ft corresponds approximately to a total porosity (PHIT) value of 20%. In general, the Lower Cretaceous limestones are marly deposits, and therefore PHIT is herein preferred for porosity evaluations. There is a direct correspondence between sonic log porosity and PHIT, but in Upper Cretaceous chalks the

shale volume is low and it may be anticipated that PHIT = PHIE. The latter assumption cannot be applied to Lower Cretaceous limestones due to the high clay content.

Firstly, a GRnorm baseline was used to separate the limestones from clayey and marly intervals. Secondly, a DT baseline was used to subdivide the limestones belonging to the Rødby, Sola and Tuxen formations into only two porosity classes. The Leek Member marlstone was treated separately.

Class	Porosity range PHIT	DT range (micro-sec/ft)	Colour code
High porosity limestone	> 20%	> 100	Light blue
Low porosity limestone	< 20%	< 100	Medium blue
Clay/Marl		Independent of DT	Brown
Leek Mb marlstone			Dark blue

Additional GR/DT log facies

The Cretsys study also includes information on classifying of Upper Jurassic and Lower Cretaceous sandstones. Hence, the Cretsys study deals with sandstone layers belonging to the Vyl and Poul formations together with a number of Upper Jurassic turbiditic sandstones. The porosity interpretation of these sandstones is based a conventional petrophysical evaluation, and only two porosity classes are considered: PHIE<20% and PHIE>20%.

Vyl, Poul, and turb. sandstones	PHIE > 20%	Based on GR, DT and neutron-density	Red
	PHIE < 20%		Light red

4.6 Quantification and illustration of GR/DT log facies

For a particular well, the thickness of the GR/DT log facies can be extracted from the Cretsys website (press 'Wells' – 'GR/DT Log Facies'). The GR/DT Log Facies module contains a bar diagram for each well illustrating the thickness of each lithostratigraphic unit facies accompanied by a GR/DT Log Facies distribution. For each well, the thickness of a particular facies is plotted in a supplementary bar diagram. All thicknesses (in metres) are also tabulated in tables.

In addition, the GR/DT Log Facies can be plotted as pie diagrams for each lithostratigraphic unit or formation. Press ‘Map’ in the main menu – then ‘Cretsys website’ – followed by ‘MAP DATA’ – and next ‘GR/DT Log Facies’.

4.7 Database with core analysis data

Conventional core analysis data (CCAL) are available from the Cretsys website. The data comprise porosity, permeability and grain density measurements. The data can be plotted as histograms for each well or for specific lithostratigraphic units. The data can be downloaded as an Excel file.

Press ‘Wells’ in the main menu – then ‘Core analysis’ to get access to the core analysis data originating from selected wells penetrating the Cretaceous succession.

5 Hydrocarbon shows/discoveries database

The following note gives at brief description of the hydrocarbon shows/discoveries database that was established as part of the Cretsys project and which is available on the Cretsys website.

All data have been compiled from completion reports. Data are presented at depth levels and stratigraphic levels, using the revised lithostratigraphic subdivision established in the project.

Shows/discoveries at depth level are presented for the total drilled sequence. The Jurassic lithostratigraphy has been taken from the Petsys project. The Mandal Formation has been added and corresponds to the following sequences: Volg-4, Ryaz-1 and Ryaz-2, if present.

Data can be addressed at map level and at well level.

5.1 Access at map level

Select “Map” and press “Map data”

Select “Shows/Discoveries”

Select “lithostratigraphic unit”, i.e. Formation/Member

For each well the various show categories will be plotted, example Tor_Upper (Fig. 5.1):

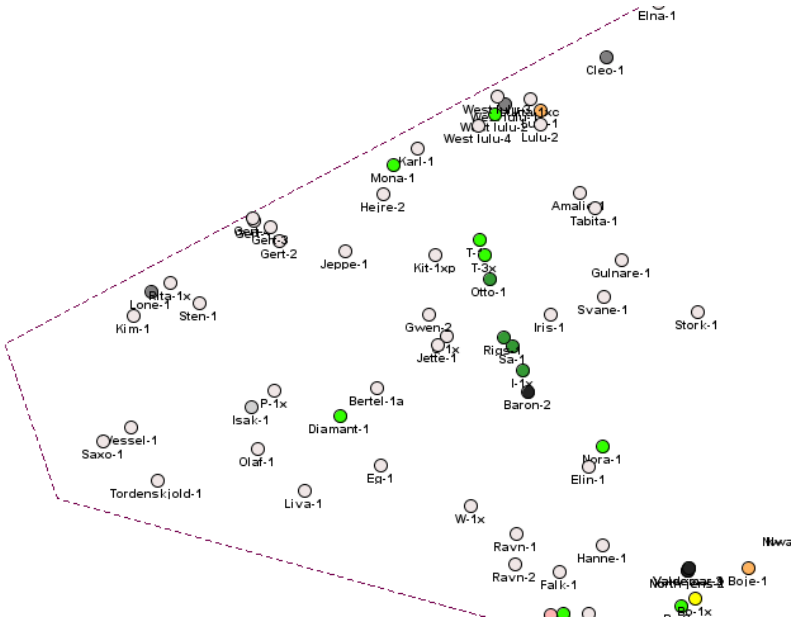

Fig. 5.1

Entry at well level using Map view. Press Wells and Well name (Fig. 5.2):

Fig. 5.2

Select well on map (Fig. 5.3):

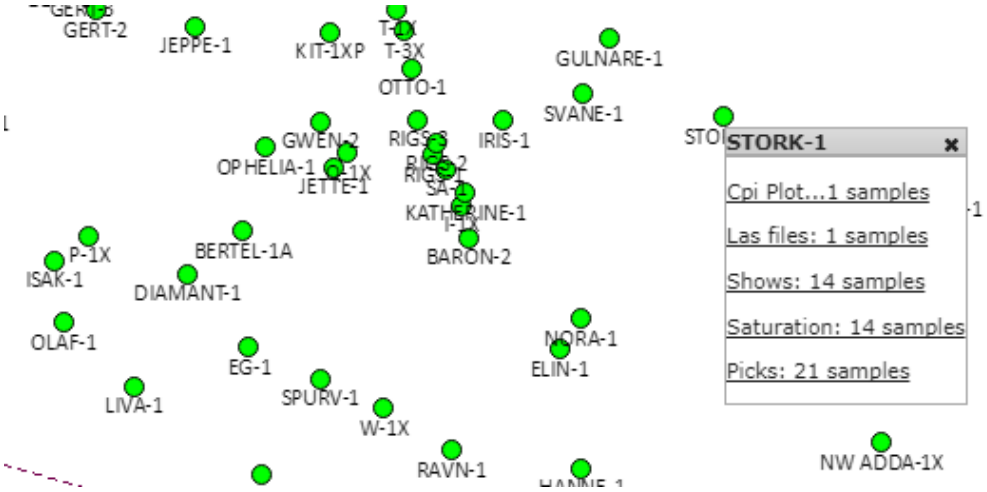

Fig. 5.3

For the Stork-1 well information on shows is given as a table with the distribution of shows/discoveries at lithostratigraphic levels. Press Shows and see table (Fig. 5.4):

STORK-1

Formation	Showtype
Ekofisk	Dry
Tor_Upper	Dry
Tor_Lower	Dry
Hod_D	Dry
Hod_C	Dry
Hod_B	Dry
Hod_A	Dry
Herring-Blodoks	Dry
Hidra	Dry
Rødby Formation	Unit not present
Sola Formation	Dry
Tuxen Formation	Dry
Valhall Formation	Oil shows
Leek/Vyl	Unit not present
Formation	**Showtype**

Fig. 5.4

5.2 Access at well level

Select wells in the main menu and press hydrocarbon shows. Information is provided at two levels: lithostratigraphic and depth.

Depending on the methods used by the various companies, information at depth level is given on the following:

Percentage staining	Type of staining	Colour of staining
Direct fluorescence distribution	Direct fluorescence intensity	Direct fluorescence colour
Visible cut	Fluorescent cut	Crush cut
Fluorescent residue	Visible residue	Odour
Gas	CPI saturation	Comments

An example of information presented under comments is from the Ekofisk Formation in the Anne-3A well:

Core #1 and 2. Locally bleeding oil and gas.
Test #3 in the interval 1903.8 – 1917.2 m produced 970 BOPD and 430 MCFPD of gas.
Tests #4 and 4A in the interval 1869.6 – 1894.3 produced 350 BOPD/205 MCFPD and 780 BOPD/460 MCFPD respectively.

6 Classification of hydrocarbon saturation (%Sh)

Based on the CPI logs, the hydrocarbon saturations have been grouped into five classes with respect to %Sh:

- Dry: no Sh
- Trace: <10%
- Low: 10 – 50%
- Moderate: 50 – 70%
- High: >70%

Examples, see Figs 6.1 to 6.3:

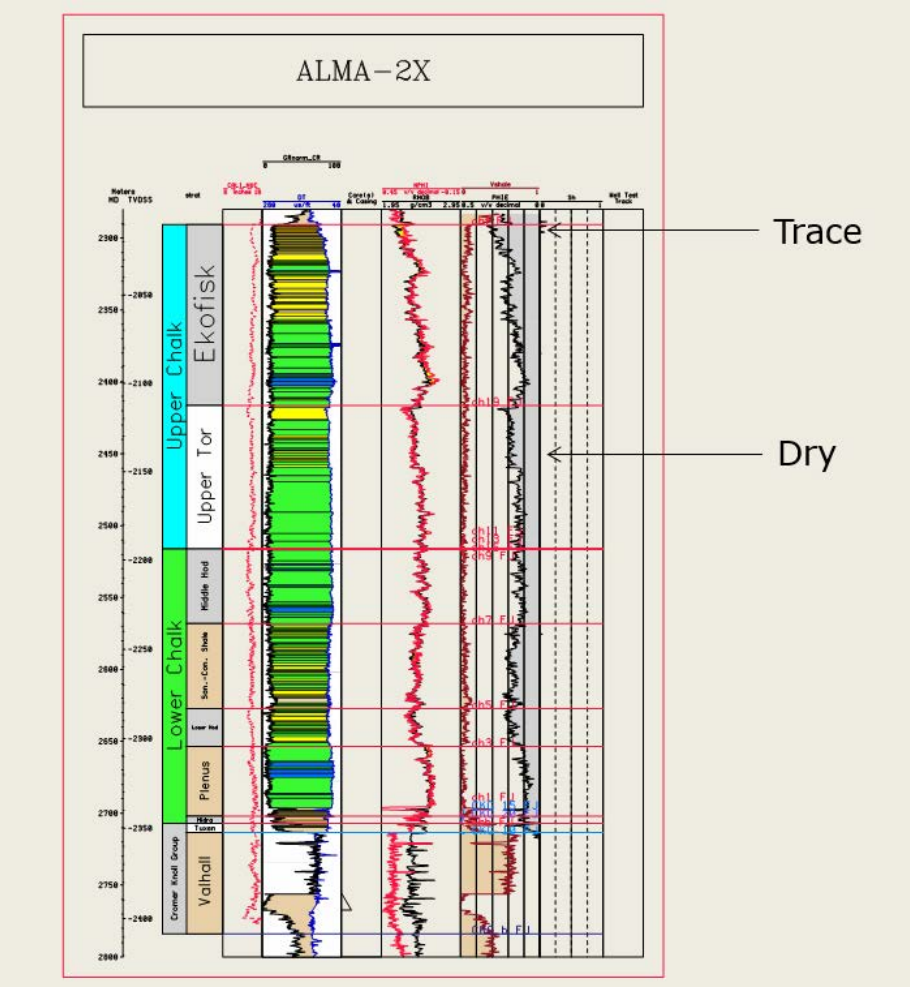

Fig. 6.1. *Example of Dry and trace saturation.*

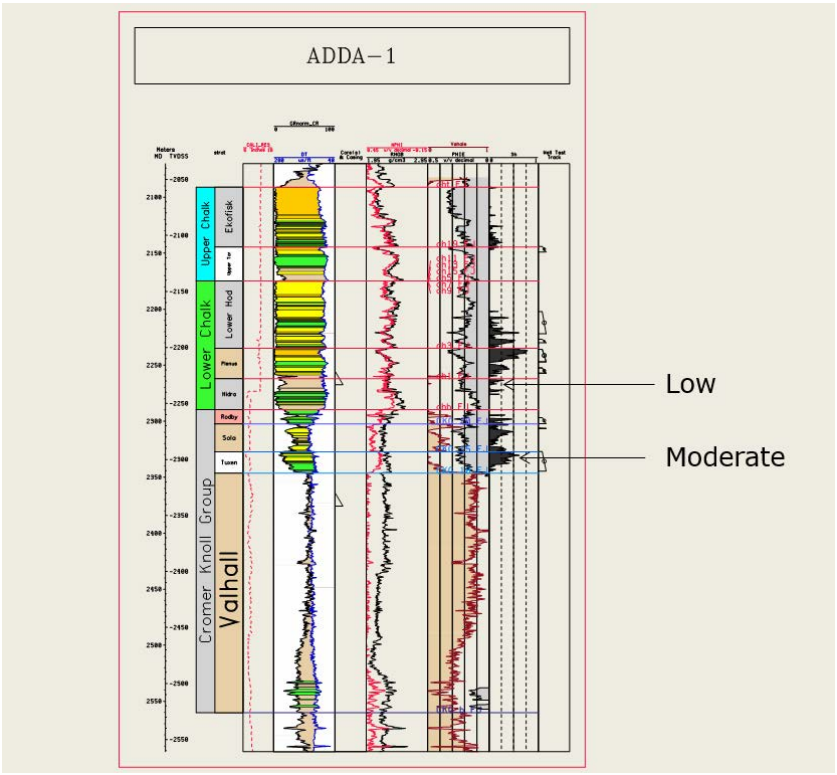

Fig. 6.2. *Example of low and moderate saturation.*

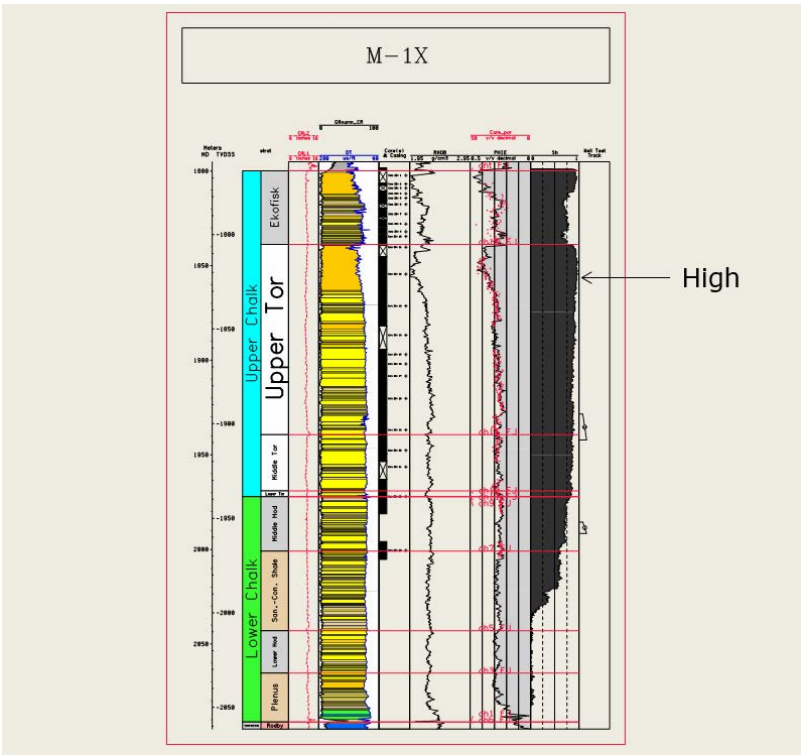

Fig. 6.3. *Example of high saturation.*

The degree of saturation can be displayed as tables and as maps.

Using “Map” and “Map data” as entry an example is presented for the Tuxen formation (Fig. 6.4):

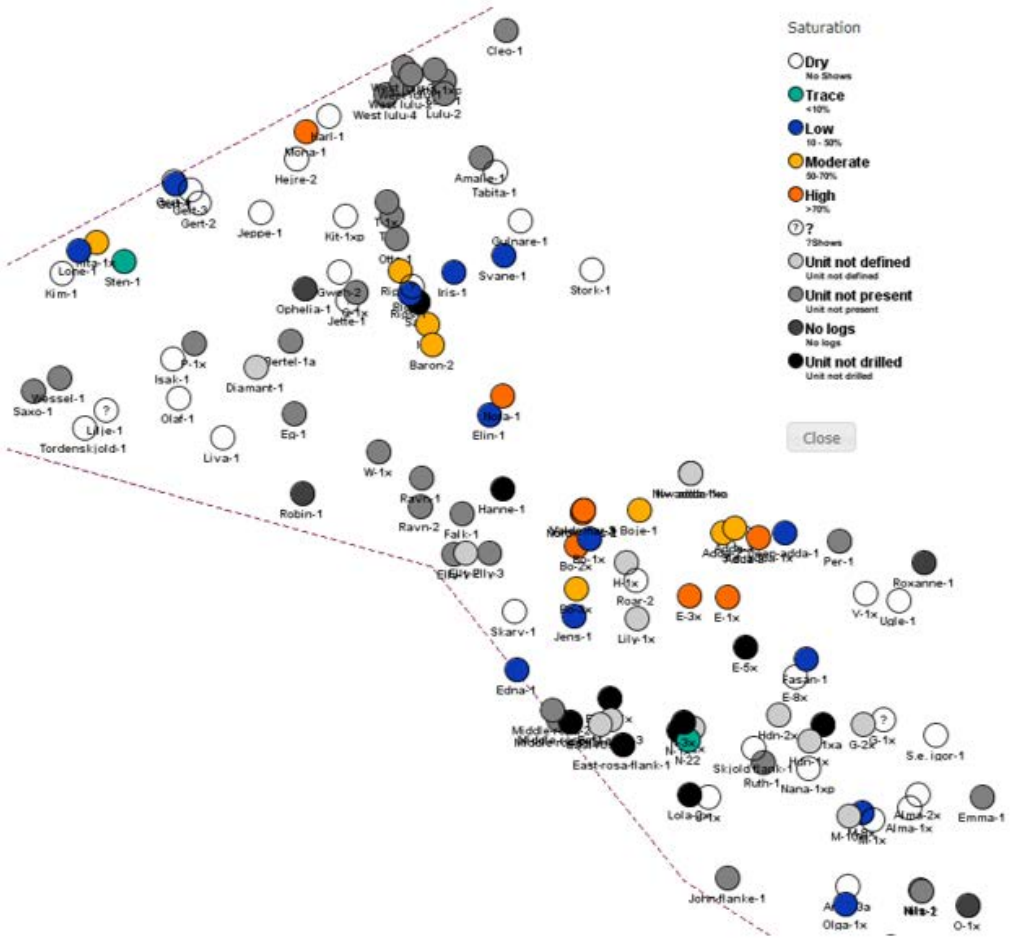

Fig. 6.4. *Classification of the hydrocarbon saturation in the Tuxen formation.*

7 Biomarker analysis and multivariate methodology applied for oil family typing in the North Sea

7.1 Introduction

This technical note on the methodology of oil family classification provides information on the biomarker analysis, data pre-treatment leading up to the data analysis and a description of the different steps in the multivariate data analysis conducted on oil, stain and sediment extracts. The biomarker database is composed of 99 analyses of oil samples extracted from the North Sea, 285 sediment extracts from cores and cuttings within the main Jurassic source rock units. The biomarkers were analysed by GC-MS-MS techniques at the Source rock Laboratory at GEUS, and constitute 43 biomarkers or ratios hereof. The subsequent data analysis resulted in the definition of four main types of oils (Oil type 1, 2, 3, 4). The main Upper Jurassic oil type (type 1) is further subdivided into four subtypes (1A, 1B, 1C, 1D). Each of the types and subtypes represent different organofacies. By reference to biomarker systematics and by comparison with sediment extract ages of the Jurassic source rock extracts, the oil types have been correlated to the sequence stratigraphical framework established for the Jurassic. The stratigraphic variation in oil types reflects the organofacies variation resulting from the tectonic evolution and flooding of the North Sea Basin. A clear geographical variation is seen in the oil types within the North Sea. Oil type 1 dominates in the southern Salt Dome Province (oil subtype 1D) and around the Tail End Graben (oil subtype 1A). Terrestrial types (oil type 2 and 3) occur more locally suggesting that several kitchen areas contributed to the accumulated oils.

A high resolution dataset consisting of 61 oil analyses from the Valdemar Field is included in the analysis. It is concluded that the oil is sourced from the main Upper Jurassic Farsund Formation source rock. The Valdemar oil represents oil subtypes 1A and 1B and reflects organofacies variation within the kitchen area(s). In addition, variation in the oil maturity in seen suggesting multiple migration episodes.

7.2 Analysis of oils and source rock extracts using GC-MS and GC-MS-MS

The experimental setup and biomarker identification is similar as for the Petsys project. Some of the main details are provided below. For detailed description see Petsys Technical Notes on biomarkers.

7.3 Experimental

Source rocks were extracted using a Soxtec System HT 2 1045 Extraction Unit using dichloromethane/methanol (93:7 vol/vol). Oils or extracts were transferred to a preweighed vial. After a couple of days, a constant weight was obtained. The residue, which consists of compounds having more than approximately 15 carbon atoms, is called the C15+ fraction. The asphaltenes were removed from the oils and extracts by precipitation in at least a 40 fold excess of *n*-pentane. The asphaltene-free oil or extract was fractionated into three fractions (saturated hydrocarbons, aromatic hydrocarbons and polar compounds or NSO) by MPLC (Radke et al., 1980).

Gas chromatography-mass spectrometry (GC-MS and GC-MS-MS) was carried out using a Hewlett-Packard 6890N gas chromatograph connected to a Waters (Micromass) Quattro Micro GC tandem quadrupole mass spectrometer (photo). The GC was fitted with an Agilent HP-5 or Phenomenex ZB-5 column (30 m x 0.25 mm i.d., film thickness 0.10 µm). The temperature program was 30°C/min from 70 to 100°C and 4°C/min from 100 to 308°C followed by 8 min at 308°C. The samples were dissolved in isooctane, and the concentration was 0.5 mg/100µl (GC-MS) or 1 mg/100µl (GC-MS-MS). Splitless injection was used.

Hopanes and steranes were quantified using GC-MS data (*m/z* 191 and 217 respectively). Only a few steranes such as the regular C_{29} steranes are separated in the *m/z* 217 mass chromatogram. In order to quantify all C_{27} – C_{30} diasteranes and steranes ((4 + 4) x 4 = 32), GC-MS-MS data must be used. Only a few sterane ratios can be measured reliably using GC-MS.

Some hopanes also coelute in the *m/z* 191 mass chromatogram. A few examples can be mentioned: 28,30-Bisnorhopane (BNH) coelutes with an unidentified C_{30} hopane and the C_{30} neohopane (C30Ts) coelutes with a norgammacerane.

7.4 Biomarker ratios

An overview of biomarkers and ratios is provided in Table 7.1. Biomarker ratios can be expressed as A/ (A+B) or A/B. It is common to use A/ (A+B) if compound A is converted to its isomer B (e.g. because of maturation). The possible range for A/ (A+B) is 0-1. In many cases, an equilibrium between A and B is reached (hopane S/(S+R) isomerization: 0.60; sterane S/(S+R) isomerization: 0.55). A/B is normally used for compounds A and B that are not isomers or when two isomers A and B have a different origin. The range for A/B is 0-∞.

Hopane ratios are self-explanatory with a single exception:

HHI = C_{35} Homohopane Index: (H35αβS + H35αβR) / (H31αβS + H31αβR + H32αβS + H32αβR + H33αβS + H33αβR + H34αβS + H34αβR + H35αβS + H35αβR).

Table 7.1. *Acronyms (Parameter) for the biomarkers (Compounds). GC-FID was used for n-alkanes and isoprenoids and GC-MS in SIM-mode for tricyclic terpanes.*

Table 1			
Index	**Parameter**	**Quantification**	**Compounds**
1	Pr/Ph	GC-FID	pristane/phytane
2	Pr/*n* C17	GC-FID	pristane/*n* -C17
3	Ph/*n* C18	GC-FID	phytane/*n* -C18
4	Ts/(Ts + Tm)	370 → 191	18α-22,29,30-trisnorneohopane/(18α-22,29,30-trisnorneohopane + 17α-22,29,30-trisnorhopane)
5	29Ts/(29Ts + H29)	398 → 191	18α-30-norneohopane/(18α-30-norneohopane + 17α,21β-30-norhopane)
6	30Ts/H30ab	412 → 191	18α-neohopane/(18α-neohopane + 17α,21β-hopane)
7	30E/H30ab	412 → 191	"early eluting C_{30} hopane"/17α,21β-hopane
8	30D/H30ab	412 → 191	C_{30} 17α-diahopane/17α,21β-hopane
9	31D-S/H30ab	412, 426 → 191	C_{31}-S 17α-diahopane/17α,21β-hopane
10	31D-R/H30ab	412, 426 → 191	C_{31}-R 17α-diahopane/17α,21β-hopane
11	30ba/H30ab	412 → 191	17β,21α-hopane/17α,21β-hopane
12	BNH/ H30ab	384, 412 → 191	28,30-bisnorhopane/17α,21β-hopane
13	H29ab/H30ab	398, 412 → 191	17α,21β-30-norhopane/17α,21β-hopane
14	31abS	412, 426 → 191	C_{31}-22S hopane /17α,21β-hopane
15	31abR	412, 426 → 191	C_{31}-22R hopane /17α,21β-hopane
16	32abS	412, 440 → 191	C_{32}-22S hopane /17α,21β-hopane
17	32abR	412, 440 → 191	C_{32}-22R hopane /17α,21β-hopane
18	33abS	412, 454 → 191	C_{33}-22S hopane /17α,21β-hopane
19	33abR	412, 454 → 191	C_{33}-22R hopane /17α,21β-hopane
20	34abS	412, 468 → 191	C_{34}-22S hopane /17α,21β-hopane
21	34abR	412, 468 → 191	C_{34}-22R hopane /17α,21β-hopane
22	35abS	412, 482 → 191	C_{35}-22S hopane /17α,21β-hopane
23	35abR	412, 482 → 191	C_{35}-22R hopane /17α,21β-hopane
24	H31S/(S+R)	426 → 191	C_{31}-22S hopane /(C_{31}-22S hopane + C_{31}-22R hopane)
25	H32S/(S+R)	440 → 191	C_{32}-22S hopane /(C_{32}-22S hopane + C_{32}-22R hopane)
26	H35/H34	468, 482 → 191	C_{34}-22S+22R hopane/ C_{35}-22S+22R hopane
27	HHI	426 – 482 → 191	C_{35} 22S+22R hopane/∑C_{31}- C_{35} 22S+22R hopanes
28	C27stD/R+D)	372 → 217	C_{27} diasteranes/(reg. steranes + diasteranes)
29	C28stD/R+D)	386 → 217	C_{28} diasteranes/(reg. steranes + diasteranes)
30	C29stD/R+D)	400 → 217	C_{29} diasteranes/(reg. steranes + diasteranes)
31	C27stS/S+R)	372 → 217	C_{27} steranes 20S/(20S + 20R)
32	C28stS/S+R)	386 → 217	C_{28} steranes 20S/(20S + 20R)
33	C29stS/S+S)	400 → 217	C_{29} steranes 20S/(20S + 20R)
34	C27stbb/bb+aa)	372 → 217	C_{27} steranes ββ/(ββ + αα)
35	C28stbb/bb+aa)	386 → 217	C_{28} steranes ββ/(ββ + αα)
36	C29stbb/bb+aa)	400 → 217	C_{29} steranes ββ/(ββ + αα)
37	%C27	372 - 400 → 217	% C_{27} diasteranes + reg. steranes (C_{27} - $_{29}$ = 100)
38	%C28	372 - 400 → 217	% C_{28} diasteranes + reg. steranes (C_{27} - $_{29}$ = 100)
39	%C29	372 - 400 → 217	% C_{29} diasteranes + reg. steranes (C_{27} - $_{29}$ = 100)
40	%C30	372 - 414 → 217	% C_{30} diasteranes + reg. steranes (C_{27} - $_{30}$ = 100)
41	T22/T21	*m/z* 191	C_{22}/C_{21} tricyclic terpanes
42	T24/T23	*m/z* 191	C_{24}/C_{23} tricyclic terpanes
43	T26/T25	*m/z* 191	C_{26}/C_{25} tricyclic terpanes

Table 7.2. *Main controls (environmental, maturity, biodegradation index etc.) of biomarkers. Legend: x: Important. (x): Some importance. (x): Only in case of severe biodegradation, this is not relevant here.*

Ratio	Biological origin	Environment	low	high	Thermal maturity	low	high	Biodegradation (ratio increases)
Pr/Ph	(x)	x	anoxic	oxic	(x)			
Pr/*n*C17								x
Ph/*n*C18								x
Ts/(Ts + Tm)		x	1) anoxic 2) carbonate	1) oxic 2) shale	x	immature	mature	(x)
29Ts/(29Ts + H29)		x	1) anoxic 2) carbonate	1) oxic 2) shale	x	immature	mature	(x)
30Ts/H30ab		x	1) anoxic 2) carbonate	1) oxic 2) shale	x	immature	mature	(x)
30E/H30ab		x	1) anoxic 2) carbonate	1) oxic 2) shale	x	immature	mature	(x)
30D/H30ab		x	1) anoxic 2) carbonate	1) oxic 2) shale	x	immature	mature	(x)
31D-S/H30ab		x	1) anoxic 2) carbonate	1) oxic 2) shale	x	immature	mature	(x)
31D-R/H30ab		x	1) anoxic 2) carbonate	1) oxic 2) shale	x	immature	mature	(x)
30ba/H30ab		x	anoxic	oxic	x	mature	immature	
BNH/ H30ab		x	oxic	anoxic	(x)	immature	mature	
H29ab/H30ab		x	shale	carbonate				
31abS		x	oxic	anoxic				
31abR		x	oxic	anoxic				
32abS		x	oxic	anoxic				
32abR		x	oxic	anoxic				
33abR		x	oxic	anoxic				
33abR		x	oxic	anoxic				
34abS		x	oxic	anoxic				
34abR		x	oxic	anoxic				
35abS		x	oxic	anoxic				
35abR		x	oxic	anoxic				
H31S/(S+R)					x	immature	mature	
H32S/(S+R)					x	immature	mature	
H35/H34		x	oxic	anoxic				
HHI		x	oxic	anoxic				
C27stD/R+D)			carbonate	shale	(x)	immature	mature	(x)
C28stD/R+D)			carbonate	shale	(x)	immature	mature	(x)
C29stD/R+D)			carbonate	shale	(x)	immature	mature	(x)
C27stS/S+R)					x	immature	mature	
C28stS/S+R)					x	immature	mature	
C29stS/S+S)					x	immature	mature	
C27stbb/bb+aa)					x	immature	mature	
C28stbb/bb+aa)					x	immature	mature	
C29stbb/bb+aa)					x	immature	mature	
%C27	x							
%C28	x							
%C29	x							
%C30	x							
T22/T21		x		carbonate				(x)
T24/T23		x	carbonate					(x)
T26/T25		x		lacustrine				(x)

7.5 Methodology of oil typing based on multivariate data analysis

Step 1: Data pre-treatment and outlier analysis of a representative oil database consisting of 99 and 285 sediment extract samples and 61 samples from the Valdemar Field measured for 43 biomarkers. The data are termed matrix A ([A]) matrix B ([B]) and matrix C ([C]) respectively. The biomarker input parameters are reduced to 37 as part of the initial analysis.

Step 2: Principal component analysis (PCA) of [A]. Identification of geological controls (i.e. maturity, organofacies, biodegradation etc.) on biomarker data. Locate clustering of data. For the classification purpose followed here, the PCA axis dependant on organofacies is used for identification of the four main oil families (oil type 1 to 4).

Step 3: Perform a new PCA of [A] + [B] + [C]. Identify outliers and identify zone of interest within the [A] + [B] sample space for the subsequent data analysis, i.e. where Jurassic oil families (oil type 1, 2, and 3 i.e. excluding oil type 4) and sediment [B] overlaps. The reduced [A] and [B] are termed [A*] and [B*].

Step 4: Perform PCA analysis of [A*] + [B*] + [C]. Identify the main controlling factors on the PC axis. For the classification purpose followed here, the PCA axis dependant on organofacies is used. A detailing of the oil family 1 into subtype (subtype A to D) is made for [A*] + [B*] + [C].

Oil typing and determination of oil families are described in more details in Chapter 8F.

Chapter 8

Selected topics

Sub-chapters:

8A	Structural setting
8B	Cretaceous basin development
8C	Base Cretaceous Unconformity (BCU)
8D	Mandal Formation
8E	Overpressure distribution and porosity-depth trends in the Chalk Group
8F	Oil family classification and source rock typing
8G	Hydrocarbon aspects

8A Structural setting

The base of the Cretaceous succession, the *BCU*, is a North Sea Basin-wide seismic marker that represents a hiatus and/or a facies change, which in basin centres separates the anoxic sedimentation of the upper Farsund/Mandal Formation from oxic depositional conditions above the surface. A detailed description of *BCU* is given in a separate chapter (8C). A 3D presentation the *BCU* seen from the North-west is given in Fig. 8A.1 but for further details the reader is referred to the time-structure map found on the website. The depth to the surface in the Danish Central Graben increases from south towards north, from about 2.0 sec. (equivalent to about 2340 m) to more than 3.8 sec. (equivalent to about 4800 m). The southern area is dominated by Zechstein salt piercement structures and pillows giving rise to the rather dramatic relief.

It is noteworthy that the *BCU* is shallower in the graben area along the south-eastern segments of the Coffee Soil Fault Zone than on the adjoining part of the stable Ringkøbing-Fyn High. This is the result of intra-Cretaceous compressional tectonism with minor thrust faults that propagate from the tips of former extensional basement attached faults in the substrate. The major faults (both normal and reverse) affecting the *BCU* are highlighted in Fig. 8A.2. In order to give an impression of small-scale discontinuities and the general structural grain at the *BCU,* a merged edge detection attribute map is shown in Fig. 8A.3. Apart from artifacts at survey boundaries it illustrates a generally smooth surface over rather large areas (e g. over the Heno Plateau and further to the North-west) with few fault cuts. Strong colors in the Salt Dome Province indicate structural dips associated with rim-synclines.

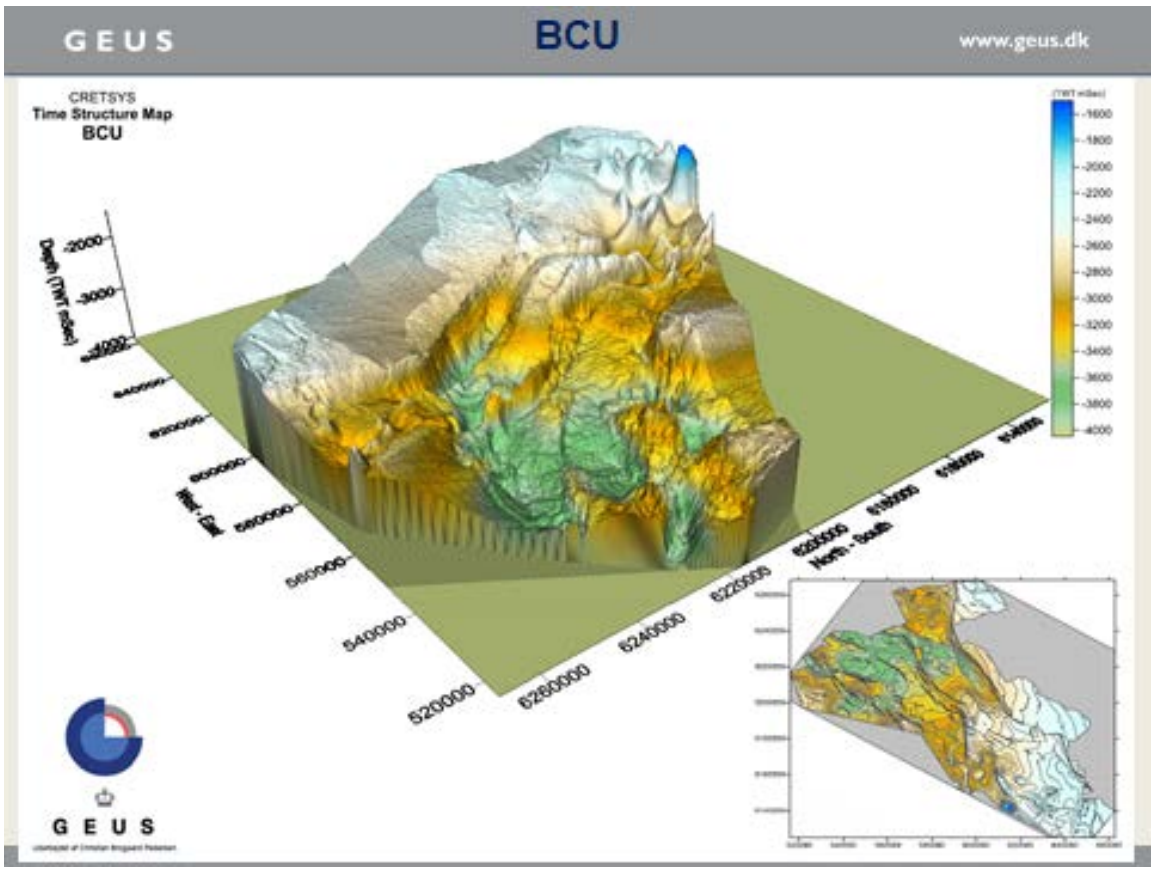

Fig. 8A.1. *3D presentation of the time-structure map of the BCU as viewed from the NW towards the SE.*

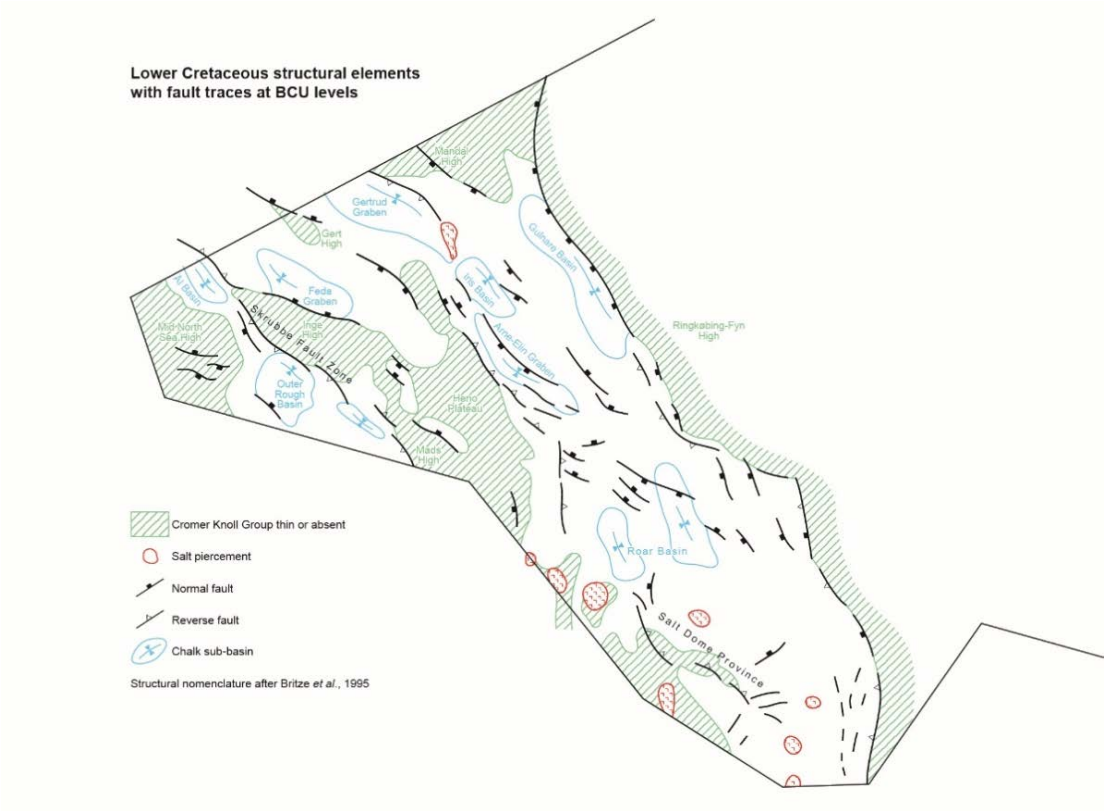

Fig. 8A.2. *Lower Cretaceous structural elements with fault traces at the BCU level.*

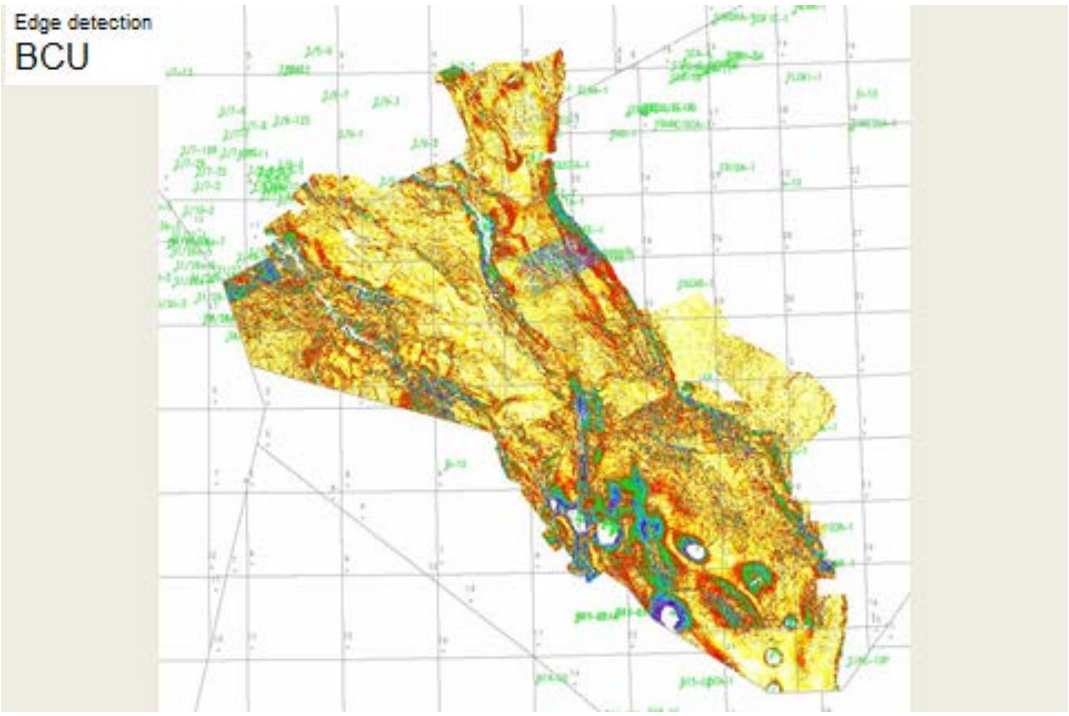

Fig. 8A.3. *Edge detection attribute of BCU surface*

8A.1 Lower Cretaceous

The post-rift Lower Cretaceous (the Cromer Knoll Group) accumulated under early thermal subsidence infilling the inherited basin-floor topography following the late Jurassic rifting stages in the DCG. The Cromer Knoll Group has a more restricted occurrence than the underlying late Jurassic deposits being absent on the Mid North Sea High, Heno Plateau, Søgne Basin and the south-western part of the Salt Dome Province (Fig. 8A.2). However, a number of distinct Lower Cretaceous depocentres are mapped overlying the major depocentres of the Middle Volgian – Early Ryazanian part of the Farsund Formation (interval PSS31 – BCU of the PETSYS project), e.g. the Feda Graben, Gertrud Graben, Arne-Elin Graben and major parts of the former Tail End Graben (Figs. 8A.2 & 8A.4). Here the total thickness of the Cromer Knoll Group may locally exceed 800 m (Britze et al. 1995). New structural elements were the development of the Outer Rough Basin and Ål Basin with thick Lower Cretaceous both located south-west of the complex Skrubbe Fault Zone extending from Norwegian water south-eastwards into German waters.

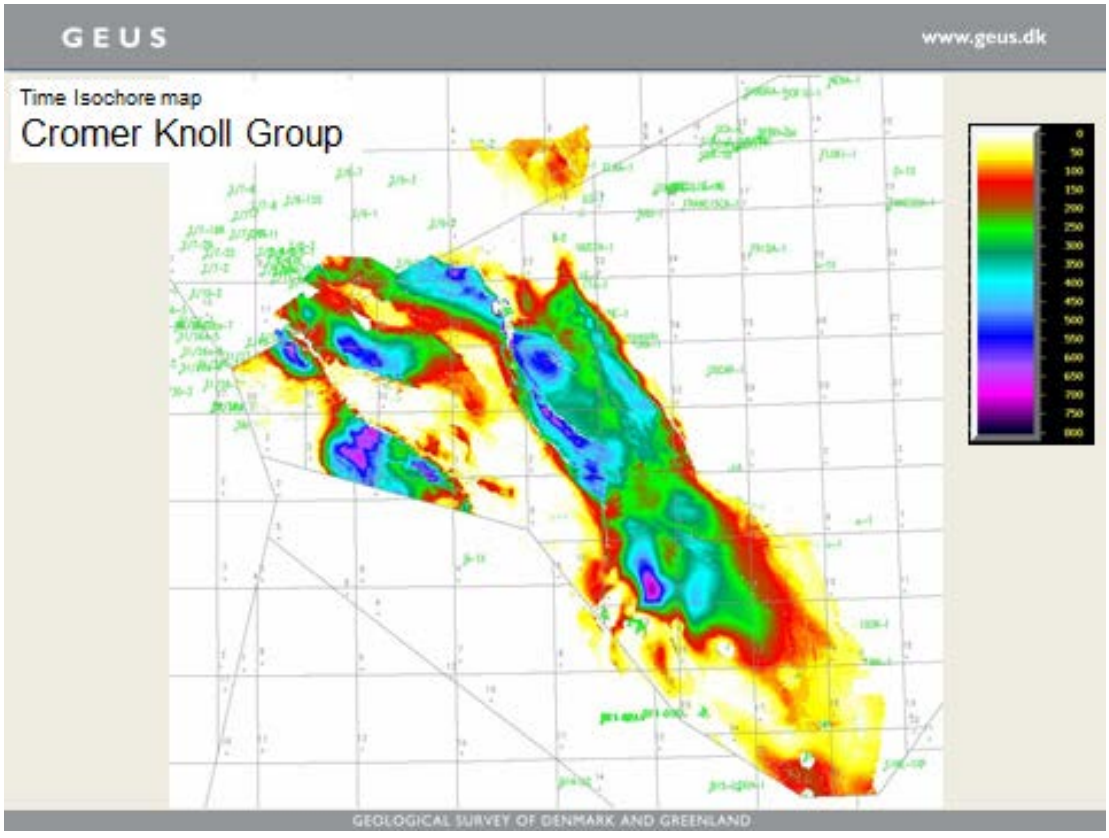

Fig. 8A.4. *Time isochore map of the Cromer Knoll Group (screen dump from Seisworks)*

8A.2 Upper Cretaceous

From the Cenomanian to the Danian, representing a time interval of about 40 myr, deposition of the Chalk Group took place over large parts of NW Europe. This period was characterized by high sea levels and a peak in carbonate production. Late Cretaceous regional subsidence in the study area was modified by halokinesis of the Zechstein salt and was punctuated by widespread structural inversion in the form of compression along old extensional fault trends, flexuring and asymmetric folding of basin infill (e.g. Vejbæk & Andersen 2002; van Buchem et al. 2017). This resulted in the development of areas with bathymetric elevations and the formation of local depocentres in the intervening lows. The structural movements gave rise to unconformities that are recognized as truncations and onlap surfaces on the seismic profiles and to stratigraphic hiatuses. Van Buchem et al. (2017) proposed that the inversion climax was one major event during Campanian times. As a result of changes in sea-floor topography, the pelagic chalk deposits were subjected to redistribution by various processes. These include down-slope mass flow movements caused by slope instability as well as along-slope currents that caused seafloor geometry modifications in the form of incised valleys, channels, drifts, ridges and mounds described by several authors (e.g. Lykke-Andersen & Surlyk 2004, Esmerode et al. 2008, Back et al. 2011, and van Buchem et al. 2017).

The general impact of inversion may be illustrated with the Chalk Group time-isochore map (Fig. 8A.5) and the structural element map (Fig. 8A.6). The main inversion zones from the Igor-Emma Ridge, the Arne Ridge, the Bo-Jens Ridge, the Mona Ridge, and the Lindesnes ridge clearly stand out as inversion ridges with thinly developed Chalk Group coinciding with Early Cretaceous depocentres . Another important observation is that the Chalk Group depocentres on the southern part of the RFH, and the Jeppe, Eg and Karl Basins coincide with areas of thinly developed or absent Lower Cretaceous. The inversion thus not only changed areas of subsidence and deposition into areas of uplift and erosion, but also previously uplifted areas into areas of subsidence and deposition. The inverted zones are expressed as generally asymmetric anticlines with predominantly NW-SE and N-S tending axes reflecting the pre-Cretaceous structural grain, often arranged in en-echelon patterns. Vejbæk & Andersen (2002) argued that apart from obvious shortening perpendicular to the graben axis; i.e. suggesting NE-SW compression, the often left-stepping of faults associated with the ridges is consistent with a dextral component.

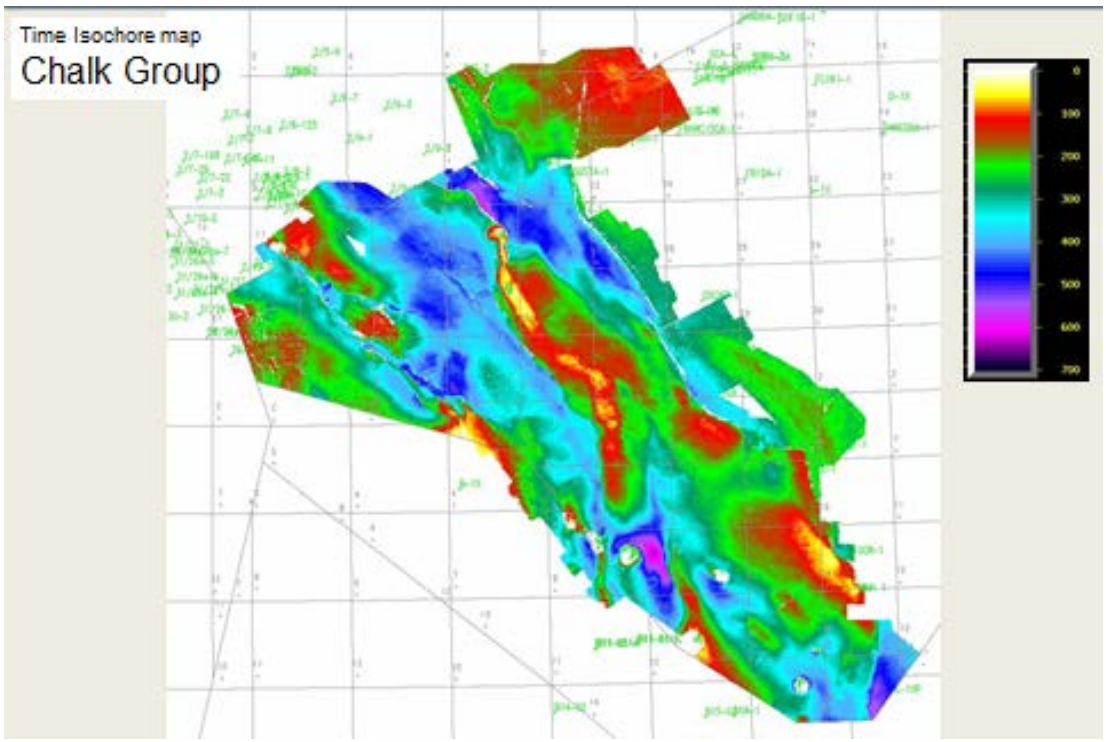

Fig. 8A.5. *Time-isochore map of the Chalk Group (screen-dump from Seisworks)*

The upper boundary of the Chalk Group at the Danian-Selandian boundary is an easily recognized reflector marking the change from carbonate deposition to post-Danian siliciclastic deposition. However, phase reversals occur on top of gas accumulations. Time- and depth structure maps to the Top Chalk Group are found on the map menu on the website. Apart from salt-piercement structures caused by continued halokinetic movements during post-Danian times, the relief of the surface is gentle compared for example to the *BCU* with depth in the south of about 2.0 sec. increasing to a maximum of 3.2 sec. in a rim-syncline east of the Svend Field in the north. Outside halokinetic structures the surface is almost devoid of faults; only in the North-east can minor normal faults be mapped along the Coffee Soil Fault Zone.

The structure maps display the effects of continued post-Danian inversion movements with the development of a broad, low relief NW-SE trending anticline *(Tyra-Igor Ridge)* displaced westwards relative to the intra-Cretaceous inversion ridges (Fig. Ss.6). The top Chalk reflector represents the top of the Ekofisk Formation when present. On the crestal parts of the Tyra-Igor Ridge in the Valdemar area and further north where also the Tor Formation is thin to absent, the marker may locally represent the top of the Hod Formation. The reflector represents an even deeper cut into the Hod Formation on the crest of the post-Chalk Robin Inversion Ridge (part of the Skrubbe Fault Zone trend).

Fig. 8A.6. *Upper Cretaceous structural element with fault traces at Base Chalk level.*

References

Back, S., van Gent, H., Reuning, L., Grøtsch, J. Niederau; J & Kukla, P. 2011. 3D seismic geomorphology and sedimentology of the Chalk Group, southern Danish North Sea. *Journal of the Geological Society, London, Vol. 168, pp.393-405*

Britze, P., Japsen, P. & Andersen, C. 1995c: Geological map of Denmark. 1: 200,000: The Danish Central Graben. 'Base Cretaceous' and the Cromer Knoll Group (two-way-traveltime and depth, thickness and interval velocity). Danm. Geol. Unders., Map Series 49, 7 pp and 4 maps.

Lykke-Andersen, H. & Surlyk, F. 2004. The Cretaceous-Palaeogene boundary at Stevns Klint, Denmark: inversion tectonics or sea-floor topography? *Journal of the Geological Society, London, Vol. 161, pp 343-352.*

Esmerode, E.V., Lykke-Andersen, H. & Surlyk, F. 2008. Interaction between bottom currents and slope failure in the Late Cretaceous of the southern Danish Central Graben, North Sea. *Journal of the Geological Society, London, Vol.165, pp. 55-72.*

Van Buchem, F.S.P., Smit, F.W.H, Buijs, G.J.A., Trudgill, B. & Larsen, P.-H. 2017: Tectonostratigraphic framework and depositional history of the Cretaceous – Danian succession of the Danish Central Graben (North Sea) – new light on a mature area. In: Bowman, M. & Levell, B. (eds) *Petroleum Geology of NW Europe: 50 Years of Learning – Proceedings of the 8th Petroleum Geology Conference.*

Vejbæk, O.V. & Andersen, C. 2003: Post Mid-Cretaceous Inversion Tectonics in the Danish Central Graben – regionally synchronous tectonic events. *Bulletin of the Geological Society of Denmark*. Vol. 49, pp 129-144

8B Cretaceous basin development

A more detailed description of the Cretaceous basin development based on the seismic data and maps is given in the following chapter. It will primarily make use of the seismic structural profiles shown on the website and the 11 up-loaded time-isochore maps, the latter also shown as small scale pdf-maps at the end of the chapter as Appendix 8B. In addition, a number of 'seismic feature maps' of the upper five mapped chalk intervals highlight various features of geo-morphologic significance.

8B.1 Lower Cretaceous

The lower mapped interval *BCU – CKG10* comprises the claystone-dominated Valhall Formation of Valanginian to Hauterivian age. There are considerable drilled thickness variations across the DCG from absent on the Mid North Sea High, Inge High, Søgne Basin and Heno Plateau to more than 600 m in the Sten-1 well located in the Feda Graben. The main depocentres are mapped as elongate troughs or sub-basins parallel to the basin axis and as well as the Feda Graben include the Gertrud Graben, Arne-Elin Graben, Iris Basin, Gulnare Basin along the Coffee Soil Fault Zone and the Roar Basin to the south. The latter is separated by a NE-SW trending threshold (Pollerne Ridge of Vejbæk 1986) from the northern sub-basins. However, the location of the post-rift Vallhal Formation depocentres is to a large extent coincident with the depocentres of the late-rift phase parts of the upper Farsund/Mandal Formation.

The basin fill geometry in the northern sub-basins is illustrated in Figs 8B.1 & 8B.2 (seismic structural profile 5 & 11) located in the Feda Graben and Arne-Elin Graben, Gulnare Basin, respectively. Here, the rather seismically transparent *BCU – CKG10* interval shows basal onlap onto the *BCU* along basin margins.

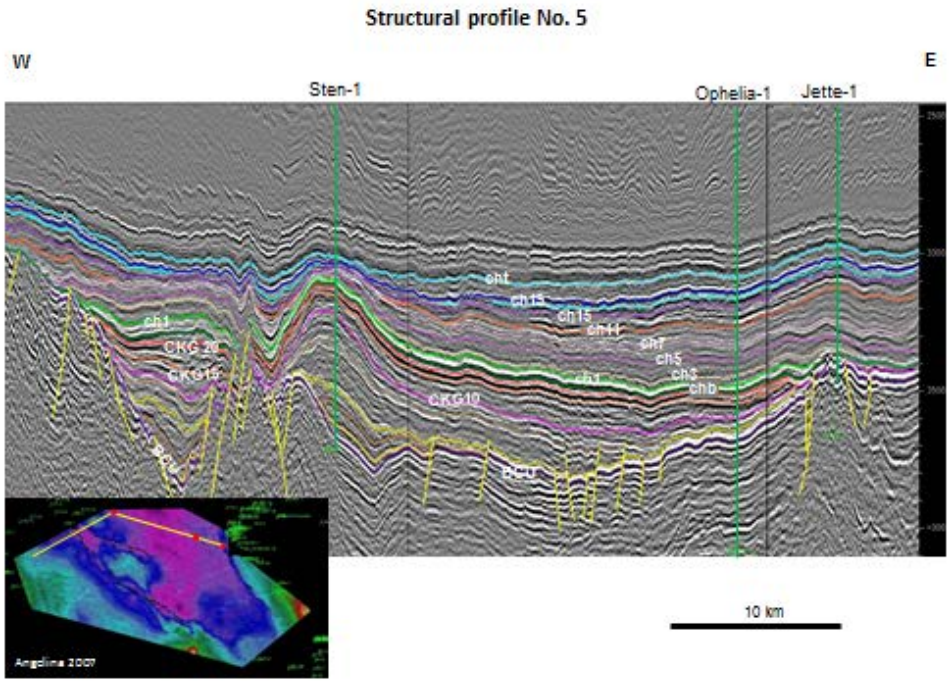

Fig. 8B.1. *Structural profile 5 across the Lindesnes Ridge and the Feda Graben. Note the basal onlaps of the BCU – CKG10 interval to the east.*

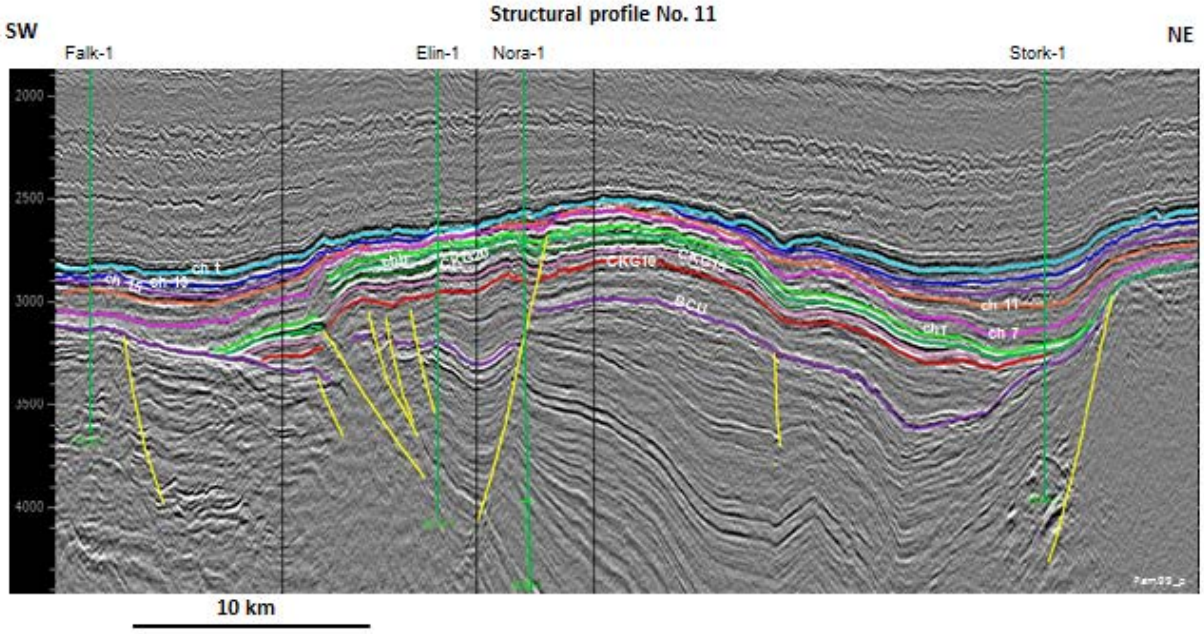

Fig. 8B.2. *Structural profile 11 across the Arne-Elin Graben and the Gulnare Basin to the east showing basal onlap onto the BCU.*

The basin fill geometry is different in the southern part of the Roar Basin with the presence of basinward dipping reflections resempling clinoforms that prograde towards the basin centre from east to west (Fig. 8B.3). The maximum topographical relief on these clinoforms has been estimated to be in the order of 400 m (Vidalie et al. 2014). Based on flattening at the Base Chalk Group Vidalie et al. (2014) have mapped a pattern of laterally continuous sequences over a distance of more than 20 km representing south-westward migration of a shelf, and taken as an indication of the underfilled nature of the Early Cretaceous basin. An alternative interpretation of the apparent clinoforms in this area is that the dipping surfaces represent gently tilted strata due to a progressive westward shift in the depocentre accompanying incipicent inversion in the Adda-Tyra area.

Synsedimentary tectonic control during deposition of the interval is demonstrated in the Tyra-Adda area where a system of WNW-ESE oriented normal faults with a vertical displacement of about 100 m at BCU level occurs (Fig. 8B. 4). The fault activity gradually waned during deposition of the Valhall Formation with hardly any displacement seen at *CKG10* level.

The basin development changed during deposition of the overlying chalks and marly chalks of the Hauterivian - Barremian Tuxen Formation, as testfied by the time-isochore of the *CKG10 – CKG15* interval. This interval has a slightly more restricted extension compared to the underlying *BCU – CKG10* seismic unit caused by truncation by the Base Chalk Group (*chb*) reflection both in the Søgne Basin and in the south. Depocentres with time-thicknesses above 100 mSec. are mapped in the Feda Graben area and in the southern part of the Arne-Elin Graben. A new structural element was introduced with the development of the Outer Rough Basin located SW of the Skrubbe Fault Zone. Furthermore, a thick development of the unit is mapped in the south-western part of the Roar Basin. This depocentre is believed to be the result of salt withdrawal.

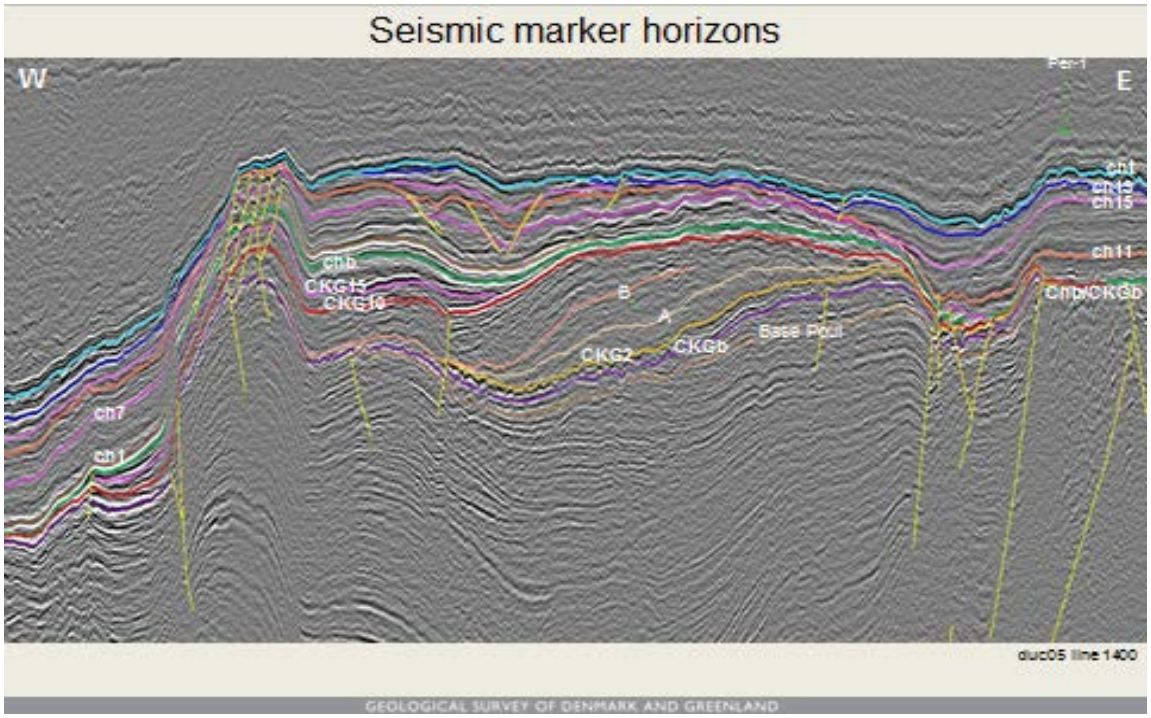

Fig. 8B.3. *Westward dipping clinoforms in the Valhall Formation (BCU – CKG10 interval). Note the westward shift of the depocentre of the CKG10 – chb interval in the southern Roar Basin. (seismic line DUC05 1400).*

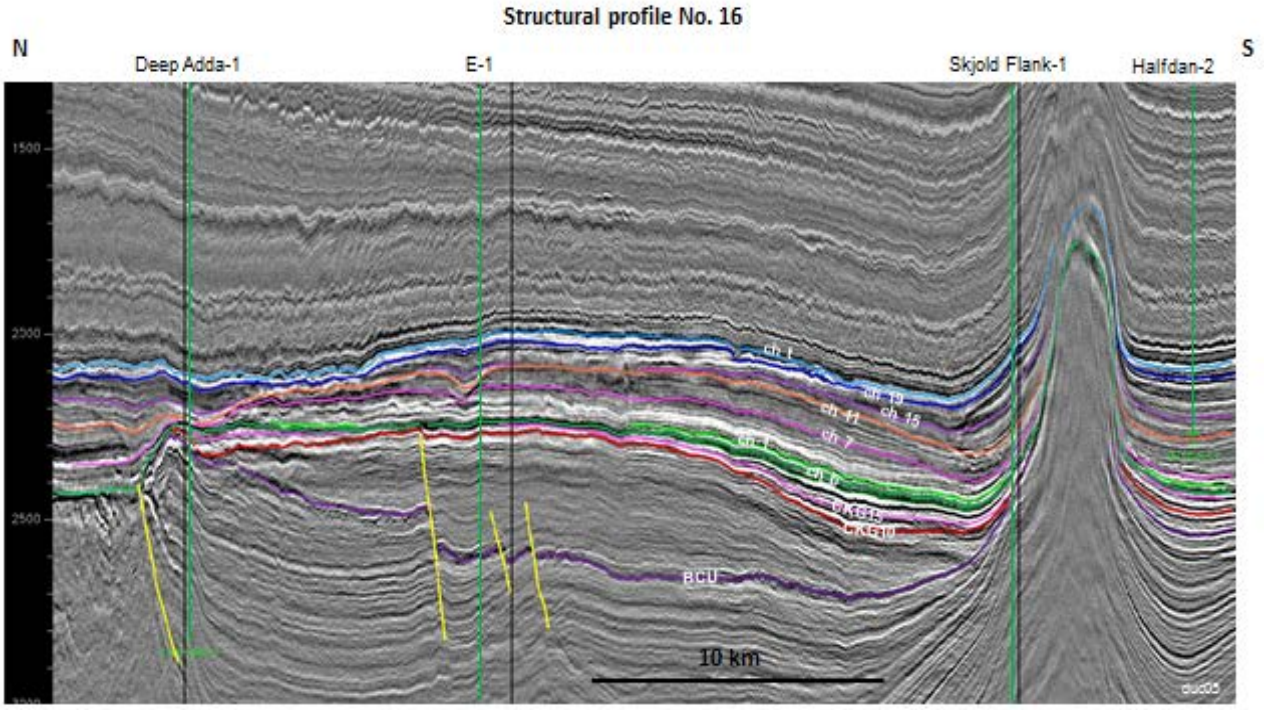

Fig. 8B.4. *Structural profile 11 showing faults active during the deposition of the Valhall Formation.*

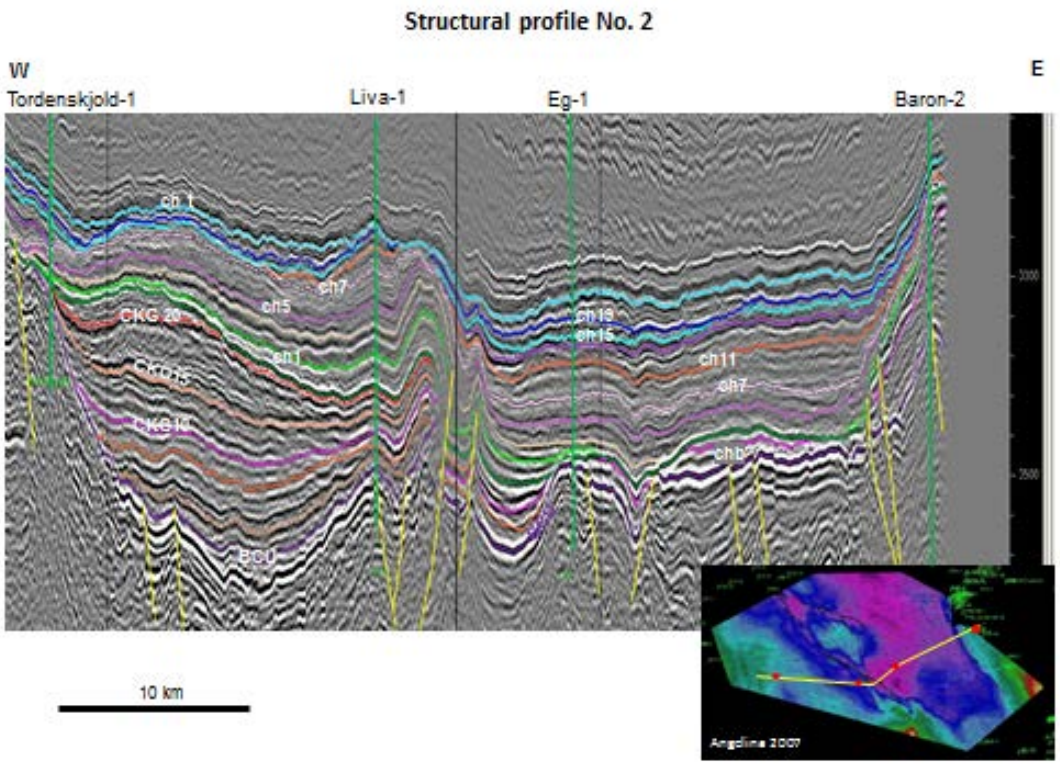

Fig. 8B.5. *Structural profile 2 crossing the Outer Rough Basin and the Skrubbe Fault Zone*

The base of the *CKG15 – CKG20* interval is everywhere picked in a seismic trough marking the contact of the chalk and marly chalk of the Tuxen Formation below and the marls and claystones of the Sola Formation of Late Barremian –Early Albian age above. The upper boundary of the interval is over most of the area picked in a peak marking the transition from the claystones of the upper part of the Sola Formation, the Fanø Member as defined by van Buchem et al (2017), to the marls of the overlying Albian marls of the Rødby Formation (*CKG20 – chb* interval).

Compared to the *CKG10 – CKG15,* interval the *CKG15 – CKG20* interval exhibits a slightly reduced lateral extent in the southern and southeastern part of the DCG due to truncation by the Base Chalk reflector; otherwise, the time-isochore map shows similarities with the same location of depocentres, e.g. the Arne-Elin Graben and southeastern Roar Basin (Figs 8D.2 & 8D.5). The central part of the Outer Rough Basin stands out with a maximum thickness of more than 150 mSec.

The *CKG20 – chb* interval comprising the Rødby Formation is thinly developed over most of the study area where there is poor separation between the CKG20 and the distinct Base Chalk seismic marker. However, the Outer Rough Basin is also anomalous at this stratigraphic level showing extraordinary thicknesses. It is stressed that the central part of this basin is without well control. The only seismic tie is provided by the Lilje-1 well, located at the western basin margin.

As mentioned above the Lower Cretaceous succession is truncated by the Base Chalk in the southern part of the Søgne Basin. This is illustrated in Fig. 8B.6 (structural profile 8), clearly showing the truncation features affecting the entire succession. This indicates that this area experienced uplift prior to deposition of the Chalk Group.

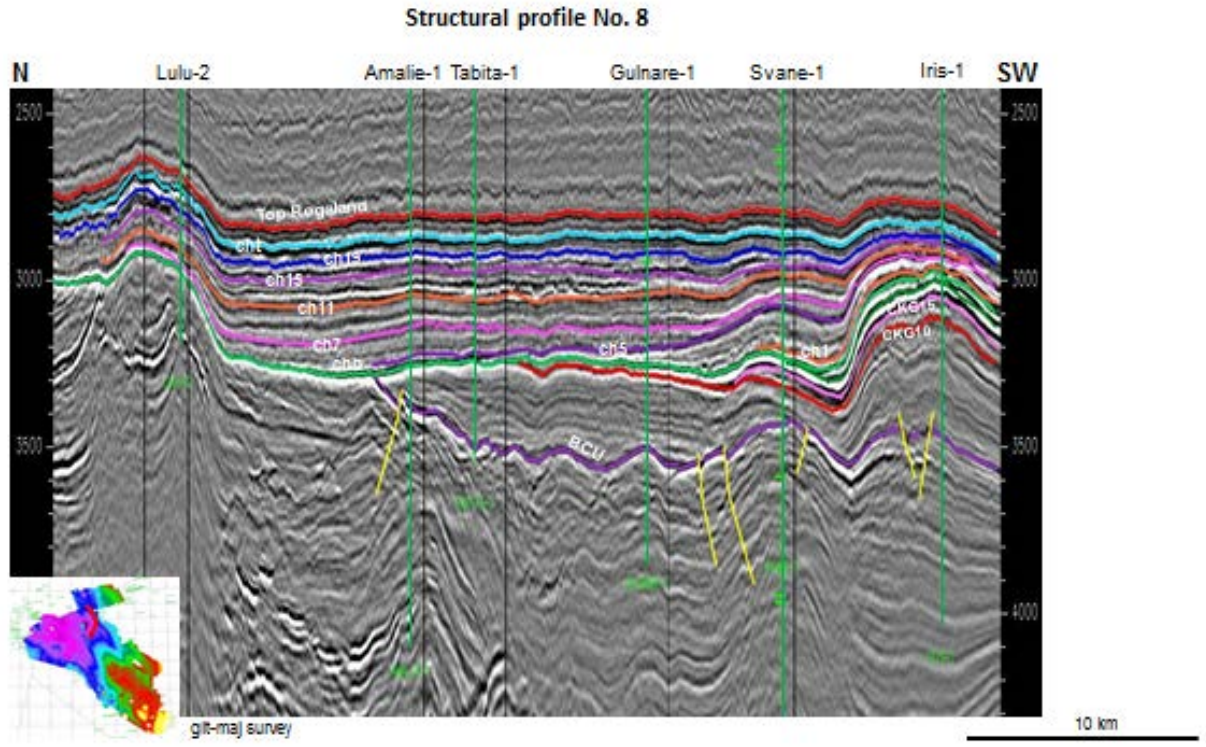

Fig. 8B.6. *Truncation of the Lower Cretaceous succession by the Base Chalk reflection in the southern Søgne Basin area.*

8B.2 Upper Cretaceous

The chalk depositional system in the DCG was established during the Cenomanian with deposition of the Hidra Formation, corresponding to seismic unit *chb – ch1*. The top of the unit is picked in a peak tying to the so-called Plenus Marl or Roar member of van Buchem et al. (2017). The marker onlaps the Base Chalk (*chb*) along the basin margins. The interval is thin, never exceeding 50 mSec with exception of a narrow zone located SW of the Skrubbe Fault Zone with maximum drilled thickness of more than 150 m encountered in the Liva-1 well.

The *ch1 – ch7* interval comprises the Blodøks, Herring and Hod A+B lithostratigraphic units (equivalent to the Kraka Formation of van Buchem et al., 2017) of Turonian through Santonian age. The seismic unit has an overall transgressive nature with onlap and overstepping of the Early Cretaceous depocentres. The internal seismic reflections mostly show high continuity and only local evidence of deformation. Exceptions are related to local uplift along deeper-seated faults inherited from the Jurassic rift phases (e.g. Arne-Elin Graben and Bo-Jens Ridge where the interval is thin. Maximum thicknesses (above 200 mSec) are mapped in narrow zones along the Skrubbe Fault Zone, along the western margin of the Arne-Elin Graben and in the Karl Basin.

The top of the interval is in most area a distinct high amplitude peak that is easily traced and marks the interface between the chalks of the Hod C unit above and lower impedance marly chalks of unit Hod B below. The horizon is in several places developed as an unconformity surface with truncation of the Hod B unit and is further characterized by several incisions. An example with truncation at the ch7 marker on the Iris structure in the northern DCG is shown in Fig. BD.7. This is taken as evidence that onset of inversion movements of this structure took place by the end of deposition of the Hod A+B unit. The timing to late Santonian or Early Campanian is constrained by ties to the West Lulu-1 well shown in structural profile 9 on the website, where core data provide high-quality biostratigraphic dating in the lower part of the Hod C chalk section. Another example is taken from the Jens structure in the south also showing truncation at top Hod B (Fig. 8B.8).

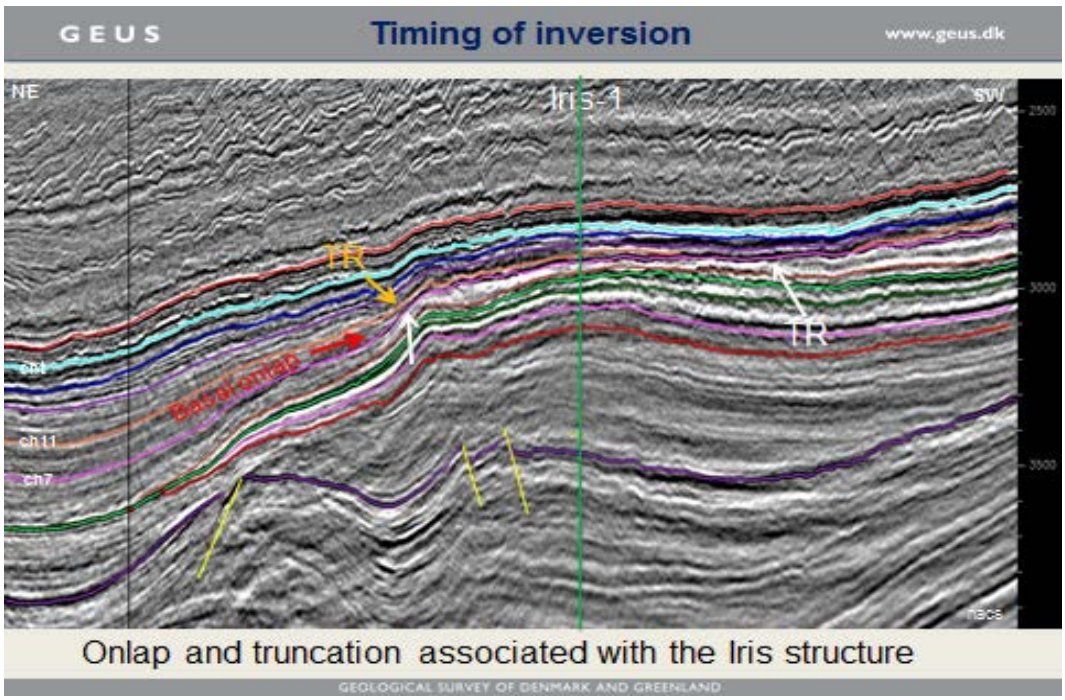

Fig. 8B.7. *Truncation of ch7 marker.*

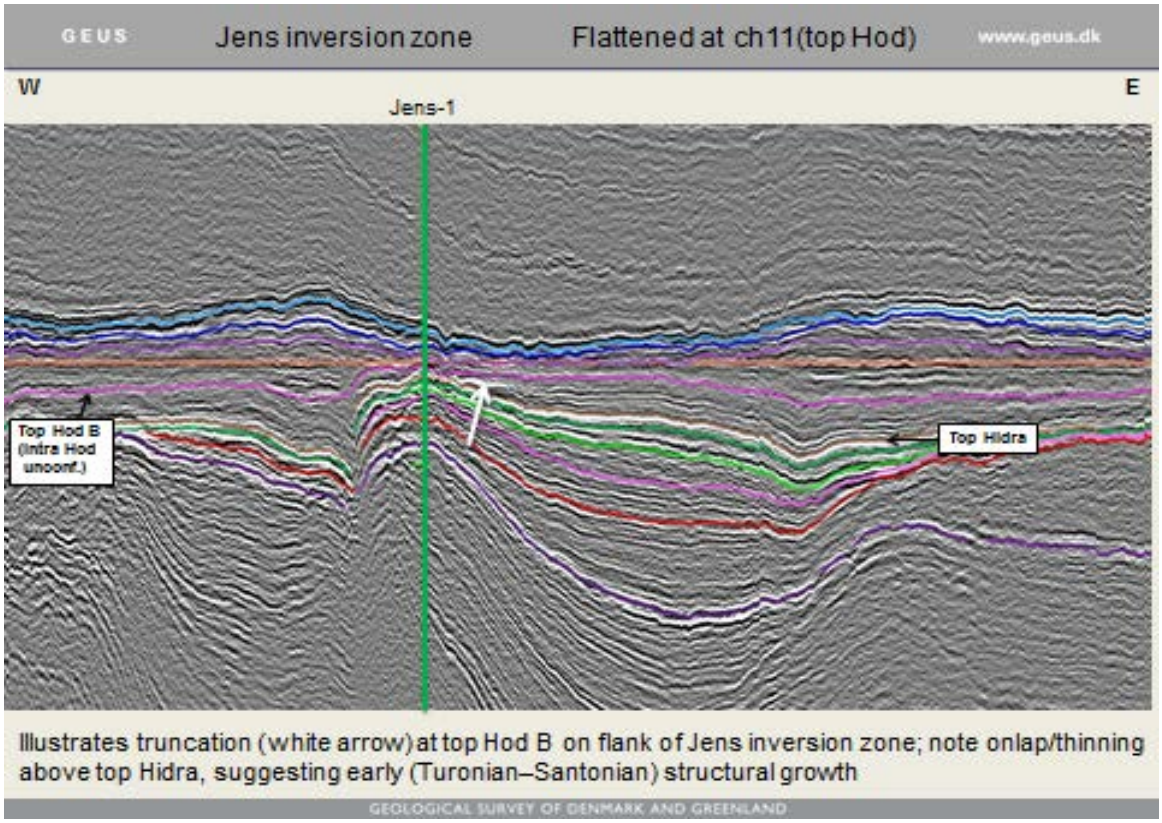

Fig. 8B.8. *Seismic section across the Jens structure, flattened at ch11.*

Both channel incisions cut the *ch7* surface and small scale disruptions and discontinuity of reflectivity indicating creep, slumping and sliding are widespread. The location of channels and mass transport complexes are shown on Fig. 8B.9.

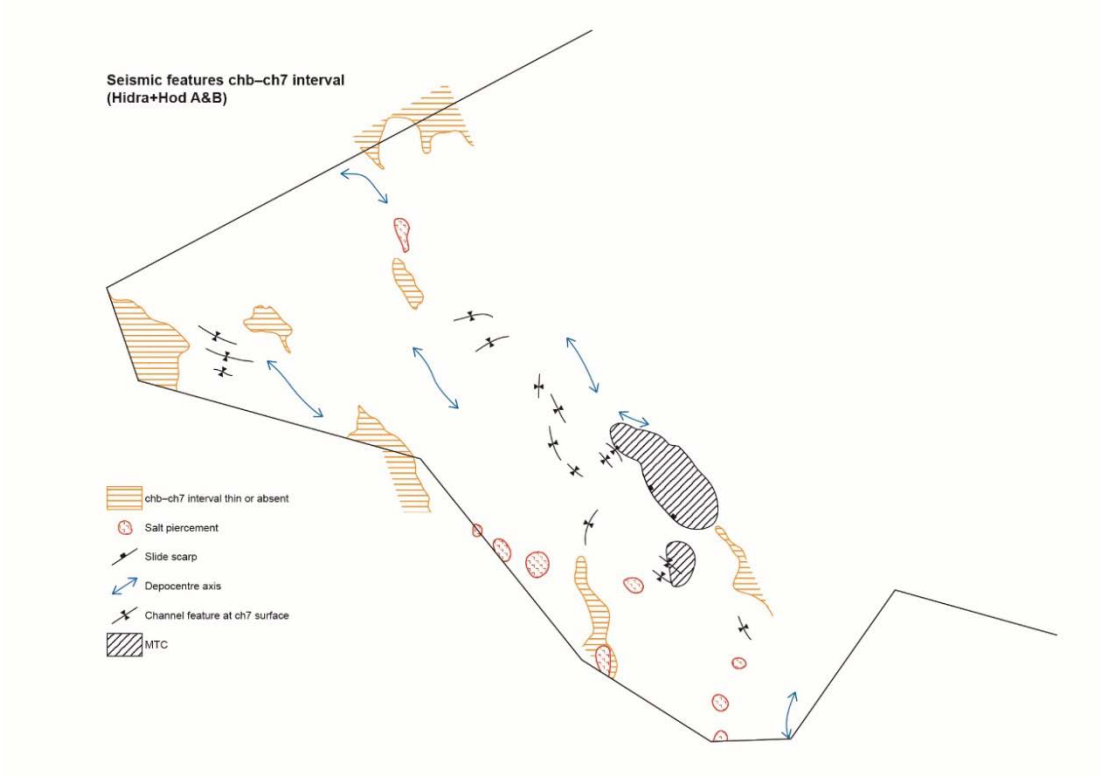

Fig. 8B.9. *Seismic features, chb – ch7 interval:*

Fig. 8B.10 (structural profile 13) shows an example of a complex channel feature with several generations of channelling in the Boje area. These features are believed to reflect a change in sea-floor topography caused by the onset of inversion movements. As a result, chalk sedimentation patterns changed with condensation and non-deposition on inverted highs, mass wastage deposits on the flanks, and thick accumulation of in-situ chalk in the new depocentres. Chalk redeposition is represented by mass wastage deposits, recording debris flow, slumping and channelling, which have been dealt with recently by several authors (Esmerode et al. 2008; Back et al. 2011; van Buchem et al. 2017).

The channel cuts on the *ch7* surface are also indicated as NW-SE trending elongate thickness lows on the time-isochore map of the *ch1-ch7* interval in the DUC05 survey area in Fig. 8B.10. This channel system is described in detail by Esmerode et al. (2008). These workers interpreted the channels to have formed by along slope processes caused by long-lived SE-directed bottom currents. An alternative mechanism has been favored by Back et al. (2011), who noted that the channel system displays many of the architectural elements of a classic gravity-driven deep-water turbidite system.

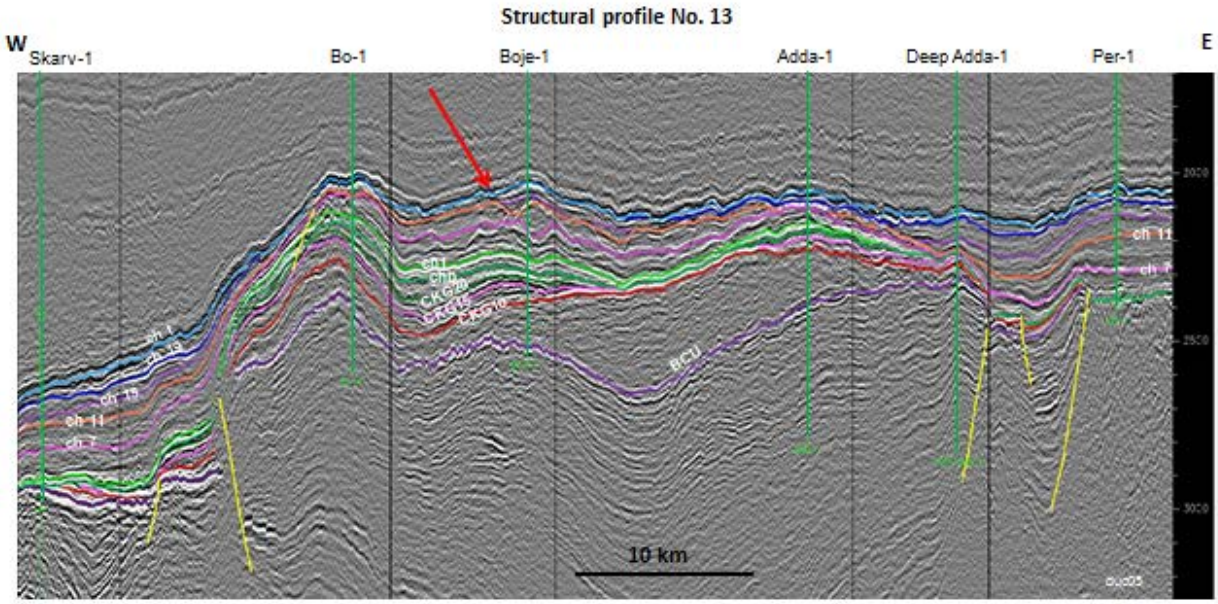

Fig. 8B.10. *Structural profile 13 showing the channel complex in the Boje area (red arrow).*

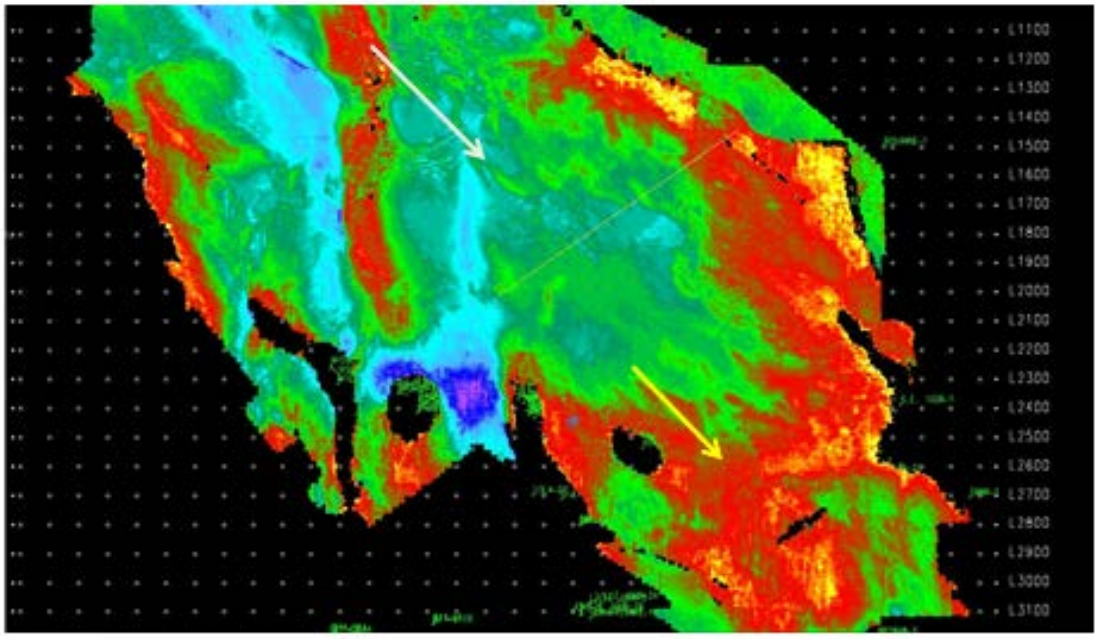

Fig. 8B.11. *Seisworks screen dump of time-isochore of the ch1 – ch7 interval in the DUC05 area. The thickness lows in the north (white arrow) show channel cuts on the ch7 surface.*

An example of a creep feature with small scale-scale discontinuities in the *ch1-ch7* interval in the Halfdan area, also described by van Buchem et al. (2008), is shown in Fig. 8B.12. The creep was caused by slope failure at a slump scar at the head of a sea-floor valley or channel. The feature is also expressed as NW- SE oriented thickness lows on the time-isochore in Fig. 8B.11 (yellow arrow).

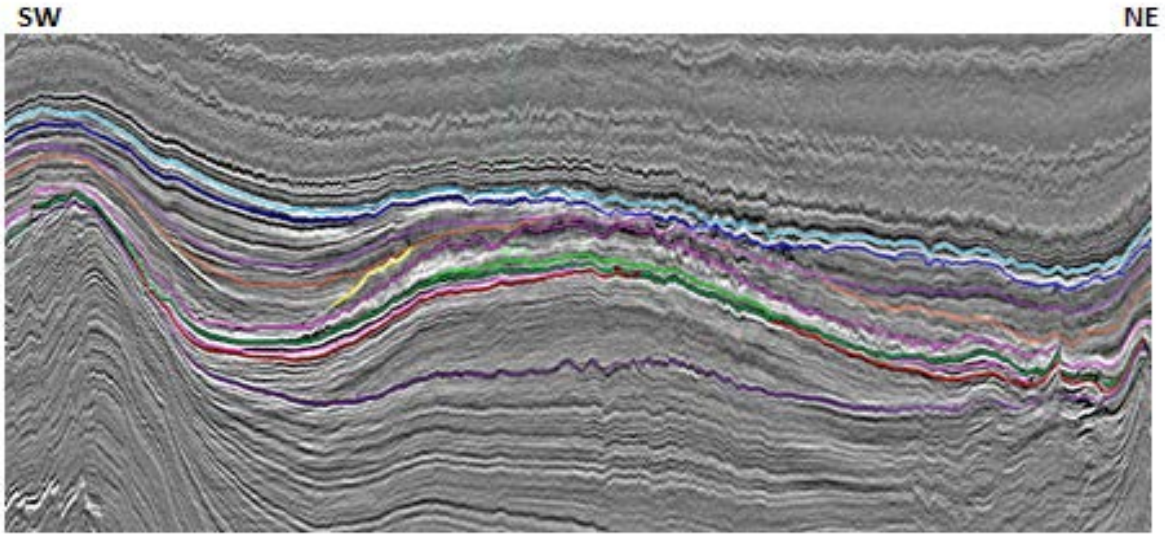

Fig. 8B.12. *Creep and slump structure in the Halfdan area with disrupted and discontinuous ch7 reflection*.

The seismic *ch7 – ch11* interval corresponding to the lithostratigraphic interval Hod C+D of Campanian age (equivalent in part to the Gorm Formation of van Buchem et al. 2017) was deposited during the climax of inversion tectonics. The interval is mapped to cover the entire study area apart from the Mid North Sea High and the central part of the Robin Ridge. Thicknesses above 100 mSec occur to the north-east in the Karl and Gulnare Basins and towards south-west in rim-synclines in the Salt Dome Province and adjoining parts of the RFH. The interval is thin on the inverted zones due to truncation and the upper bounding reflector *ch11* merges locally with the distinct *ch7* marker. Similar to the underlying *ch1-ch7* interval, channels, slides and MTCs have been observed with locations shown on Fig. 8B.13. The channel complex in the Boje area discussed above is also expressed as elongate thickness lows on the time-isochore of the interval in Fig. 8B 14. The crescent-shaped thickness low east of the Fasan-1 well represents the head scarp of a major mass transport complex along the north-eastern slope of the uplifted inversion ridge. This feature caused by slope instability has been dealt with in detail by Esmerode et al. (2008) and van Buchem et al. (2017).

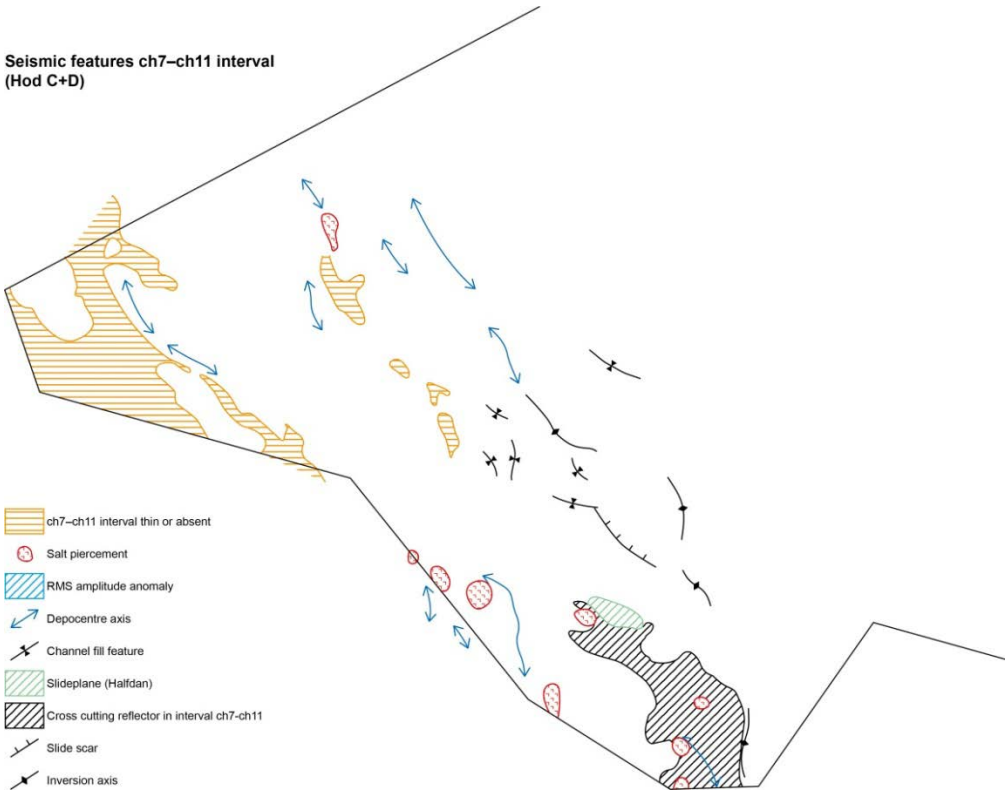

Fig. 8B.13. *Seismic features, ch7 – ch11 interval (Hod C+D)*

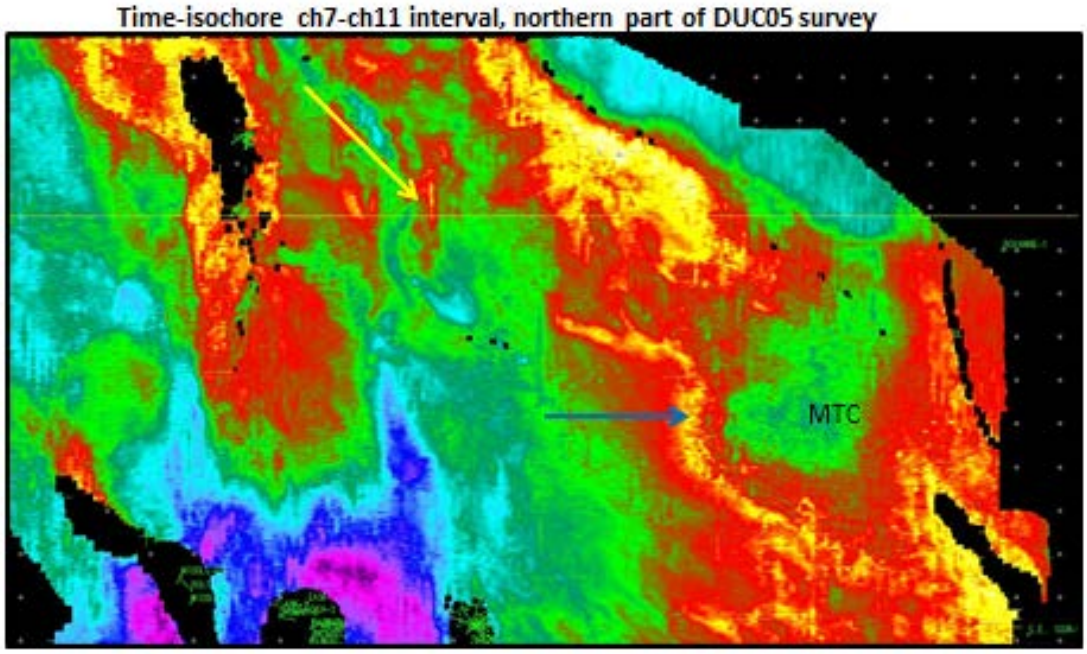

Fig. 8B.14. *Location of channel scars (yellow arrow) and head scarp of MTC (blue arrow).*

A major SSW dipping slide plane affecting the ch11 reflection (Fig. 8B.15) can be mapped in the Halfdan area NE of the Skjold salt piercement structure and shown on the seismic feature map. The slide plane was drilled in the Nana-1X well and is marked by a log break with an abrupt increase in sonic velocity.

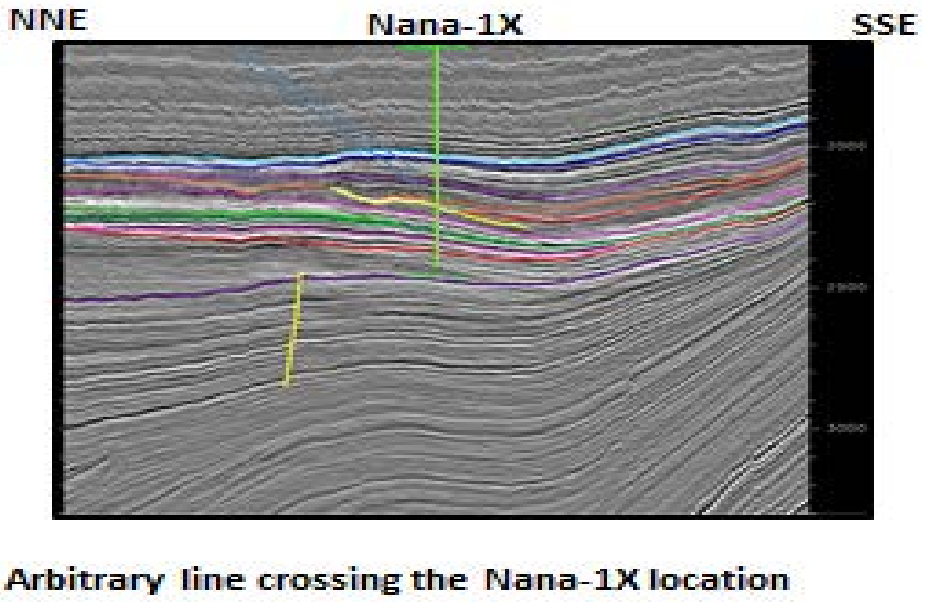

Fig. 8B.15. *Slide plane affecting the ch11 marker in the Halfdan area. Note increased reflection strength above.*

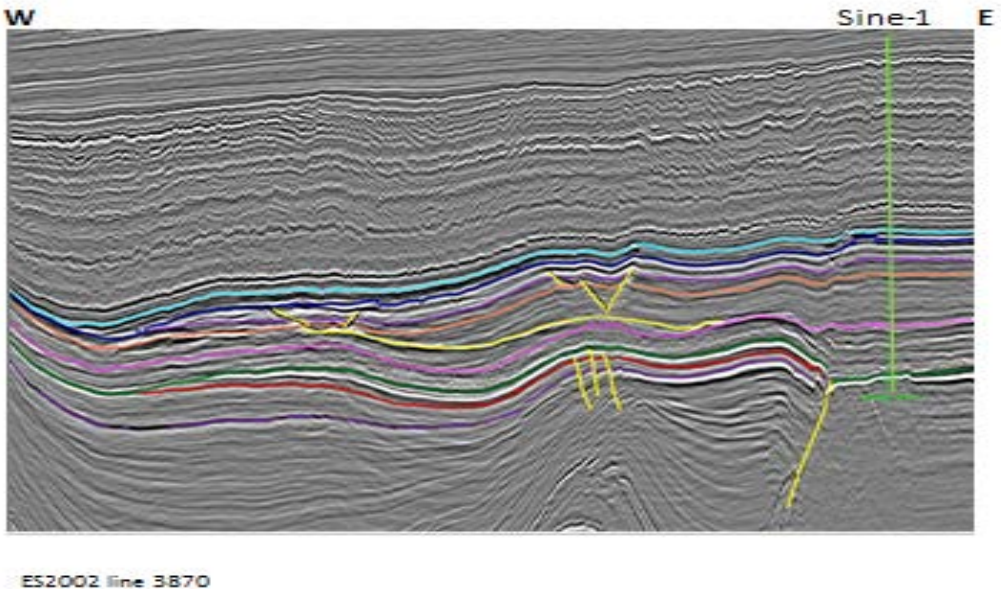

Fig. 8B.16. *Cross-cutting reflector in the ch7 –ch11 interval in the southern DCG (yellow marker).*

A cross-cutting reflector onlapping *ch7* in the east and truncated by *ch11* in the west exists over a large area south of the Halfdan slide plane. It has the character of a well-developed seismic sequence boundary and represents a puzzle. The interpreted locations of both *ch7* and *ch11* are, however, consistent with the reviewed stratigraphy in neighboring tie wells and the integrity of these surfaces is not considered flawed. An eastward tilt of this part of the basin during deposition of the *ch7 –ch7* interval may represent a possible interpretation.

The seismic interval *ch11 – ch15* corresponding to the lithostratigraphic Lower Tor formation of Maastrichtian age was deposited after the climax of inversion movements. The unit is characterized by basal onlap onto the newly inverted basin highs, where it is thin to absent (Fig. 8B.17). The amount of uplift of the basin centre was estimated by van Buchem et al. (2017) to be of the order of 300-400 m prior to deposition of the *ch11 – ch15* interval creating substantial sea-floor relief. The lower Tor depocentres concentrated in the north and in rim-synclines in the south may therefore be in a favorable position to contain intervals with reworked material shed off the bathymetric highs into the deeper-water sub-basins.

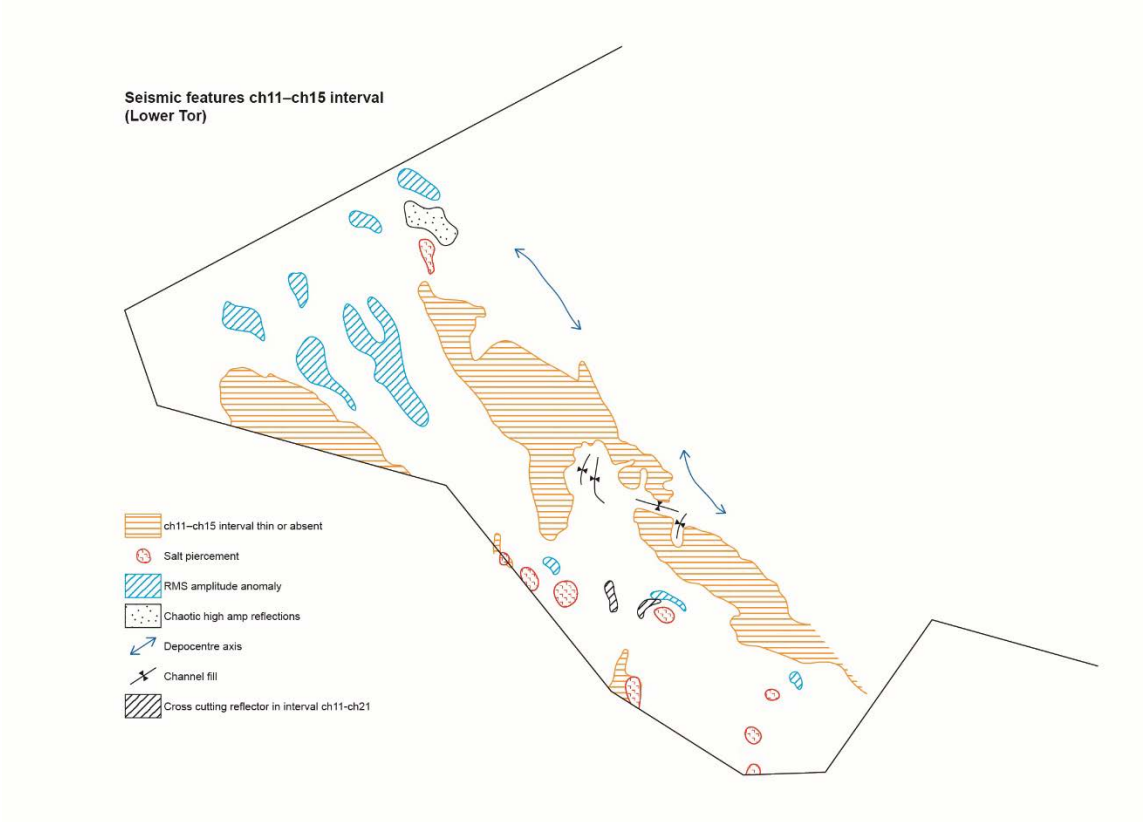

Fig. 8B.17. *Seismic features of the ch11 – ch15 interval showing the location of channel fill of pre-existing channel incisions on the central inversion axis and RMS anomalies in the depocentres.*

RMS amplitudes have been extracted for the *ch11 – ch15* interval in an attempt to locate potential areas that may display intervals with elevated porosities. An example from the Angelina area in the North-west is shown in Fig. 8B 18. Amplitude anomalies are here located in 3 areas, along the north and south-east of the flanks of Inge High and in a NW-SE trending area in the basin area comprising the Spurv-1 location. This well drilled an amplitude anomaly on a gentle structural nose and encountered a porous interval in the *ch11 – ch15* unit according to prognosis, albeit dry. The anomaly is shown on the structural profile No. 6 (Fig. 8B.19).

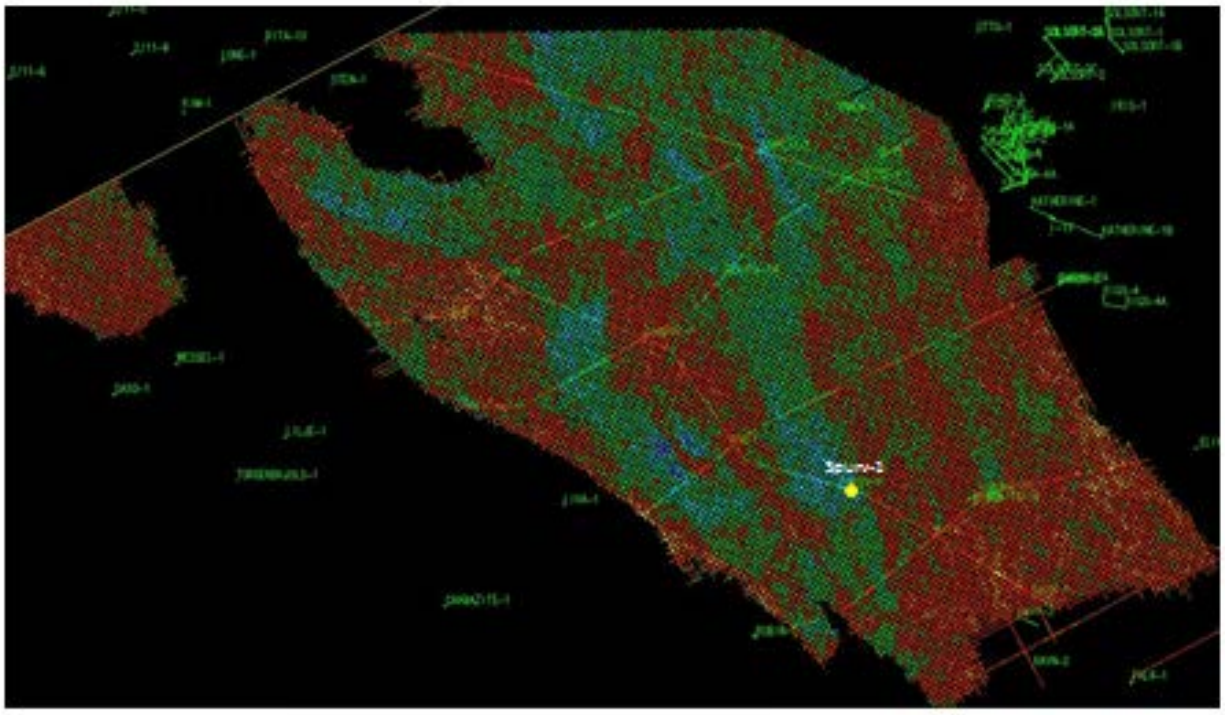

Fig. 8B.18. *SeisWorks screen dump of RMS amplitudes of the ch11 – ch15 in the Angelina survey area. Green and blue colors indicate high amplitudes.*

Two areas with high amplitude cross-cutting reflectors affecting the interval are marked on the seismic feature map west and east of the Gorm Field, respectively. They are shown in Fig. 8B.20 with a red color. The reflector on the Gorm west flank is almost horizontal and cuts all seismic units from *ch11* to *ch21*. This is in contrast to the eastern area where the reflector is inclined and broken into smaller segments with the interval above appearing transparent. We are at present not in a position to offer an interpretation of the two features, and they remain as a puzzle. Do they represent diagenetic surfaces or in the eastern feature a slide plane phenomenon?

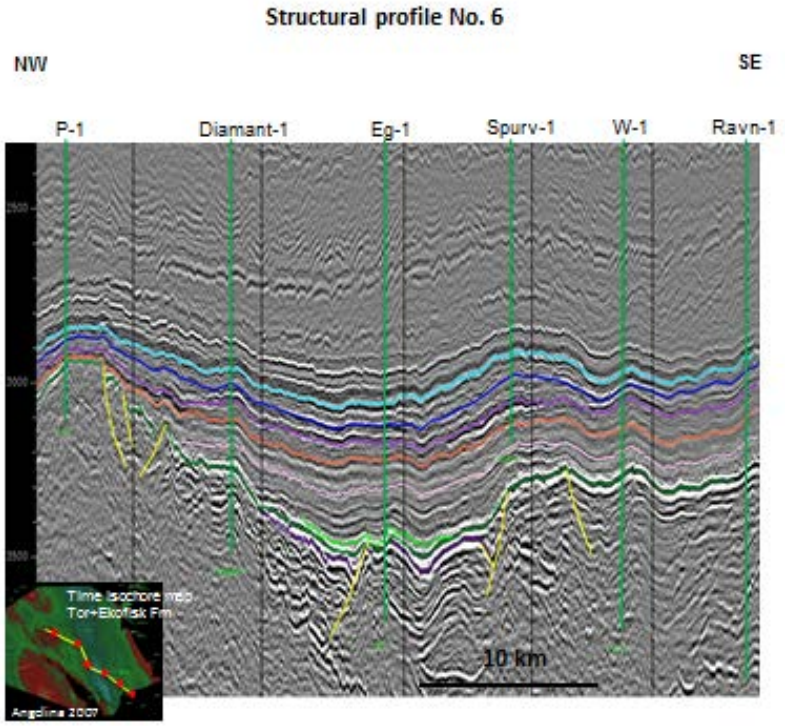

Fig. 8B.19. *Structural profile 6 with a distinct amplitude anomaly in the ch11 – ch15 interval (between lilac and red horizons) at the Spurv-1 location corresponding to a drilled porous interval.*

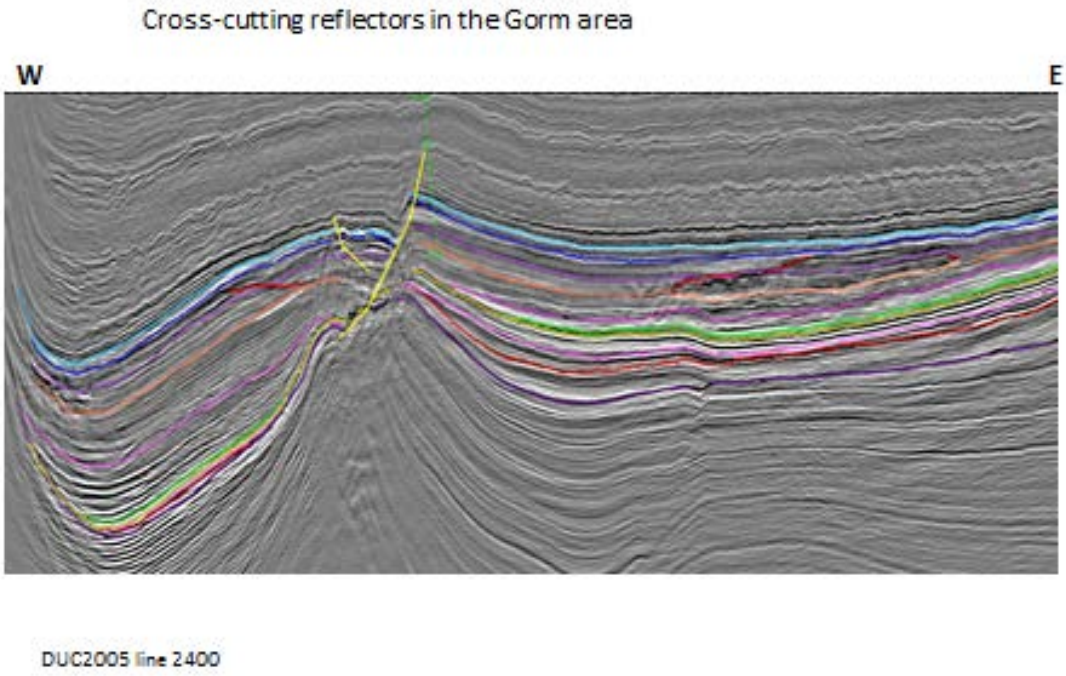

Fig. 8B.20. *Cross-cutting reflector in the Gorm area.*

The *ch15 – ch19* interval comprises the Upper Tor Formation of Late Maastrichtian age. This part of the Tor Formation is characterized by generally higher porosities than the underlying Tor interval. The depositional pattern is a continuation of the *ch11 – ch15* interval, although with rather gentle thickness variations. The only indication of a marked shift in depocentre is that a thick interval is present on the Mid North Sea High in the west.

The Tor Formation is the most important reservoir in chalk fields in the North Sea region having typically the highest porosities and permeability of all chalk reservoirs. During the last two decades several wells have been drilled with targets in the Upper Tor outside structural closures; results have been generally disappointing apart from the prolific Halfdan discovery located in a non-structural trap with the oil zone in disequilibrium (Albrechtsen et al. 2001). Most of the wells have been based on amplitude anomalies, usually further de-risked by seismic inversion for acoustic impedance. As a general rule, the expected porosity anomalies were confirmed but were dry, possibly due to non-existing traps or unfavorable migration routes from the underlying Upper Jurassic source rocks. RMS amplitudes have been extracted over the entire interval and locations of anomalies are shown on Fig. 8B.20, and an example from the Angelina survey is given in Fig. 8B.21. Compared to the underlying interval, amplitude anomalies in Upper Tor are widespread and may represent areas with high porosity intervals in reworked chalk even at depths exceeding 3200 m. Fig. 8B.22 is a correlation diagram with log porosities through 5 wells from the northern area showing intervals in the upper Tor with porosities above 20%. The blocky nature of the log motifs suggests the presence of redeposited units.

Fig. 8B.20. *Seismic feature map of the ch15 – ch19 interval with the locations of RMS amplitude anomalies.*

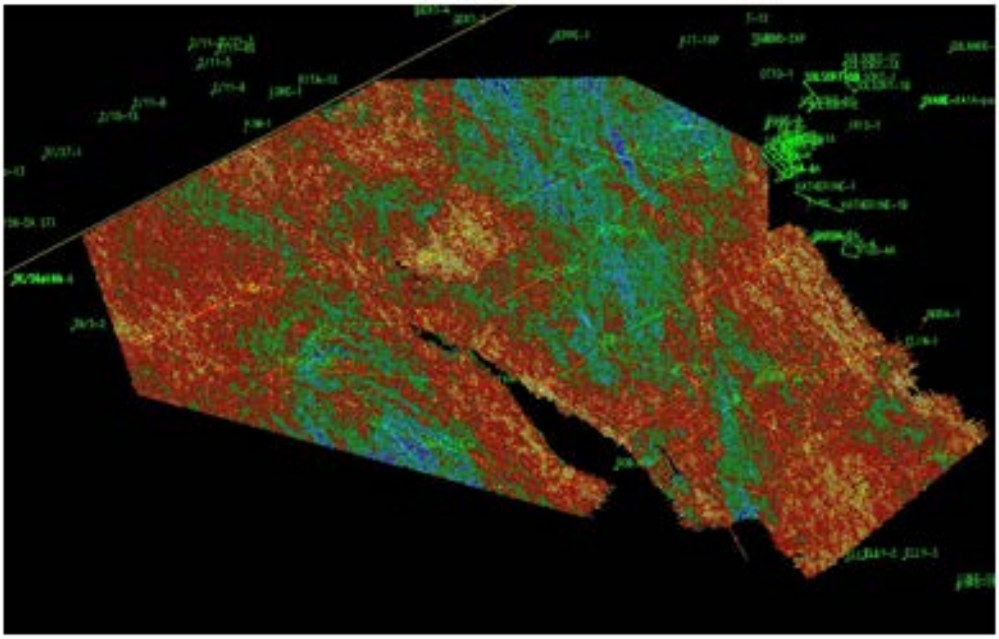

Fig. 8B.21. *SeisWorks screen dump of RMS amplitudes of the ch15 – ch19 interval in the Angelina survey area. Green and blue colors indicate high amplitudes.*

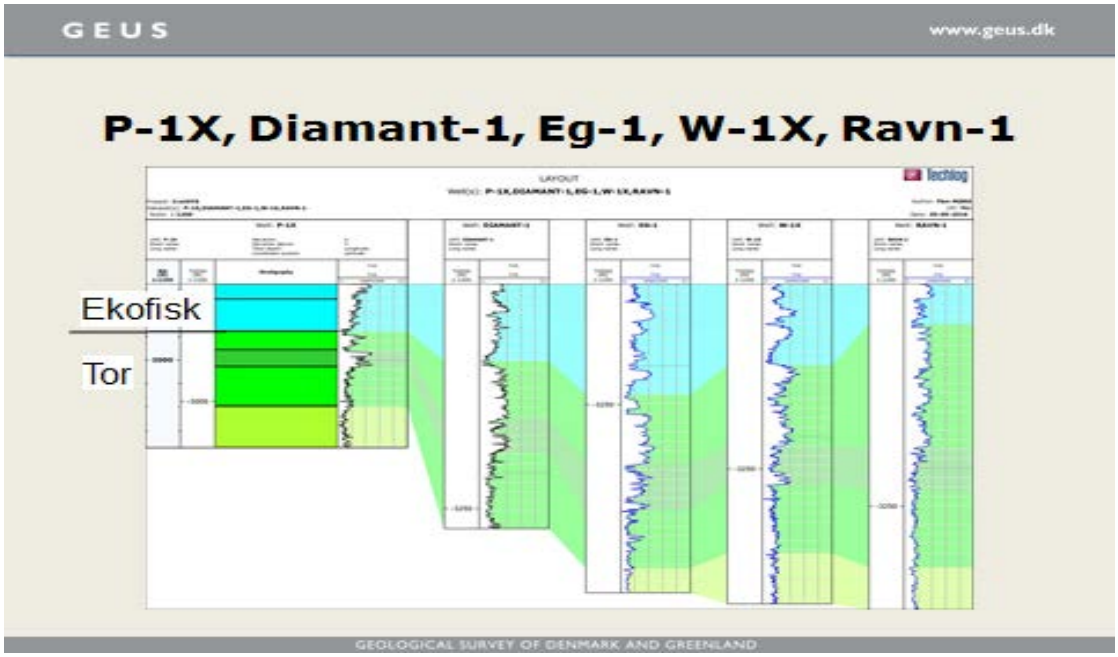

Fig. 8B. 22. *Log correlation between 5 northern wells with log porosities.*

The seismic interval *ch19 – cht* comprises the Ekofisk Formation of Danian age. The unit is mapped in most parts of DCG but is absent on the crest of the Robin Inversion ridge and thin to absent on the northern part of the Tyra-Igor Ridge. Maximum time-thickness (up to 100 mSec) is found in an NW-SE trending elongate zone between the

inversion ridges along the Skrubbe Fault Zone to the west and the Arne- and Bo-Jens Ridges to the east (Fig. 8B.23). The wells in this depocentre contain several intervals of redeposited chalk with high porosities in the Ekofisk Formation and expressed with a blocky log-motif (Fig. 8B.22).

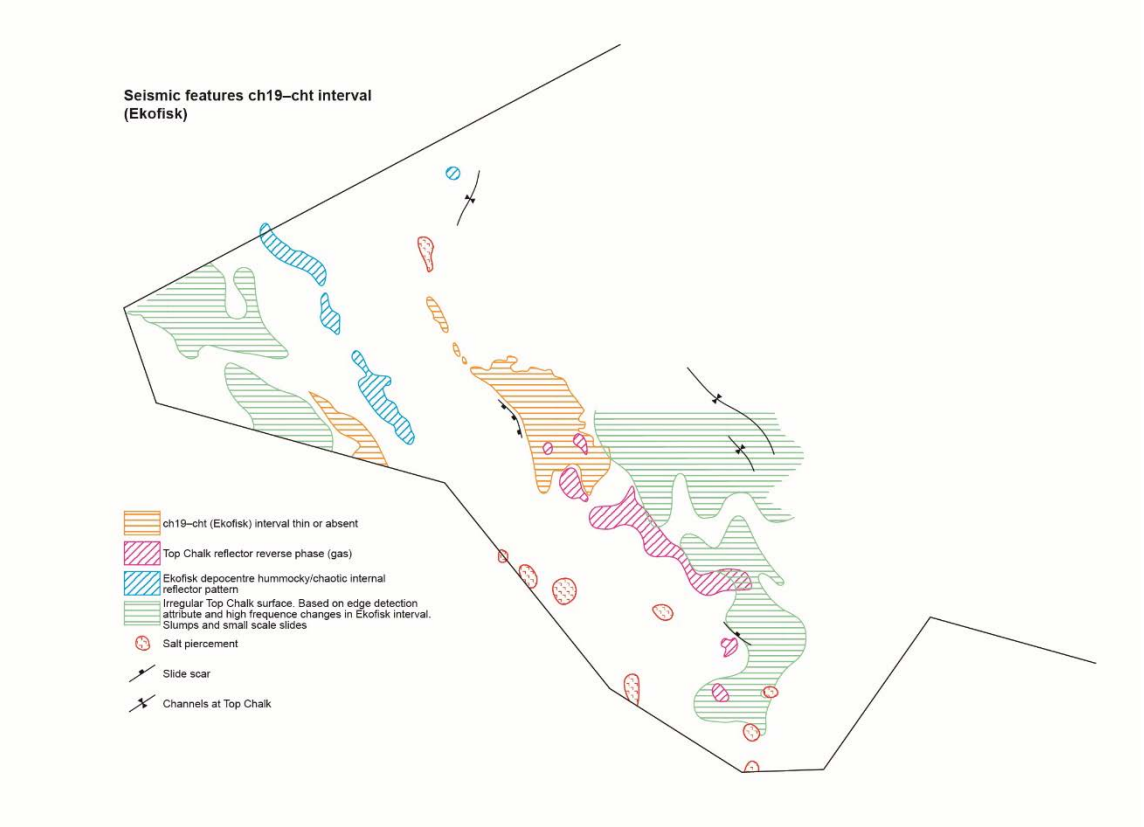

Fig. 8B.23. *Seismic feature map, ch19 – cht interval.*

Although the time-structure map of the Top Chalk surface on a regional scale appears smooth with gentle dips apart from the salt piercement structures, it is in fact often irregular and rugged when studied in detail. Phase reversals of the cht marker disturb the surface in areas with gas-saturation (Fig. 8B.23). The rugged surface is caused by post-Danian small scale slumping and sliding due to slope instability. These features are illustrated below with examples from the DUC2005 area in the south. Fig. 8B.24 is a screen dump from Seisworks of details of the Ekofisk time-isochore showing high frequency thickness variations caused by an irregular cht surface and a rather smooth lower *ch19* surface. The ruggedness caused by slumping is further illustrated in the edge detection attribute map in Fig. 8B.25. The sliding and slumping features are conspicuous in the area northeast of the Dan Field as illustrated by the seismic profile in Fig. 8B.26 and the detailed Top Chalk structure map showing circular and crescent-shaped geometries (Fig. 8B.27).

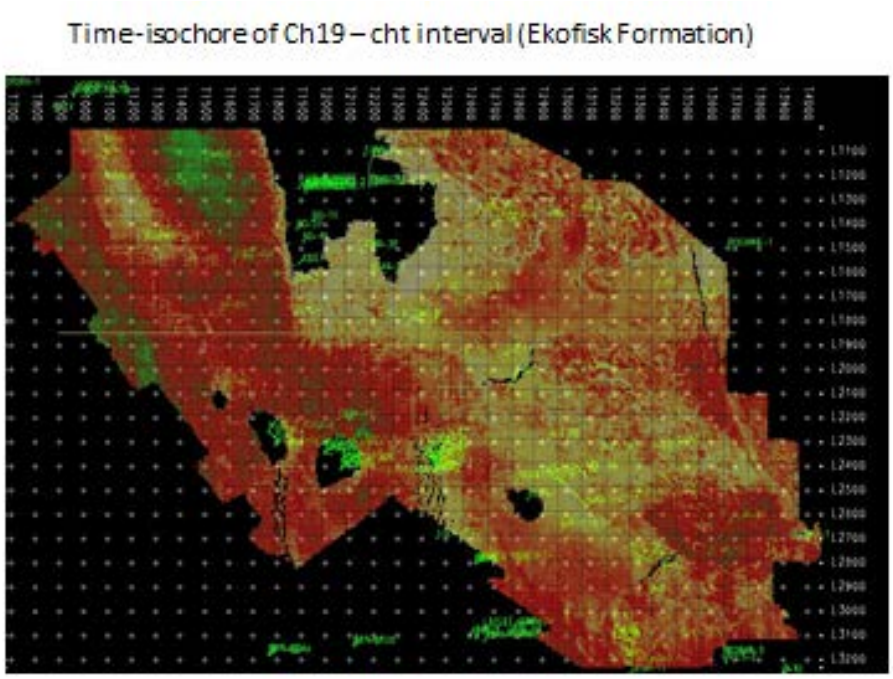

Fig. 8D.24. *Time-isochore of the ch19 –cht interval in DUC2005 survey area.*

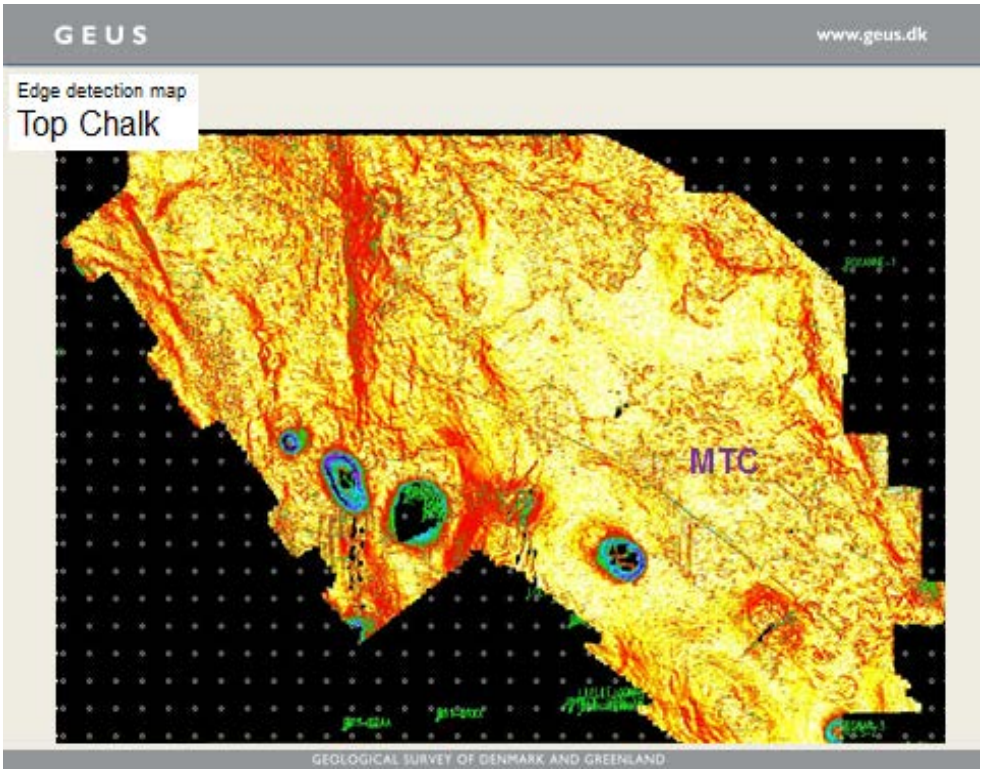

Fig. 8B.25. *Edge detection of Top Chalk in the DUC2005 area showing slumping and sliding to the east.*

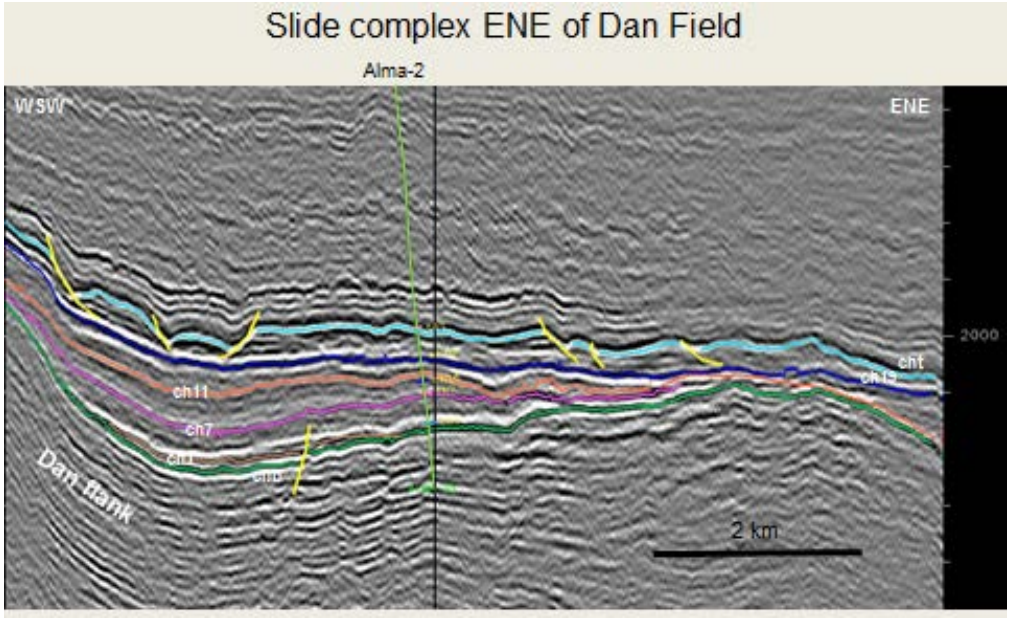

Fig. 8B.26. *Slump and slide complex in ch19 – cht interval ENE of the Dan Field.*

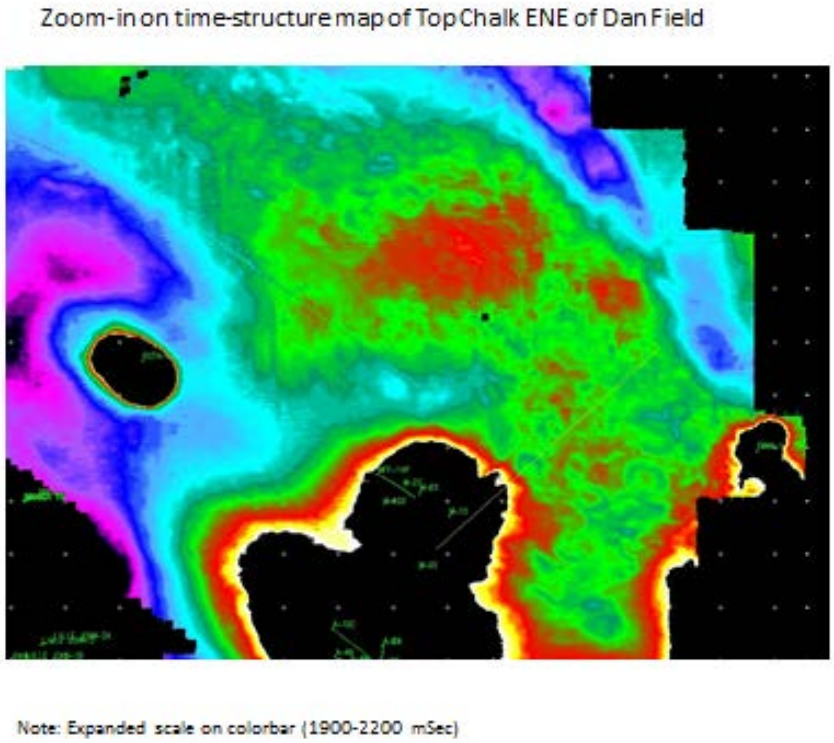

Fig. 8B.27. *Detail of Top Chalk structure map in the area ENE of the Dan Field.*

8B.3 Summary of Cretaceous basin development

The following brief summary of the basin development is based on composite time-isochore maps of the following 4 intervals found on the website: 1) *BCU – C*KG10 (Valhall Fm), 2) *CKG11 – chb* (combined Tuxen, Sola and Rødby Fms), 3) *chb – ch11* (Hidra and Hod Fms) and 4) *ch11 – cht* (Tor and Ekofisk Fms).

The lower mapped interval *BCU – CKG10* interval comprises the claystone-dominated Valhall Formation of latest Ryazanian to Hauterivian age. It was deposited as a result of early thermal subsidence infilling the inherited basin-floor topography following the late Jurassic rifting stages. It has a more restricted occurrence than the underlying late Jurassic deposits, however, being absent at the basin margins including the Mid North Sea High, Heno Plateau, Søgne Basin and the south-western part of the Salt Dome Province. The locations of the post-rift Valhall Formation depocentres are to a large extent coincident with depocentres of the late-rift phase part of the upper Farsund/Mandal Formation. They form elongate troughs or sub-basins parallel to the DCG basin axis. These include the Feda Graben, Gertrud Graben, Iris Basin, Gulnare Basin and to the south, the Roar Basin. The maximum drilled thickness is over 600 m in the Sten-1 well located in the Feda Graben.

The interval *CKG10 – chb* interval encompasses the mixed carbonate - siliciclastics of the Tuxen, Sola and Rødby Formations spanning the age interval from Hauterivian through Albian, a time span of about 30 Ma. The interval has a slightly more restricted extention compared to the Valhall Formation due to truncation by the Base Chalk Group reflector both in the Søgne Basin and in the south. The location of depocentres shifted westwards with maximum thickness of the combined interval of more than 300 m drilled in the Elin-1 well in the Arne-Elin Graben. A new structural element is the Outer Rough Basin located west of the Skrubbe Fault Zone; the combined time-thickness in this basin is atypically large, locally exceeding 300 mSec. It is, however, stressed that the central of the basin is without well control. The only seismic tie is provided by the Lilje-1 well located at the western margin of the basin.

The interval *chb – ch11* comprises the chalks of the Blodøks, Herring, Hidra and Hod Formations. This interval shows an overall 'transgressive' nature with onlap and overstepping of the Early Cretaceous basin margins. The climax of upper Cretaceous inversion movements took place in Campanian times during deposition of unit Hod C+D. The inversion movements resulted ina change of sea-floor topography and led to deposition of reworked chalk in basin lows away from the newly formed structural highs. Unconformities, channel development and mass transport complexes are widespread as a result of the inversion tectonics. The time-isochore map therefore expresses the combined pre-inversion and syn-inversion development. The inversion ridges stand out as elongate thickness lows, separated by intervening depocentres.

The Interval *ch11 – cht* encompasses the prospective Tor and Ekofisk Formations with abundant hydrocarbon-bearing intervals of high porosity. It was deposited after the climax of inversion tectonism during the Maastrichtian and Danian and is characterized by basal onlap on the inversion highs. Compared to interval *chb – ch11* the thickness variations are much less dramatic. The depocentres in the North are in a favorable position to contain reworked chalk intervals originating from slope instability on the flanks of the highs. The development of rim-synclines in the south suggests continued halokinetic movements during this time period.

References

Albrechtsen, T., Andersen, S.J., Dons, T., Engstrøm, F., Jørgensen, O. & Sørensen, F.W. 2001. Halfdan: Developing non-structurally trapped oil in North Sea Chalk. *SPE paper, 71327: 11pp.*

Back, S., van Gent, H.,Reuning, L., Grøtsch, J. Niederau; J & Kukla, P. 2011. 3D seismic geomorphology and sedimentology of the Chalk Group, southern Danish North Sea. *Journal of the Geological Society, London, Vol. 168, pp.393-405*

Esmerode, E.V., Lykke-Andersen, H. & Surlyk, F. 2008. Interaction between bottom currents and slope failure in the Late Cretaceous of the southern Danish Central Graben, North Sea. *Journal of the Geological Society, London, Vol.165, pp. 55-72.*

Van Buchem, F.S.P., Smit, F.W.H, Buijs, G.J.A., Trudgill, B. & Larsen, P.-H. 2017. Tectonostratigraphic framework and depositional history of the Cretaceous – Danian succession of the Danish Central Graben (North Sea) – new light on a mature area. In: Bowman, M. & Levell, B. (eds) *Petroleum Geology of NW Europe: 50 Years of Learning – Proceedings of the 8th Petroleum Geology Conference.*

Vejbæk, O.V. 1986. Seismic stratigraphy and tectonic evolution of the Lower Cretaceous in the Danish Central Trough. *Danmarks Geologiske Undersøgelse. Serie A. Nr. 11.*

Vidalie, M., van Buchem, F., Schmidt, I. & Uldall, A. 2014. Seismic stratigraphy of the Lower Cretaceous Valhall Formation (Danish Graben, North Sea. *First Break. 32, 71-80.*

Appendix 8B

List of contents.

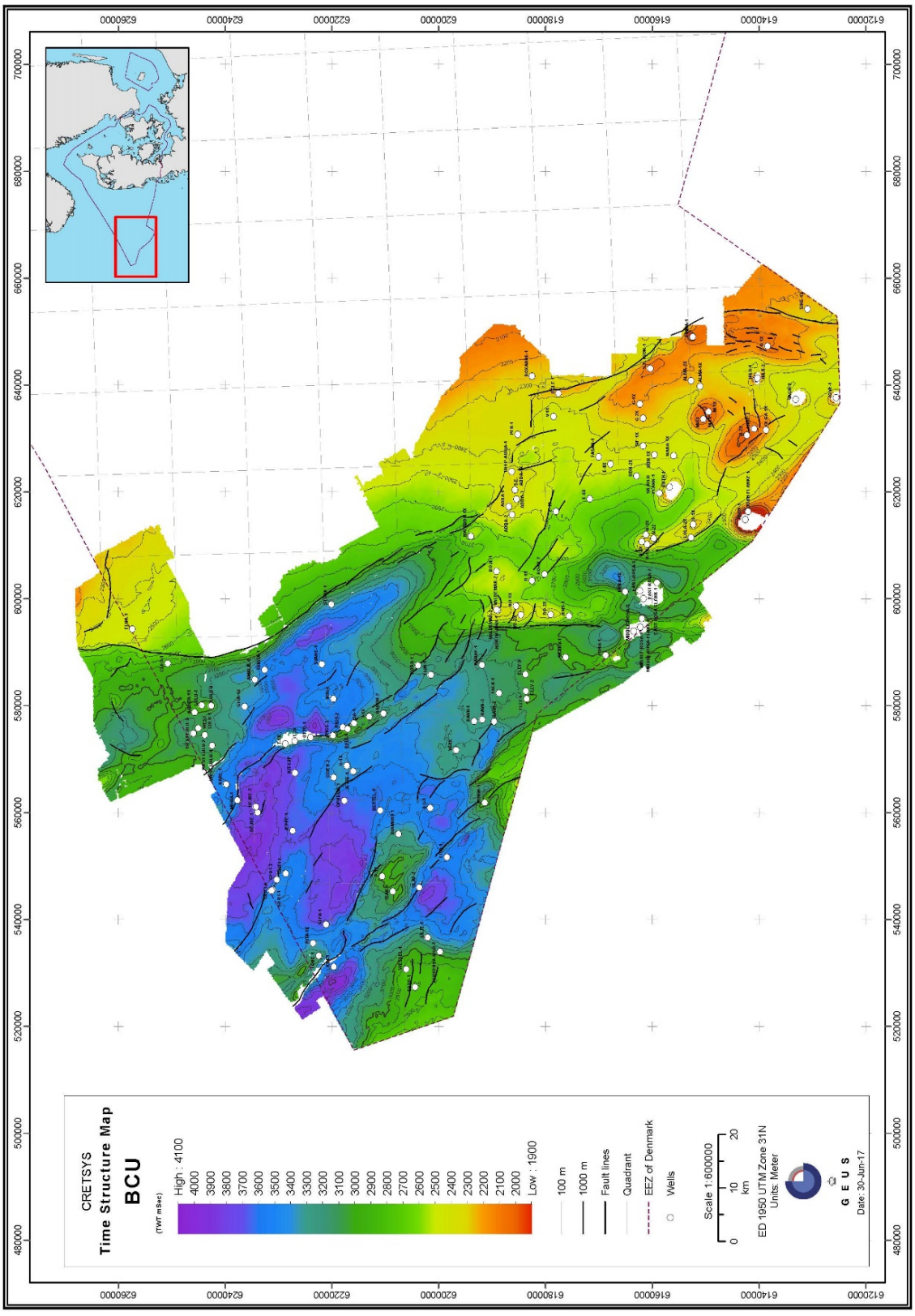

App. 8B: Time structure map: **BCU**

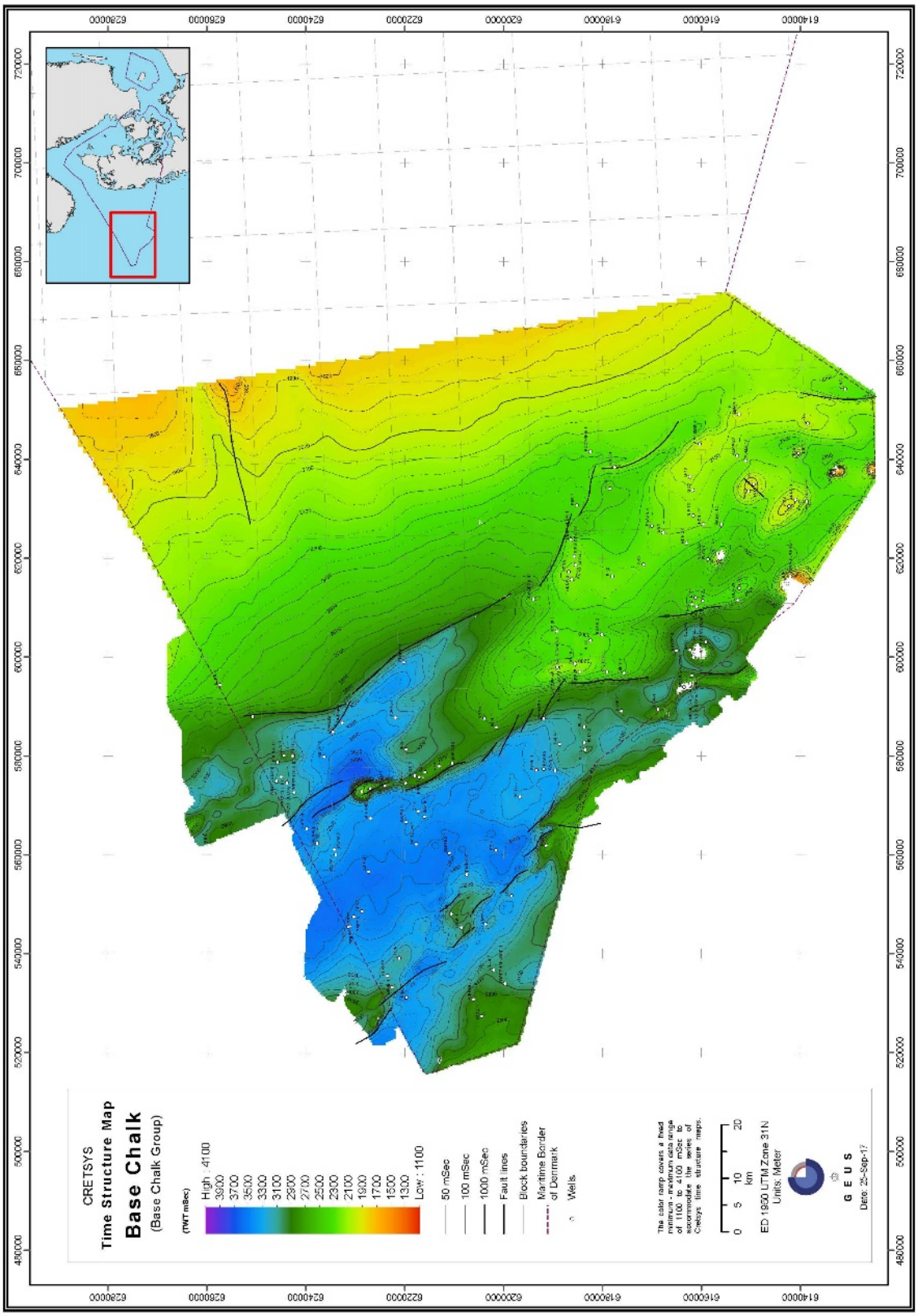

App. 8B: Time structure map: **Base Chalk**

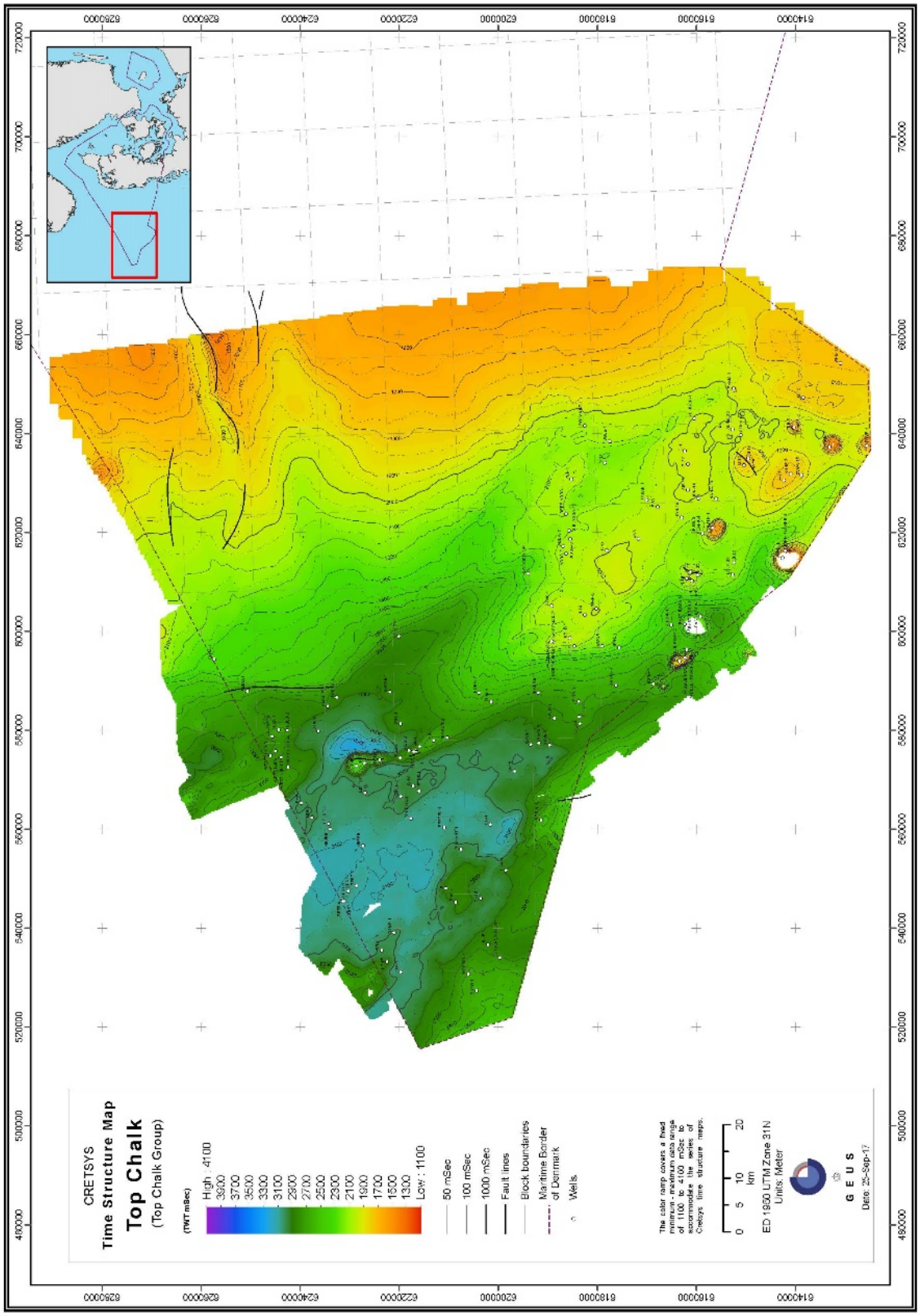

App. 8B: Time structure map: **Top Chalk**

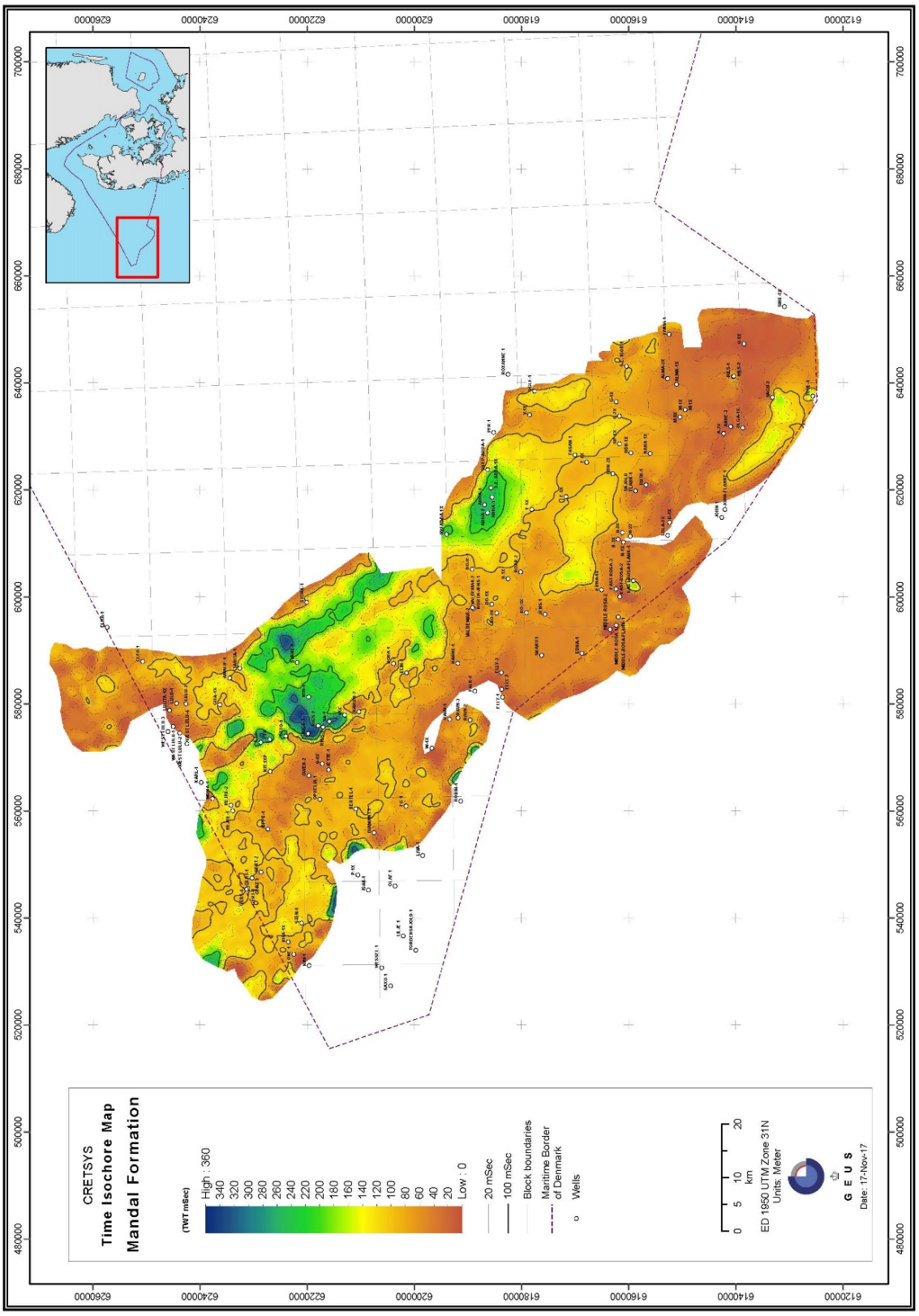

App. 8B: Time isochore map: **Mandal Formation**

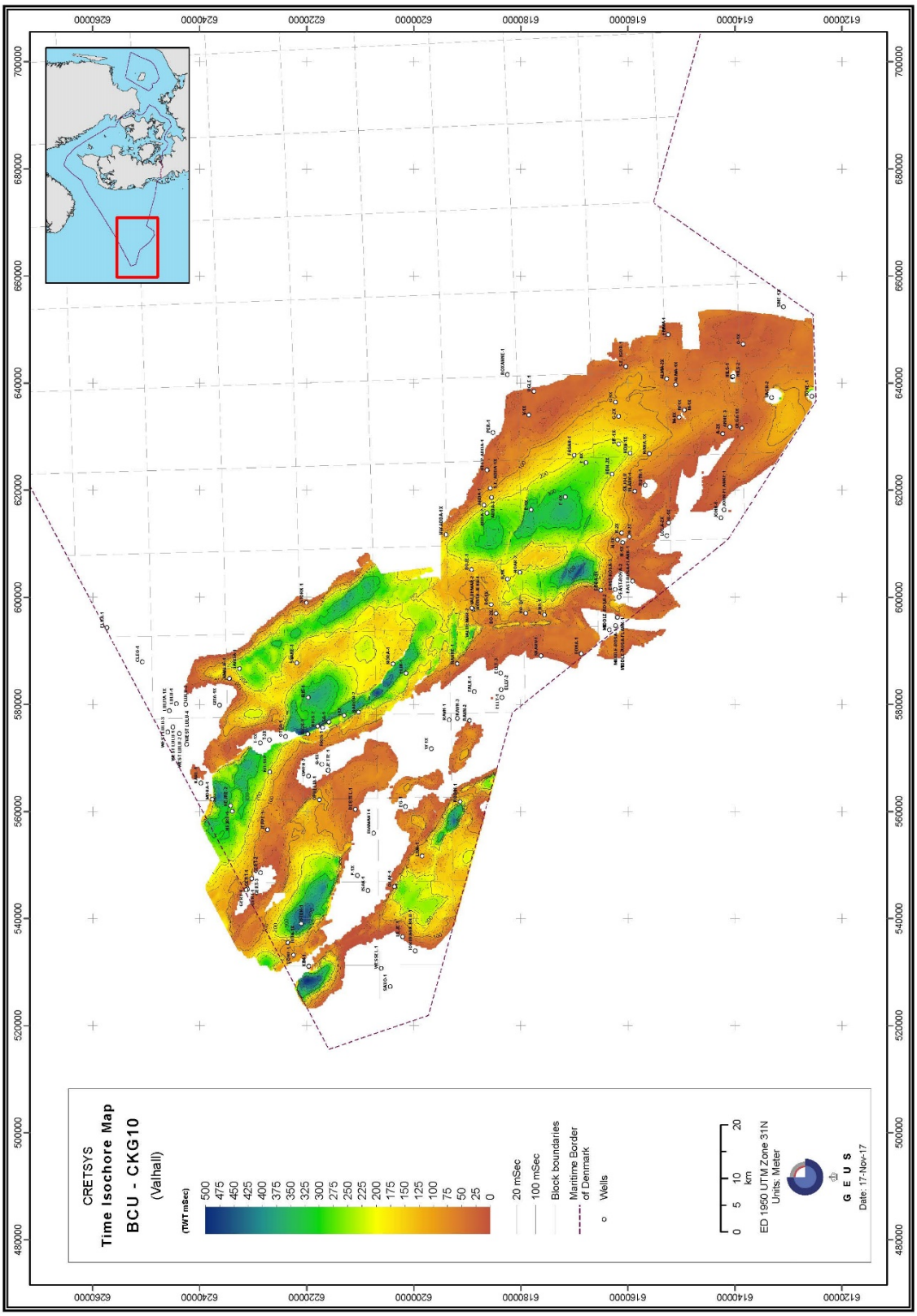

App. 8B: Time isochore map: **BCU – CKG10** (Valhall)

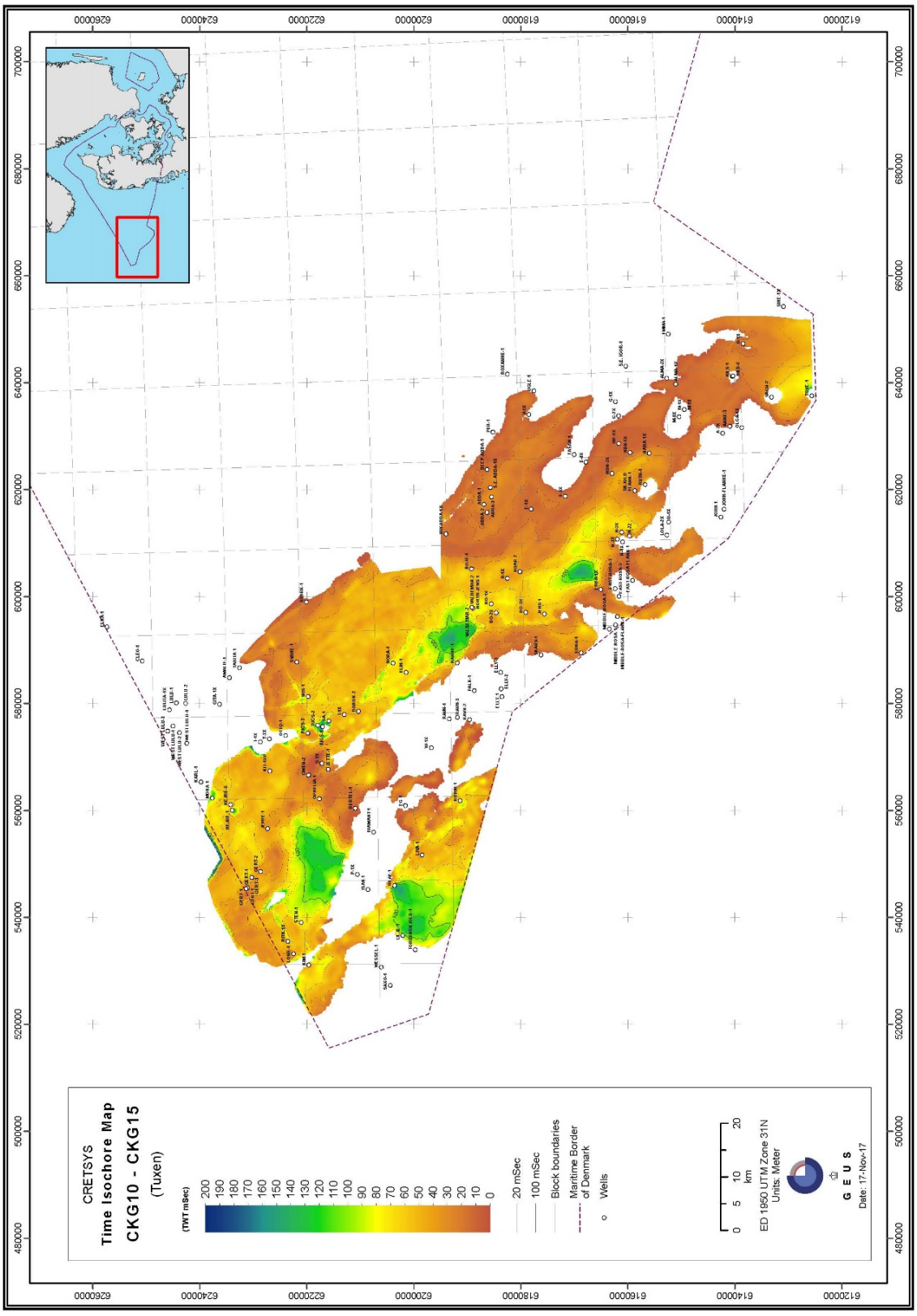

App. 8B: Time isochore map: **CKG10 – CKG15** (Tuxen)

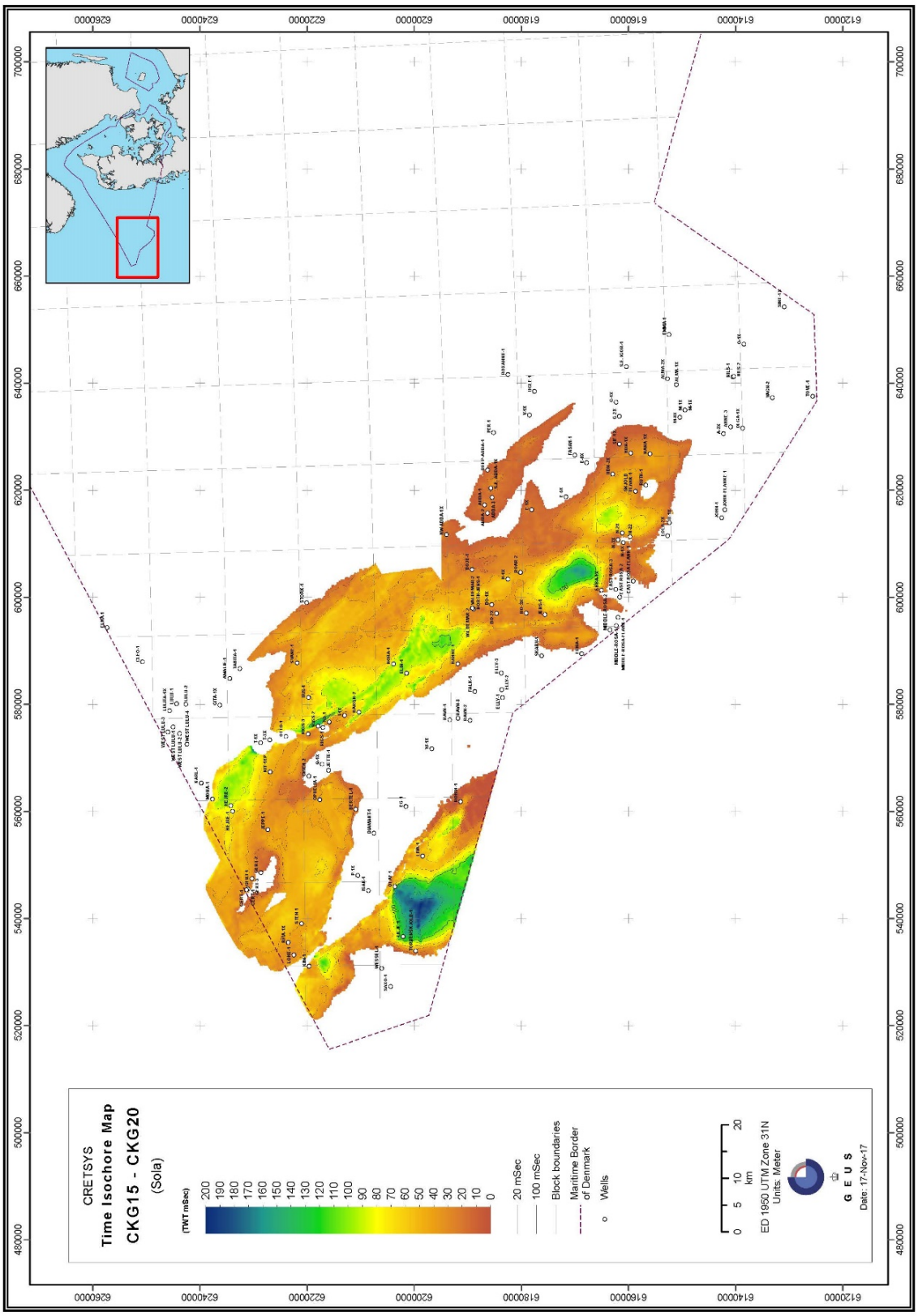

App. 8B: Time isochore map: **CKG15 – CKG20** (Sola)

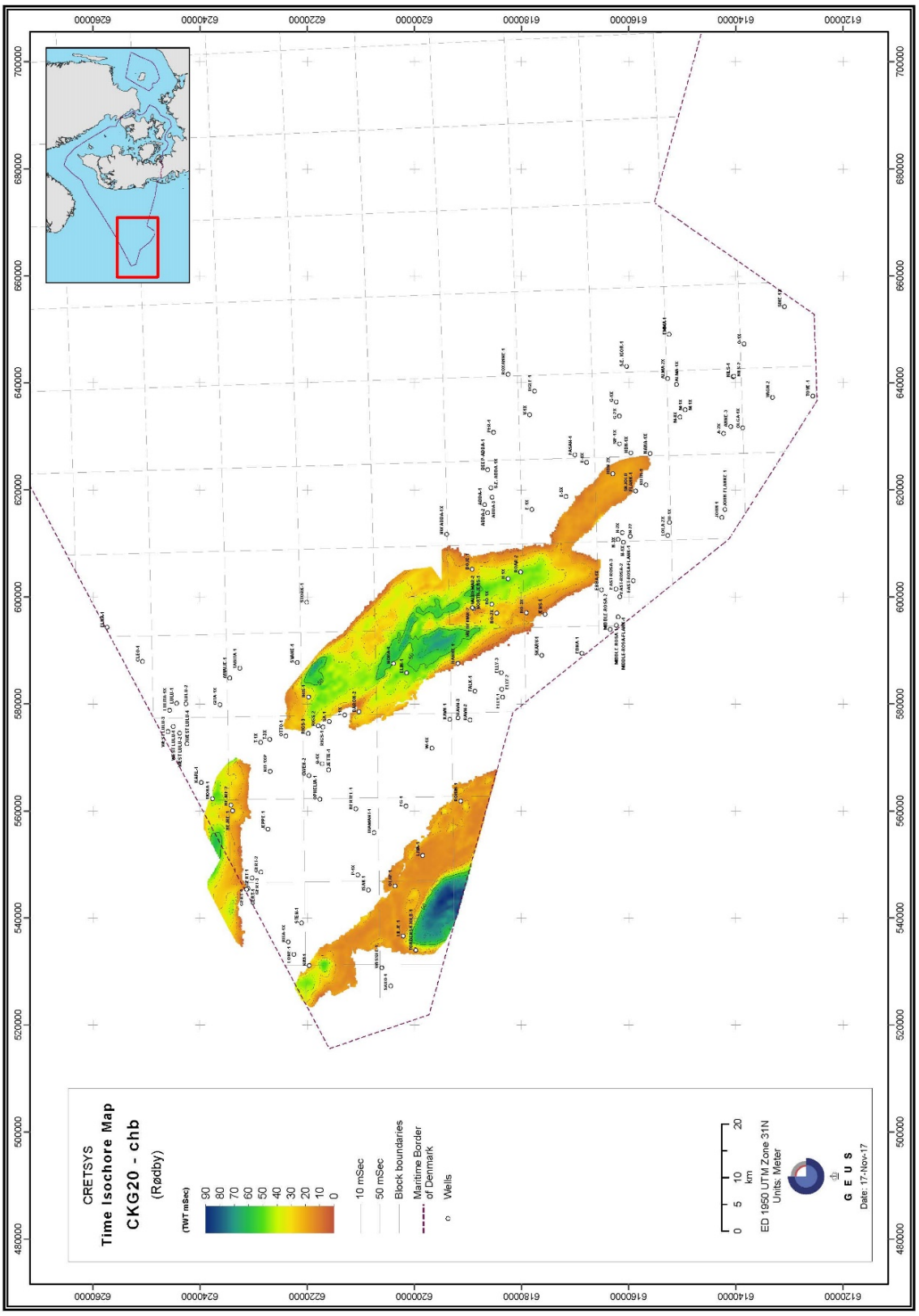

App. 8B: Time isochore map: **CKG20 – chb** (Rødby)

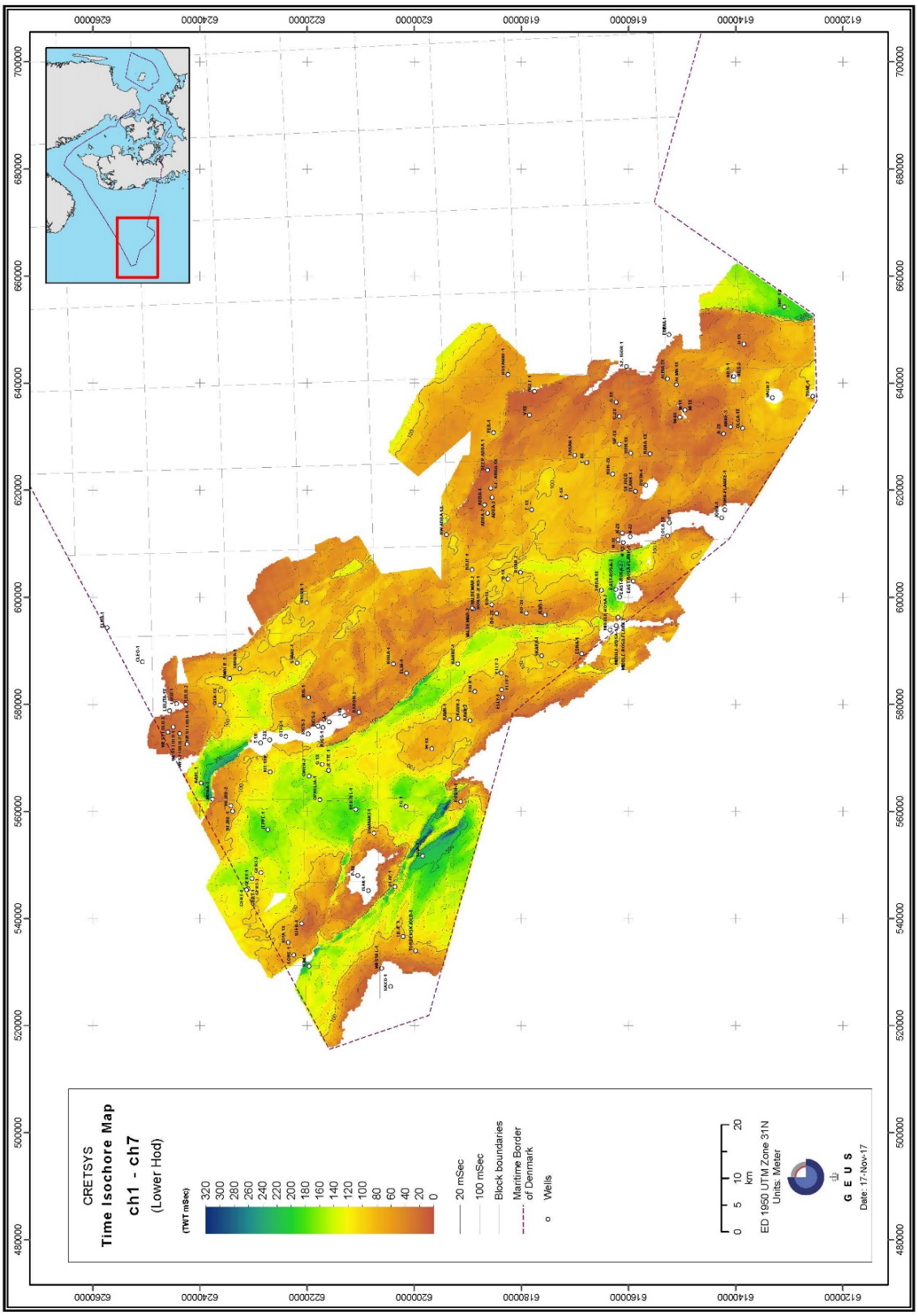

App. 8B: Time isochore map: **chb – ch1** (Hidra)

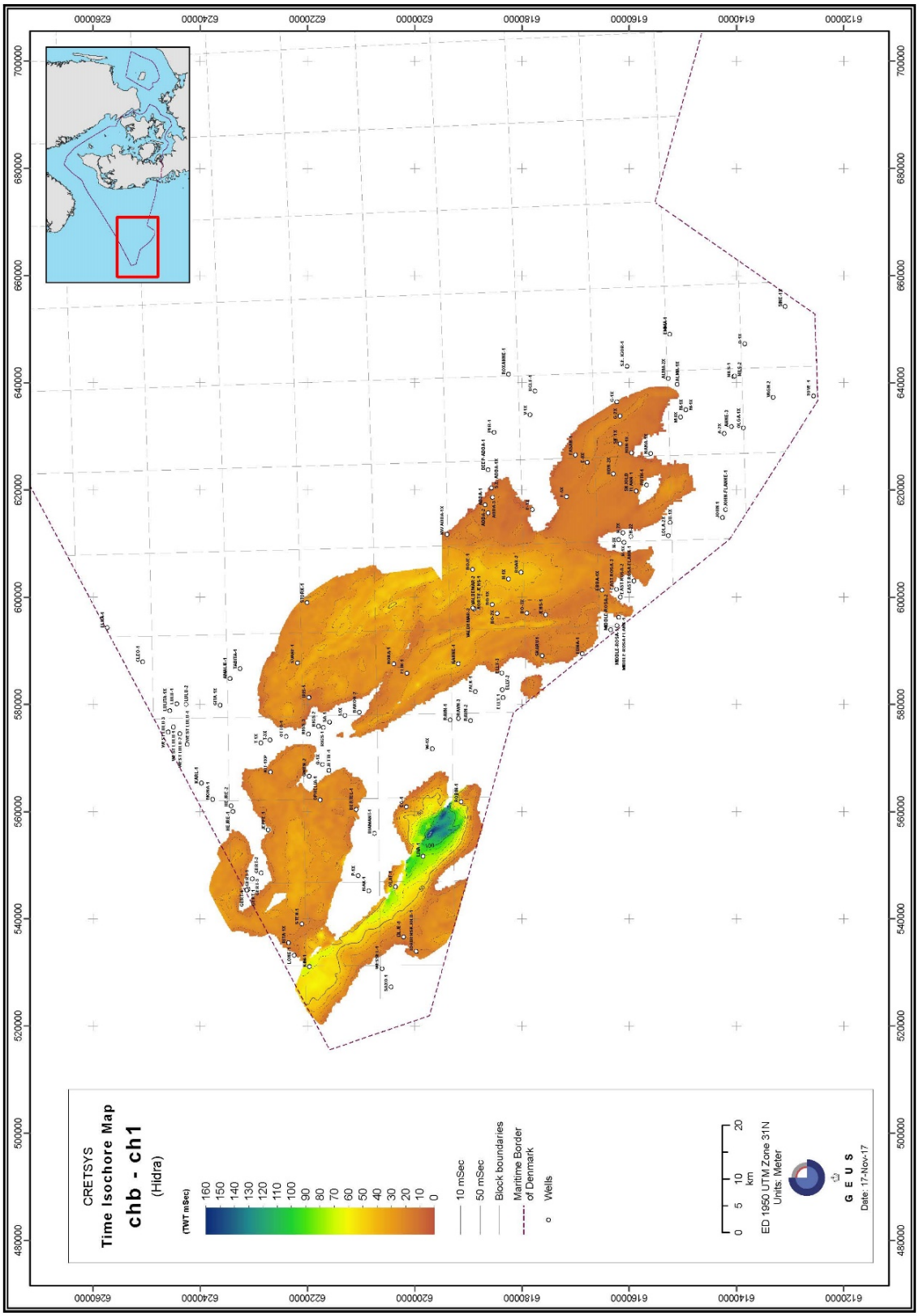

App. 8B: Time isochore map: **ch1 – ch7** (Hod A+B)

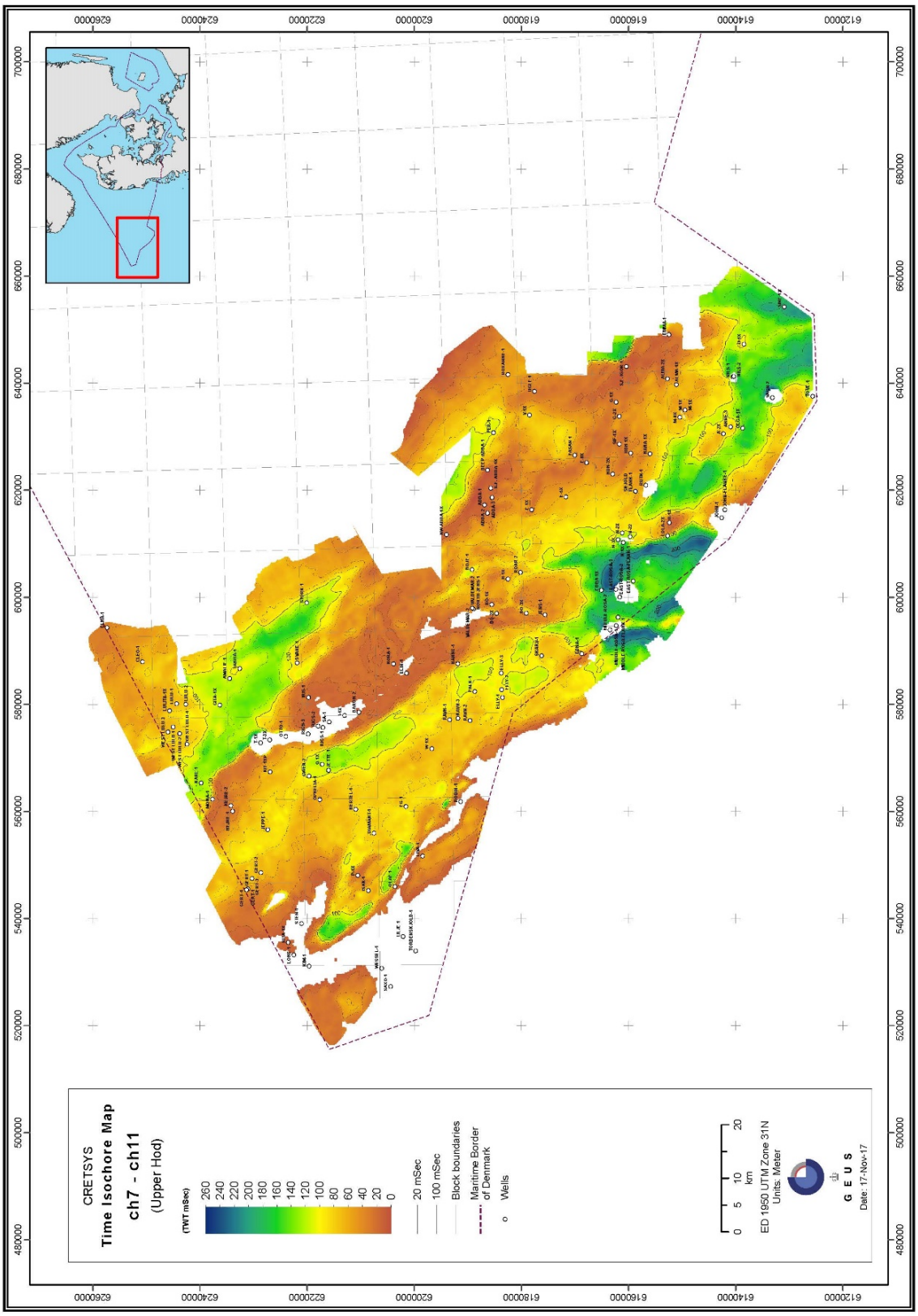

App. 8B: Time isochore map: **ch7 – ch11** (Hod C+D)

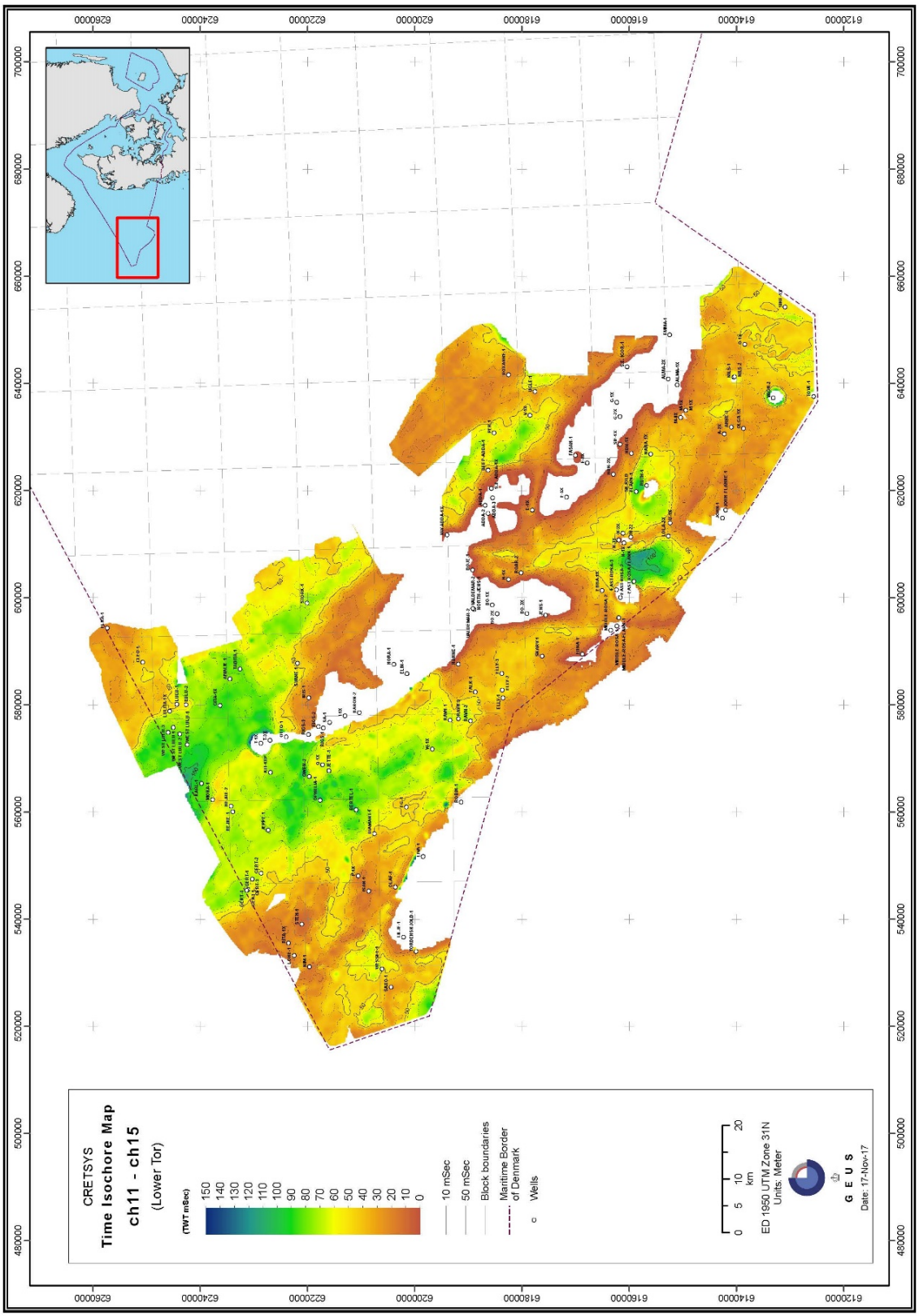

App. 8B: Time isochore map: **ch11 – ch15** (lower Tor)

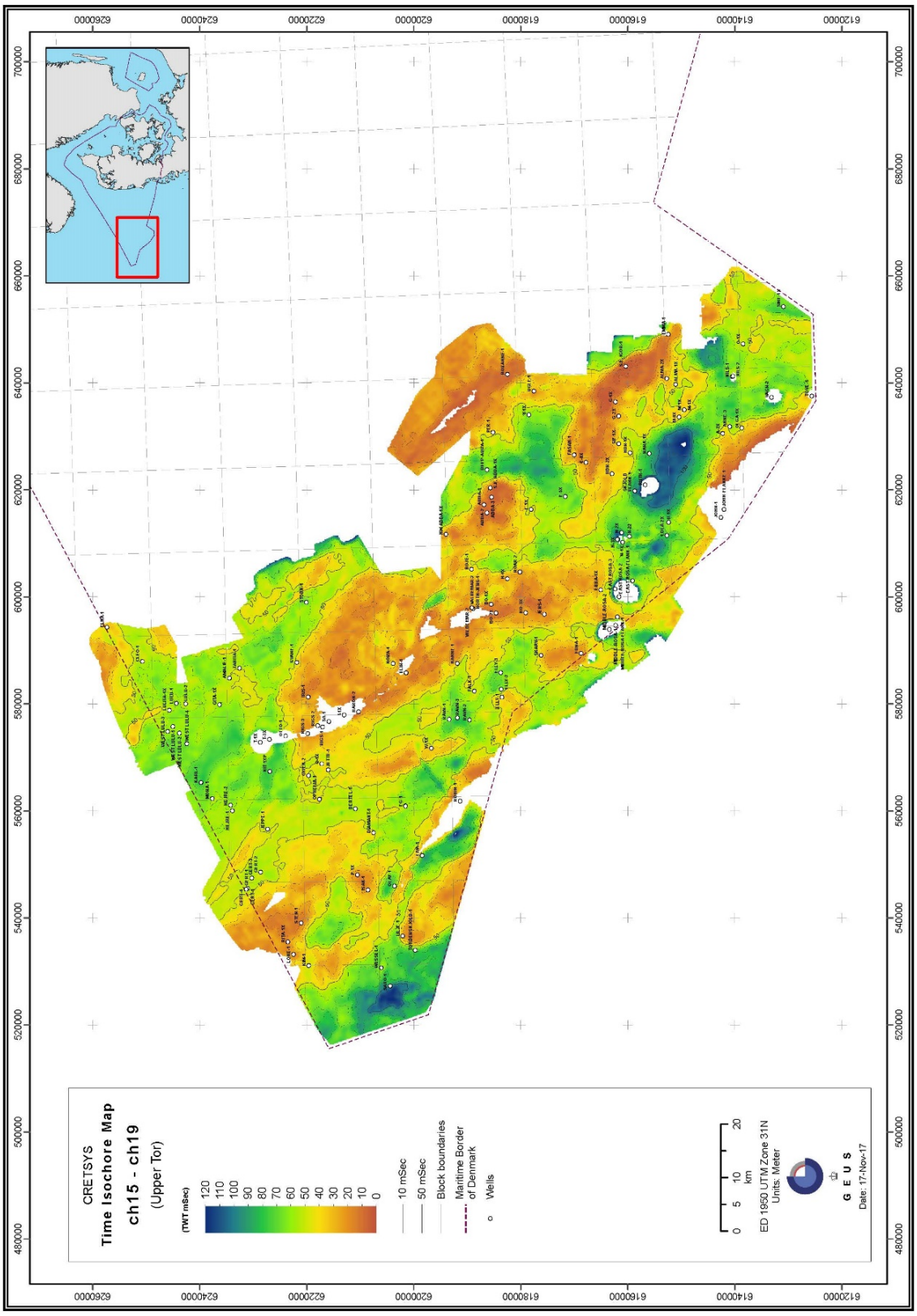

App. 8B: Time isochore map: **ch15 – ch19** (Upper Tor)

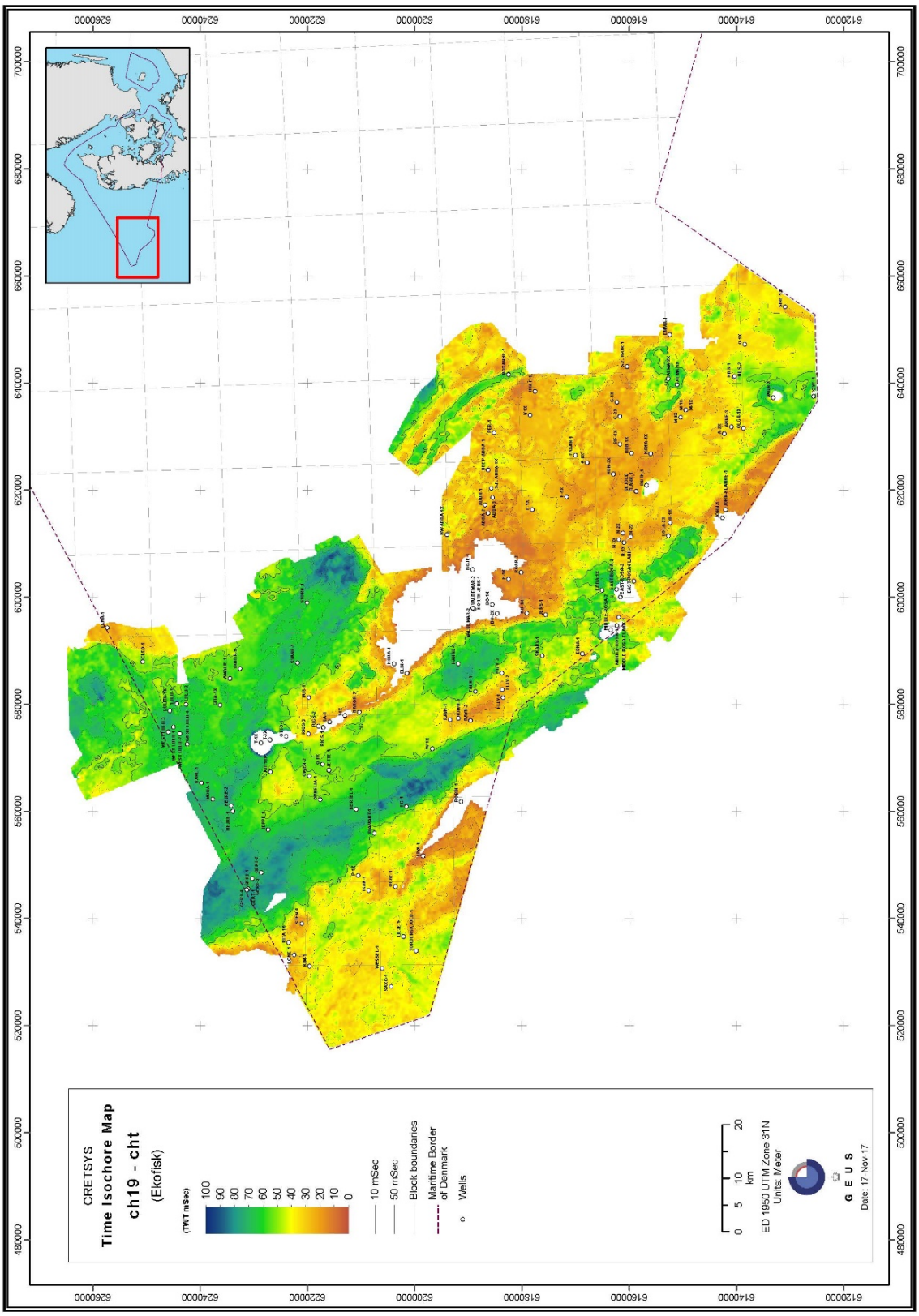

App. 8B: Time isochore map: **ch19 – cht** (Ekofisk)

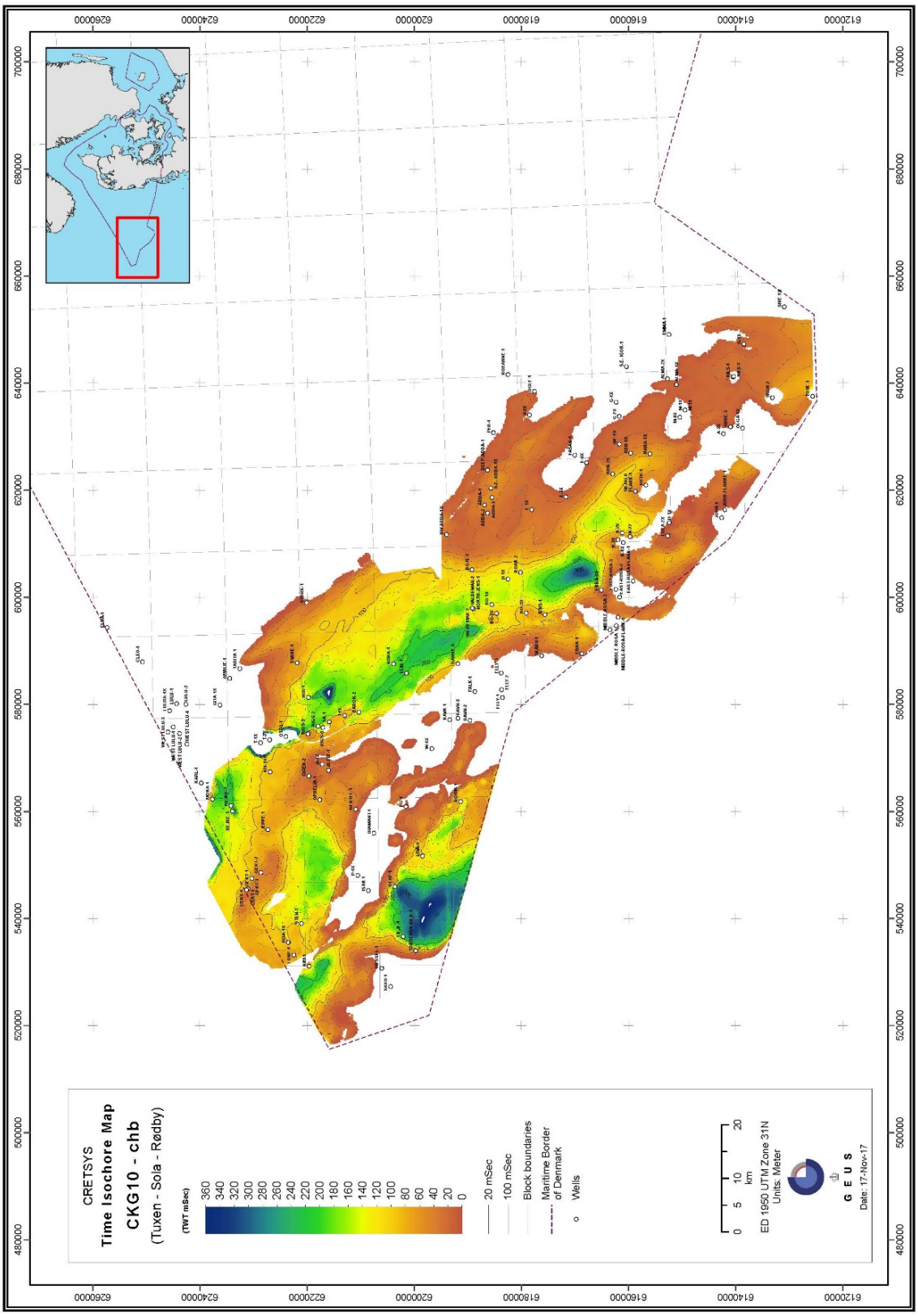

App. 8B: Time isochore map: **CKG10 – chb** (Tuxen, Sola Rødby)

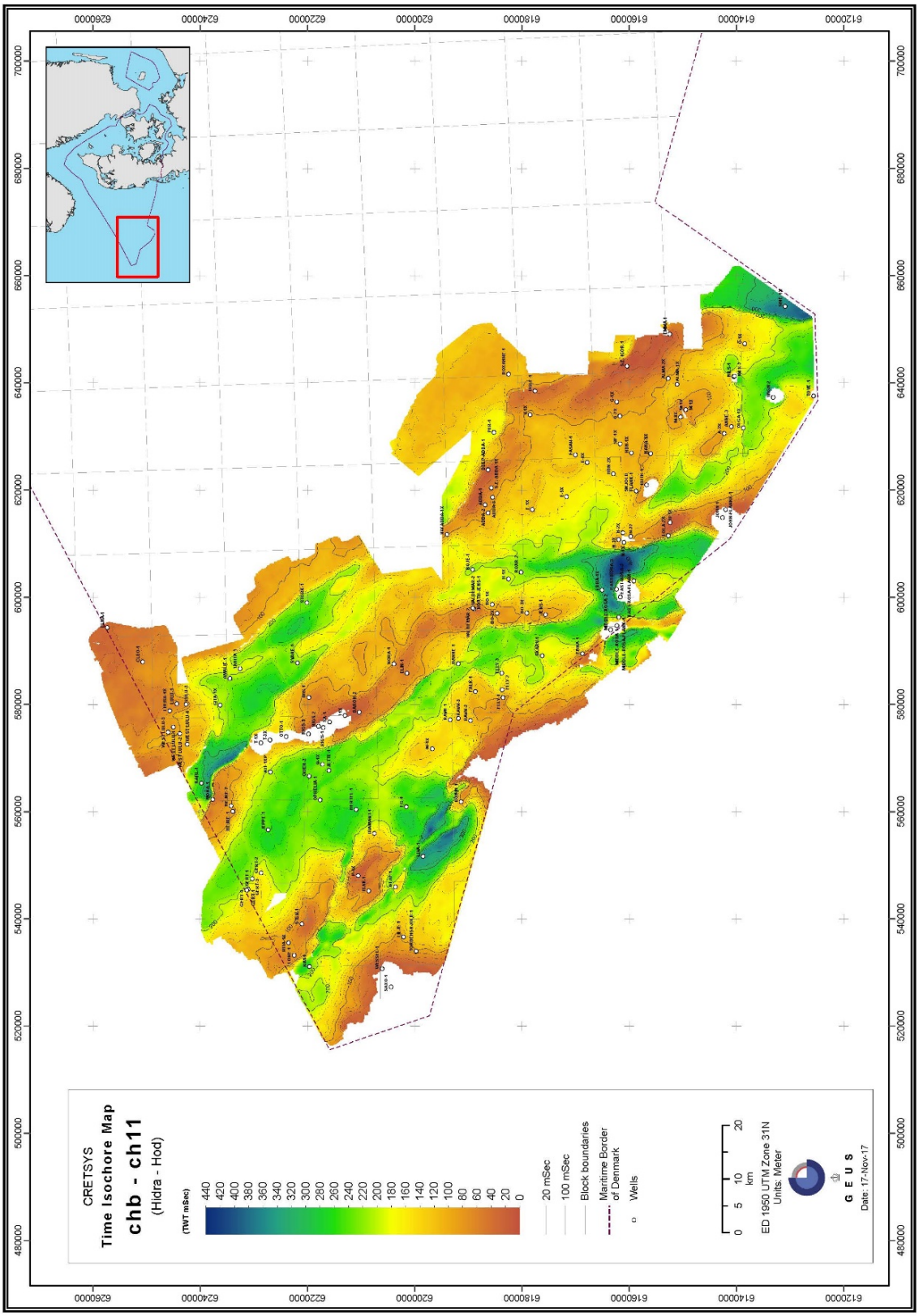

App. 8B: Time isochore map: **chb – ch11** (Hidra, Hod)

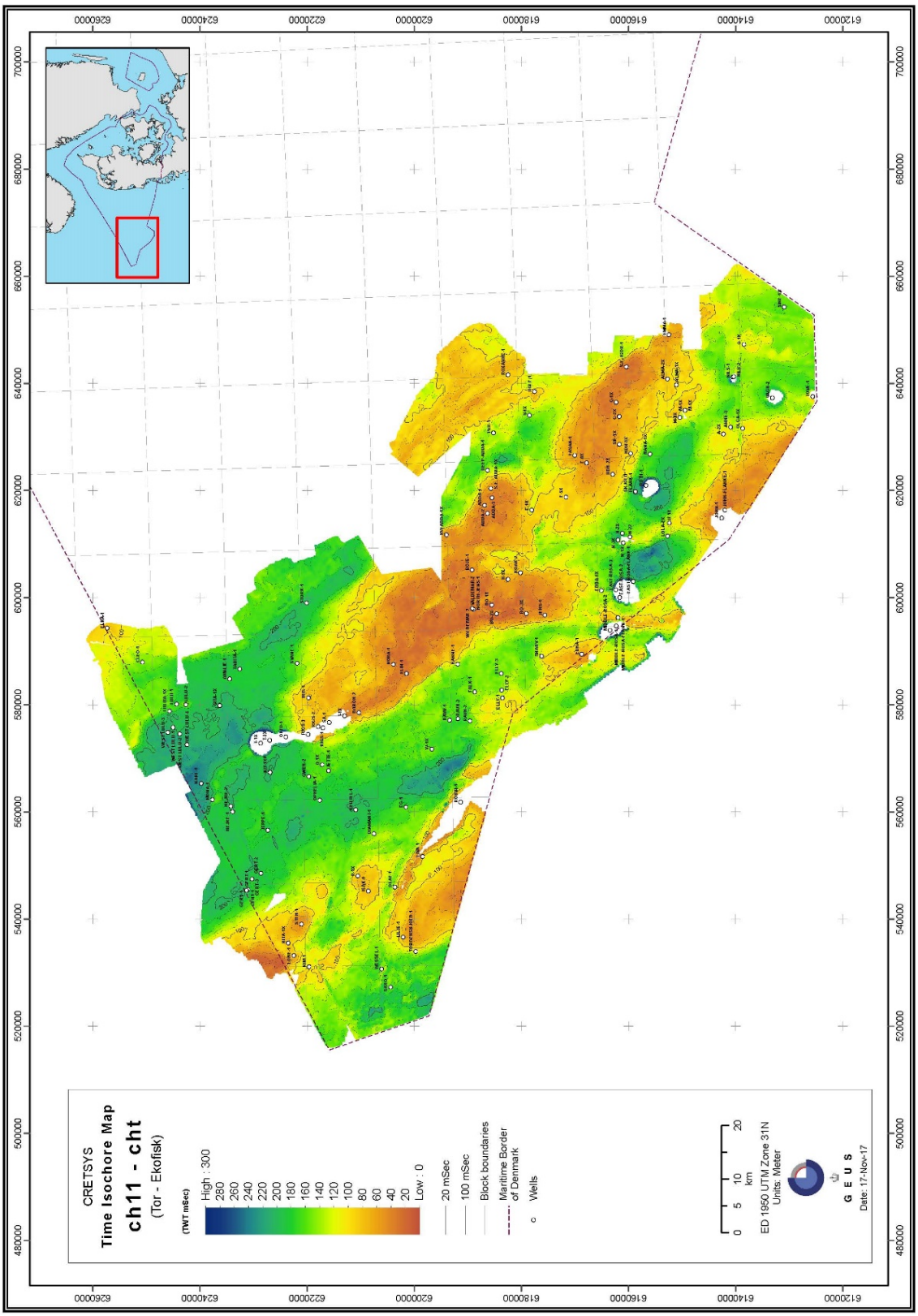

App. 8B: Time isochore map: **ch11 – cht** (Tor, Ekofisk)

8C Base Cretaceous Unconformity (BCU)

In the Danish Central Graben the Base Cretaceous Unconformity (BCU) defines the Jurassic-Cretaceous boundary separating the Jurassic syn-rift sequence from the Cretaceous post-rift sequence.

The BCU can be identified throughout large areas of the North Sea basin. The BCU is clearly defined from wireline logs and has a distinct seismic character making it an important marker that can be correlated and mapped in major parts of the North Sea.

The BCU is not a single event but represents the merging of surfaces (Kyrkjebø et al. 2004). The unconformity displays great local complexity and great variability on a regional scale and the seismic character varies throughout the Central Graben. The unconformity associated with the BCU marker demonstrates nonconformities, disconformities, angular unconformities as well as hiatuses spanning long periods of time. These variations reflect the different structural setting within a diversity of basins.

8C.1 Log definition of the BCU

In most of the Danish Central Graben the BCU is an unconformity representing a time gap of varying duration and is easily identified by a distinct shift in the log pattern representing the change from Cromer Knoll Group marly mudstones to Upper Jurassic claystones. In many wells located in the basin centre the BCU represents the boundary between the organic rich sediments of the Upper Jurassic Mandal Formation and the sediments of the Valhall Formation (including the Leek Member and Vyl Formation). The transition is normally characterised by an upwards decrease in gamma ray response and a corresponding increase in sonic velocity related to the change in lithology.

However, this is not always the case. Along the western flank of the Ringkøbing Fyn High the Upper Jurassic and Early Cretaceous succession comprises sandy/silty intervals and the BCU is interpreted as marking the transition between the sandstone and the overlying Cromer Knoll Group marl- and claystones. In the V-1 well the sandstone referred to the Vyl Formation by Jensen et al. (1986) is located above the seismic BCU marker and the sandstone interval is considered as part of the Cromer Knoll Group (Fig. 8C.1). Biostratigraphic data from the sandstone interval indicate a (Early Ryazanian to) Lower Valanginian age for the Vyl sand.

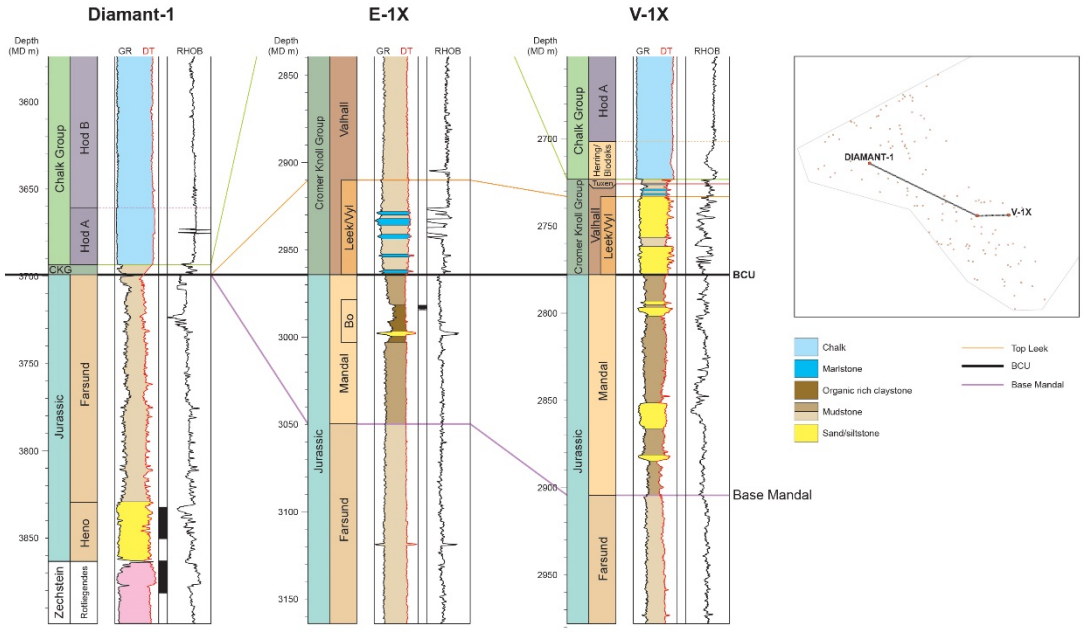

Fig. 8C.1. *Log correlation between wells with different BCU interpretations. In Diamant-1 the BCU is associated with a major hiatus (a time gap spanning the Volgian to Santonian). The BCU in E-1 is defined at the boundary between the Mandal Formation and the Valhall Formation with a well-developed Leek Member. In V-1 the BCU is associated with the base of the Vyl Formation.*

8C.2 Seismic determination of the BCU

In large parts of the Danish Central Graben the BCU seismic marker corresponds to the lithological change from Upper Jurassic/Ryazanian shales to the marly deposits of the Cromer Knoll Group. Synthetic seismograms demonstrate that this transition is associated with a characteristic distinct positive seismic reflector (peak). A similar distinct seismic reflector appears when Lower Cretaceous successions overlie pre-Jurassic strata. In the area along the Coffee Soil Fault, the BCU reflector is less distinct at the transition from the sandy Jurassic to the Lower Cretaceous.

The time structure map on the BCU is shown in Fig. 8C.2.

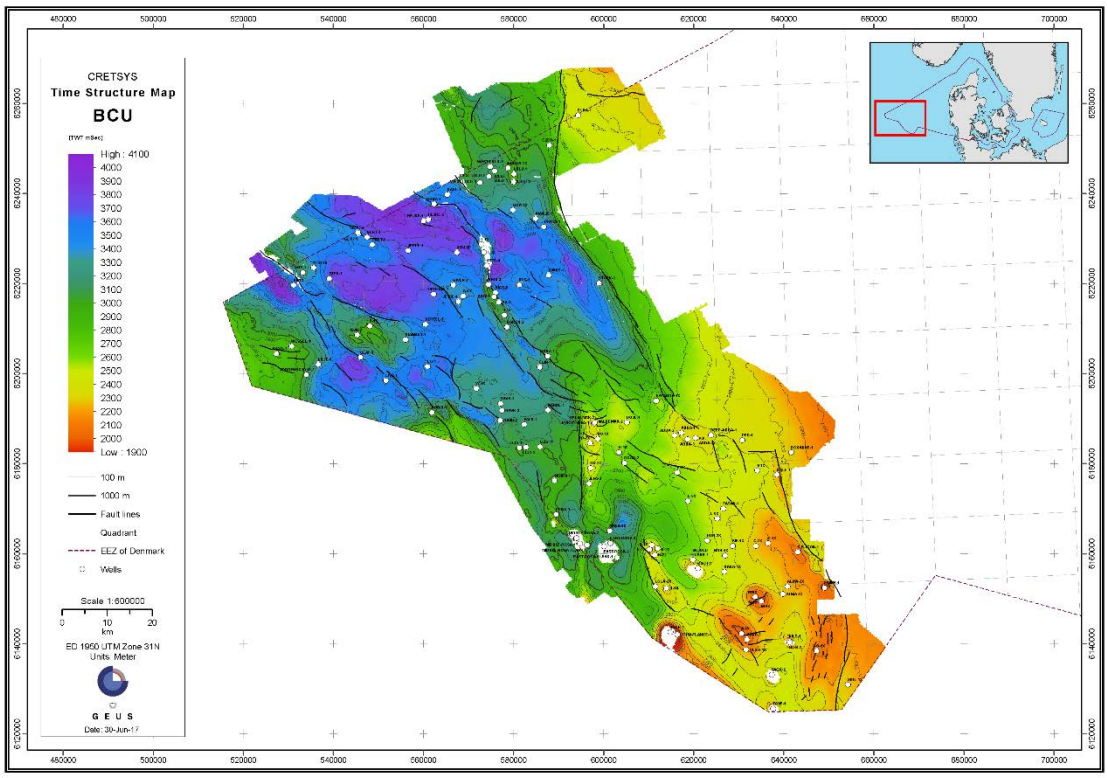

Fig. 8C.2. *Time structure map on the BCU with indication of fault traces at BCU level.*

8C.3 Geological setting

The transition from a syn-rift setting during the Jurassic to post-rift regimes during the Cretaceous is associated with tectonic activity and changes in the basin development which can be illustrated by comparison of BCU sub-crop and super-crop formations. The transition coincides with the Late Ryazanian transgression that generated a marked facies shift. In the Danish Central Graben the transition from syn-rift to post-rift tectonic regimes is relatively gentle, with the most active period of extension ending in the Ryazanian (in the Norwegian sector the extension period terminated locally as early as the Volgian (Færseth et al. 1995)). In some places, however, faulting continued well into the Cretaceous.

The present day structural situation of the BCU shows evidence of significant impact of post-Jurassic tectonic activity, which includes normal faulting as well as inversion and reverse faulting. In most cases, the faulting is associated with reactivation of older Jurassic faults and thus controls the structural development during the Cretaceous (Fig. 8C.2).

8C.4 BCU sub-crop and super-crop

BCU sub-crop

The Jurassic succession sub-cropping the BCU shows evidence of truncation (Petsys project). The degree of truncation depends on the structural position within the basin. The truncation of the Jurassic is generally moderate in most parts of the Central Graben, but locally severe erosion of the Jurassic is seen, and also on structural highs, where the Jurassic is absent (Fig. 8C.3).

Fig. 8C.3. *BCU sub-crop map with indications of degree of truncation into the Jurassic. Gentle truncation is associated with fault activity in the central part of the Central Graben. On structural highs deep erosion of the Jurassic is recognised. On the Ringkøbing Fyn High and on the Inge High the BCU marker forms the top of Paleozoic or older rocks (basement).*

BCU super-crop

In most of the Central Graben sediments of the Lower Cretaceous Cromer Knoll Group overlie the BCU. The structural situation associated with the BCU indicates a surface with a palaeo-relief of some magnitude. The earliest Lower Cretaceous deposits are found in basin centres. The Valhall Formation appears as a transgressive event and successive younger deposits are found along the basin margins. On highs and platforms the BCU is overlain by Late Cretaceous sediments (Fig. 8C.4).

The oldest Cromer Knoll Group deposits are found in the basin center and are associated with calcareous claystones-marlstones of the Leek Member (Jensen et al. 1986). The Leek Member is a slightly diachronous lithological unit and gradually younger deposits are found up-slope in the basin. The Leek Member is thickest in the basin centre (often overlain by claystone related to a transgressive systems tract). On the basin slopes the Leek Member becomes thinner and the top of the Leek Member corresponds to a MFS (maximum flooding surface) towards the basin margins.

High areas such as the Heno Plateau and the Mid North Sea High were subsequently submerged during the Cretaceous. Upper Cretaceous chalk is found directly overlying the BCU on the Inge High and on the Ringkøbing Fyn High.

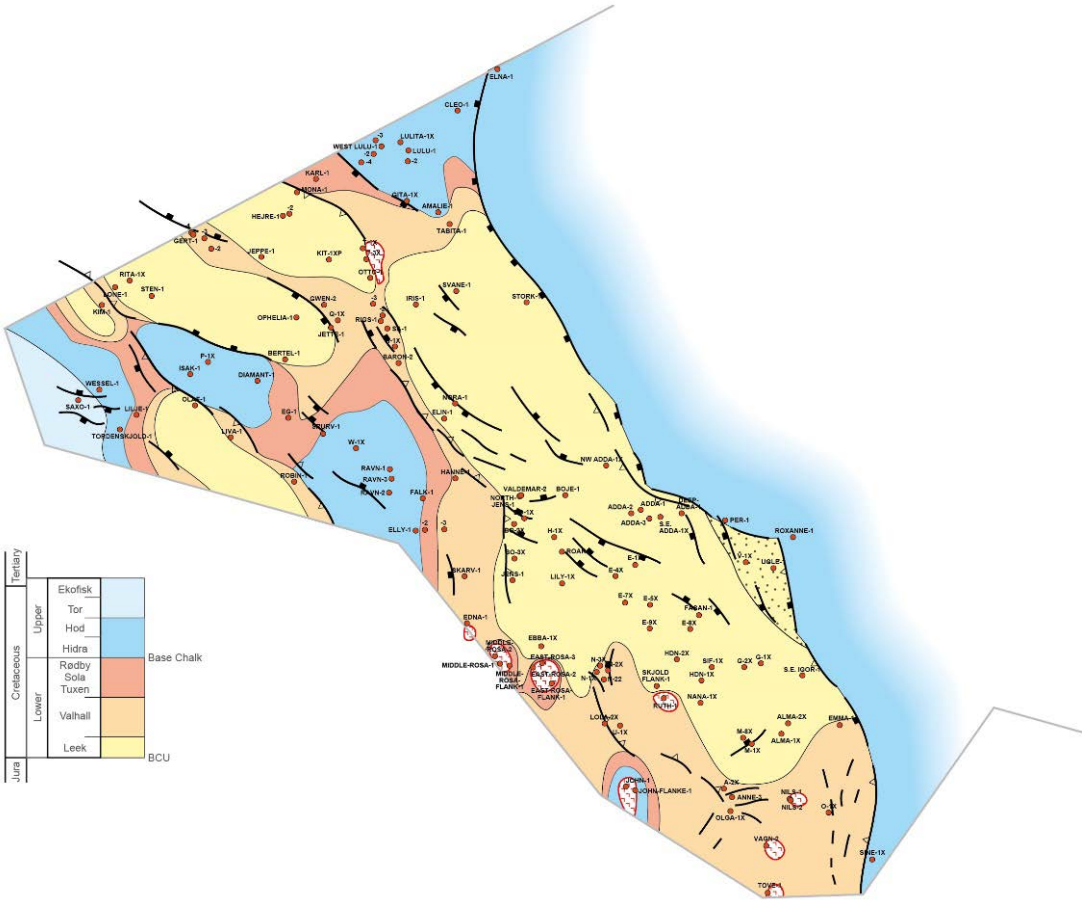

Fig. 8C.4. *BCU super-crop map. The initial Early Cretaceous sedimentation (deposition of the Leek Member) took place in the local basin centres. In a narrow zone along the Ringkøbing Fyn High the sandy Vyl Formation was deposited. During the succeeding transgression the rims of the basins were submerged. Platforms and highs were flooded during late Late Cretaceous.*

In the V-1 well the BCU seismic marker is interpreted as being below the sandy Vyl Formation of Late Ryazanian to earliest Valanginian age (Jensen et al. 1986). In the Petsys project the Vyl Formation was included in the sandy Poul Member, but as the interval is separated from the underlying sandy interval (Poul Member) by the distinct BCU marker, the Vyl Formation is considered as part of the Cromer Knoll Group in this study (Fig. 8C.5).

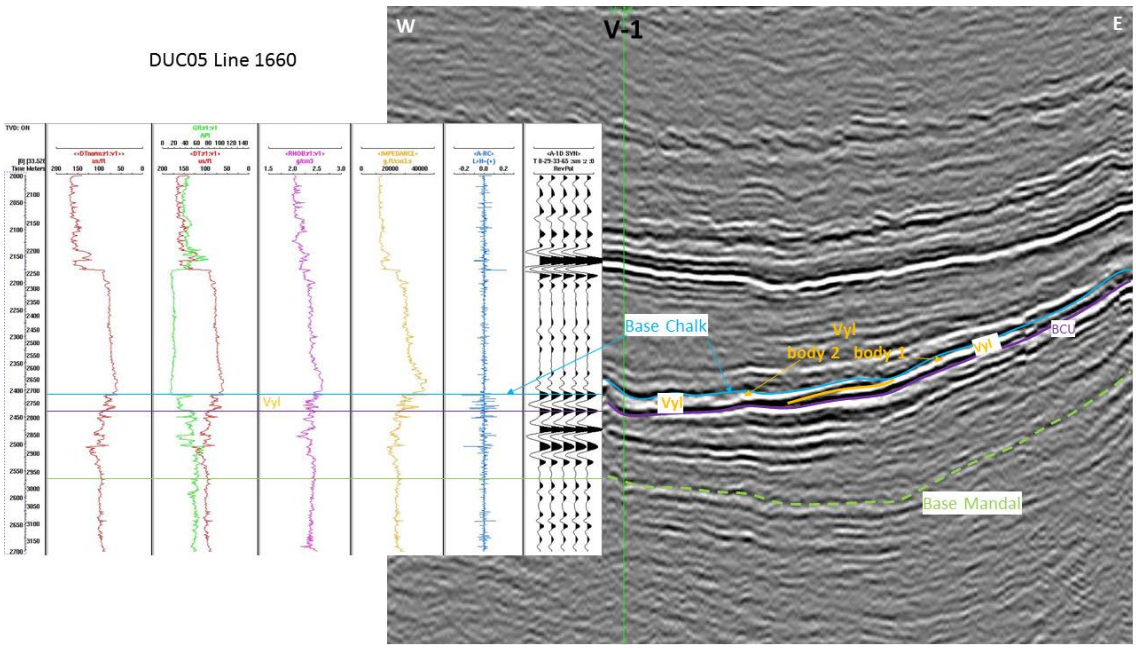

Fig. 8C.5. *Seismic interpretation of the Vyl Formation in the V-1 well. The seismic data indicate the presence of two sedimentary bodies (lobes) associated with the Vyl Formation between the Base Chalk and the BCU seismic markers. (DUC05 line 1660).*

The distribution of the Vyl Formation is restricted to a narrow zone along the Coffee Soil Fault and may be associated with a structural development similar to the Upper Jurassic Poul Member. This indicates that fault activity during Late Jurassic along the fault zone continued into the Early Cretaceous.

Only two wells encounter Vyl Formation sensu stricto (the V-1 and Ugle-1 wells). However, thin sand intervals of indeterminate Ryazanian-Valanginian age have been drilled in the Amalie-1 and Tabita-1 wells. These sand intervals are found at the seismic BCU marker and may represent a Vyl Formation equivalent.

References

Færseth R.B., Sjøblom. T.S., Steel, R.J., Liljedahl, T., Sauar, B.E. & Tjelland, T. 1995. Tectonic controls on Bathonian-Volgian syn-rift successions on the Visund fault block, northern North Sea. *In:* Steel, R.J., Felt, V.L., Johannesen, E.P. & Mathieu, C. (eds) Sequence Stratigraphy on the NW European Margin. Norwegian Petroleum Society Special Publication, **5**, 325-346.

Jensen, T.F., Holm, L., Frandsen, N. & Michelsen, O. 1986. Jurassic – Lower Cretaceous lithostratigraphic nomenclature for the Danish Central Trough. Danmarks Geologiske Undersøgelse, serie A, nr. 12.

Kyrkjebø, R., Gabrielsen, R.H. & Faleide, J.I. 2004. Unconformities related to the Jurassic-Cretaceous synrift - post-rift transition of the northern North Sea. Journal of the Geological Society, London, **161**, 1-17.

PETSYS 2015. Skaarup et al.: The Jurassic Petroleum System in the Danish Central Graben. Technical notes. Danmarks og Grønlands geologisk Undersøgelse, Rapport 2015/22. (Confidential)

8D Mandal Formation

In the Cretsys project the Mandal Formation has been added to the Cretaceous stratigraphy. The Mandal Formation is a well-defined stratigraphic unit in the Norwegian sector (Vollset & Doré 1984) but has an unclear distribution towards the south into the Danish sector. In large parts of the Danish Central Graben the uppermost Upper Jurassic succesion exhibits close similarities with the Mandal Formation in the Norwegian sector and it is therefore possible to extend the Mandal Formation into the Danish sector.

In the Petsys project, the uppermost Jurassic succesion is referred to the Farsund Formation comprising the Bo Member (the informal "Hot Unit", Jensen et al. 1986) in the basin centre, and the Poul Member (embracing the Poul Formation (Michelsen et al. 2003) and Vyl Formation (Jensen et al. 1986)) along the margins of the Coffee Soil Fault.

The uppermost part of the Farsund Formation is time equivalent to the Mandal Formation defined in the Norwegian sector (Vollset & Doré 1984). Several attempts have been made to introduce the Mandal Formation to the Danish Sector (Ineson et al. 2003 and Dybkjær 1998), but a formal definition of a Mandal Formation has not yet been established. The use of the Mandal Formation in the Danish sector is mostly restricted to the northern part of the Central Graben (towards the Norwegian border), but Dybkjær (1998) found evidence in the Bo-1 well (type well for the Bo Member (Hot unit)) that Mandal Formation palynological characteristics can be found as far south as the Salt Dome Province in the southern Danish Central Graben.

In the Cretsys study we assign the uppermost Jurassic succession in the entire Central Graben to the Mandal Formation, but for the time being the Mandal Formation may still be considered as an informal stratigraphic unit in the Jurassic/Cretaceous section.

8D.1 Comparison of the Mandal Formation in the Norwegian and Danish sectors of the North Sea

The Mandal Formation as established in the Norwegian sector by Vollset and Doré (1984) consists of a dark grey-brown to black, slightly calcareous, carbonaceous claystone becoming fissile in places. It is characterised by a very high level of radioactivity, which is a function of organic carbon content. In addition it has an anomalously low velocity, a high resistivity and a low density. It may contain thin stringers of limestone/dolomite and in some areas, sandstone. The contacts of the Mandal Formation with underlying and overlying sediments are easily recognised on logs due to its high gamma ray and resistivity readings and its low velocity and density.

Palynological investigation of the organic rich Mandal Formation in the type well 7/12–3A, indicates that the age of the formation is mainly Late Volgian to Late Ryazanian, although the lower part may extend into the Middle Volgian. Dating is based on the last occurrence of *Rotosphaeropsis thula* at the upper boundary of the formation and of *Glossodinium dimorphum* immediately above the lower boundary. Identification of a number of stratigraphically important bioevents has permitted a detailed correlation of the Mandal Formation in its type well with the equivalent organic-rich shales in the Bo-1 well from the Danish Central Graben (Fig. 8D.1, from Dybkjær, 1998).

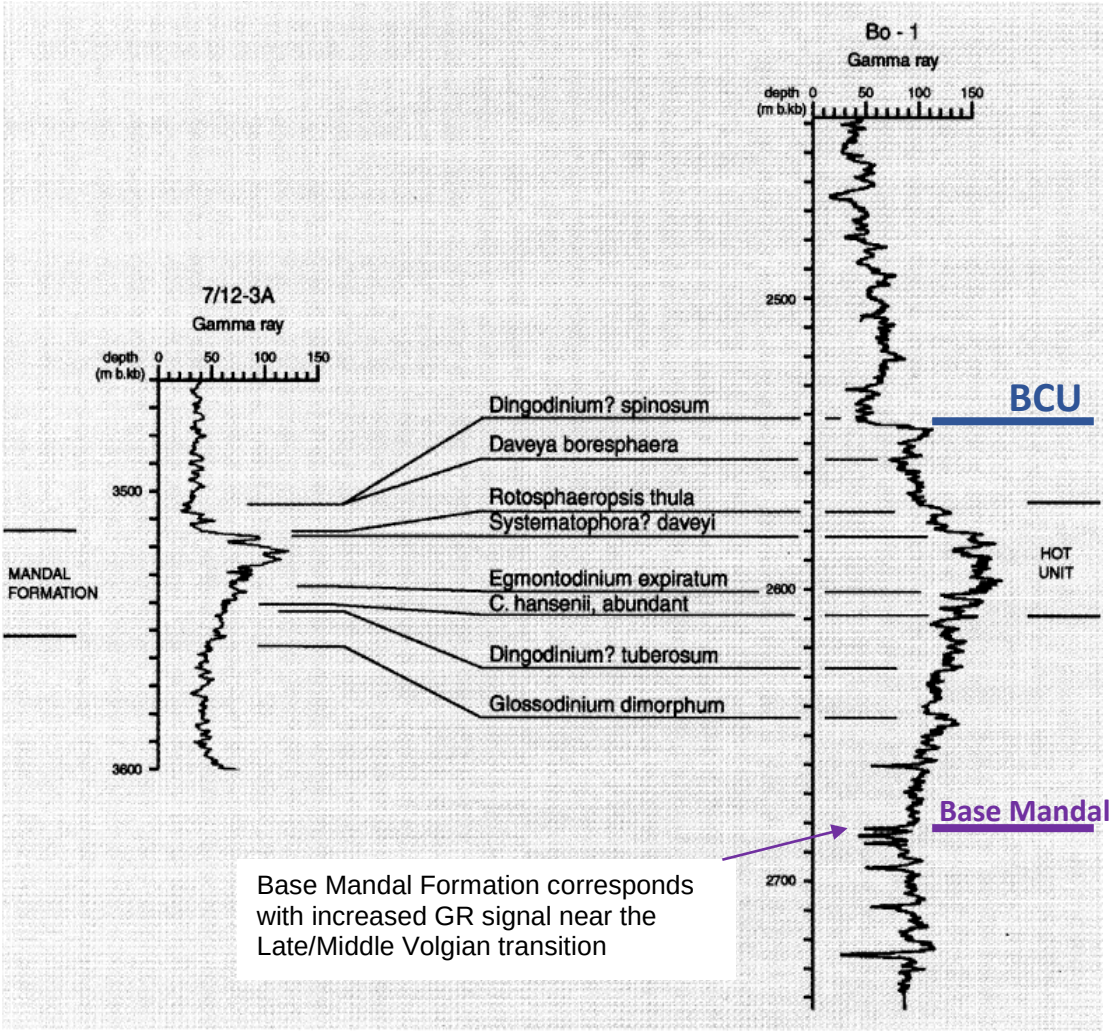

Fig. 8D.1. *Correlation between the Mandal Formation in the Norwegian reference well 7/12-3A and the time equivalent succession in the Bo-1 well. The delineation of the Mandal Formation in the Danish Central Graben is indicated. The Base Mandal Formation corresponds with an increase in the gamma ray near the Late/Middle Volgian boundary. Top Mandal Formation is associated with the BCU. Modified from Dybkjær 1998.*

8D.2 Lithostratigraphy

The introduction of the Mandal Formation into the Danish Central Graben requires a revision of the Upper Jurassic lithostratigraphy. In the present study a new lithostatigraphic subdivision for the Latest Jurassic to Early Cretaceous interval has been introduced (Fig. 8D.2).

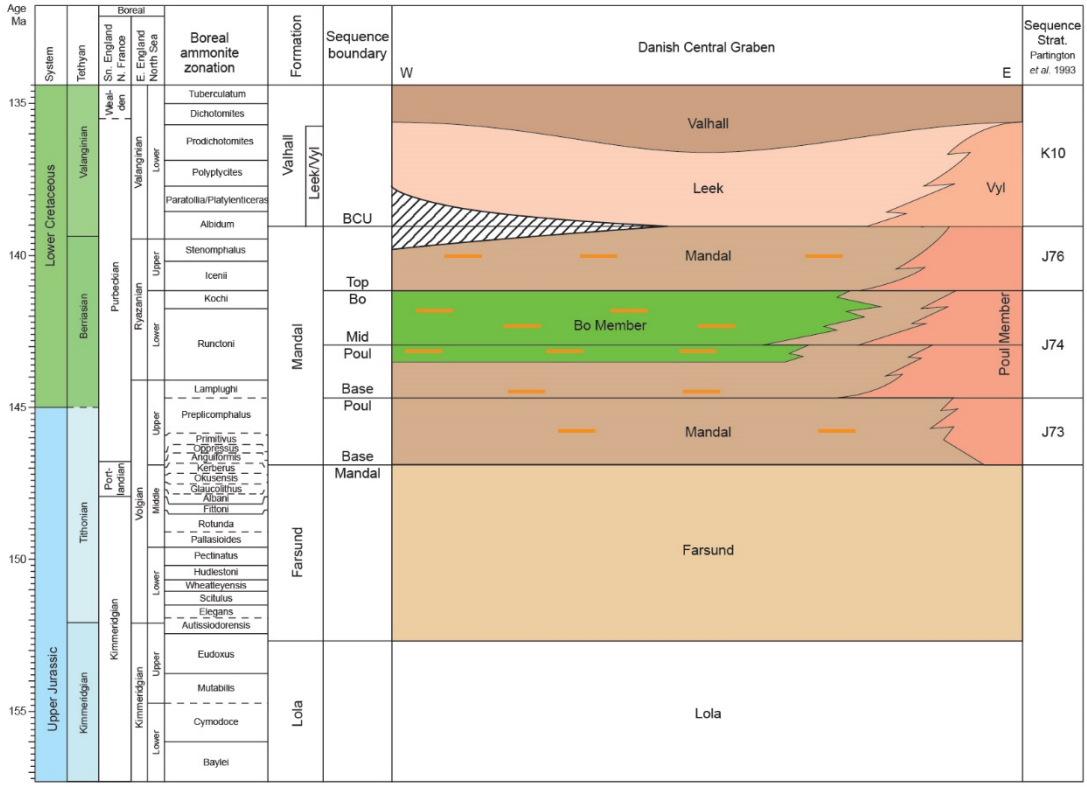

Fig. 8D.2. *Lithostratigraphic scheme covering the transition from the Upper Jurassic to Lower Cretaceous in the Danish Central Graben.(Chronostratigraphy from Gradstein 2012).*

In the new lithostratigraphy the uppermost part of the Farsund Formation as defined by Michelsen et al (2003) is substituted by the Mandal Formation. The Mandal Formation ranges in age from Late Volgian to Late Ryazanian (?Early Valanginian). The Mandal Formation includes the Bo Member and the Poul Member. The present study indicates that the Vyl Formationof Jensen et al. (1986) forms part of the Cromer Knoll Group and may be contemporaneous with the Leek Member.

The dark grey-brown to black, slightly calcareous, carbonaceous claystones of the Mandal Formation represent a change from the open marine claystone deposits of the Farsund Formation to a more restricted deep-water environment.

The Bo Member represents an organic rich interval and is recognised by high gamma ray values distinctly separate from the gamma ray values of the surrounding claystone.

There are no specific minimum GR values defining the upper and lower boundaries of the Bo Member and in many wells the determination of the boundaries is often based on subjective assumptions. The Bo Member as defined by high GR values, disappears towards the marginal parts of the basin, partly due to the increasing content of coarse clastic deposits. Locally, the Bo Member comprises stringers and intervals of silt/sandstone, and along the margin of the Ringkøbing Fyn High the Bo Member gradually grades into the Poul Member.

The Poul Member comprises upwards fining units grading from fine sands and siltstones to more clay-rich deposits. The Poul Member is predominantly associated with gravity-flow sandstones. The sandstone occurs as massive sand beds and as isolated lobes. Along the Coffee Soil Fault stacked sandy/silty deposits dominate the Poul Member. Basinwards claystone dominates the succession and only the sandy intervals are considered as part of the Poul Member.

Gravity flow deposits formed by turbidite currents are common throughout the Mandal Formation in the basin centre. The turbidites are most likely connected to the gravity flow deposits of the Poul Member, but are not included in the Poul Member as the turbidites are often found as isolated sandstone beds disconnected from the Poul Member.

8D.3 Seismic interpretation

The distribution of the Mandal Formation in the Danish Central Graben has been evaluated from seismic data. The top of the Mandal Formation is associated with the well-defined Base Cretaceous Unconformity. The Base Cretaceous Unconformity is an easily recognised seismic event in basinal areas (strong peak) marking the top of the underlying Mandal/Farsund shales which are characterized by low impedance.

The base of the Mandal Formation is picked in a weak trough marking a downwards increase in acoustic impedance (Fig. 8D.3). It is tied into selected wells and marks the base of TOC-rich mudstones of Late Volgian and Ryazanian age with elevated GR-readings.

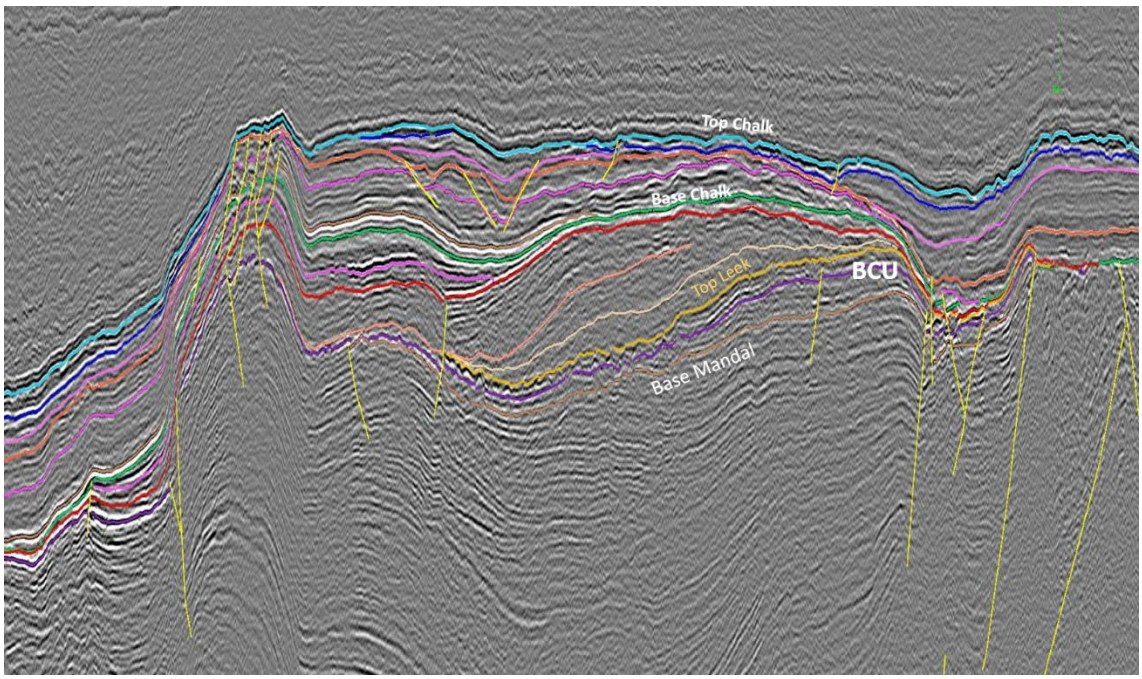

Figure 8D.3. *Seismic profile showing seismic markers related to the Mandal Formation. (DUC05 line 1400)*

A time structure map on Base Mandal is shown in Fig. 8D.4. (The map is uploaded onto the Cretsys website). The map indicates a widely distributed Mandal Formation in the central part of the Central Graben. The formation is bounded to the east by the Ringkøbing Fyn High and to the west by the Mid North Sea High.

The isochore map of the Mandal Formation (Fig. 8D.5) reveals differential subsidence within the complex rift basin of the Central Graben. The deposition of the Mandal Formation took place while the tectonic regime changed from a phase of active extension and rapid fault-controlled subsidence in the Late Jurassic to regional subsidence in the Cretaceous. During the Late Jurassic the Danish Central Graben was segmented into a number of NW–SE-trending depocentres, separated by elongate highs or broad plateaus (Johannessen & Andsbjerg 1993; Andsbjerg & Dybkjær 2003; Johannessen 2003).

A thick Mandal Formation is found along the Coffee Soil Fault and along the major Mona Fault in the Gertrud Graben as a result of the synsedimentary fault activity. The Mandal Formation pinches out along inversion structures in the basin centre and onto the Heno Plateau to the west.

The Mandal Formation is absent on structural highs (e.g. the Ringkøbing Fyn High and the Mandal High, Fig. 8D.5), as it is considered that these platform areas were partly sub-aerially exposed and subject to erosion. These areas are considered as sources for clastic input for the density flow deposits.

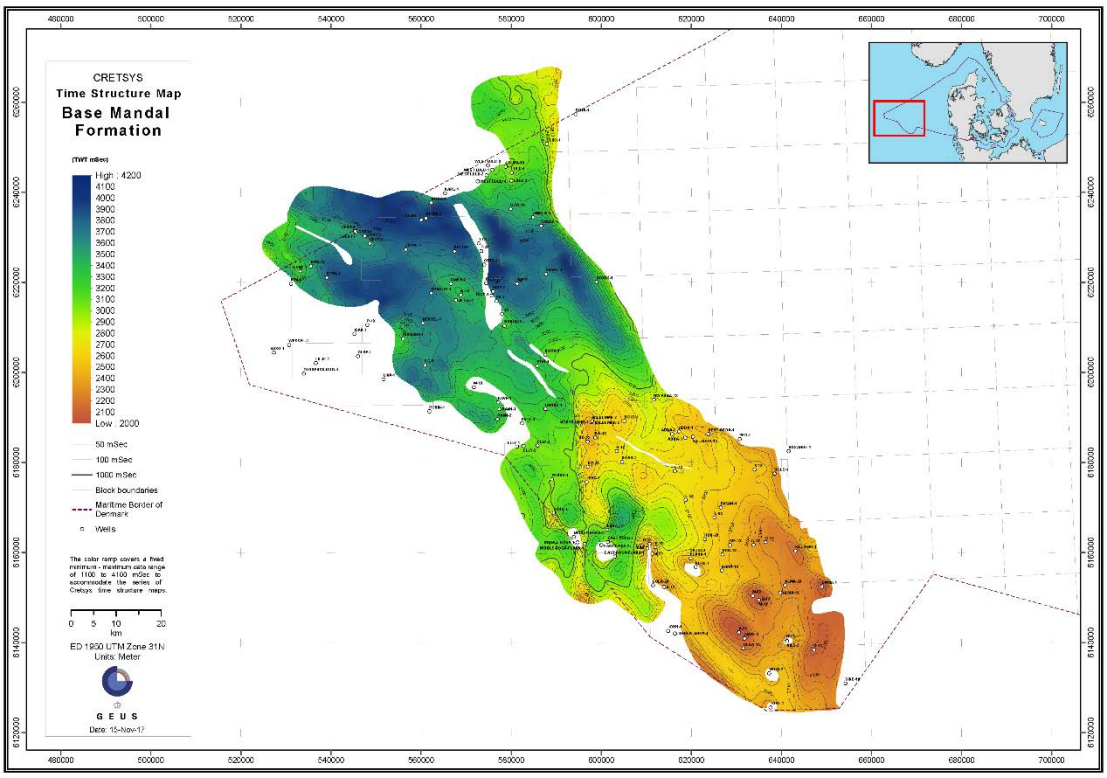

Fig. 8D.4. *Time structure map of the Base Mandal Formation. The Mandal Formation is absent on the Ringkøbing Fyn High, the Mandal High and on the Mid North Sea High.*

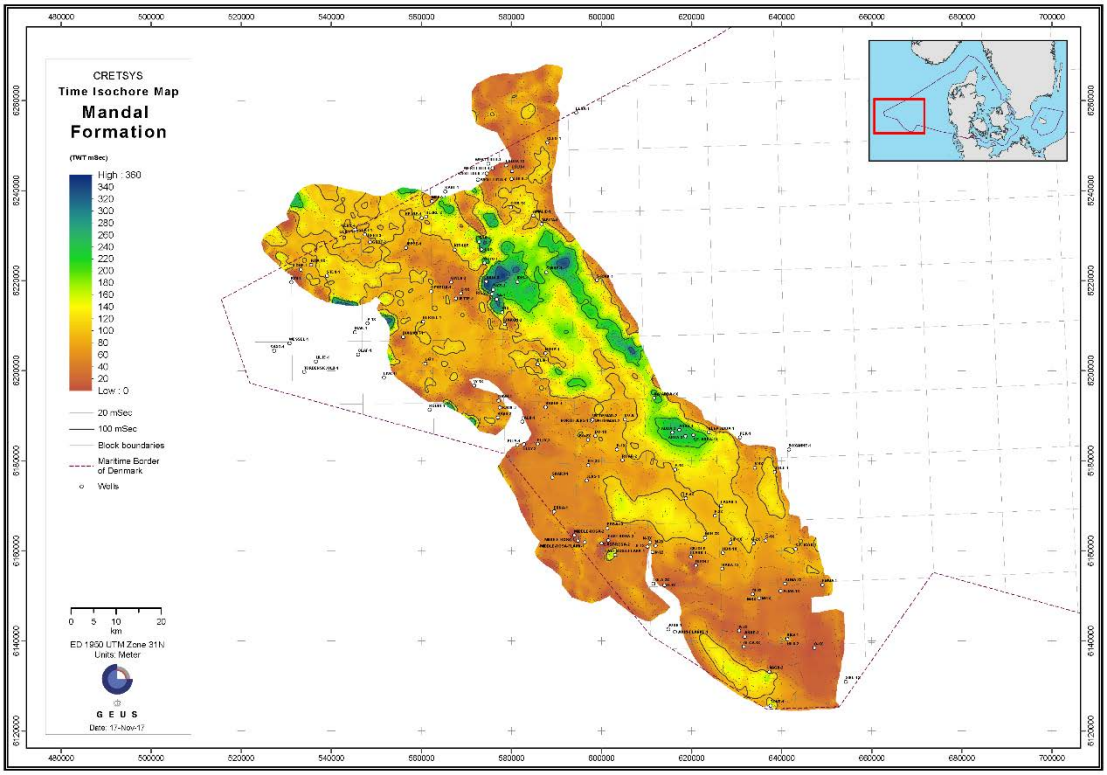

Fig. 8D.5. *Time isochore map of the Mandal Formation.*

8D.4 Log character

The Mandal Formation in the centre of the Danish Central Graben is recognised based on log character. Generally, the interval is characterised by high gamma ray and resistivity readings accompanied by low velocity and density values. An irregular pattern on the gamma ray log is due to sandy intervals, and along the Coffee Soil Fault the gamma ray readings are low due to the increase in the content of sandy/silty deposits (Fig. 8D.6).

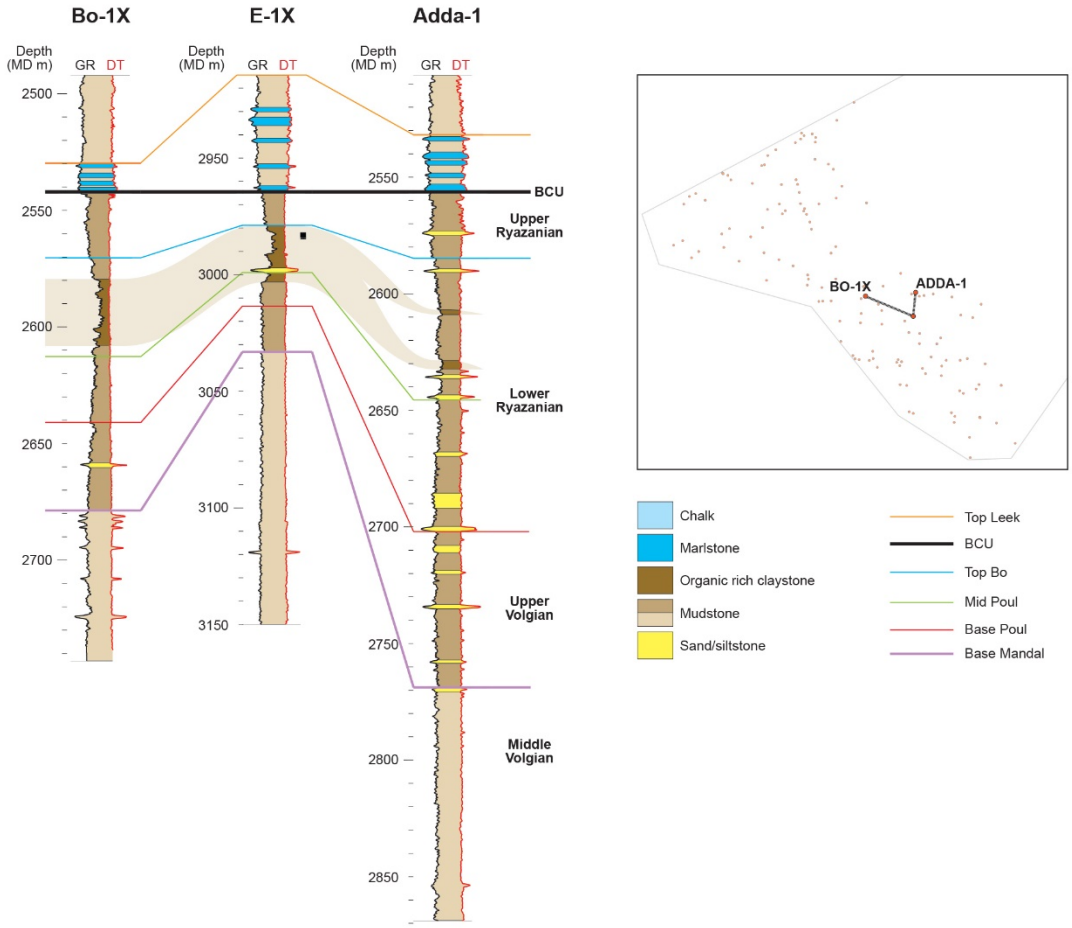

Fig. 8D.6. *Log correlation between the Bo-1, E-1 and Adda-1wells. In the basin centre (the Bo-1 and E-1 wells) the Mandal Formation is characterised by high GR readings in organic rich deposits. Along the Coffee Soil Fault (Adda-1) an increase in clastic components suppresses the gamma ray values.*

The base of the Mandal Formation corresponds to increased gamma ray values at the transition from the Middle Volgian to Upper Volgian succession. The base Mandal Formation boundary is associated with a weak seismic marker, which can be mapped in most of the Danish Central Graben (see Time Structure Map of the Base Mandal Formation, Fig. 8D.4).

The lower part of the Mandal Formation exhibits an upwards increase in gamma ray readings ('warming-upwards' interval, Ineson 2003) but the increase is less significant compared with that of the overlying Bo Member.

The Bo Member is defined by the characteristly high gamma ray values. In the Bo-1 well, the background gamma-ray values of the mudstones are in the 75–100 API range, but occasionally the Bo Member shows values ranging from 120 to 160 API with marked upwards shifts to higher and lower values defining the lower and upper boundaries of the member, respectively.

The Bo Member is not delineated by specific gamma ray value and because of variation in the degree in the development of the lower part of the Mandal Formation the location of the base (and the top) of the Bo Member is ambiguous.

Upwards the Bo Member grades into claystone with lower gamma ray readings. The interval above the Bo Member appears as a heterogeneous claystone with inter-fingering silty/dolomitic sandstone beds. The upper boundary of the Mandal Formation corresponds to the BCU and is overlain by the Cromer Knoll Group sediments.

In the eastern part of the Danish Central Graben, increased siliciclastic supply suppresses the organic signal related to the Bo Member and less distinct gamma ray values are common (e.g. Adda-1 in Fig. 8D.6).

8D.5 Distribution and development

Correlation of the Mandal Formation across the Central Graben (Figs 8D.7, 8D.8 and 8D.9) can be carried out with high confidence although some differences appear in the log character of wells located in the basin centre and wells located along the basin margin i.e. along the Coffee Soil Fault.

The Mandal Formation in the basin centre can be divided into a basal warming-upwards interval, an intermediate interval with high gamma ray readings (the Bo Member) and an upper heterogeneous claystone interval.

The intensity of the Bo Member gamma ray readings varies throughout the Central Graben with the highest gamma ray values in the basin centre and the lowest values near the basin margins. Sandy/silty stringers are often seen in the Bo Member and low gamma ray values in the Bo Member interval are interpreted to be a result of increased input of clastic and non-organic material, which suppresses the gamma ray values. The increased contribution of clastic deposits towards the basin margins reduces the thickness and number of "high gamma ray" beds and the Bo Member, sensu stricto, vanishes towards the basin margins.

In the marginal zone along the Ringkøbing Fyn High, the Mandal Formation encompasses sandy and silty intervals related to the Poul Member. The high gamma ray readings associated with the organic rich Bo Member are poorly developed (or absent) and here the Mandal Formation is dominated by interbedded sands/siltstones and claystones. The accumulated thickness of sands/siltstones decreases towards the basin centre.

In the wells drilled near the Ringkøbing Fyn High, the Mandal Formation reveals 4 depositional events representing upwards fining units (Fig. 8D.7). With a basal sandy/silty interval grading upwards into more silty/shaly deposits, the Mandal Formation is suggested to comprise 4 depositional sequences upwards bounded by maximum flooding surfaces.

In wells situated in a basinal setting, the Mandal Formation is generally more clay-rich and appears somewhat different compared with wells with a marginal setting. It is however, possible to identify 4 upwards fining sequences in the clay rich package (Figs 8D.6, 8D.7, 8D.8 and 8D.9). In most wells sandy/silty deposits represent the base of the sequences.

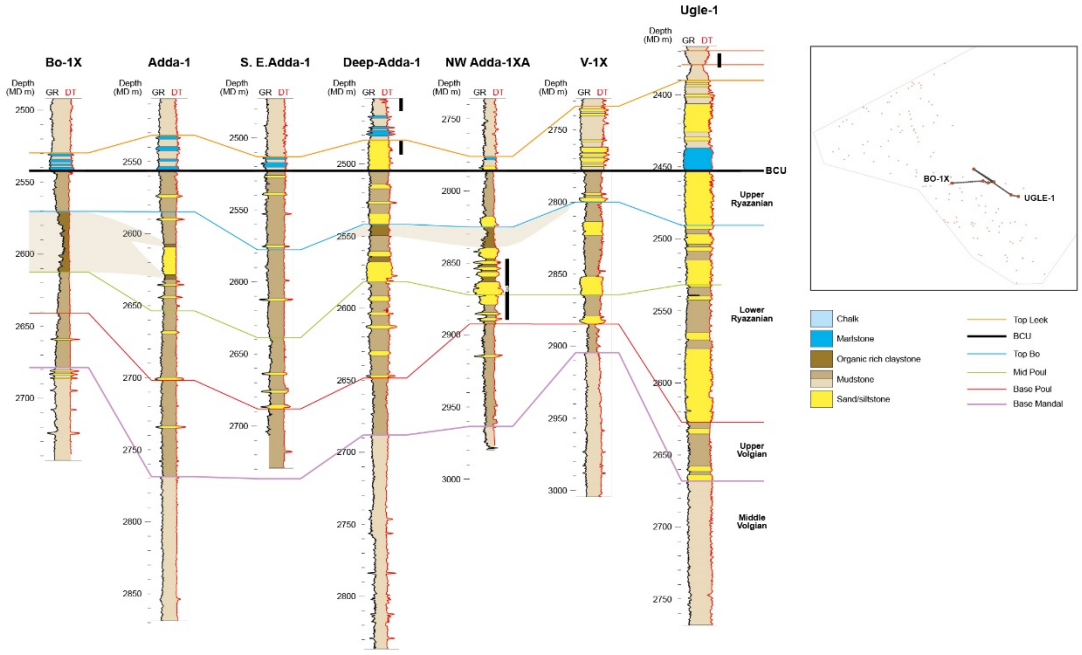

Fig. 8D.7. *Log correlation between wells in the Adda area. The log pattern in the wells exhibits 4 upwards fining sequences. The gamma ray values are surpressed by the influence of clastic input. Interbedded organic rich claystone and gravity-flow deposits are seen in the NW-Adda-1 cores.*

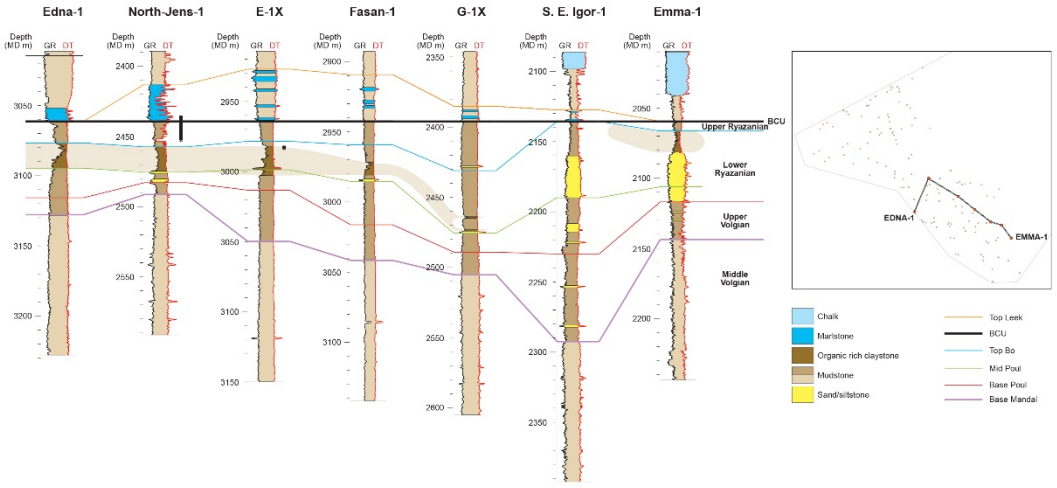

Fig. 8D.8. *Log correlation between wells in the southern Tail End Graben. The log pattern in the wells exhibits 4 upward finings sequences. High gamma ray intervals (Bo Member) are found within the clastic rich deposits along the Coffee Soil Fault (Emma-1).*

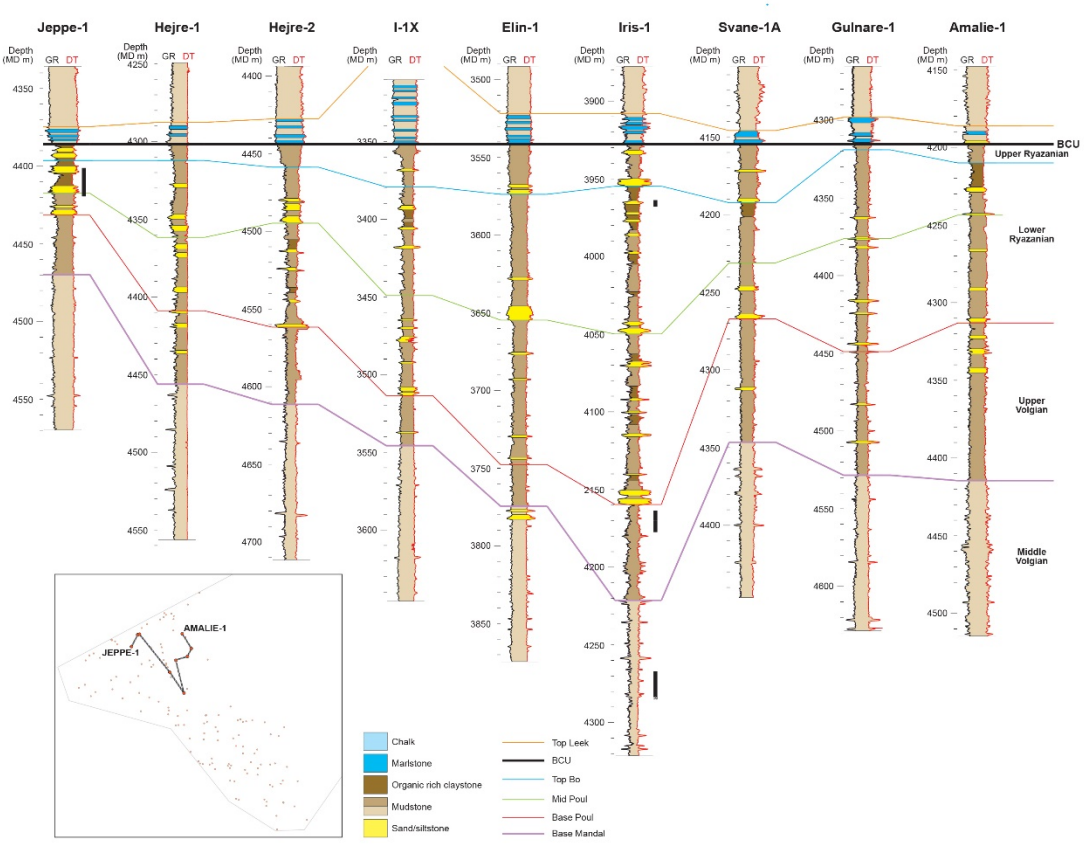

Fig. 8D.9. *Correlation of the Mandal Formation between wells in the northern part of the Central Graben. Thick turbidite rich sections dominate the area.*

8D.6 Sequence stratigraphy

The Mandal Formation encompases the Late Volgian to Late Ryazanian interval of the succession at the Jurassic/Lower Cretaceous boundary. The age determination of the Mandal Formation is based on results from palynological investigations carried out under the Petsys project. (PETSYS Stratigraphic summary charts).

Confidence in the age determination of the Mandal Formation varies from well to well and may occasionally be slightly ambiguous. There is however, evidence of close correlation between the fining upwards sequences and bioevents related to the succession. This relationship endorses a sequence stratigraphic subdivision of the Mandal Formation. A tentative sequence stratigraphy for the Mandal Formation in the Danish Central Graben is indicated in Table 8D.1.

Unit	Sequence boundary	Age
Valhall/Leek/Vyl		Valangian
	Top Mandal (BCU)	Ryazanian/Valanginian transition
Upper Mandal		Late Ryazanian
	Top Bo Member	Late/Early Ryazanian transition
Bo Member		Early Ryazanian
	Mid Poul	Early Ryazanian
Middle Mandal		Early Ryazanian
	Base Poul	Early Ryazanian/Late Volgian transition
Lower Mandal		Late Volgian
	Base Mandal	Late Volgian/Middle Volgian transition

Table 8D.1. *Cretsys nomenclature for the Mandal Formation. (NB: The delineation of the Bo Member in this study differs from the original description by Michelsen et al. 2003*).

The identification of sequences within the Mandal Formation succession concurs with work from the Petsys project. The sequence boundaries Volg-4 and base Ryaz-1 from the Petsys project correspond with the Base Mandal and Base Poul sequence boundaries, respectively.

A comparison with the sequence stratigraphy of the Jurassic established by Partington et al. (1993) indicates a possible correlation of the Lower Mandal unit to sequence J73, Middle Mandal unit and the Bo Member unit correlate with the J74 sequence and that the Upper Mandal unit can be linked to the J76 sequence.

8D.7 Facies and depositional environment

The Mandal Formation is encountered in several exploration wells in the Danish Central Graben but only a few cores are cut in this succession. These cores have wide geographic and stratigraphic spread (Fig. 8D.10), but provide valuable information on the depositional environment during deposition of the Mandal Formation.

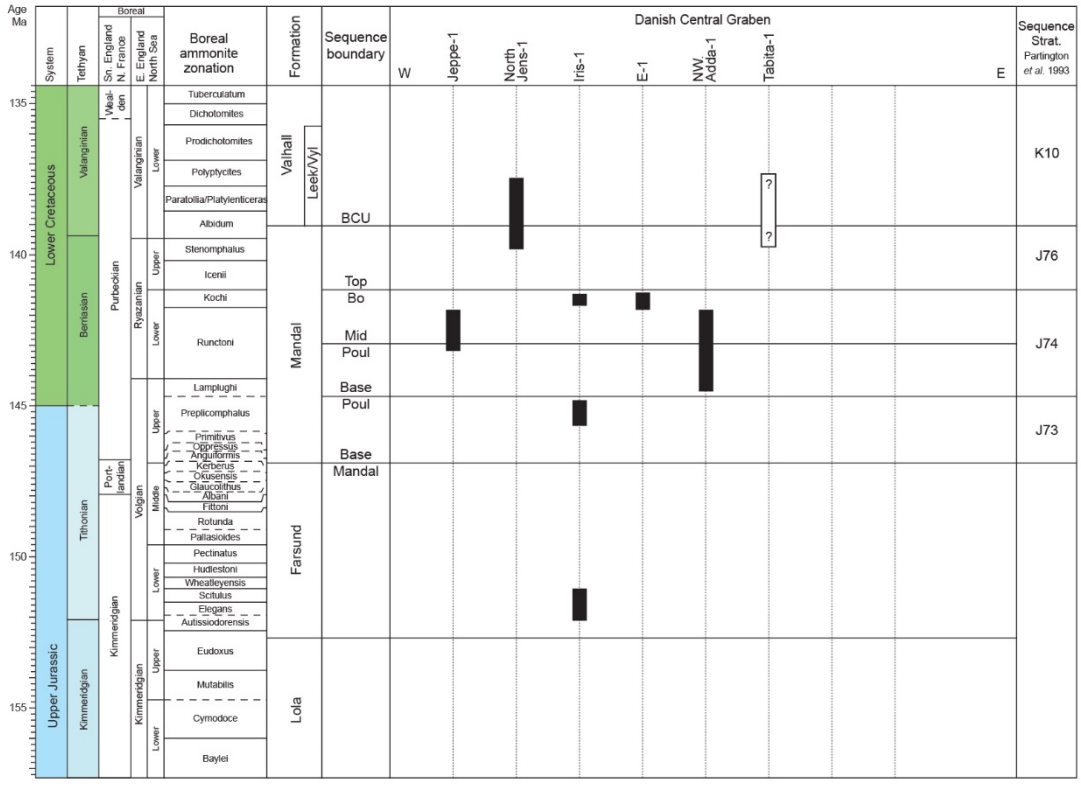

Fig. 8D.10. *Stratigraphic scheme with indication of the stratigraphic coverage of cores from the Mandal Formation.*

The basal part (Lower Mandal unit) comprises a dark grey, slightly calcareous and carbonaceous claystone deposited in a low-energy marine environment. The interval displays an upward increase in gamma-ray values due to an increase in the carbonaceous content indicative of a change towards more oxygen-deficient conditions. In the Iris-1 well the core displays a clay dominated section with evidence of turbidites. Thin sandy stringers prevail in the claystone but the core also displays thick beds of coarse-grained sand, occasionally with a conglomeratic base.

A prominent lithotype of the Mandal Formation is the organic-rich claystone related to the Bo Member. The Bo Member consists of a dark grey-brown to black, non-calcareous, carbonaceous claystone becoming fissile in places. It is characterised by a very high level of radioactivity which is a function of organic carbon content. The organic rich Bo Member represents the most prolific source rock for hydrocarbons in the Jurassic. The unit was deposited in a low-energy anaerobic marine environment with high organic productivity.

The Bo Member is cored in the Jeppe-1, Iris-1 and E-1 wells.

The E-1 and Iris-1 cores consist solely of laminated, organic-rich, hemipelagic mudstones that accumulated under suboxic–anoxic bottom conditions. Turbidites and gravity-flow deposits are not recorded in the cored sections but are identified from well logs from the Bo Member of both wells.

The core in the Jeppe-1 well comprises laminated, organic-rich claystone, turbiditic sandstone and debris flow deposits. The cored section shows evidence of deposition in a low-energy marine environment characterised by background sedimentation of muds and subordinate thin sands from dilute, muddy turbidity currents and by suspension settling through the water column. Slump sheets of turbiditic sandstone and mudstone and associated debris flow deposits provide evidence of intrabasinal slopes near the well.

The Upper Mandal sequence above the Bo Member comprises a dark grey, slightly calcareous claystone and indicates reappearance of less restricted marine conditions. In the North Jens-1 well approximately 10 m of the uppermost Upper Mandal sequence is cored. The cored section consists of laminated dark to very dark grey mudstone with minor indications of slump features.

Along the Coffee Soil Fault the Mandal Formation is dominated by dark grey siltstones and light grey, very fine grained sandstones related to the Poul Member. The succession comprises upwards fining sequences with a sandy/silty base. The siltstones are partly argillaceous and grade into claystone. The sequences contain glauconite and pyrite. The sandstones may be calcite cemented. The sandstone occurs as massive sand beds and as isolated lobes and is interpreted as due to gravity flow deposition.

In the NW Adda-1 well, a thick sandy interval in the Poul Member is cored. Here the interval is composed of heterolithic interbedded mudstones, siltstones and sandstones and some intervals of laminated black mudstone. The silt- and sandstone deposits are interpreted as turbidite channels, crevasse splays and levee deposits. The laminated mudstone are interpreted as hemipelagic mudstones accumulated under anoxic bottom conditions and represent basin floor sediments deposited in between active turbidite channels.

8D.8 Depositional setting for the Mandal Formation

Based on implications from the core data combined with information from the log stratigraphy and the basin development, an overall depositional model for the Mandal Formation in the Danish Central Graben has been established.

The increase in gamma ray readings at the base of the Mandal Formation indicates a gradual change from open marine conditions during deposition of the Farsund Formation to gradually more restricted conditions. The deposition took place in a low-energy, oxygen-deficient marine environment distal from terrestrial influence. Laminated, organic-rich, hemipelagic mudstones accumulated under suboxic–anoxic bottom conditions and culminated with deposition of the organic rich Bo Member.

In the basin centre the low-energy claystone is interbedded with turbidites and gravity-flow deposits. The turbidites and debris-flow deposits represent dynamic depositional events in a generally low-energy marine environment. The number and thickness of the turbidites varies throughout the basin but seems to be closely related to the structural development. In distal parts of the basin, thin turbiditic sand stringers prevail.

Towards the basin margins there seems to be an increase in the number and thickness of the turbidites. Slump sheets of turbiditic sandstones and mudstones and associated debris flow deposits provide evidence of intrabasinal slopes and proximity to structural highs. The Mandal Formation succession in the Gertrud Graben encounters numerous and thick gravity flow deposits. The Gertrud Graben is bounded to the east by the Mandal High, which may have acted as a source area for the turbidite sands.

Towards the basin margin along the Ringkøbing Fyn High, the Mandal Formation grades into clastic dominated deposits of the Poul Member. The transition is evident from the gradual suppression of the high gamma ray values typical of the Bo Member claystone.

The silt- and sandstone deposits of the Poul Member are interpreted as turbidite channels, crevasse splay and levee deposits and may represent a more marginal facies type than the turbidites and density flow deposits in the basin.

Thin intervals of laminated organic-rich claystone similar to the organic rich Bo Member claystone are found in the Poul Member sequence. These claystones are interpreted as a hemipelagic mudstone accumulated under anoxic bottom conditions and represent basin floor sediments deposited in between active turbidite channels.

The presence of the organic-rich claystones in the Poul Member indicates that low-energy suboxic–anoxic bottom conditions can be found further to the east in the Central Graben than anticipated on the basis of the gamma ray values. The evidence of low-energy bottom conditions is however, suppressed by the numerous gravity-flow deposits shed into the basin along the Coffee Soil Fault.

8D.9 Hydrocarbon aspects

Hydrocarbons have been encountered in sandstones of the Mandal Formation, suggesting a prospective succession.

With the mutual occurrence of an internal prolific source rock for hydrocarbons (the Bo Member) and potential reservoirs (Poul gravity-flow sand and turbidites) the Mandal Formation may be considered as an interval with interesting prospectivity.

The organic rich Bo Member represents the most prolific source rock in the Jurassic succession. Although immature in some areas of the Central Graben the Bo Member is considered as source rock for a large number of hydrocarbon accumulations in the Cretaceous.

In the Mandal Formation hydrocarbons are found in porous sandstone beds related to the Poul Member (NW Adda-1) and in turbidites in the Gertrud Graben (Hejre-1, -2 and Jeppe-1). None of the hydrocarbon findings have been declared commercial. Uncertainties regarding evaluation of the discoveries are the thickness of the sand beds, the reservoir quality and migration and filling of the reservoir.

Whereas reservoir quality is difficult to predict from the available data, the thickness and possible filling can be estimated from the present study. The study indicates thick sandstone intervals in juxtaposition with mature source rocks along the Coffee Soil Fault and in the Gertrud Graben. These areas may be considered as the most prospective areas regarding the Mandal Formation.

References

Andsbjerg, J. & Dybkjær, K. 2003: Sequence stratigraphy of the Jurassic of the Danish Central Graben. In: Ineson, J.R. & Surlyk, F. (eds): The Jurassic of Denmark and Greenland. Geological Survey of Denmark and Greenland Bulletin 1, 265-300.

Dybkjær, K. 1998: Palynological dating of the Mandal Formation (uppermost Jurassic – lowermost Cretaceous, Norwegian Central Graben) and correlation to organic-rich shales in the Danish sector. Marine and Petroleum Geology 15, 495-503.

Gradstein, F.M., Ogg, J.G., Schmitz, M.D., Ogg, G.M. 2012. The geological timescale 2012. Elsevier, Oxford, UK.

Ineson, J.R., Bojesen-Koefoed, J.A., Dybkjær, K. & Nielsen, L.H. 2003: Volgian-Ryazanian "hot shales" of the Bo Member (Farsund Formation) in the Danish Central Graben, North Sea stratigraphy, facies and geochemistry. In: Ineson, J.R. & Surlyk, F. (eds): The Jurassic of Denmark and Greenland. Geological Survey of Denmark and Greenland Bulletin 1, 403-436.

Jensen, T.F., Holm, L., Frandsen, N. & Michelsen, O. 1986: Jurassic – Lower Cretaceous lithostratigraphic nomenclature for the Danish Central Trough. Danmarks Geologiske Undersøgelse, Serie A 12, 65pp.

Johannessen, P.N. 2003: Sedimentology and sequence stratigraphy of paralic and shallow marine Upper Jurassic sandstones in the northern Danish Central Graben. In: Ineson, J.R. & Surlyk, F. (eds): The Jurassic of Denmark and Greenland. Geological Survey of Denmark and Greenland Bulletin 1, 367-402.

Johannessen, P.N. & Andsbjerg, J. 1993: Middle to Late Jurassic basin evolution and sandstone reservoir distribution in the Danish Central Trough. In: Parker, J.R. (ed): Petroleum geology of Northwest Europe: proceedings of the 4th conference, 271-283. London. Geological Society.

Michelsen, O., Nielsen, L.H., Johannessen, P.N., Andsbjerg. J. & Surlyk, F. 2003: Jurassic lithostratigraphy and stratigraphic development onshore and offshore Denmark. In: Ineson, J.R. & Surlyk, F. (eds): The Jurassic of Denmark and Greenland. Geological Survey of Denmark and Greenland Bulletin 1, 147-216.

Partington, M.A., Copestake, P., Mitchener, B.C & Underhill, J.R. 1993: Biostratigraphic calibration of genetic stratigraphic sequences in the Jurassic-lowermost Cretaceous (Hettanginian to Ryazanian) of the North Sea and adjacent areas. In: Parker, J.R. (ed): Petroleum geology of Northwest Europe: proceedings of the 4th conference, 371-386. London. Geological Society.

PETSYS 2015. Skaarup et al.: The Jurassic Petroleum System in the Danish Central Graben. Technical notes. Danmarks og Grønlands geologisk Undersøgelse, Rapport 2015/22. (Confidential).

Vollset, J. & Doré, A.G. (eds) 1984: A revised Triassic and Jurassic lithostratigraphic nomenclature for the Norwegian North Sea. Norwegian Petroleum Directorate Bulletin 3, 53pp.

8E Overpressure distribution and porosity-depth trends in the Chalk Group

In general, the upper part of the Chalk Group of the Danish Central Graben is characterised by high porosities. The high porosities are related directly to overpressuring as overpressure supports porosity retention. The Cromer Knoll Group, the Chalk Group and major parts of the Cenozoic deposits (mainly the Paleogene sediments) are overpressured. The overpressuring is due the rapid subsidence of the basin in late Cenozoic time, but also the low permeability of the clays and chalks contributes to the overpressure build-up. The rapid subsidence and the low permeability prevent vertical and lateral escape of pore fluids, leading to under-compaction and overpressure build-up. Many authors suggest that the top of the Mid Miocene sediments coincides with the top of the overpressured zone (in other words, the on-set of the overpressure corresponds approximately to top Mid Miocene). Herein the overpressure is considered to correspond to the difference between pore pressure and hydrostatic pressure.

In order to map the variation in the magnitude of the overpressure, we analysed pressure data from various sources (DSTs, RFTs, MDTs, flow test, production tests etc. conducted in wells). The overpressure at top chalk level as mapped by GEUS is shown in Fig. 8E.1. Data from UK and N are used as guiding points.

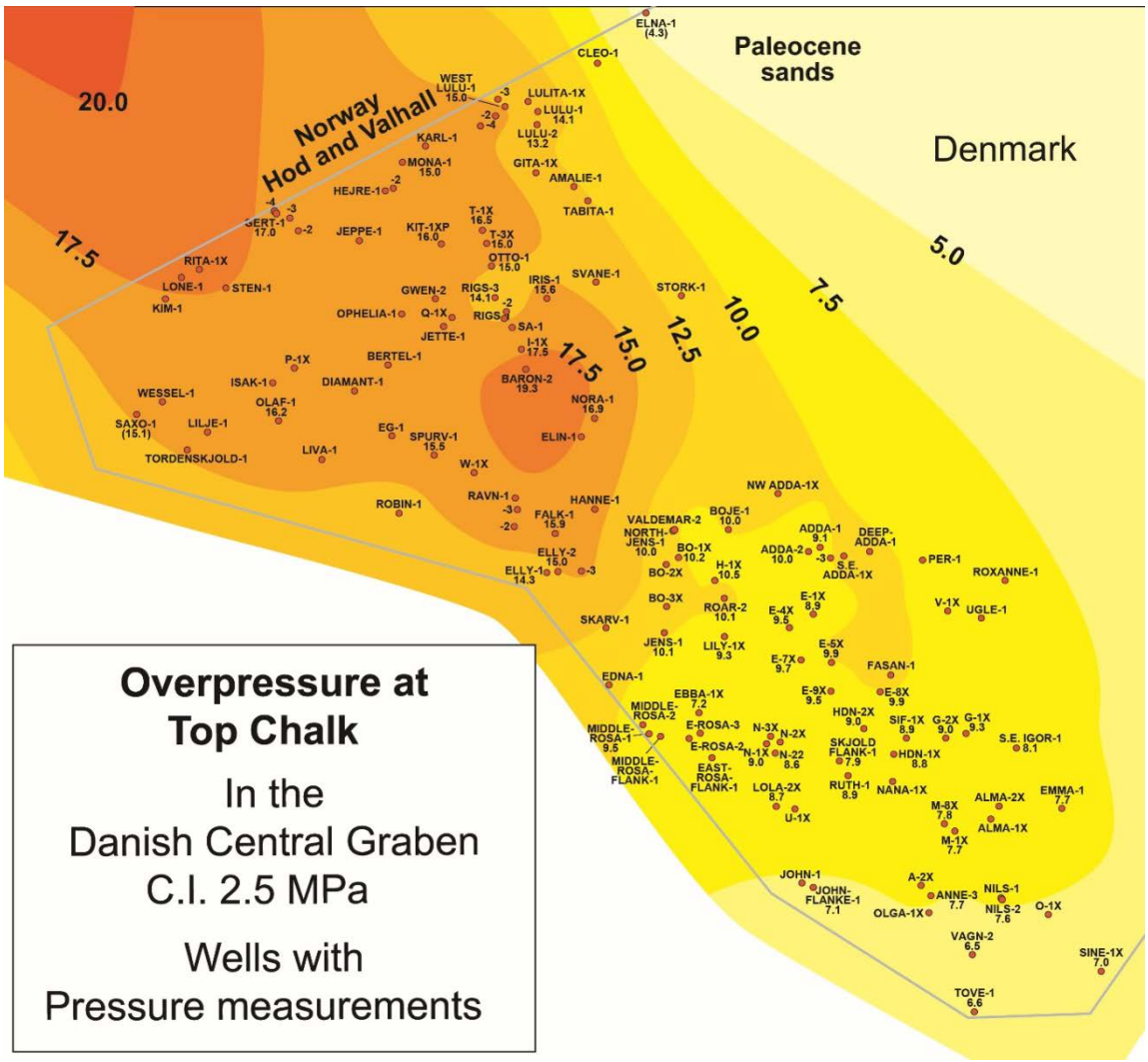

Fig. 8E.1: *Overpressure at Top Chalk level. Contour Interval (C.I.): 2.5 MPa. (yy) represent estimated values*

The overpressure generally increases from Southeast to Northwest in the Danish Central Graben and ranges from *c.* 6 MPa towards SE to *c.* 18 MPa towards NW. The maximum overpressure in the Chalk Group corresponds to the Cenozoic depocentre in the Norwegian sector. The overpressure bleeds off towards Northeast due to the presence of rather high-permeable Paleocene sandstones in this area. Based on these observations, it may be concluded that the overpressure in the Chalk Group is connected primarily to burial depth – or more correctly: to the thickness of the Cenozoic shales combined with the depositional history of the Cenozoic sediments. The Cenozoic shales are generally characterised by high sealing capacities.

The data plotted on the overpressure map (Fig. 8E.1) originate from interpretation of well test data and wireline test data from more than 60 wells combined with information extracted from Pressure-Depth plots. An example of a Pressure-Depth plot is shown for the N.W. Adda-1X well (Fig. 8E.2). Wireline pressure data (RFT data) are plotted along with a simplified mud weight curve. In addition, formation tops and leak off test data are included.

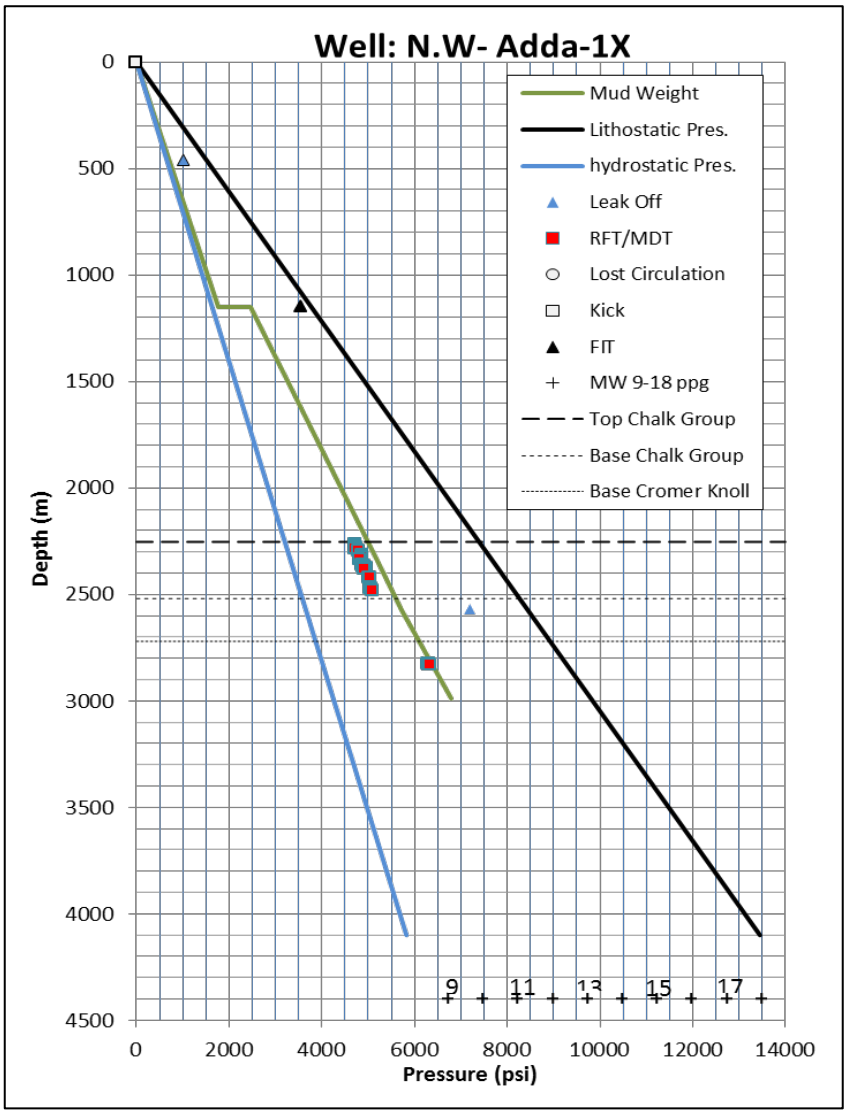

Fig. 8E.2: *Pressure-Depth plot for the N.W. Adda-1X well. A curve based on the hydrostatic pressure gradient (0.44 psi/ft) and a curve based on the lithostatic pressure gradient (1 psi/ft) form the framework of the plot. The red squares point out pressure measurements (RFT data). See legend.*

The pressure data are uploaded onto the Cretsys website as Excel files on a well-to-well basis. The Excel files includes raw and processed RFT/MDT data together with an assessment of the initial pore pressure as interpreted from well test data. Apart from pressure data, each Excell file also includes information about formation tops and a Pressure-Depth plot similar to the plot shown in Fig. 8E.2. Each plot displays the pore pressure distribution at a particular depth and provides information about the overpressure (the difference between pore pressure and hydrostatic pressure). For each pore pressure measurement, the overpressure data have been computed. Finally, the overpressure data were included in the database.

8E.1 Pressure Models

(a) Pore Pressure-Depth relationship

For each well, a representative pore pressure value is assigned to the upper part of the Chalk Group and to the Cromer Knoll Group, if the pressure and well data allow such assessments. The Chalk Group pressure data are plotted versus depth in Figure 3. The majority of the pore pressure measurements stem from the upper part of the Chalk Group, because most data represent intervals tested for hydrocarbons. A regression line illustrates a 'GEUS Pore Pressure Model', indicating that the pore pressure with good confidence is related to depth, at least when dealing with the upper part of the Chalk Group within the Danish Central Graben. We derived the following equation for modelling pore pressure as a function of depth:

Modelled pore pressure (in psi) = 2.4·Actual Depth(in m) – 614

Modelled pore pressure (in MPa) = [2.4·Actual Depth(in m) – 614]/145

The assumed correlation between pressure and depth is not perfect but on the other hand, the correlation coefficient (least-square-mean) is still >90%. A number of outliers are observed among the plotted data points. Some of the data points that plot above the trend line represent salt piercement structures are characterised by somewhat ab-normal pressure-depth relationships due to structural uplift, for example:

Well name	Depth (m)	Actual pore pressure (psi)	Modelled pore pressure (psi)
East Rosa-1	1300	3079	2400
T-1X	2276	5611	4750
T-3X	2517	5751	5325
Otto-1	2462	5672	5200

Summary: In these four wells, the actual pore pressure is considerably higher than modelled.

Despite not drilled on a salt piercement structure, the Baron-2 pressure-depth data also deviates from the GEUS model, and i.e. the pore pressure is higher than indicated by the trend line. The Baron-2 well is located in a flank area of a domal structure related to structural inversion:

Well Name	Depth (m)	Actual pore pressure (psi)	Modelled pore pressure (psi)
Baron-2	2822	6923	6050

Summary: In the Baron-2 well, the actual pore pressure is significantly higher than modelled.

A few data points plot below the trend line. For example, the pressure-depth data from the Ebba-1 well data plot far below the trend line. The actual pore pressure is thus significantly lower that modelled.

Well name	Depth (m)	Actual pore pressure (psi)	Modelled pore pressure (psi)
Ebba-1	2800	5022	6000

Summary: In the Ebba-1 well, the actual pore pressure is significantly lower than modelled.

The low pore pressure compared to depth in Ebba-1 is presumably due to the presence of chalk with exceptionally high porosity, and the high-porosity chalk probably bleeds off pressure. The Ebba-1 well penetrated a porosity anomaly identified from seismic data.

(b) Overpressure-Depth relationship

Similarly, it appears from the figure that the overpressure (the difference between pore pressure and hydrostatic pressure) also is related to depth. For modelling purposes, we assume that the overpressure increases linearly with depth and that the on-set of the overpressure is equal to a fixed depth value (herein 800 m). The depth value of 800m is, however, subject to discussion, and it may turn out that the on-set of the overpressure actually corresponds to a somewhat higher depth value (e.g. 1200 m) depending on the exact position of the trend line. The trend line may deviate from a linear line at shallow depths as observed elsewhere; see the graphic illustration (diagram) below:

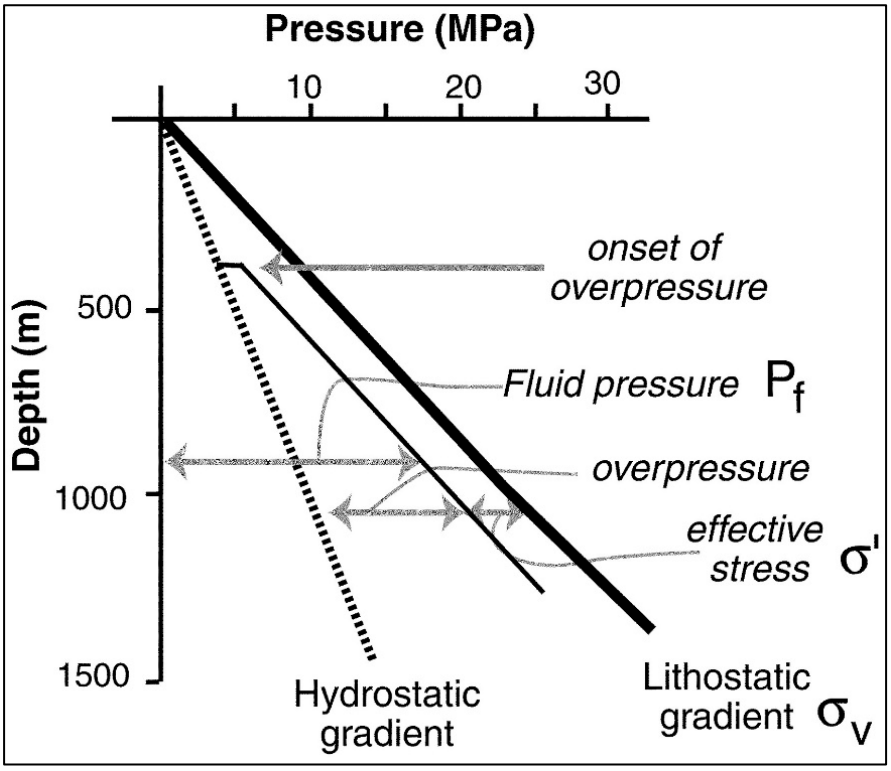

GEUS derived the following equation for modelling the overpressure (ΔP) as function of depth; cf. Fig. 8E.3:

ΔP (in MPa) = 0.006393·Actual Depth (in m) – 4.23

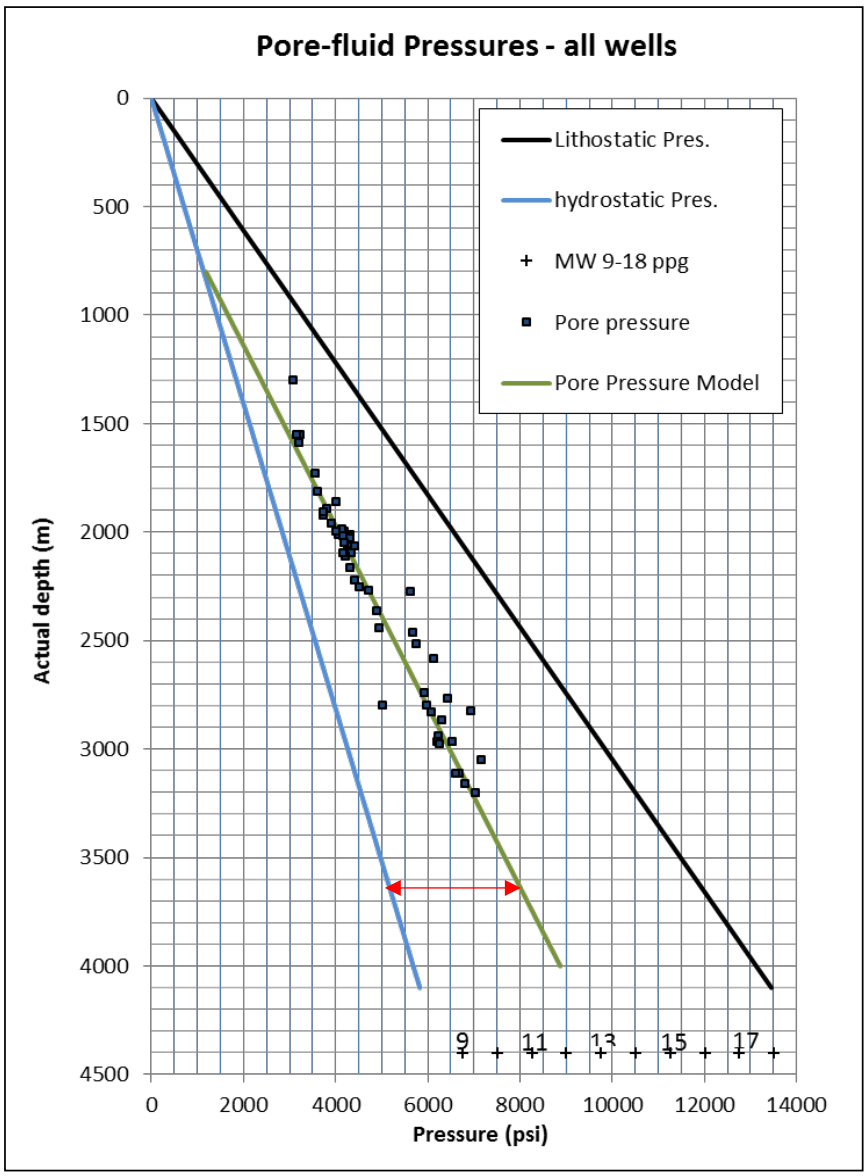

Fig. 8E.3: *Composite pressure-depth plot including all wells with pressure measurements. Most of the data represent interpreted DST and RFT data from the upper part of the Chalk Group. The red arrow illustrates the overpressure (ΔP), meaning Pore pressure – Hydrostatic Pressure. The following equation expresses the overpressure (ΔP): ΔP (in MPa) = = 0.006393·Actual_Depth (in m) - 4.23*

8E.2 Porosity model

A porosity-depth curve for normally compacted chalk in the Danish Central Graben is constructed on the basis of a conventional Scholle curve (Scholle, 1977) combined with information about chalk porosity in areas with no overpressure, i.e. areas located outside the Central Graben area (Fig. 8E.4):

$$\text{Porosity} = 69 \cdot \text{EXP}(-0.001 * \text{Actual\_Depth}) \qquad (1)$$

At least two mechanisms lead to porosity preservation in chalk: overpressuring and the effect of hydrocarbon saturation – and in addition, reworking may also contribute porosity preservation. The expected correspondence between porosity, overpressure and depth is discussed in detail below. In order to quantify the effect of overpressure on the porosity preservation, Japsen et al. (2005) introduced an 'effective depth' term, i.e. overpressure-corrected depths. In case of overpressure, the 'Effective Depth' should replace 'Actual Depth'. Japsen et al. (2005) suggested calculating the Effective Depth (in metres) as follows:

$$\textbf{Effective Depth (}\text{m}\textbf{) = Actual\_Depth (}\text{m}\textbf{) - 100·}\Delta\textbf{P (}\text{MPa}\textbf{)} \qquad \textbf{(2)}$$

Where ΔP is the overpressure in MPa. When inserting the Effective Depth term in Equation 1, we have:

$$\textbf{Porosity = 69 · EXP (-0.001·(Actual Depth (m) - 100·}\Delta\textbf{P (}\text{MPa}\textbf{))} \quad \textbf{(3)}$$

The overpressure may be estimated from the map shown in Figure 1. When the overpressure is known, the porosity may be modelled using Equation no. 3 or alternatively, from the type-curves plotted in Fig. 8E.4. These type-curves are calculated on the basis of Equation no. 3 using the Actual Depth and four selected overpressure values (5, 10, 15 and 20 MPa) as input data. Accordingly, the porosity of the chalk section is herein simply considered a function of two variables: depth and overpressure.

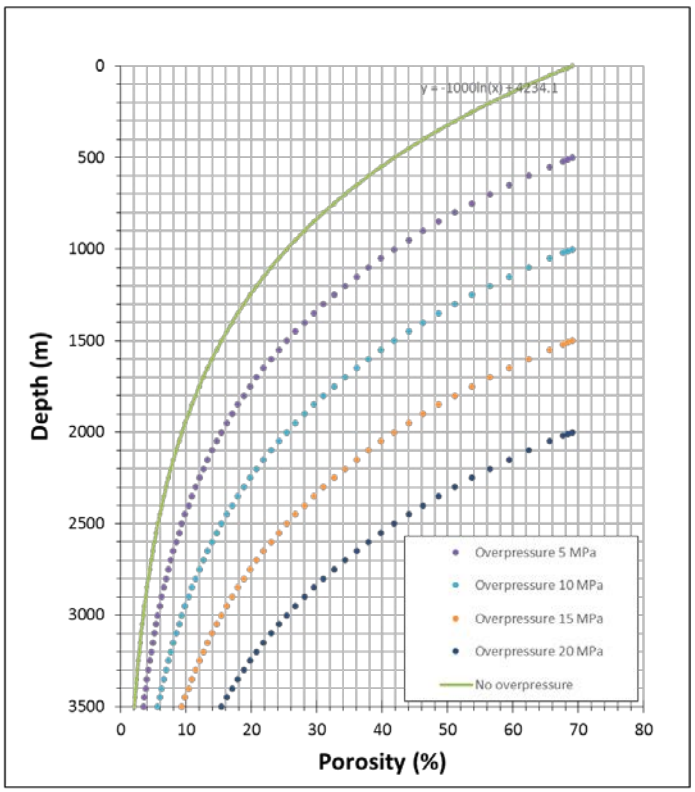

Fig. 8E.4: *The GEUS model for estimating chalk porosity as function of depth and overpressure.*

Previously it was found that the overpressure *(ΔP)* may be estimated using the GEUS Pore Pressure Model, i.e. *ΔP (in MPa) = 0.006393·Actual_Depth (in m) - 4.23.* Inserting this expression into Equation 3 and upon re-arranging, we have

Porosity(%) = 69·EXP(-0.00036·Actual_Depth - 0.423) (4)

In this latter case, it has been assumed that the overpressure increases linearly with depth (reference is made to Fig. 8E.3). Furthermore, it has been assumed that the chalk is pelagic and that the onset of the overpressure corresponds to a fixed value throughout the Danish Central Graben (800 m; but the exact depth value is subject to discussion as described above). It is, however, difficult to fulfil these assumptions and Equation 4 just reflects a simple model for porosity modelling and prediction. However, the model gives a good indication of the expected porosity level as illustrated in Fig. 8E.5. This figure compares log-derived and modelled porosities. The assumption of pelagic chalk reflects slow deposition rates, but pelagic chalk also signifies that hydrostatic pressure conditions prevailed during deposition and afterwards until a sufficiently high sealing capacity of the overlying shaly sediments was obtained.

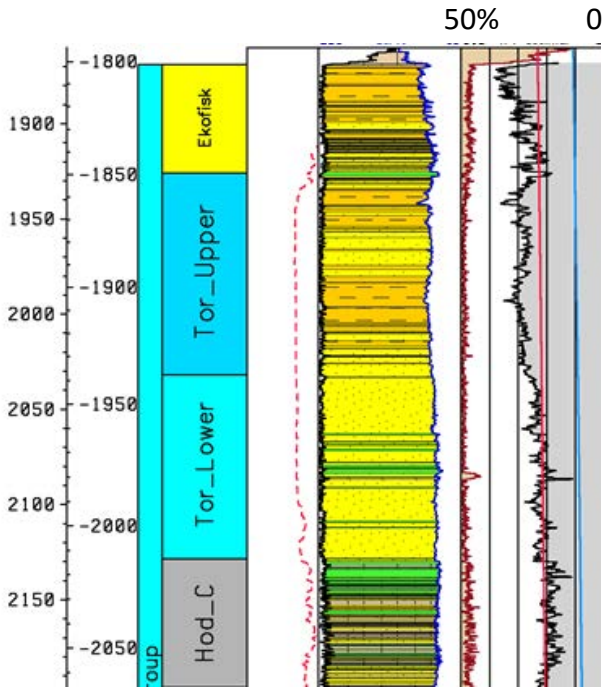

Fig. 8E.5: *Stratigraphy, lithology and porosity distribution in in the Anne-3 well. The log-derived porosity is in grey, the modelled porosity based on a normal compaction model is in blue and the red curve shows the porosity as calculated from the porosity model expressed by Equation 4. Note the porosity scale: the porosity increases from right (0%) to left (50%). The well porosity (grey) is obviously higher than estimated from a normal compaction model (blue). With respect to the Hod_C and Tor_Lower units, excellent agreement between modelled porosity (red) and log-derived porosity (grey) is observed. The modelled porosity (red) is lower than the log-derived porosity (grey) in the Ekofisk Formation and the Tor_Upper unit.*

8E.3 Fracture pressure

In the Danish area, the formation strength has been estimated from leak off tests (LOTs) conducted at casing points in the drilled formations. Leak off tests from primarily non-chalk sections in Anne-3, Baron-2, Gert-1, Skjold Flank-1 and NW Adda-1 were analysed, and these LOT data form the basis of establishing a fracture pressure trend for the Danish area (Figure 6). As the amount of leak off tests conducted in the chalk section is sparse when dealing with the Danish sector, we suggests using the Norwegian trend line that is based on all LOT data (both chalk and non-chalk) from the southern part of the Norwegian Central Graben. Furthermore, the Norwegian line corresponds to a minimum leak off pressure (LOP) trend, and this trend line may be a better estimate of the fracture pressure in the chalk section than the Danish line.

The plotted pore pressure data in Fig. 8E.6 indicate that the fracture pressure has not been reached in the Danish wells in recent times. With respect to the Norwegian Fields, the fracture pressure is reached in the Valhall Field, where leakage occurs as indicated by gas cloud located above the Chalk Group. In the Hod Field leakage occurred when the fracture pressure was lower than to day (Caillet et al., 1997).

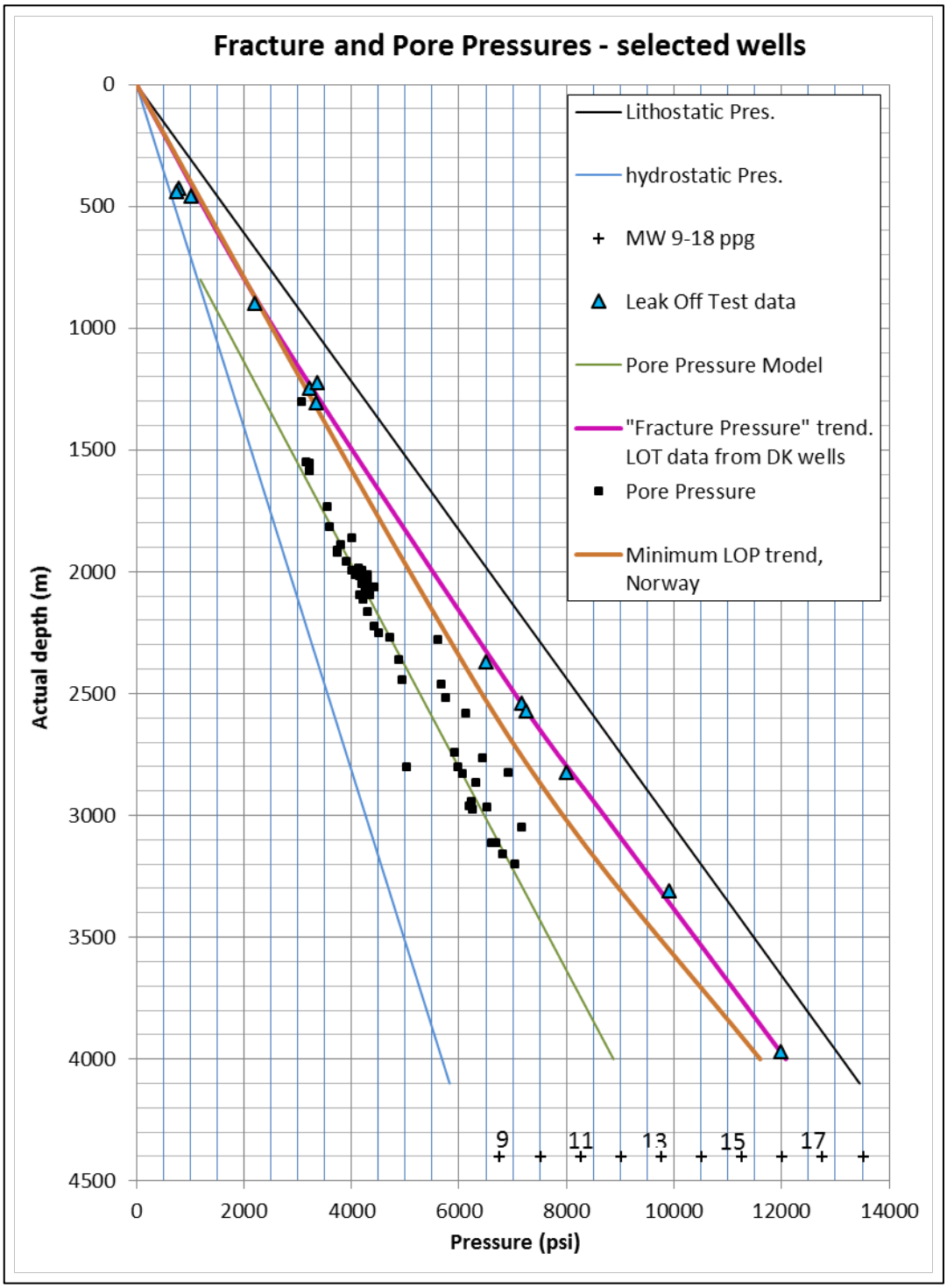

Fig. 8E.6. *Approx. fracture pressure curves from Denmark and Norway. Estimated pore pressures in the Chalk Group, based on pressure data from selected wells located in the Danish Central Graben, are also shown in the figure.*

References

Andersen, M. 1995: Petroleum Research in North Sea chalk. Amoco Norway Oil Company and RF-Rogaland Research. Joint Chalk Research Phase IV (1984–1986).

Bassinot, F., Marsters, J.C., Mayer, L.A., Wilkins, R.H., 1993. Variations of porosity in calcareous sediments from the Ontong Java Plateau. Proceedings of the Ocean Drilling Program: Scientific Results, Vol. 130, pp. 653-661.

Caillet G., Judge, N.C., Bramwell, N.P., Meciani, L., Green, M. & Adam, P. 1997: Overpressure and hydrocarbon trapping in the Chalk of the Norwegian Central Graben. Petrol. Geoscience, **v**.3, pp. 33-42.

Dennis, H., Bergmo, P. and Holt, T. 2005: Tilted oil−water contacts: modelling the effects of aquifer heterogeneity. *In Doré & Vining (eds)* Petroleum Geology: NW Europe and Global Perspectives−Proceedings of the 6th Petroleum Geology Conference, pp. 145−158. Geological Society, London.

Gaarenstroom, L., Tromp, R.A.J., deJong, M.C. & Brandenburg, A.M. 1993: Overpressures in the Central North Sea. Implications for trap integrity and drilling safety. *In: J.R. Parker (ed)* Petroleum geology of Northwest Europe: Proceedings of the 4th Conference.

Japsen, P., G. Mavko, L. Gommesen, I. L. Fabricius, F. Jakobsen, O. V. Vejbæk, R. Rasmussen and C. R. Schiøtt, 2005: Chalk background velocity: Influence of effective stress and texture, paper presented at 67th Conference and Exhibition, Eur. Assoc. of Geol. and Eng., Madrid, 13–16 June.

Japsen, P., Dysthe, D.K., Hartz, E.H., Stipp, S.L.S., Yarushina, V.M. & Jamtveit, B. 2011: A compaction front in North Sea chalk. Journal of Geophysical Research, **v**. 116 (B11).

Rasmussen, E.S., Piasecki, S., Andsbjerg, J., Dybkjær, K., Vejbæk, O.V., Jacobsen, C., Britze, P. & Bryde-Auken, M. 2005. Cenozoic maps of the Danish North Sea area. GEUS report 2005/33.

Scholle, P. A., 1977: Chalk diagenesis and its relation to petroleum exploration: oil from chalks, a modern miracle? AAPG Bull., v. 61, p. 982-1009.

Zhang, J., 2013: Effective stress, porosity, velocity and abnormal pore pressure prediction accounting for compaction disequilibrium and unloading. Marine and Petroleum Geology, **v.** 45, 2–11

8F Oil family classification and source rock typing

8F.1 Introduction

This technical note on the methodology of oil family classification provides information on the biomarker analysis, data pre-treatment leading up to the data analysis and a description of the different steps in the multivariate data analysis conducted on oil, stain and sediment extracts. The biomarker database is composed of 99 analyses of oil samples extracted from the North Sea, 285 sediment extracts from cores and cuttings within the main Jurassic source rock units. The biomarkers were analysed by GC-MS-MS techniques at the Source rock Laboratory at GEUS, and constitute 43 biomarkers or ratios hereof. The subsequent data analysis resulted in the definition of four main types of oils (Oil type 1, 2, 3, 4). The main Upper Jurassic oil type (type 1) is further subdivided into four subtypes (1A, 1B, 1C, 1D). Each of the types and subtypes represent different organofacies. By reference to biomarker systematics and by comparison with sediment extract ages of the Jurassic source rock extracts, the oil types have been correlated to the sequence stratigraphical framework established for the Jurassic. The stratigraphic variation in oil types reflects the organofacies variation resulting from the tectonic evolution and flooding of the North Sea Basin. A clear geographical variation is seen in the oil types within the North Sea. Oil type 1 dominates in the southern Salt Dome Province (oil subtype 1D) and around the Tail End Graben (oil subtype 1A). Terrestrial types (oil type 2 and 3) occur more locally suggesting that several kitchen areas contributed to the accumulated oils.

A high resolution dataset consisting of 61 oil analyses from the Valdemar Field is included in the analysis. It is concluded that the oil is sourced from the main Upper Jurassic Farsund Formation source rock. The Valdemar oil represents oil subtypes 1A and 1B and reflects organofacies variation within the kitchen area(s). In addition, variation in the oil maturity in seen suggesting multiple migration episodes.

8F.2 Analysis of oils and source rock extracts using GC-MS and GC-MS-MS

The experimental setup and biomarker identification is similar as for the Petsys project. Some of the main details are provided below. For detailed description see Petsys Technical Notes on biomarkers.

8F.3 Experimental

Source rocks were extracted using a Soxtec System HT 2 1045 Extraction Unit using dichloromethane/methanol (93:7 vol/vol). Oils or extracts were transferred to a preweighed vial. After a couple of days, a constant weight was obtained. The residue, which consists of compounds having more than approximately 15 carbon atoms, is called the C15+ fraction. The asphaltenes were removed from the oils and extracts by precipitation in at least a 40 fold excess of *n*-pentane. The asphaltene-free oil or extract was fractionated into three fractions (saturated hydrocarbons, aromatic hydrocarbons and polar compounds or NSO) by MPLC (Radke et al., 1980).

Gas chromatography-mass spectrometry (GC-MS and GC-MS-MS) was carried out using a Hewlett-Packard 6890N gas chromatograph connected to a Waters (Micromass) Quattro Micro GC tandem quadrupole mass spectrometer (photo). The GC was fitted with an Agilent HP-5 or Phenomenex ZB-5 column (30 m x 0.25 mm i.d., film thickness 0.10 µm). The temperature program was 30°C/min from 70 to 100°C and 4°C/min from 100 to 308°C followed by 8 min at 308°C. The samples were dissolved in isooctane, and the concentration was 0.5 mg/100µl (GC-MS) or 1 mg/100µl (GC-MS-MS). Splitless injection was used.

Hopanes and steranes were quantified using GC-MS data (*m/z* 191 and 217 respectively). Only a few steranes such as the regular C_{29} steranes are separated in the *m/z* 217 mass chromatogram. In order to quantify all C_{27} – C_{30} diasteranes and steranes ((4 + 4) x 4 = 32), GC-MS-MS data must be used. Only a few sterane ratios can be measured reliably using GC-MS.

Some hopanes also coelute in the *m/z* 191 mass chromatogram. A few examples can be mentioned: 28,30-Bisnorhopane (BNH) coelutes with an unidentified C_{30} hopane and the C_{30} neohopane (C30Ts) coelutes with a norgammacerane.

8F.4 Biomarker ratios

An overview of biomarkers and ratios is provided in Table 7F.1. Biomarker ratios can be expressed as A/ (A+B) or A/B. It is common to use A/ (A+B) if compound A is converted to its isomer B (e.g. because of maturation). The possible range for A/ (A+B) is 0-1. In many cases, an equilibrium between A and B is reached (hopane S/(S+R) isomerization: 0.60; sterane S/(S+R) isomerization: 0.55). A/B is normally used for compounds A and B that are not isomers or when two isomers A and B have a different origin. The range for A/B is 0-∞.

Hopane ratios are self-explanatory with a single exception:

HHI = C_{35} Homohopane Index: (H35αβS + H35αβR) / (H31αβS + H31αβR + H32αβS + H32αβR + H33αβS + H33αβR + H34αβS + H34αβR + H35αβS + H35αβR).

Table 8F.1. *Acronyms (Parameter) for the biomarkers (Compounds). GC-FID was used for n-alkanes and isoprenoids and GC-MS in SIM-mode for tricyclic terpanes.*

Table 1			
Index	**Parameter**	**Quantification**	**Compounds**
1	Pr/Ph	GC-FID	pristane/phytane
2	Pr/*n* C17	GC-FID	pristane/*n* -C17
3	Ph/*n* C18	GC-FID	phytane/*n* -C18
4	Ts/(Ts + Tm)	370 → 191	18α-22,29,30-trisnorneohopane/(18α-22,29,30-trisnorneohopane + 17α-22,29,30-trisnorhopane)
5	29Ts/(29Ts + H29)	398 → 191	18α-30-norneohopane/(18α-30-norneohopane + 17α,21β-30-norhopane)
6	30Ts/H30ab	412 → 191	18α-neohopane/(18α-neohopane + 17α,21β-hopane)
7	30E/H30ab	412 → 191	"early eluting C_{30} hopane"/17α,21β-hopane
8	30D/H30ab	412 → 191	C_{30} 17α-diahopane/17α,21β-hopane
9	31D-S/H30ab	412, 426 → 191	C_{31}-S 17α-diahopane/17α,21β-hopane
10	31D-R/H30ab	412, 426 → 191	C_{31}-R 17α-diahopane/17α,21β-hopane
11	30ba/H30ab	412 → 191	17β,21α-hopane/17α,21β-hopane
12	BNH/ H30ab	384, 412 → 191	28,30-bisnorhopane/17α,21β-hopane
13	H29ab/H30ab	398, 412 → 191	17α,21β-30-norhopane/17α,21β-hopane
14	31abS	412, 426 → 191	C_{31}-22S hopane /17α,21β-hopane
15	31abR	412, 426 → 191	C_{31}-22R hopane /17α,21β-hopane
16	32abS	412, 440 → 191	C_{32}-22S hopane /17α,21β-hopane
17	32abR	412, 440 → 191	C_{32}-22R hopane /17α,21β-hopane
18	33abS	412, 454 → 191	C_{33}-22S hopane /17α,21β-hopane
19	33abR	412, 454 → 191	C_{33}-22R hopane /17α,21β-hopane
20	34abS	412, 468 → 191	C_{34}-22S hopane /17α,21β-hopane
21	34abR	412, 468 → 191	C_{34}-22R hopane /17α,21β-hopane
22	35abS	412, 482 → 191	C_{35}-22S hopane /17α,21β-hopane
23	35abR	412, 482 → 191	C_{35}-22R hopane /17α,21β-hopane
24	H31S/(S+R)	426 → 191	C_{31}-22S hopane /(C_{31}-22S hopane + C_{31}-22R hopane)
25	H32S/(S+R)	440 → 191	C_{32}-22S hopane /(C_{32}-22S hopane + C_{32}-22R hopane)
26	H35/H34	468, 482 → 191	C_{34}-22S+22R hopane/ C_{35}-22S+22R hopane
27	HHI	426 – 482 → 191	C_{35} 22S+22R hopane/$\sum C_{31}$- C_{35} 22S+22R hopanes
28	C27stD/R+D)	372 → 217	C_{27} diasteranes/(reg. steranes + diasteranes)
29	C28stD/R+D)	386 → 217	C_{28} diasteranes/(reg. steranes + diasteranes)
30	C29stD/R+D)	400 → 217	C_{29} diasteranes/(reg. steranes + diasteranes)
31	C27stS/S+R)	372 → 217	C_{27} steranes 20S/(20S + 20R)
32	C28stS/S+R)	386 → 217	C_{28} steranes 20S/(20S + 20R)
33	C29stS/S+S)	400 → 217	C_{29} steranes 20S/(20S + 20R)
34	C27stbb/bb+aa)	372 → 217	C_{27} steranes ββ/(ββ + αα)
35	C28stbb/bb+aa)	386 → 217	C_{28} steranes ββ/(ββ + αα)
36	C29stbb/bb+aa)	400 → 217	C_{29} steranes ββ/(ββ + αα)
37	%C27	372 - 400 → 217	% C_{27} diasteranes + reg. steranes (C_{27} - $_{29}$ = 100)
38	%C28	372 - 400 → 217	% C_{28} diasteranes + reg. steranes (C_{27} - $_{29}$ = 100)
39	%C29	372 - 400 → 217	% C_{29} diasteranes + reg. steranes (C_{27} - $_{29}$ = 100)
40	%C30	372 - 414 → 217	% C_{30} diasteranes + reg. steranes (C_{27} - $_{30}$ = 100)
41	T22/T21	*m/z* 191	C_{22}/C_{21} tricyclic terpanes
42	T24/T23	*m/z* 191	C_{24}/C_{23} tricyclic terpanes
43	T26/T25	*m/z* 191	C_{26}/C_{25} tricyclic terpanes

Table 8F.2. *Main controls (environmental, maturity, biodegradation index etc.) of biomarkers. Legend: x: Important. (x): Some importance. (x): Only in case of severe biodegradation, this is not relevant here.*

Ratio	Biological origin	Environment	low	high	Thermal maturity	low	high	Biodegradation (ratio increases)
Pr/Ph	(x)	x	anoxic	oxic	(x)			
Pr/*n*C17								x
Ph/*n*C18								x
Ts/(Ts + Tm)		x	1) anoxic 2) carbonate	1) oxic 2) shale	x	immature	mature	(x)
29Ts/(29Ts + H29)		x	1) anoxic 2) carbonate	1) oxic 2) shale	x	immature	mature	(x)
30Ts/H30ab		x	1) anoxic 2) carbonate	1) oxic 2) shale	x	immature	mature	(x)
30E/H30ab		x	1) anoxic 2) carbonate	1) oxic 2) shale	x	immature	mature	(x)
30D/H30ab		x	1) anoxic 2) carbonate	1) oxic 2) shale	x	immature	mature	(x)
31D-S/H30ab		x	1) anoxic 2) carbonate	1) oxic 2) shale	x	immature	mature	(x)
31D-R/H30ab		x	1) anoxic 2) carbonate	1) oxic 2) shale	x	immature	mature	(x)
30ba/H30ab		x	anoxic	oxic	x	mature	immature	
BNH/ H30ab		x	oxic	anoxic	(x)	immature	mature	
H29ab/H30ab		x	shale	carbonate				
31abS		x	oxic	anoxic				
31abR		x	oxic	anoxic				
32abS		x	oxic	anoxic				
32abR		x	oxic	anoxic				
33abR		x	oxic	anoxic				
33abR		x	oxic	anoxic				
34abS		x	oxic	anoxic				
34abR		x	oxic	anoxic				
35abS		x	oxic	anoxic				
35abR		x	oxic	anoxic				
H31S/(S+R)					x	immature	mature	
H32S/(S+R)					x	immature	mature	
H35/H34		x	oxic	anoxic				
HHI		x	oxic	anoxic				
C27stD/R+D)			carbonate	shale	(x)	immature	mature	(x)
C28stD/R+D)			carbonate	shale	(x)	immature	mature	(x)
C29stD/R+D)			carbonate	shale	(x)	immature	mature	(x)
C27stS/S+R)					x	immature	mature	
C28stS/S+R)					x	immature	mature	
C29stS/S+S)					x	immature	mature	
C27stbb/bb+aa)					x	immature	mature	
C28stbb/bb+aa)					x	immature	mature	
C29stbb/bb+aa)					x	immature	mature	
%C27	x							
%C28	x							
%C29	x							
%C30	x							
T22/T21		x		carbonate				(x)
T24/T23		x	carbonate					(x)
T26/T25		x		lacustrine				(x)

8F.5 Methodology of oil typing based on multivariate data analysis (Steps 1-4)

Step 1: Data pre-treatment and outlier analysis of a representative oil database consisting of 99 and 285 sediment extract samples and 61 samples from the Valdemar Field measured for 43 biomarkers. The data are termed matrix A ([A]) matrix B ([B]) and matrix C ([C]) respectively. The biomarker input parameters are reduced to 37 as part of the initial analysis.

Step 2: Principal component analysis (PCA) of [A]. Identification of geological controls (i.e. maturity, organofacies, biodegradation etc.) on biomarker data. Locate clustering of data. For the classification purpose followed here, the PCA axis dependant on organofacies is used for identification of the four main oil families (oil type 1 to 4).

Step 3: Perform a new PCA of [A] + [B] + [C]. Identify outliers and identify zone of interest within the [A] + [B] sample space for the subsequent data analysis, i.e. where Jurassic oil families (oil type 1, 2, and 3 i.e. excluding oil type 4) and sediment [B] overlaps. The reduced [A] and [B] are termed [A*] and [B*].

Step 4: Perform PCA analysis of [A*] + [B*] + [C]. Identify the main controlling factors on the PC axis. For the classification purpose followed here, the PCA axis dependant on organofacies is used. A detailing of the oil family 1 into subtype (subtype A to D) is made for [A*] + [B*] + [C].

Step 1: Data Analysis

For multivariate data analysis 99 oil samples from various Danish oil fields (termed matrix A), 285 sediment extracts from various Jurassic potential source rock intervals (termed matrix B) and 61 oil samples from the Valdemar Field (termed matrix C) were included in the analysis. The sequence stratigraphic interval of the sediment samples established in the Petsys project was used to provide the relative stratigraphic subdivision.

Multivariate data analysis was carried out on biomarker analytical data supplied as conventional biomarker ratios. Variable sub-sets, traditionally reported as closed sub-sets, i.e. percentages summing to 100%, were not included here, instead the individual variable data and simple ratios were relied upon.

The data were centered w.r.t. column means and standardised, i.e. each centred variable was multiplied with the term 1/SDev calculated for all observations included in the analysis (this is termed 'auto-scaling' in data modelling. Several other types of potentially useful pre-processing were attempted (simple logarithmic or '*icl*' ratio logarithmic transformations and square root transformations) but none succeeded in providing a clearer picture of the resolution of the known oil families. Principal Component Analysis (PCA) was therefore carried out based on auto-scaled data directly.

The multivariate data analysis was carried out using the Unscrambler® program, version 10. All data modelling used sequential outlier identification/deletion, see Esbensen (2012); Esbensen & Geladi (2009).

Step 2: Identification of main oil families

The oils belonging to matrix A are classified into groups defined using their biomarker signature by examining a PCA model of all oil samples (Figs 8F.1 & 8F.2). The two first components of the PCA model represent 65% of the variance (Figs 8F.1a & 8F.1b). Along the first PC component biomarkers mainly related to thermal maturity cluster and they represent a trend from relative high maturity (positive values) to low maturity (negative values).

The loading PC2 vs PC3 plot of the biomarker data for matrix A (Fig. 8F.2b) displays biomarkers more dependent on facies changes rather than maturity. The PC2 displays biomarker related to terrestrial aspects (positive values) versus biomarkers related to marine anoxic aspects of the depositional environment (negative values) (Fig. 8F.2b). It was therefore decided to use the PC2 vs PC3 score plot as a basis for the oil classification and four natural groupings among the oil samples: oil type 1, oil type 2, oil type 3 and oil type 4 (see Fig. 8F.2a).

In terms of organofacies the oil types represent:

Oil type 1: Marine anoxic conditions to slightly oxic organofacies

Oil type 2: Mainly marine oxic to slightly terrestrial influenced organofacies

Oil type 3: Terrestrial influenced organofacies

Oil type 4: Marine anoxic organofacies.

The four oil types are largely similar to those defined in Petersen et al. (2016). Oil type 1 characterises the bulk of the oil samples and represent the main Upper Jurassic Farsund Formation source rock. Oil type 2 and type 3 represents terrestrial source rock organofacies, typically Middle Jurassic deposits, and are less common in Upper Jurassic organofacies. Oil type 4 represents oil that occurs in the Outer Rough Basin and represents a Permian rather exotic organofacies (see Petersen et al. 2016 for a more detailed discussion and definition).

It should be stressed that subdivision of each main group can be carried out if detailed analysis is required. In this study a subdivision of the oil type 1 is made in Step 4.

Oil classification is presented in Appendix 8F-A and the score results are found in Appendix 8F-B.

Table 8F.3. *PCA loadings of [A] and environmental control on biomarkers (c.f. Table 8F.2). Red and green boxes indicate relatively high positive and low negative loadings respectively.*

Ratio	Environment	low	high	Thermal maturity	low	high		PC-1	PC-2	PC-3
Pr/Ph	x	anoxic	oxic	(x)			Pr/Ph	0,00	0,17	0,04
Ts/(Ts + Tm)	x	anoxic	oxic	x	immature	mature	Ts/(Ts + Tm)	0,01	0,25	-0,08
29Ts/(29Ts + H29)	x	anoxic	oxic	x	immature	mature	29Ts/(29Ts + H29	0,10	0,23	-0,17
30Ts/H30ab	x	anoxic	oxic	x	immature	mature	30Ts/H30ab	0,18	0,01	-0,26
30E/H30ab	x	anoxic	oxic	x	immature	mature	30E/H30ab	0,15	0,20	-0,21
30D/H30ab	x	anoxic	oxic	x	immature	mature	30D/H30ab	0,15	0,20	-0,24
31D-S/H30ab	x	anoxic	oxic	x	immature	mature	31D-S/H30ab	0,17	0,18	-0,24
31D-R/H30ab	x	anoxic	oxic	x	immature	mature	31D-R/H30ab	0,16	0,19	-0,24
30ba/H30ab	x	anoxic	oxic	x	mature	immature	H30ba/H30ab	-0,04	0,00	-0,21
BNH/ H30ab	x	oxic	anoxic	(x)	immature	mature	BNH/H30ab	-0,16	-0,04	0,18
H29ab/H30ab	x	shale	carbonate				H29ab/H30ab	0,05	-0,13	0,03
31abS	x	oxic	anoxic				31abS	0,22	-0,15	-0,02
31abR	x	oxic	anoxic				31abR	0,21	-0,15	-0,16
32abS	x	oxic	anoxic				32abS	0,25	-0,13	-0,07
32abR	x	oxic	anoxic				32abR	0,22	-0,16	-0,12
33abR	x	oxic	anoxic				33abS	0,21	-0,17	-0,05
33abR	x	oxic	anoxic				33abR	0,18	-0,19	-0,11
34abS	x	oxic	anoxic				34abS	0,19	-0,21	-0,04
34abR	x	oxic	anoxic				34abR	0,18	-0,21	-0,08
35abS	x	oxic	anoxic				35abS	0,18	-0,22	0,02
35abR	x	oxic	anoxic				35abR	0,16	-0,23	0,01
H31S/(S+R)				x	immature	mature	H31S/(S+R)	0,04	-0,01	0,39
H32S/(S+R)				x	immature	mature	H32S/(S+R)	0,12	0,10	0,25
H35/H34	x	oxic	anoxic				H35/H34	0,12	-0,21	0,16
HHI	x	oxic	anoxic				HHI	0,15	-0,22	0,06
C27stD/R+D)		carbonate	shale	(x)	immature	mature	C27stD/(R+D)	0,14	0,23	0,06
C28stD/R+D)		carbonate	shale	(x)	immature	mature	C28stD/(R+D)	0,14	0,23	0,06
C29stD/R+D)		carbonate	shale	(x)	immature	mature	C29stD/(R+D)	0,14	0,23	0,04
C27stS/S+R)				x	immature	mature	C27stS/(S+R)	0,21	0,09	0,27
C28stS/S+R)				x	immature	mature	C28stS/(S+R)	0,23	0,10	0,21
C29stS/S+S)				x	immature	mature	C29stS/(S+R)	0,23	0,09	0,24
C27stbb/bb+aa)				x	immature	mature	27st bb/(bb+aa)	0,22	0,13	0,19
C28stbb/bb+aa)				x	immature	mature	28st bb/(bb+aa)	0,23	0,13	0,16
C29stbb/bb+aa)				x	immature	mature	29st bb/(bb+aa)	0,22	0,15	0,16
%C30							%C30	-0,11	-0,05	0,14

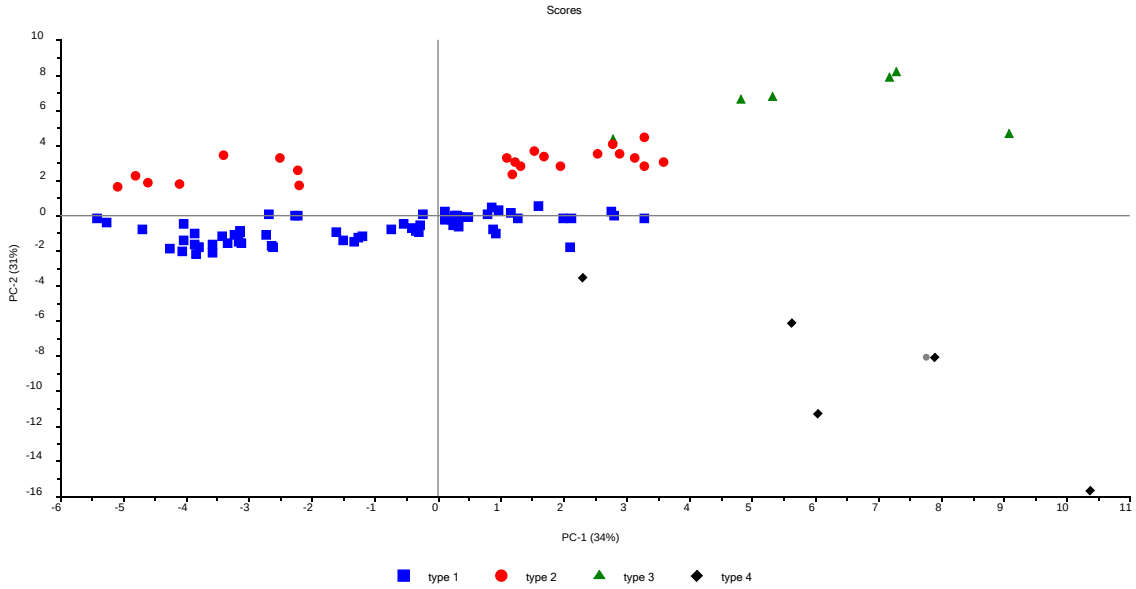

Fig. 8F.1a. *PCA score plot of (PC1 vs PC2) of 99 oil samples (matrix A).*

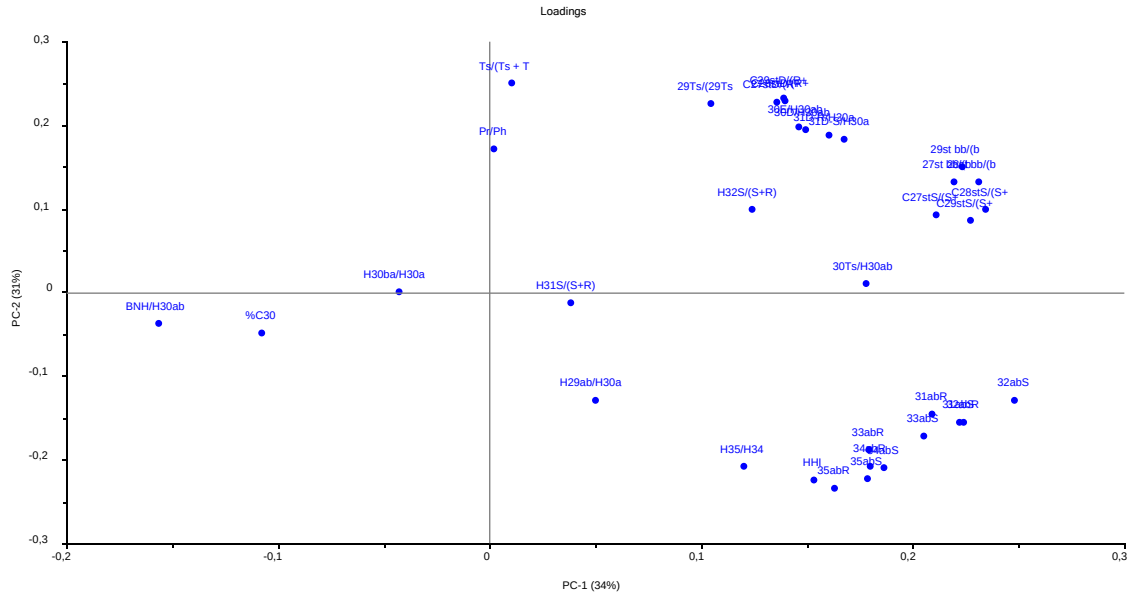

Fig. 8F.1b. *PCA loading plot (PC1 vs PC2) of 99 oil samples (matrix A).*

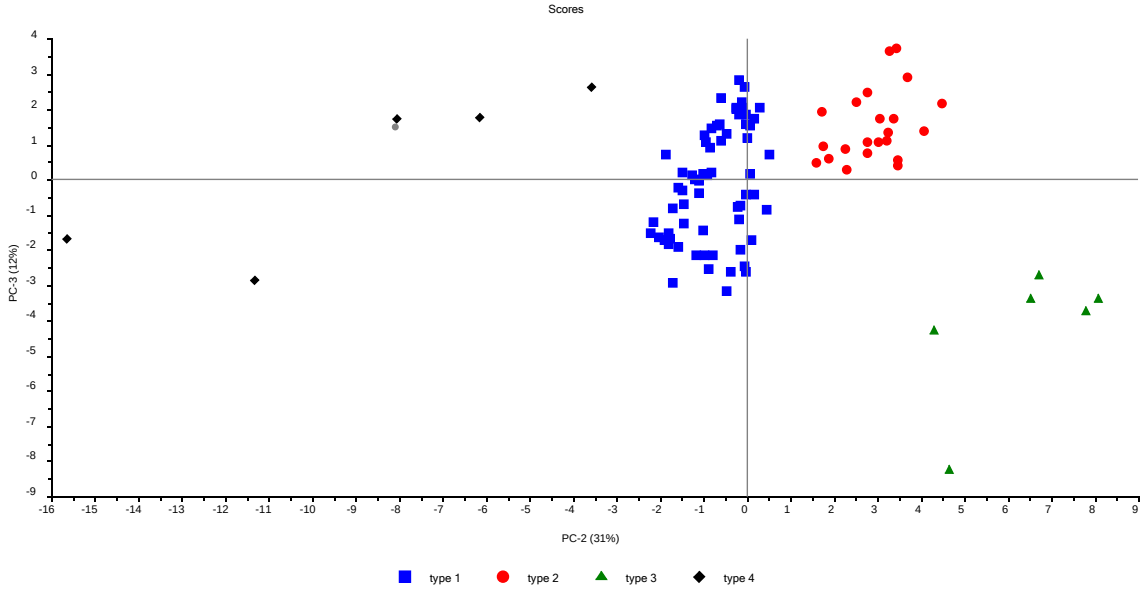

Fig. 8F.2a. *PCA score plot (PC2 vs PC3) of 99 regionally selected oil samples (matrix A). This diagram forms the basis for defining the four naturally occurring oil types (oil type 1 to oil type 4).*

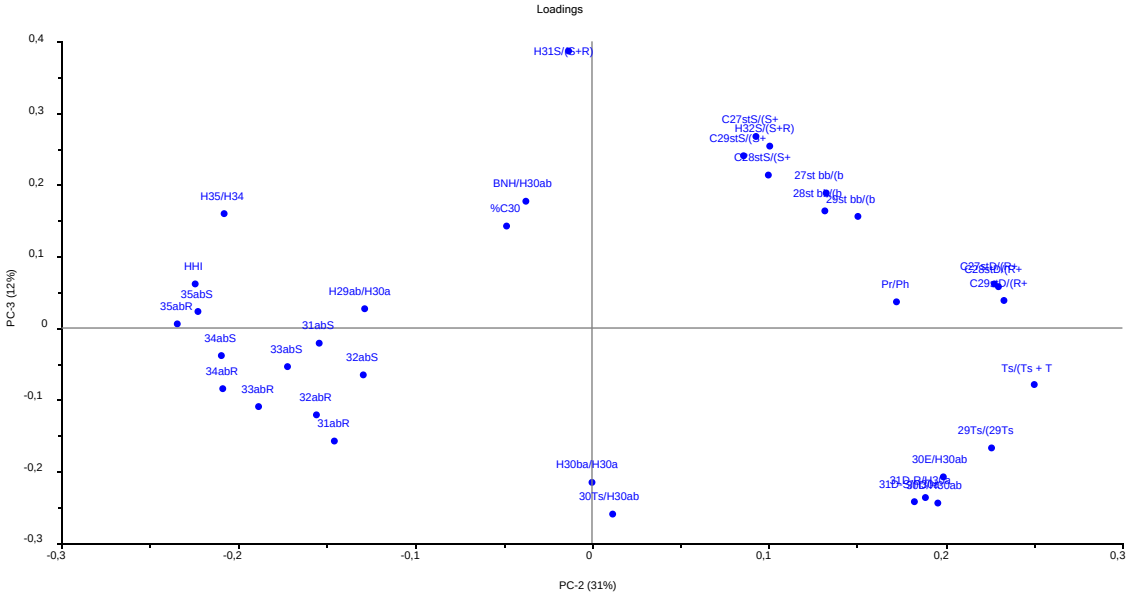

Fig. 8F.2b. *PCA loading plot (PC2 vs PC3) of 99 regionally selected oil samples (matrix A).*

Step 3: PCA analysis of oil samples with sediment extract samples

A PCA model was prepared and analysed in order to jointly classify oil types and sediment extract data. In addition it was decided to include a sample set from the Valdemar Field to examine the intra field variation.

The data included was: 99 oil samples previously classified into four main types (oil type 1-4), 285 sediment extracts and 61 oil extracts from the Valdemar Field. The data are termed matrix A, B and C respectively.

The first PC axis in the model of [A]+[B]+[C] represents 38% of the variance. High positive values are related to high maturity and high negative values reflect thermally immature biomarker samples (Figs 8F.3a & 8F.3b). Oils plot with lower PC 1 scores than -2 whereas sediment extract samples plot with PC1 score values down to -8.5. This reflects that sediments with PC1 values less than -2 are thermally immature and thus no oils have been generated.

The PC2 vs PC3 loading plot model of [A]+[B]+[C] accounts for 33% of the variance and displays biomarkers that code for organofacies variations (Figs 8F.4A & 8F.4B). All oil type 4 (Permian oils) and one sample from the Mona-1 well plot on the PC2>0 (Fig. 8F.4a). To focus the analysis on Jurassic oils and their likely source rocks only, the analyses has been limited to deal only with samples having PC2 < 0. By doing so the Mona-1 oil sample is regarded as an outlier from other type 1 oils. The reduced sample A matrix is termed [A*]. The reduced B matrix is termed [B*].

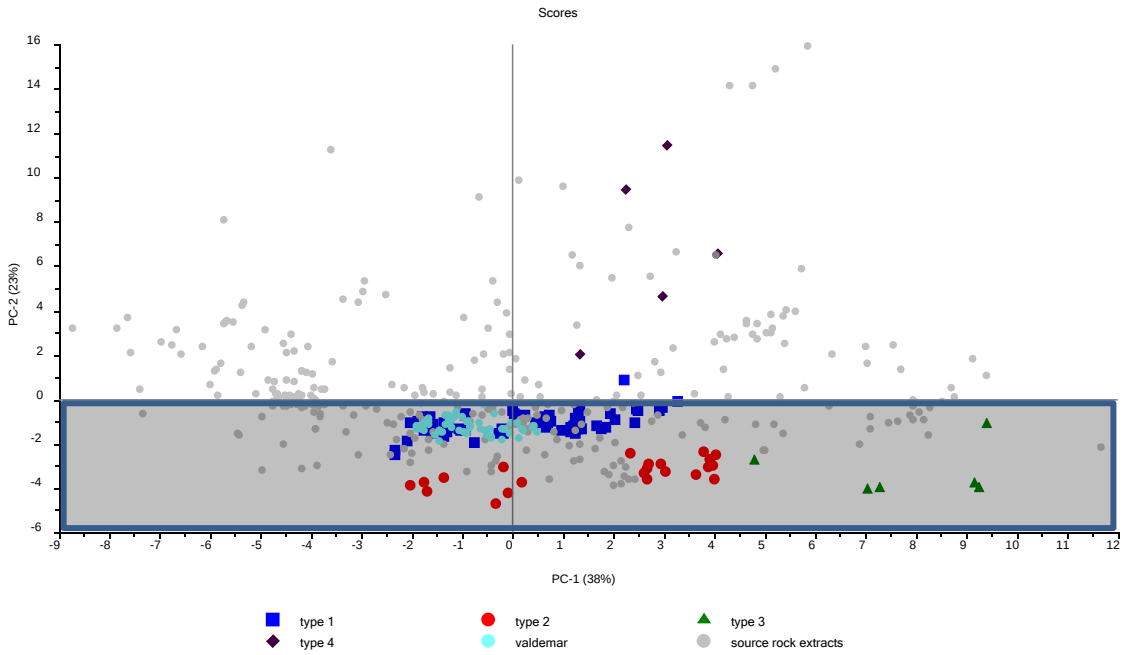

Fig. 8F.3a. *Score plot for PC1 vs PC2 for a model including oil extracts (regional North Sea), sediment extracts and oil samples from the Valdemar Field ([A]+[B]+[C]). The four main oil types (type 1 to type 4) are defined above. The rectangle (PC2<0) encloses the zone of interest for further data analysis i.e. [A*]+[B*]+[C] samples.*

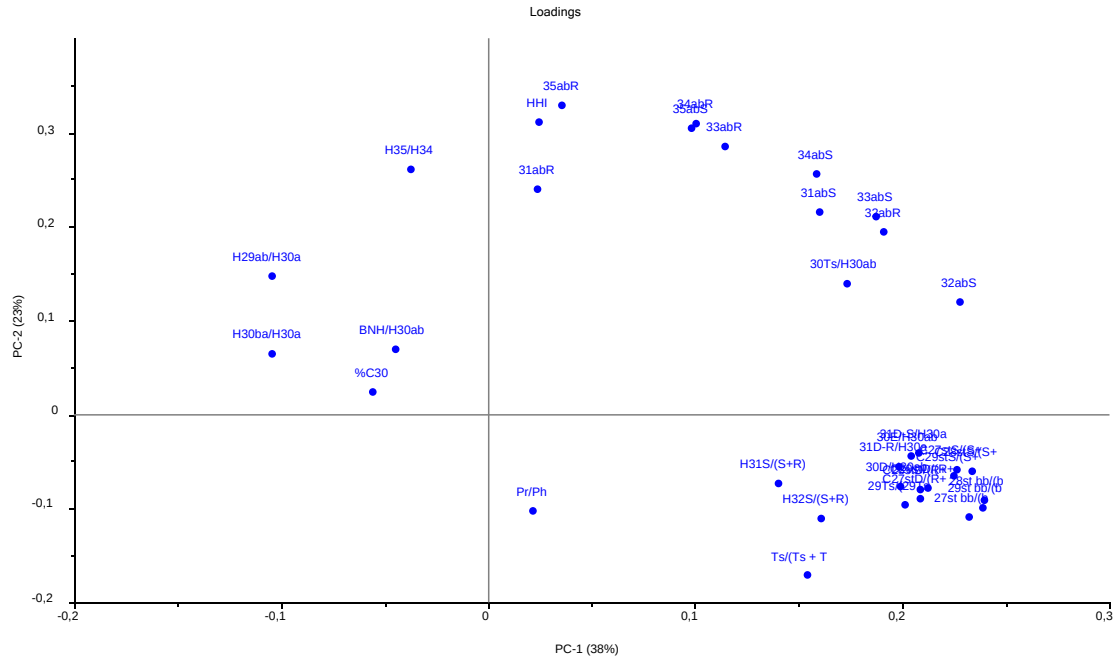

Fig. 8F.3b. *Loading plot PC1 vs PC2 for a model including oil extracts (regional North Sea), sediment extracts and oil samples from the Valdemar Field ([A]+[B]+[C]).*

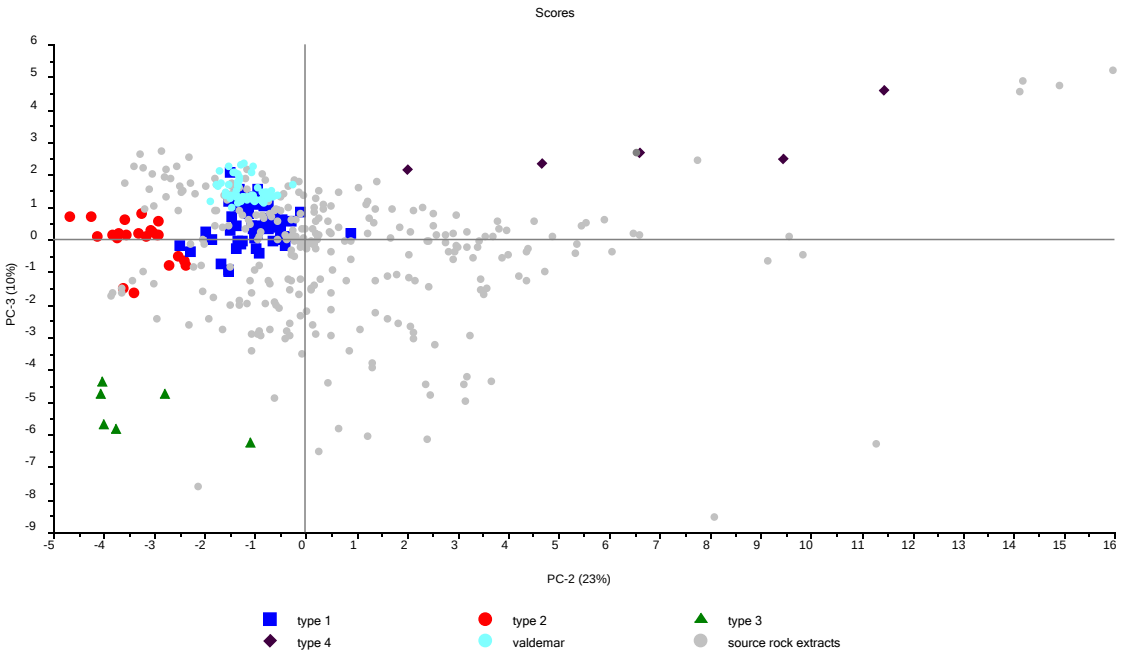

Fig. 8F.4a. *PC2 versus PC3 Score for a model including oil extracts (regional North Sea), sediment extracts and oil samples from the Valdemar field ([A]+[B]+[C]).*

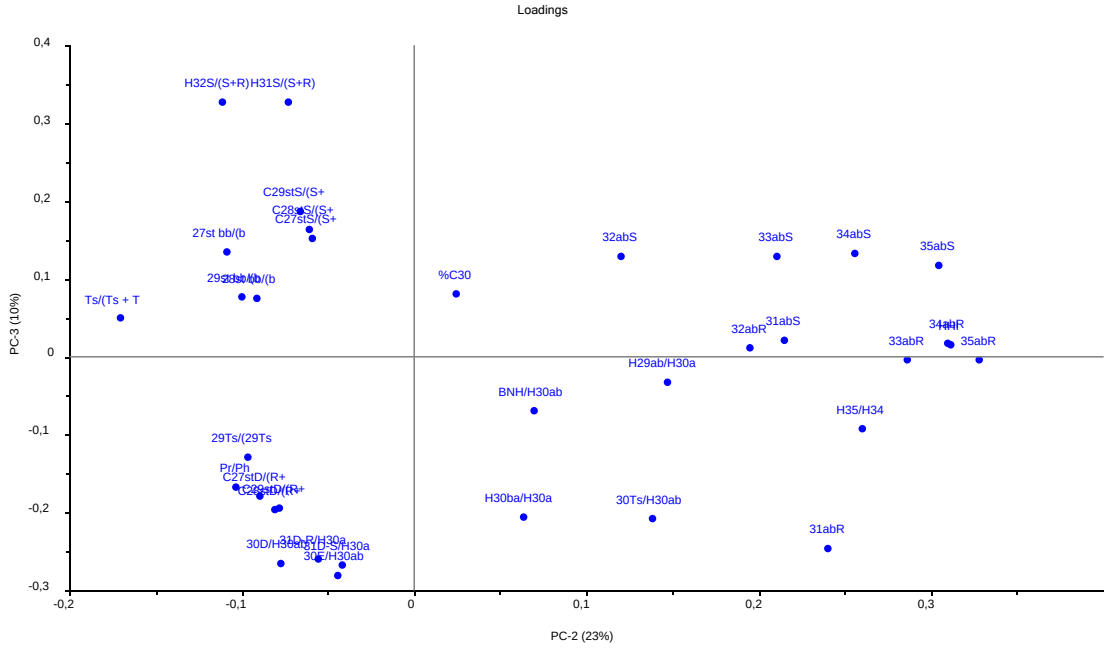

Fig. 8F.4b. *PC2 versus PC3 loading plot for a model including oil extracts (regional North Sea), sediment extracts and oil samples from the Valdemar field ([A]+[B]+[C]).*

Step 4: Subtypes within the oil type 1 family

In order to focus on Jurassic oils only and their relation to sediment extracts, the reduced data matrix of [A] and [B] i.e. [A*] and [B*] was applied for further analysis. No reduction is needed in [C] as these samples all plot within the Jurassic oil types (cf. Fig. 8F.4a).

The PC1 and PC2 axes of this analysis models 59% of the variance (Figs 8F.5a & 8F.5b). The PC2 vs PC3 score plot forms the basis for a subdivision of Oil type 1 into subclasses (Fig. 8F.6a). The subtyping is made by labelling the four quadrants defined by PC2 and PC3 in Fig. 8F.6a.

The labelling of the subtypes are:

Type 1A - quadrant I i.e. >0,>0;

Type 1B - quadrant II i.e.<0,>0;

Type 1C - quadrant III i.e. <0,<0;

Type 1D - quadrant IV i.e. >0,<0.

The division between Oil type 1B and Oil type 2 and between Oil type 1C and Oil type 3 is placed at a -1.8 PC2 score value (Fig. 8F.6a).

Following this approach, the following subtypes within Oil type 1 (i.e. marine anoxic to slightly oxic conditions) have been defined (see also Fig. 8F.7):

Oil type 1A: A subtype influenced by HHI and %C30. Marine anoxic.

Oil type 1B: A subtype influenced by high Pr/Ph ratios and thus relatively terrestrial rich. The type grades into Oil type 2.

Oil type 1C: A subtype influenced by high Pr/Ph ratios and thus relatively terrestrial rich. The Oil type grades into Oil type 3

Oil type 1D: Subtype influenced by HHI and %C30. Marine anoxic.

The above classification was applied to samples in [A*], [B*] and [C]. Samples from [B] not included in [B*] were labelled “no match” since the [B*] matrix was prepared to only include extract samples that overlap in composition with known Jurassic oil types. The “no match” thus refers to no match with known Jurassic oils from Danish North Sea reservoirs. Analysis of new samples may lead to another classification.

Table 8F.4. *PCA loadings of [A*] + [B*]+[C] and environmental control on biomarker (c.f. Table 2). Red and green boxes indicate relative high positive and low negative loadings respectfully.*

Ratio	Environment	low	high	Thermal maturity	low	high	PC-1	PC-2	PC-3
Pr/Ph	x	anoxic	oxic	(x)			0,02	-0,27	-0,05
Ts/(Ts + Tm)	x	anoxic	oxic	x	immature	mature	0,18	0,10	0,07
29Ts/(29Ts + H29)	x	anoxic	oxic	x	immature	mature	0,21	0,02	-0,07
30Ts/H30ab	x	anoxic	oxic	x	immature	mature	0,19	-0,01	-0,22
30E/H30ab	x	anoxic	oxic	x	immature	mature	0,19	-0,14	-0,20
30D/H30ab	x	anoxic	oxic	x	immature	mature	0,19	-0,14	-0,19
31D-S/H30ab	x	anoxic	oxic	x	immature	mature	0,21	-0,11	-0,20
31D-R/H30ab	x	anoxic	oxic	x	immature	mature	0,19	-0,11	-0,20
30ba/H30ab	x	anoxic	oxic	x	mature	immature	-0,11	-0,15	-0,20
BNH/ H30ab	x	oxic	anoxic	(x)	immature	mature	-0,03	0,13	0,16
H29ab/H30ab	x	shale	carbonate				-0,11	-0,19	-0,03
31abS	x	oxic	anoxic				0,19	0,04	-0,13
31abR	x	oxic	anoxic				0,12	-0,03	-0,24
32abS	x	oxic	anoxic				0,23	0,09	-0,05
32abR	x	oxic	anoxic				0,20	0,11	-0,17
33abR	x	oxic	anoxic				0,20	0,21	-0,04
33abR	x	oxic	anoxic				0,16	0,25	-0,15
34abS	x	oxic	anoxic				0,21	0,20	-0,02
34abR	x	oxic	anoxic				0,17	0,25	-0,16
35abS	x	oxic	anoxic				0,17	0,23	0,08
35abR	x	oxic	anoxic				0,12	0,29	-0,02
H31S/(S+R)				x	immature	mature	0,06	0,10	0,19
H32S/(S+R)				x	immature	mature	0,11	-0,02	0,33
H35/H34	x	oxic	anoxic				0,01	0,16	0,12
HHI	x	oxic	anoxic				0,07	0,28	0,13
C27stD/R+D)		carbonate	shale	(x)	immature	mature	0,20	-0,21	0,00
C28stD/R+D)		carbonate	shale	(x)	immature	mature	0,20	-0,19	-0,01
C29stD/R+D)		carbonate	shale	(x)	immature	mature	0,20	-0,19	-0,02
C27stS/S+R)				x	immature	mature	0,18	-0,16	0,27
C28stS/S+R)				x	immature	mature	0,19	-0,15	0,26
C29stS/S+S)				x	immature	mature	0,17	-0,15	0,28
C27stbb/bb+aa)				x	immature	mature	0,21	-0,09	0,24
C28stbb/bb+aa)				x	immature	mature	0,22	-0,08	0,20
C29stbb/bb+aa)				x	immature	mature	0,22	-0,08	0,20
%C30							-0,06	0,29	0,11

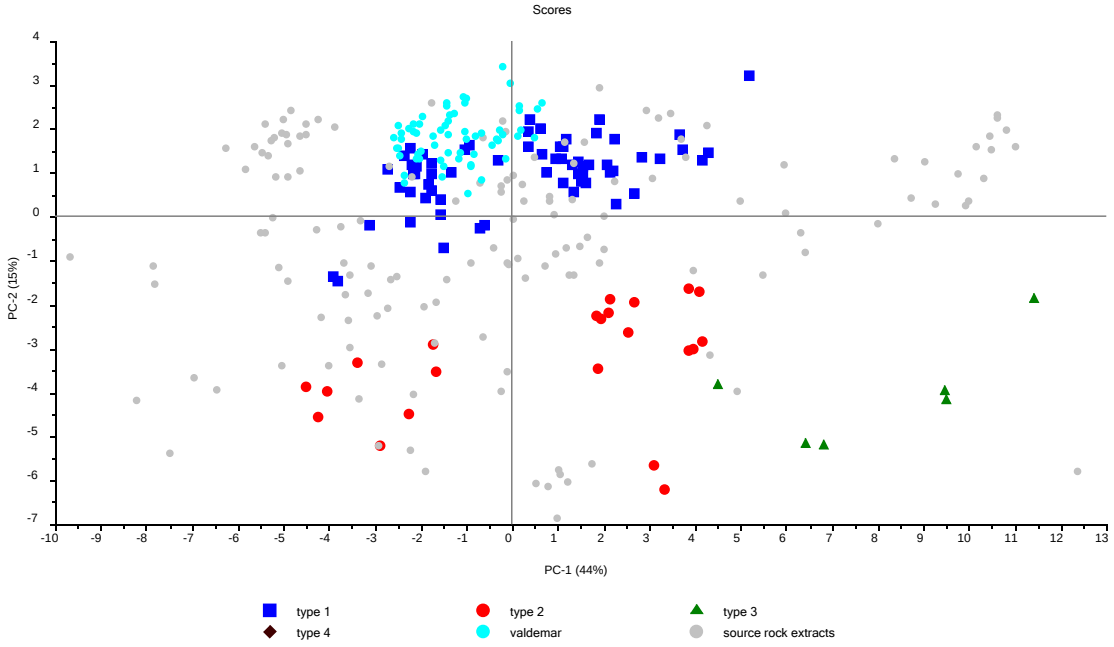

Fig. 8F.5a. *PC1 versus PC2 score plot of the samples with a PC2<0 defined in Fig. 8F.4 ([A*]+[B*]+[C]).*

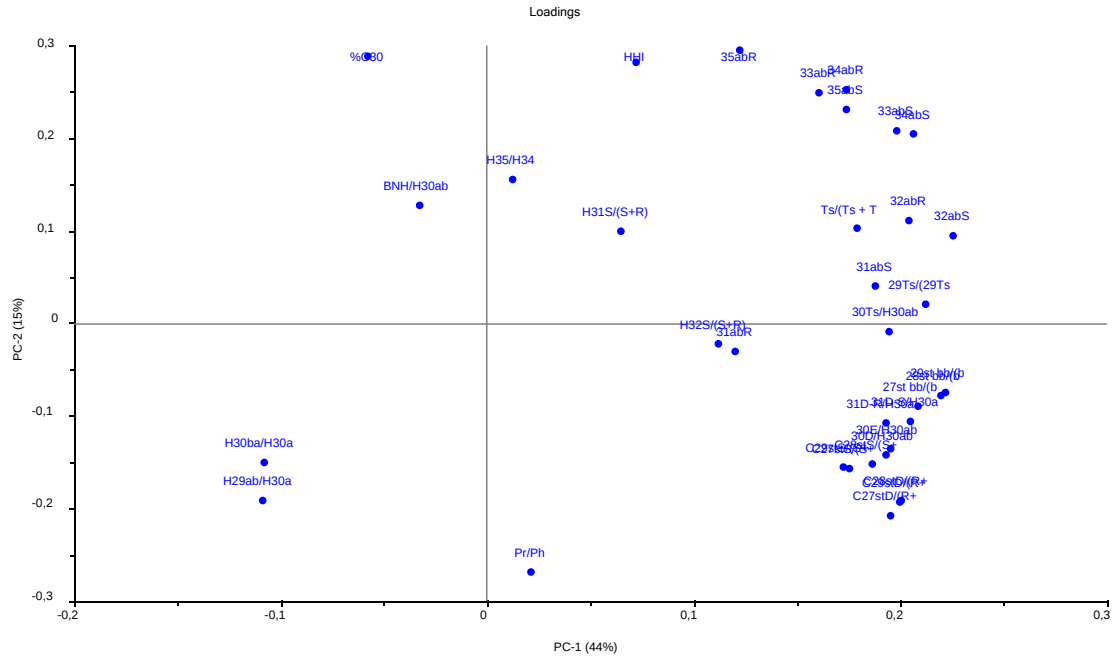

Fig. 8F.5b. *PC1 versus PC2 loading plot for ([A*]+[B*]+[C]).*

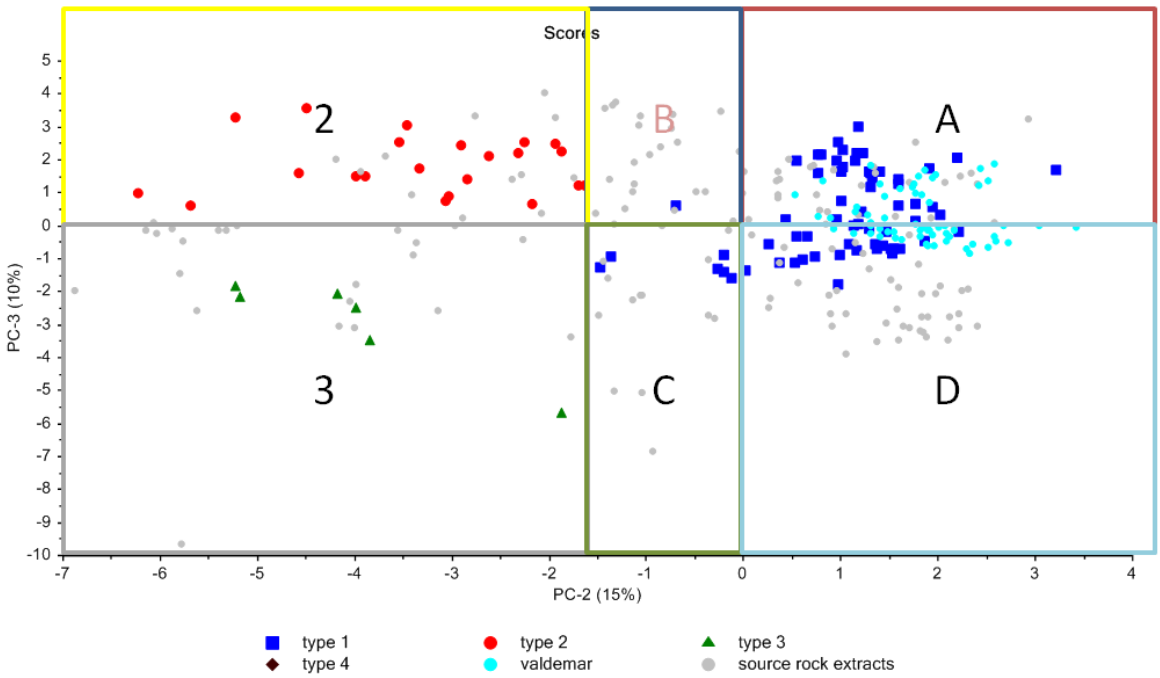

Fig. 8F.6a. *PC2 versus PC3 score plot of the selected samples ([A*]+[B*]+[C]). "A-D"; oil subtypes with oil type 1. "2": oil type 2. "3": oil type 3.*

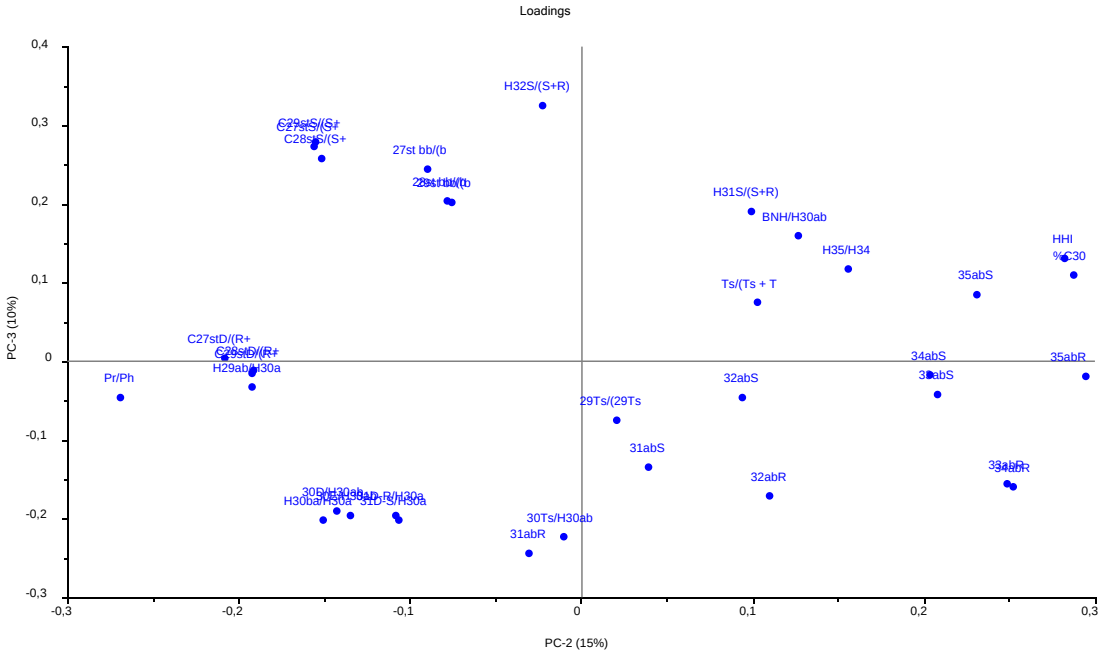

Fig. 8F.6b. *PC2 versus PC3 loading plot for ([A*]+[B*]+[C]).*

8F.6 Oil types and Jurassic sequence ages of sediment extracts

Following Step 4 the sediment extract samples in [B] has been classified together with the oil types (i.e. Fig. 8F.6a). Since all the samples also have a defined age according to the sequence stratigraphic nomenclature established in the Petsys project for the Jurassic source rocks, an analysis of the relative age on the oil types can be made (Fig. 8F.8).

The Jurassic sequence up to the Kimm-1 sequence mainly represents source rocks that generated terrestrial oils. These source rocks are found within the Bryne, Lola, and Lulu formations. Source rocks generating marine type 1A and 1B oils occur within the Kimm-1 and Kimm-2 sequences. These reflect marine anoxic organofacies (Type 1A). A more oxic terrestrial organofacies (Type 1B) is found within the Lola and basal part of the Farsund formations.

By the time of deposition of Kimm-3, two new oil types appear suggesting a diversification of the depositional environment into more types of organofacies including a terrestrial dominated marine type (Type 2), a mixed terrestrial and marine type (Type 1C) and a marine anoxic organofacies (Type 1D) all of which occur within the Farsund Formation. By Kimm-4 to Volg-2 times the oils are dominated by the marine anoxic organofacies (1D type); oil Type 2 does not occur and oil subtypes 1A and 1B only marginally. From the Volg-3 to the Ryaz-2 sequences oil type 1D is reduced in abundance and the relative abundance within the data set of oil type 1A, 1B and 1C increases together with the re-appearance of oil type 2. This suggests a renewed diversification of the organofacies types within the basins corresponding to the upper part of the Farsund and the Mandal formations.

A clear geographic variation is seen in the oil types within the North Sea (Fig. 8F.9). Type 1 dominates in the southern Salt Dome Province (subtype 1D) and around the Tail End Graben (subtype 1A). Terrestrial types (type 3 and 2) occur locally concentrated; type 3 in the Outer Rough Basin and type 2 in the Søgne Basin and in the greater Ravn area. Subtypes 1B and 1C occur in the greater Valdemar area (Fig. 8F.9). The distribution clearly suggests that several kitchen areas contributed to the accumulated oils.

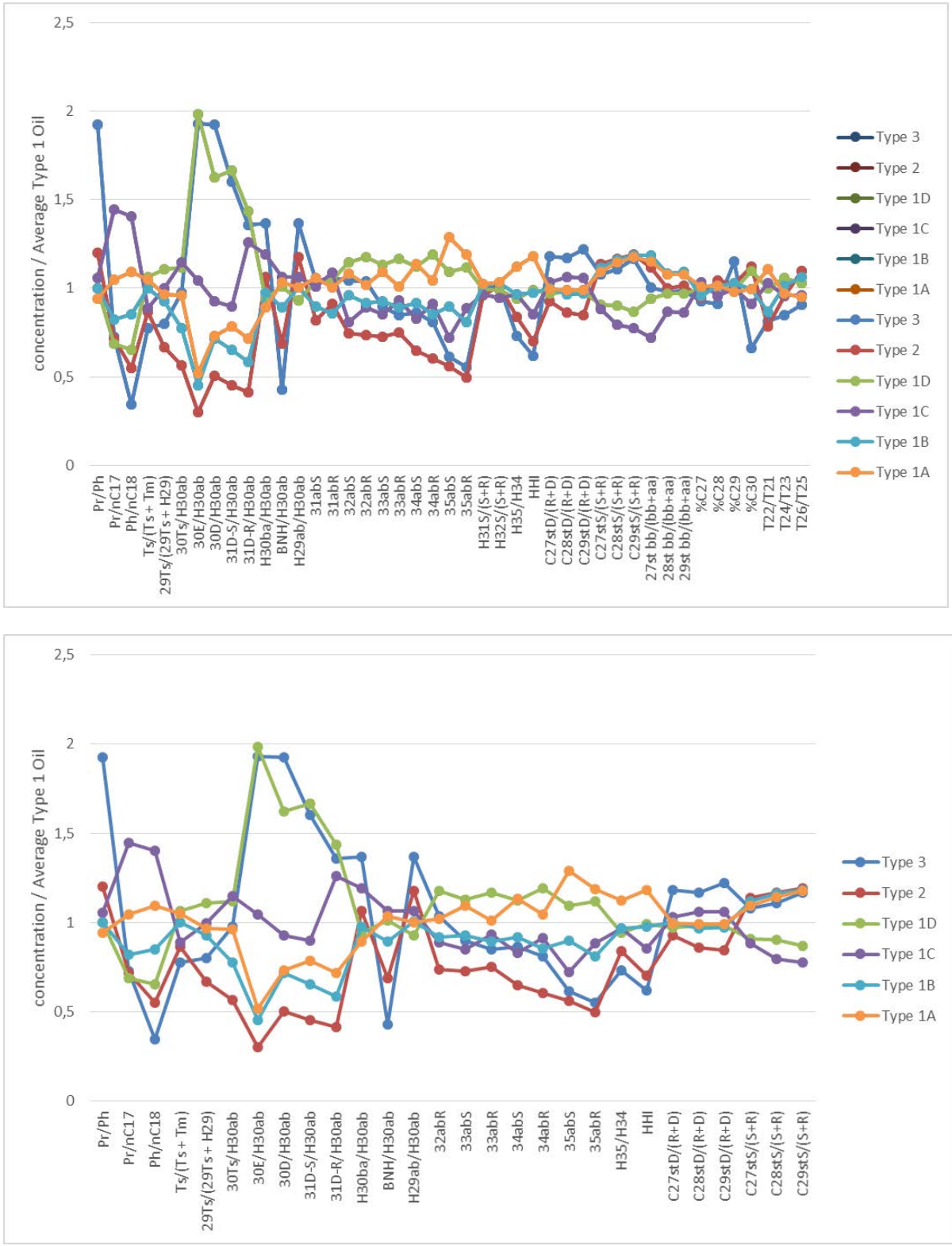

Fig. 8F.7. *Composition of the Jurassic oil types normalised to the type 1 composition (the compositions calculated from the sediment samples [B*]). Diagram above show all measured biomarker and diagram below shown selected biomarkers. The average Jurassic oil type 1 has been calculated as arithmetic mean of the mean composition of subtype 1A, 1B, 1C and 1C.*

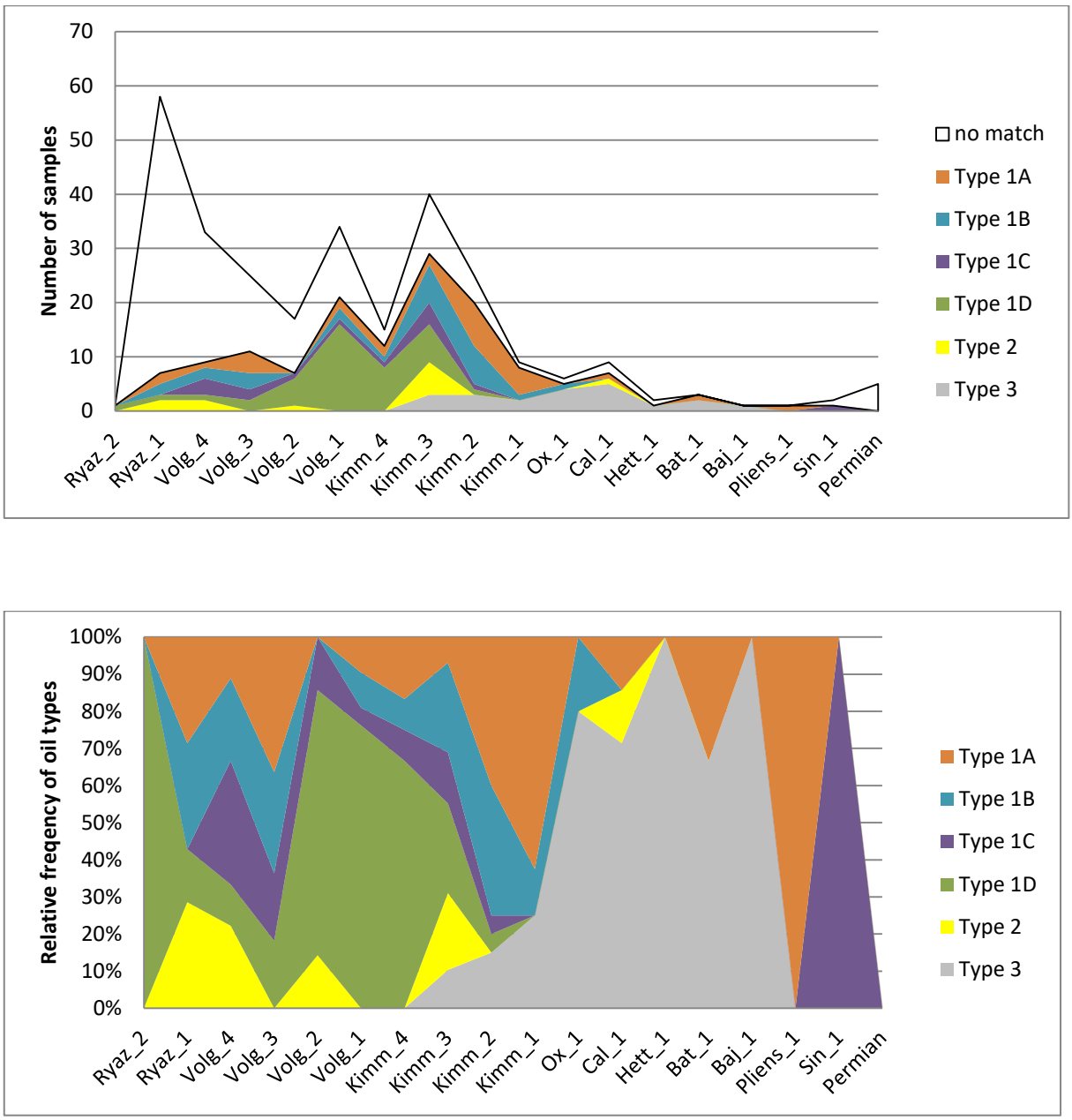

Fig. 8F.8. *Frequency of sediment extract samples vs sequence stratigraphic age of classified samples of [B*]. Diagram above represent the number of sample and the diagram below represent the relative sample frequency summed to 100%. The "no match" in the upper diagram indicates that the sediment extract samples could not be matched to a Jurassic oil family type.*

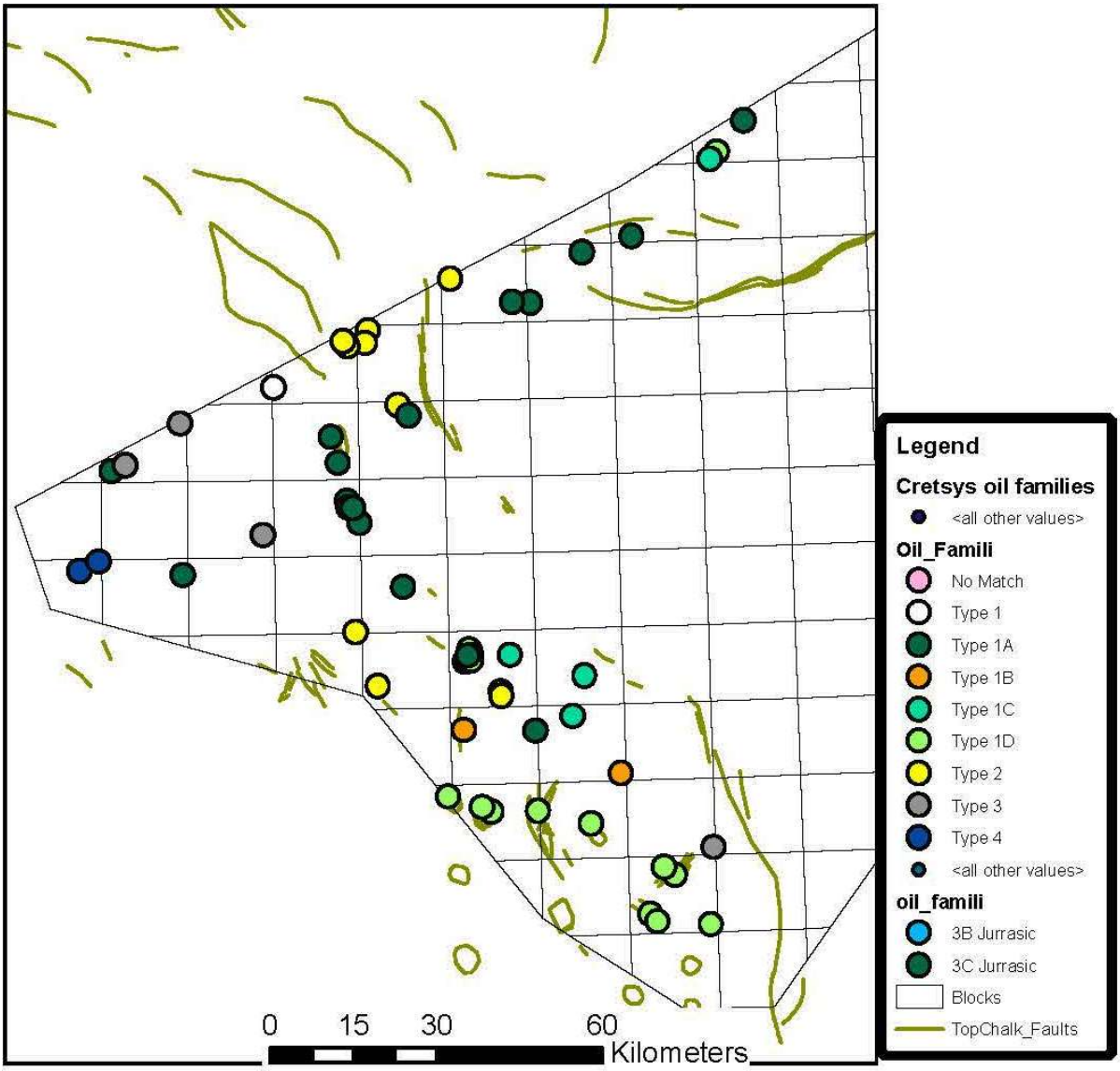

Fig. 8F.9. *Distribution of oil types in oil samples from the Danish part of the North Sea.*

8F.7 Comparison of Valdemar oils with main oil types

The Valdemar oils in matrix C are mainly composed of the most abundant Oil type 1 marine type, sourced from the Farsund Formation. The Valdemar oils represent the 1A and 1D Farsund oil subtypes (Fig. 7E.6a). The variation suggests that organofacies variation occurred within the kitchen area(s) of the Valdemar Field. The variation in the oil maturity (Fig. 7E.5a) suggests that the oil is generally of low maturity, but that oils of higher maturity also occur.

References

Esbensen, K.H. (2012) Multivariate Data Analysis – in Practice. An Introduction to Multivariate data Analysis and Experimental Design. CAMO Publ. ISBN 82-993330-3-2

Esbensen, K.H. & Geladi, P. (2009). Principal Component Analysis (PCA): Concept, geometrical interpretation, mathematical background, algorithms, history. In Brown, S, Tauler, R, Walczak, R (Eds.) Comprehensive Chemometrics, Wiley Major Reference Works, vol. 4, pp 211-226. Elsevier.

Petersen, H.I., Hertle, M., Juhasz, A., Krabbe, H., 2016. Oil family typing, biodegradation and source rock affinity of liquid petroleum in the Danish North Sea. Journal of Petroleum Geology 39, 247-268.

8G Hydrocarbon aspects: prospective Cretaceous intervals

The following brief summary and comments regarding prospective intervals in the Cretaceous succession is based on extraction of data uploaded on the Cretsys website. These include the application of the databases on GR-DT lithology, shows, CPI's and saturation in studied wells.

8G.1 Mandal Formation and Vyl Formation

Gravity flow sandstones have been encountered in a number of wells located along the Coffee Soil Fault Zone. The sandstones occur both below and above the BCU in the Poul Member of the Mandal Formation (below BCU) and the Vyl Formation of the Cromer Knoll Group (above BCU). Hydrocarbon saturations have been recorded in sandstones of the Poul Member in the NW Adda-1 well, while the most spectacular exploration result are from the Amalie-1 well in the northern part of the Central Graben. Here high oil rates were produced from a thin, porous sandstone interval located at the BCU boundary under HTHP-conditions at a depth of 4300 m. Unfortunately, a nearby appraisal well only found traces of sand with minor shows. Distal sandy turbidites with oil in the Mandal Formation are furthermore drilled in the Gertrud Graben in the Hejre–Jeppe area.

Although this sandstone play has not been focus of exploration activities for two decades, a renewed interest has emerged recently. The schematic play area for potential sandstone reservoirs in the Mandal Formation and in the Vyl Formation is depicted on Fig. 8G.1. It includes a narrow area along the Coffee Soil Fault Zone where the presence of lobes of gravity flow sandstones derived from the Ringkøbing-Fyn High may be envisaged. In addition, areas in the Gertrud Graben and in the Iris Basin have been included on the map reflecting the presence of turbiditic sandstone intervals in the Mandal Formation.

Fig. 8G.1. *Schematic play map, Mandal Formation and Lower Cretaceous*

8G.2 Tuxen and Sola Formations

Chalk and marly chalk in the Lower Cretaceous Tuxen and Sola formations are the main reservoirs in the producing Valdemar/Bo Field. The same stratigraphic interval is also the reservoir in the Adda discovery (Figs. 8G.2 and 8G.3).

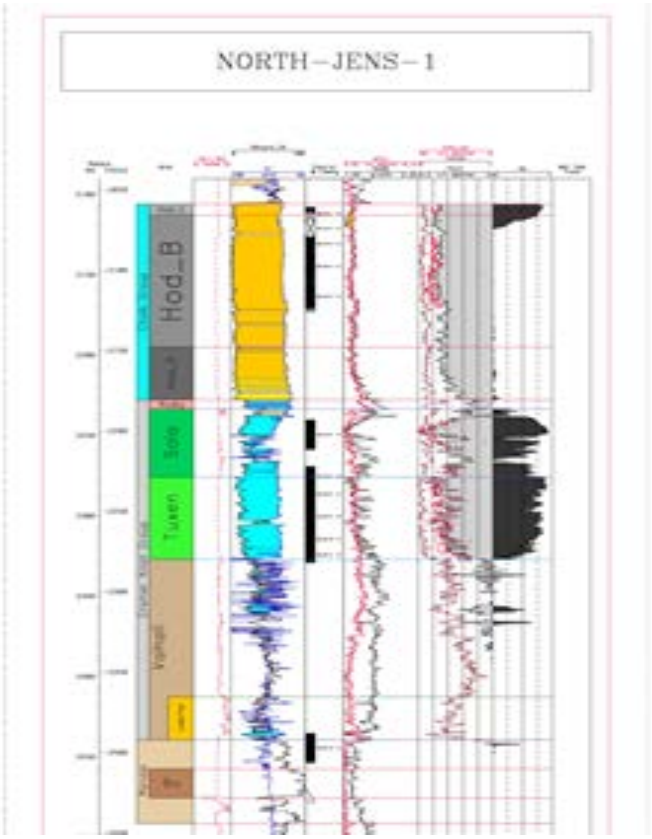

Fig. 8G.2. *CPI log with GR-DT lithology, North Jens-1*

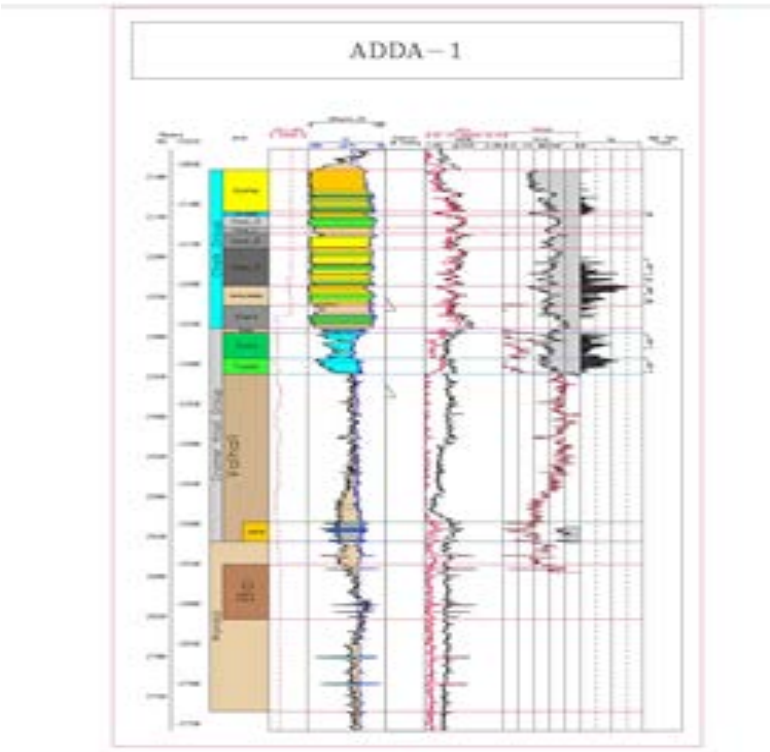

Fig. 8G.3. *CPI log with GR-DT lithology, Adda-1*

Traditionally the Tuxen/Sola interval has been considered as a secondary, deeper exploration target below structural traps identified in the overlying Chalk Group. The reservoirs consist of hemi-pelagic chalk and marly chalk in the Tuxen Formation and to a lesser extent in the overlying Sola Formation. The interval is located between the Upper Jurassic source rocks and overlying Upper Cretaceous hydrocarbon-saturated chalk reservoirs and thus in a favourable position on the migration route e.g. via fractures and faults. The reservoir quality is governed by the clay content. The porosity in the chalk reservoirs is locally very high, up to 35% in the Tuxen Formation in the Valdemar Field at a depth of 2250 m. The effective porosity decreases with increasing burial depth and clay content. The permeability is generally low resulting in reduced productivity compared with the clean chalks in the Tor Formation.

Fig. 8G.4 shows the GR-DT lithology in the wells as pie-diagrams overlying the time isochore map of the Tuxen Formation (seismic unit *CKG10 – CKG15)*. There is a maximum of clean chalk with high porosity in the central and southern parts of the Central Graben switching to dominance of marl and claystone towards the north. The maximum recorded hydrocarbon saturation in the wells is plotted on the time structure map of Top Tuxen (seismic marker *CKG15)* in Fig. 8G.5. The hydrocarbon-bearing wells are restricted to an area concentrated in the shallow central part of the DCG on the Bo-Jens and Adda inversion ridges stretching northwards in the direction of the South Arne structure. Combination of the GR-DT facies map (Fig. 8G.4) with the recorded hydrocarbon saturation map (Fig. 8G.5) led to the definition of a rather small play area for Tuxen/Sola reservoirs, centred on the above mentioned inversion ridges.

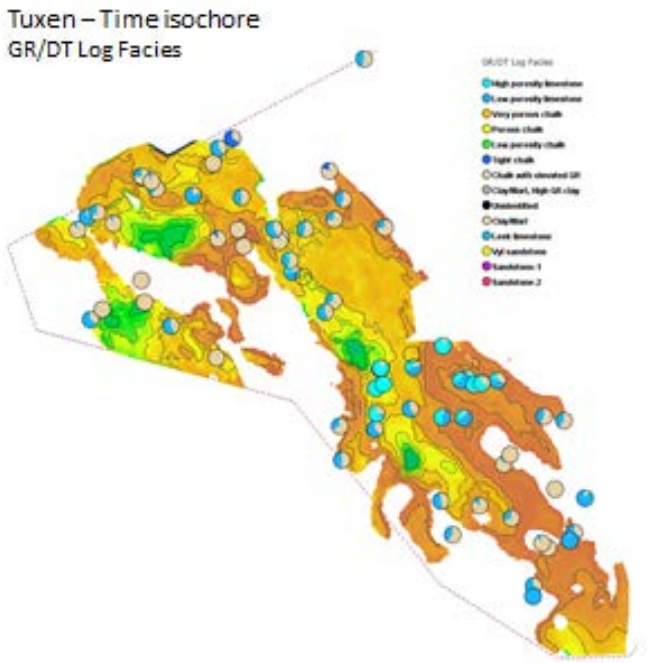

Fig. 8G.4. *GR-DT lithology on the time structure map of Tuxen Formation. Light blue colour indicates chalk intervals with porosity above 20%. Light brown colour is used for marl and clay.*

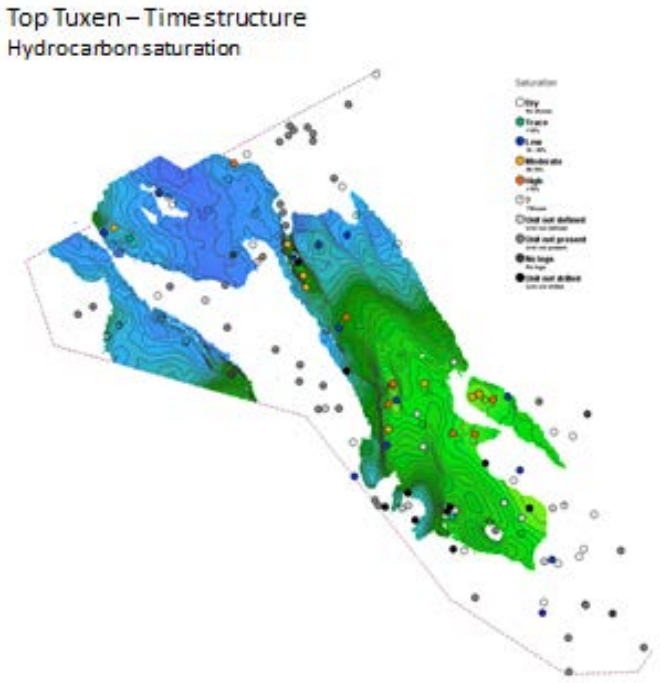

Fig. 8G.5. *Hydrocarbon saturation in the Tuxen Formation plotted on the time structure map.*

8G.3 Hidra and Hod Formations

Structurally trapped oil has been located both in the Hidra and Hod formations in the lower part of the Chalk Group (e.g. in the Adda and Bo/Valdemar area) above accumulations in the Tuxen Formation, where the top-seals have been breached as shown in Figs 8G.3 & 8G.6. These discoveries show that the chalk can act both as a reservoir and as a top-seal. High porosities can occur in the lower part of the chalk, if they contain redeposited intervals, moderate burial depth and overpressure reducing the effective stress mitigating mechanic/chemical compaction. The effects of burial depth are illustrated on Fig. 8G.7, where pie-diagrams of GR-GT log facies of the Hod C + D unist in the wells are plotted on the time structure map of top Hod D (seismic marker *ch11)*. In contrast to the southern shallow area, the chalk in the northern deep area is dominated by tight (blue) chalk. The distribution of hydrocarbons in the interval is shown on Fig. 8G.8. Saturations are recorded on inversion structures and on the southern oil and gas fields with a long hydrocarbon column stretching to below the overlying Tor Formation. The play area for intra-chalk reservoirs in the stratigraphic lower part of the Chalk Group resembles that of the Tuxen/Sola formations and is confined to the shallow located inversion anticlines in the central part of the DCG, where high porosity chalk intervals can be predicted to exist (Fig. 8G.9).

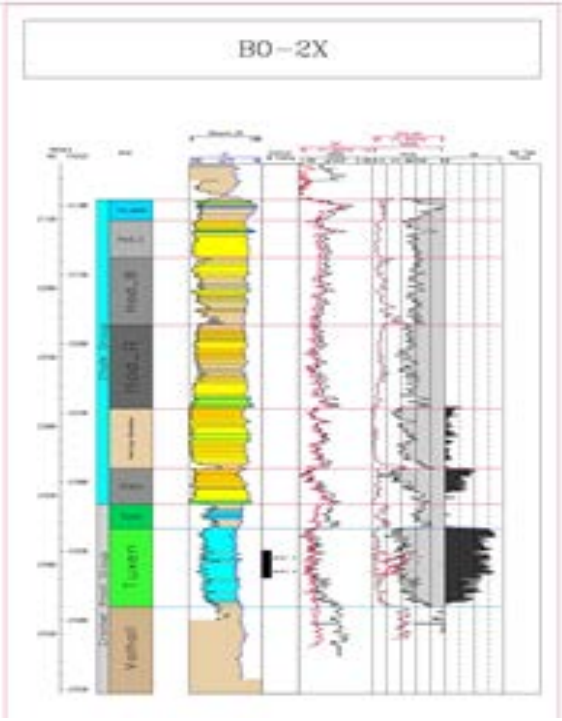

Fig. 8G.6. *CPI-log of Bo-1 with hydrocarbon saturations in both the Tuxen and Hidra Formations.*

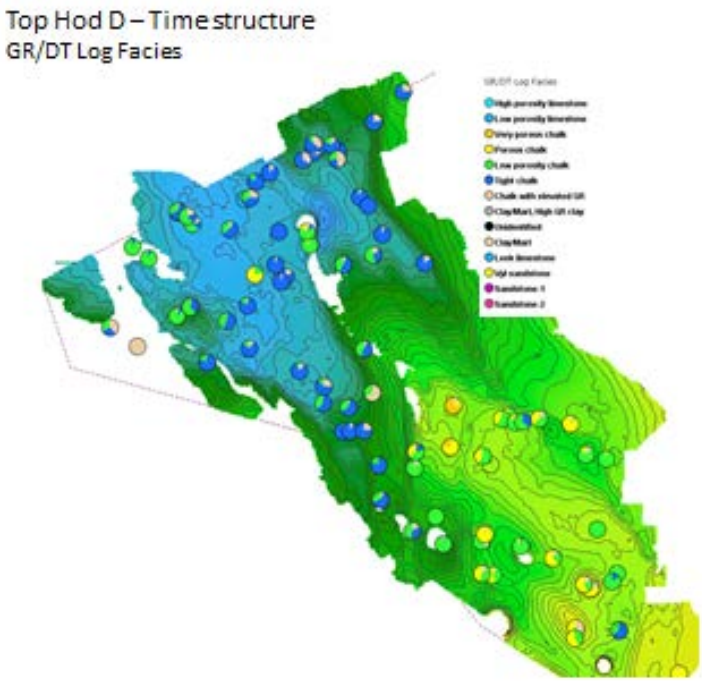

Fig. 8G.7. *GR-DT log facies of the Hod C + D unist overlying the time structure map of top Hod D (ch11)*

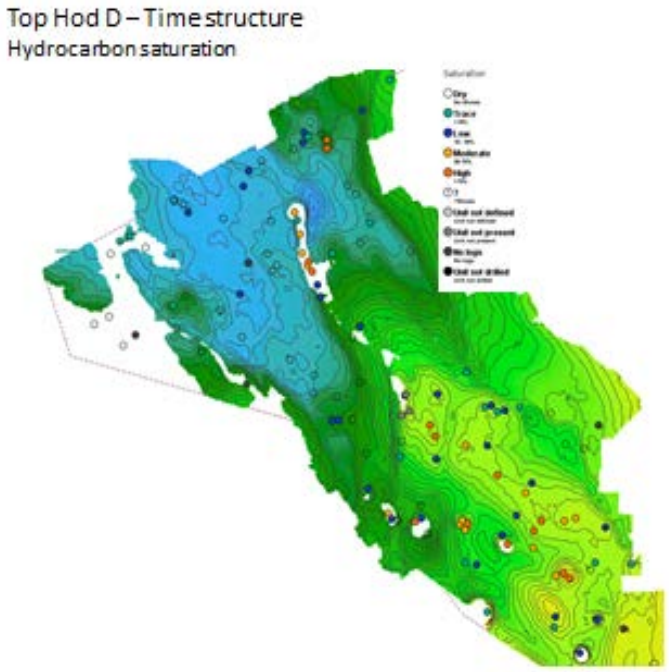

Fig. 8G.8. *Hydrocarbon saturation in the Hod C + D units plotted on the time structure map of top Hod D.*

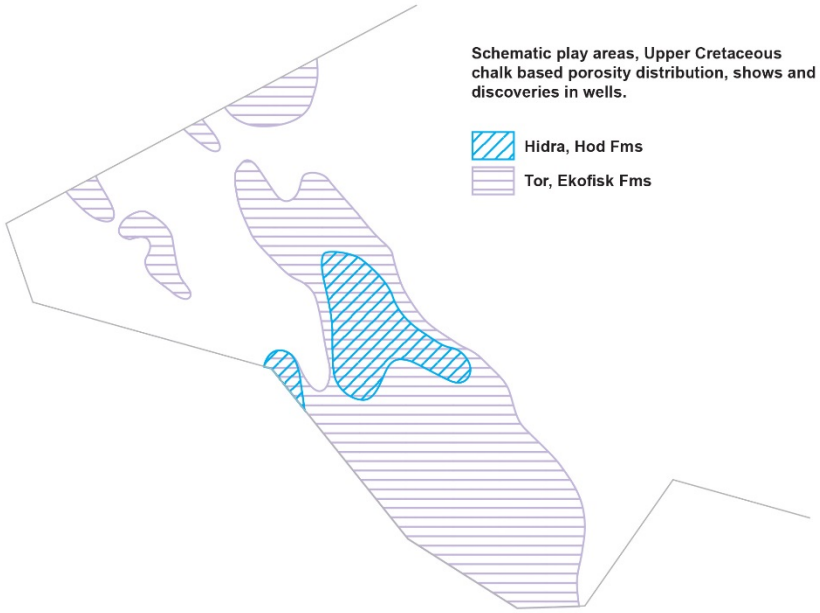

Fig. 8G.9. *Schematic play map of Upper Cretaceous chalks.*

8G.4 Tor and Ekofisk formations

The vast majority of the the Danish oil/gas production stems from porous chalk reservoirs in the Tor and Ekofisk formations. The dominant trap-type is structural, where the fields are located in 4-way dip closures over salt structures and inversion anticlines. An example is the Dan Field, where the CPI-log from the discovery well shows a more than 200 m long hydrocarbon column (Fig. 8G.10). The distribution of wells with hydrocarbon saturations in the two formations is plotted on the corresponding time structure maps on Figs 8G.11 & 8G.12. The maps show the close relationship between the presence of hydrocarbons and structure.

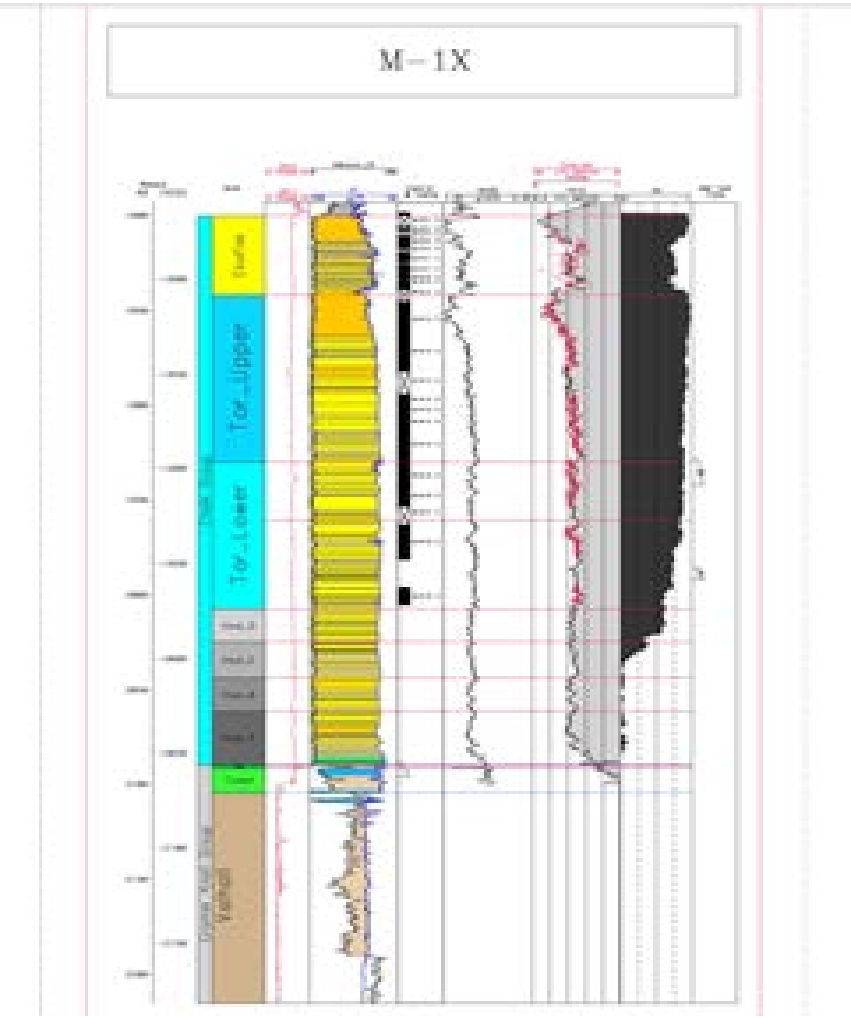

Fig. 8G.10. *CPI-log, M-1 with a 200 m hydrocarbon column*

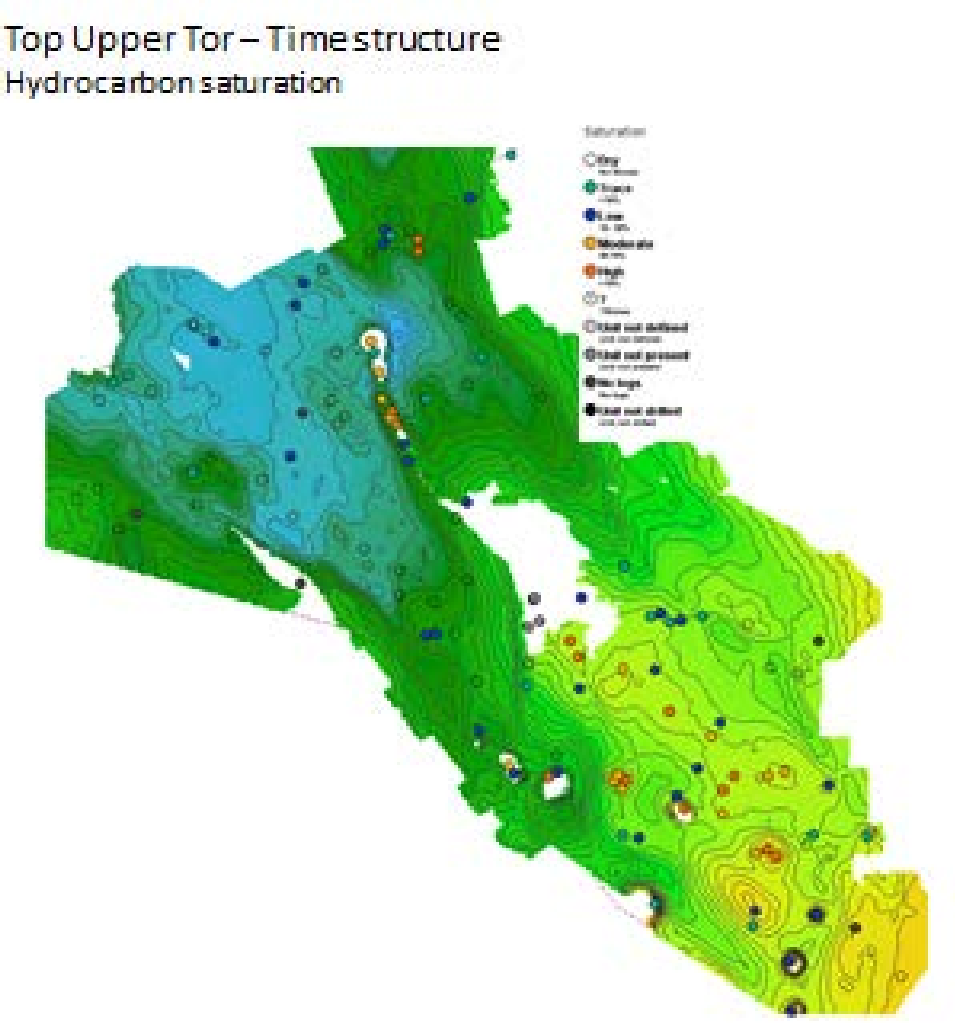

Fig. 8G.11. *Hydrocarbon saturation in the UpperTor unit unit plotted on time structure map of top Tor.*

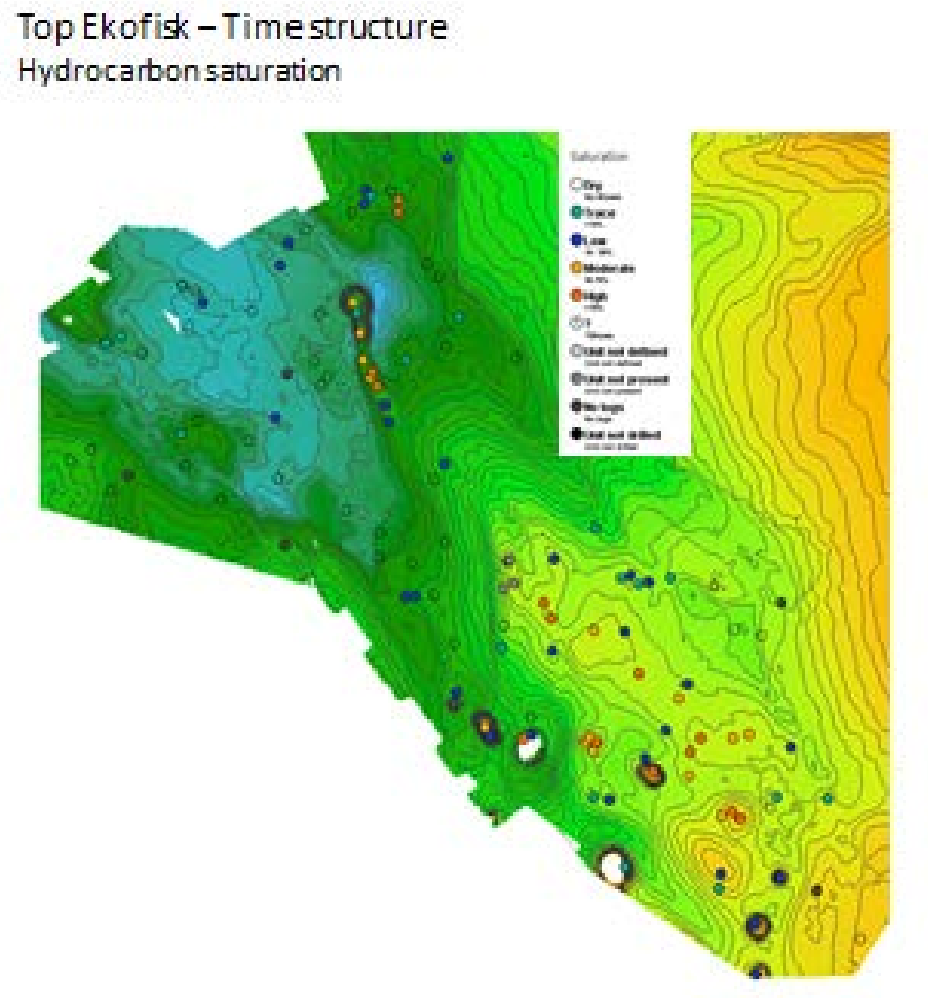

Fig. 8G.12. *Hydrocarbon saturation in the Ekofisk Formation plotted on the time structure map of top Chalk.*

The Tor-Ekofisk play is at a mature level with all structural traps already drilled. The play experienced a revival around the turn of the century due to the discovery of the prolific Halfdan Field located NW of the Dan Field. This accumulation with reserves of 100 mio. m^3 is located in a unique, non-structural trap with an inclined oil-water contact in the Tor Formation and pressure variations in the oil zone indicating disequilibrium and slow movement of the oil. Following this discovery, exploration activities have been focussed on locating non-structural and stratigraphically trapped oil; the results have generally been disappointing. Most of the wells have been based on amplitude anomalies, usually further de-risked by seismic inversion for acoustic impedance. As a general rule, the expected porosity anomalies have been confirmed but were dry, possibly due to non-existing traps or unfavourable migration routes from underlying Upper Jurassic source rocks. Although seismic inversion techniques have proved an efficient tool for locating porous intervals, the main challenge to locate

futher reserves in the upper part of the chalk is to predict the presence of hydrocarbons. This will a.o. require increased knowledge about migration routes and filling mechanisms. A further complication is that past experience has shown that inclined free water levels (FWL) are generally the rule rather than the exception.

Although porous intervals are recorded in the Tor and Ekofisk formations in almost all wells (Fig. 8G.13) we have reduced the play area shown in Fig. 8G.9 in the NW part of the DCG. Here the lower part of the chalk is both thick and tight with seal potential, and the substratum is only cut by few and insignificant faults which provide less favourable hydrocarbon migration pathways from the source.

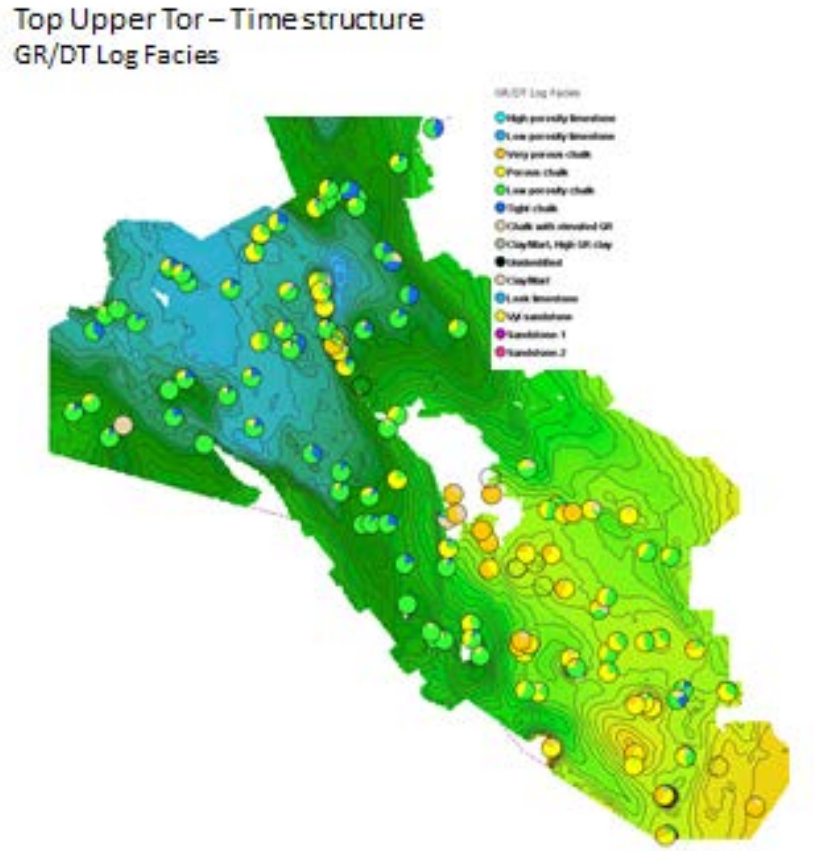

Fig 8G.13. *GR-DT log facies of the Upper Tor unit overlying the time structure map of top Tor (ch19).*

Appendix 7F

Appendix 7F-A

Oil Families

Appendix 7F-B

Principal components

Appendix A

Wellname	utmx	utmy	epth m m	Type	Field/ Seq.	Lithostrat	Oil_Families	index	Matrix
A-2	630445	6142082		Oil_stain	Kraka	Chalk Group	Type 1D	1	A
A-2	630445	6142082		Oil_stain	Kraka	Chalk Group	Type 1D	2	A
Adda-3	618524	6185266		Oil_stain	Adda	Tuxen	Type 1C	3	A
Adda-3	618524	6185266		Oil_stain	Adda	Tuxen	Type 1C	4	A
Alma-2	641782	6154193		Oil_stain	Alma	Bryne	Type 3	5	A
Amalie-1A	584738	6234249		Oil_stain	Amalie	Leek/Vyl	Type 2	6	A
Anne-3	631727	6140736		Oil_stain	Kraka	Ekofisk	Type 1D	7	A
Anne-3	631727	6140736		Oil_stain	Kraka	Ekofisk	Type 1D	8	A
Anne-3	631727	6140736		Oil_stain	Kraka	Tor	Type 1D	9	A
Bertel-1	560278	6210719		Oil_stain	Bertel-1	Gert	Type 3	10	A
Bertel-1	560278	6210719		Oil_stain	Bertel-1	Gert	Type 3	11	A
Boje-1A	605078	6189005		Oil_stain	Boje area	Tuxen	Type 1D	12	A
Boje-1A	605078	6189005		Oil_stain	Boje area	Tuxen	Type 1C	13	A
Cecilie-1	608713	6252867		Oil_stain	Cecilie	Post Chalk Group	Type 1A	14	A
Connie-1	605426	6252926		Oil_stain	Cecilie	Post Chalk Group	Type 1A	15	A
T-1X	572709	6228478		Oil_stain	Svend	Tor	Type 1A	16	A
E-1	616252	6177855		Oil_stain	Tyra	Ekofisk	Type 1C	17	A
E-2	609600	6175202		Oil_stain	Tyra	Chalk Group	Type 2	18	A
E-2	609600	6175202		Oil_stain	Tyra	Chalk Group	Type 2	19	A
E-2	609600	6175202		Oil_stain	Tyra	Chalk Group	Type 2	20	A
E-2	609600	6175202		Oil_stain	Tyra	Chalk Group	Type 1A	21	A
E-2	609600	6175202		Oil_stain	Tyra	Chalk Group	Type 1A	22	A
E-8X	625059	6167613		Oil_stain	Tyra	Chalk Group	Type 1B	23	A
Elin-1	585712	6201237		Oil_stain	Elin-1	?	Type 1A	24	A
Elly-1	581176	6183325		Oil_stain	Elly	Ravn	Type 2	25	A
Elly-1	581176	6183325		Oil_stain	Elly	?Ravn	Type 2	26	A
Elna-1	594238	6257141		Oil_stain	Elna-1	?	Type 2	27	A
E-Rosa-1	601597	6160627		Oil_stain	Dagmar	Chalk Group	Type 1D	28	A
E-Rosa-1	601597	6160627		Oil_stain	Dagmar	Zechstein	Type 1D	29	A
E-Rosa-2	599916	6161448		Oil_stain	Dagmar	Ekofisk	Type 1D	30	A
E-Rosa-2	599916	6161448		Oil_stain	Dagmar	Zechstein	Type 1D	31	A
E-Rosa-2	599916	6161448		Oil_stain	Dagmar	Zechstein	Type 1D	32	A
Gert-1	545410	6230858		Oil_stain	Freja	Gert	Type 3	33	A
Gert-1	545410	6230858		Oil_stain	Freja	Gert	Type 3	34	A
H-1	603304	6182307		Oil_stain	Roar	Tor	Type 1A	35	A
H-1	603304	6182307		Oil_stain	Roar	Tor	Type 1A	36	A
H-1	603304	6182307		Oil_stain	Roar	Tor	Type 2	37	A
H-1	603304	6182307		Oil_stain	Roar	Ekofisk	Type 2	38	A
I-1X	577846	6212796		Oil_stain	South Arne	Tor	Type 1A	39	A
Jens-1	596639	6175402		Oil_stain	Jens-1	Farsund	Type 1B	40	A
Jens-1	596639	6175402		Oil_stain	Jens-1	Farsund	Type 1B	41	A
Lone-1	533102	6222264		Oil_stain	Lone-1	?Tuxen	Type 1A	42	A
Lone-1	533102	6222264		Oil_stain	Lone-1	?Tuxen	Type 1A	43	A
Lulita-1	579377	6247668		Oil_stain	Lulita	?Lulu/Bryne	Type 2	44	A
Lulita-2	578698,6	6245467		Oil_stain	Lulita	?Lulu/Bryne	Type 2	45	A
Lulita-2	578698,6	6245467		Oil_stain	Lulita	?Lulu/Bryne	Type 2	46	A
M. Rosa-2	593824	6163257		Oil_stain	Rolf	Middle Hod/San.-Con.	Type 1D	47	A
M. Rosa-2	593824	6163257		Oil_stain	Rolf	?	Type 1D	48	A
M-1	634890	6149249		Oil_stain	Dan	Tor	Type 1D	49	A
M-1	634890	6149249		Oil_stain	Dan	Middle Hod	Type 1D	50	A
M-2	632776	6150586		Oil_stain	Dan	?	Type 1D	51	A
Mona-1	562195	6237463		Oil_stain	Mona-1	Tuxen	Type 1	52	A
N-1	610099	6160745		Oil_stain	Gorm	?	Type 1D	53	A
N-1	610099	6160745		Oil_stain	Gorm	?	Type 1D	54	A
N-1	610099	6160745		Oil_stain	Gorm	?	Type 1D	55	A
Nana-1X	610099	6160745		Oil_stain	Halfdan	Chalk Group	Type 1D	56	A
Nana-1X	610099	6160745		Oil_stain	Halfdan	Chalk Group	Type 1D	57	A
Nini-1A	642343	6280082		Oil_stain	Nini	Post Chalk Group	Type 1D	58	A
Nini-2	641077	6278856		Oil_stain	Nini	Post Chalk Group	Type 1C	59	A
Nini-2	641077	6278856		Oil_stain	Nini	Post Chalk Group	Type 1C	60	A
Nini-3	647197	6285847		Oil_stain	Nini	Post Chalk Group	Type 1A	61	A
North Jens-2	597705	6188740		Oil_stain	Valdemar	Chalk Group	Type 1A	62	A
North Jens-2	597705	6188740		Oil_stain	Valdemar	Tuxen	Type 1A	63	A
North Jens-2	597705	6188740		Oil_stain	Valdemar	Tuxen	Type 1A	64	A
Olaf-1	545874	6203388		Oil_stain	Olaf-1	?	Type 1A	65	A
Otto-1	573909	6223769		Oil_stain	Svend	Chalk Group	Type 1A	66	A
Ravn-1	577029	6193170		Oil_stain	Ravn	Ravn	Type 2	67	A
Ravn-1	577029	6193170		Oil_stain	Ravn	Ravn	Type 2	68	A
Ravn-1	577029	6193170		Oil_stain	Ravn	Ravn	Type 2	69	A
Regnar-3	641260,5	6140145,5		Oil_stain	Regnar		Type 1D	70	A
Rigs-1	575581	6216839		Oil_stain	South Arne	Chalk Group	Type 1A	71	A
Rigs-2A	575845	6215756		Oil_stain	South Arne	Chalk Group	Type 1A	72	A
Rita-1X oil	535424	6223327		Oil_stain	Rita-1	?	Type 3	73	A

Wellname	utmx	utmy	epth m m	Type	Field/ Seq.	Lithostrat	Oil_Families	index	Matrix
Roar 7B	603504,6	6181646,5		Oil_stain	Roar		Type 2	74	A
Roar-3C	603508	6181647,5		Oil_stain	Roar		Type 2	75	A
Roar-3C	603508	6181647,5		Oil_stain	Roar		Type 2	76	A
SA-1	576616,9	6215656		Oil_stain	South Arne		Type 1A	77	A
SA-12	576620,1	6215657		Oil_stain	South Arne		Type 1A	78	A
SA-14	576618,2	6215649		Oil_stain	South Arne		Type 1A	79	A
SA-16	576621,4	6215652,4		Oil_stain	South Arne		Type 1A	80	A
SA-2	576615,5	6215655,5		Oil_stain	South Arne		Type 1A	81	A
SA-3	576618,4	6215655,5		Oil_stain	South Arne		Type 1A	82	A
SA-4	576618,7	6215658,5		Oil_stain	South Arne		Type 1A	83	A
SA-5	576616,9	6215653,5		Oil_stain	South Arne		Type 1A	84	A
SA-7	576618,3	6215652,5		Oil_stain	South Arne		Type 1A	85	A
SA-9	576616,8	6215650,5		Oil_stain	South Arne		Type 1A	86	A
Saxo-1	527211	6204213		Oil_stain	Saxo		Type 4	87	A
Saxo-1	527211	6204213		Oil_stain	Saxo		Type 4	88	A
Siri-1	617987	6262004		Oil_stain	Siri		Type 1A	89	A
Siri-1	617987	6262004		Oil_stain	Siri		Type 1A	90	A
Siri-3A	626987	6264857		Oil_stain	Siri	Post Chalk Group	Type 1A	91	A
Skjold Flanke-4A	619679	6158490		Oil_stain	Skold Flanke-4	?	Type 1D	92	A
Tabita-1	586589	6232370		Oil_stain	Tabita	Post Chalk Group	Type 1A	93	A
Wessel-1	530590	6205876		Oil_stain	Wessel	Outer Rough Sand	Type 4	94	A
Wessel-1	530590	6205876		Oil_stain	Wessel	Outer Rough Sand	Type 4	95	A
Wessel-1	530590	6205876		Oil_stain	Wessel	Outer Rough Sand	Type 4	96	A
Wessel-1	530590	6205876		Oil_stain	Wessel	Outer Rough Sand	Type 4	97	A
West Lulu-1	575686	6244798		Oil_stain	Harald		Type 2	98	A
West Lulu-3	574746	6245766		Oil_stain	Harald		Type 2	99	A
Adda-1	617152	6186666	2587,8	SR_e	Ryaz-1	Farsund	No Match	100	B
Adda-1	617152	6186666	2639,6	SR_e	Ryaz-1	Farsund	No Match	101	B
Adda-1	617152	6186666	2642,6	SR_e	Ryaz-1	Farsund	No Match	102	B
Adda-1	617152	6186666	2670,0	SR_e	Ryaz-1	Farsund	No Match	103	B
Adda-1	617152	6186666	2834,6	SR_e	Volg-4	Farsund	No Match	104	B
Adda-1	617152	6186666	2840,7	SR_e	Volg-4	Farsund	No Match	105	B
Adda-1	617152	6186666	2990,1	SR_e	Volg-3	Farsund	No Match	106	B
Adda-1	617152	6186666	3045,0	SR_e	Volg-3	Farsund	No Match	107	B
Alma-1X	639612	6150851	2618,2	SR_e	Ryaz-1	Farsund	No Match	108	B
Alma-1X	639612	6150851	2743,2	SR_e	Volg-2	Farsund	No Match	109	B
Alma-1X	639612	6150851	2862,1	SR_e	Kimm-3	Farsund	No Match	110	B
Alma-1X	639612	6150851	3026,7	SR_e	Kimm-3	Farsund	Type 1C	111	B
Alma-1X	639612	6150851	3532,6	SR_e	Ox-1	Lola	Type 3	112	B
Alma-1X	639612	6150851	3642,4	SR_e	Bat-1	Bryne	Type 3	113	B
Alma-1X	639612	6150851	3644,5	SR_e	Bat-1	Bryne	Type 3	114	B
Alma-1X	639612	6150851	3650,6	SR_e	Baj-1	Bryne	Type 3	115	B
Anne-3A	631727	6140736	2682,2	SR_e	Volg-4	Farsund	No Match	116	B
Anne-3A	631727	6140736	2804,2	SR_e	Kimm-3	Farsund	No Match	117	B
Bo-1	598533	6185330	2590,8	SR_e	Ryaz-1	Farsund	No Match	118	B
Bo-1	598533	6185330	2596,9	SR_e	Ryaz-1	Farsund	No Match	119	B
Bo-1	598533	6185330	2606,0	SR_e	Ryaz-1	Farsund	No Match	120	B
Bo-1	598533	6185330	2624,3	SR_e	Volg-4	Farsund	No Match	121	B
Bo-1	598533	6185330	2651,8	SR_e	Volg-4	Farsund	No Match	122	B
Bo-1	598533	6185330	2709,7	SR_e	Volg-4	Farsund	Type 1C	123	B
Boje-1	605078	6189005	2761,2	SR_e	Ryaz-1	Farsund	No Match	124	B
Cleo-1	587853	6250521	3834,4	SR_e	Kimm-2	Farsund	Type 3	125	B
Cleo-1	587853	6250521	3898,4	SR_e	Kimm-2	Lola	Type 3	126	B
Cleo-1	587853	6250521	4410,5	SR_e	Ox-1	Lola	No Match	127	B
Cleo-1	587853	6250521	4553,7	SR_e	Cal-1	Bryne	No Match	128	B
Deep Adda-1	623686	6186118	2484,9	SR_e	Ryaz-1	Farsund	No Match	129	B
Deep-Adda-1	623686	6186118	2804,2	SR_e	Volg-4	Farsund	Type 1C	130	B
Deep-Adda-1	623686	6186118	2852,9	SR_e	Volg-3	Farsund	Type 1C	131	B
Deep-Adda-1	623686	6186118	3066,3	SR_e	Volg-2	Farsund	Type 1C	132	B
Diamant-1	555850	6207298	3712,5	SR_e	Volg-4	Farsund	No Match	133	B
Diamant-1	555850	6207298	3724,7	SR_e	Volg-3	Farsund	Type 1A	134	B
Diamant-1	555850	6207298	3733,8	SR_e	Volg-3	Farsund	No Match	135	B
Diamant-1	555850	6207298	3742,9	SR_e	Volg-3	Farsund	No Match	136	B
Diamant-1	555850	6207298	3758,2	SR_e	Volg-3	Farsund	No Match	137	B
Diamant-1	555850	6207298	3770,4	SR_e	Volg-3	Farsund	No Match	138	B
Diamant-1	555850	6207298	3800,9	SR_e	Volg-1	Farsund	No Match	139	B
Diamant-1	555850	6207298	3819,1	SR_e	Volg-1	Farsund	No Match	140	B
E-1X	616252	6177855	2982,2	SR_e	Ryaz-1	Farsund	No Match	141	B
E-1X	616252	6177855	2982,8	SR_e	Ryaz-1	Farsund	No Match	142	B
E-1X	616252	6177855	2983,1	SR_e	Ryaz-1	Farsund	No Match	143	B
E-1X	616252	6177855	2983,4	SR_e	Ryaz-1	Farsund	No Match	144	B
E-1X	616252	6177855	2983,7	SR_e	Ryaz-1	Farsund	No Match	145	B
E-1X	616252	6177855	2984,0	SR_e	Ryaz-1	Farsund	No Match	146	B
E-1X	616252	6177855	3084,6	SR_e	Volg-4	Farsund	No Match	147	B

Wellname	utmx	utmy	epth m m	Type	Field/ Seq.	Lithostrat	Oil_Families	index	Matrix
E-1X	616252	6177855	3169,9	SR_e	Volg-4	Farsund	No Match	148	B
Edna-1	589350	6168535	3026,7	SR_e	Ryaz-2	Farsund	Type 1D	149	B
Edna-1	589350	6168535	3075,4	SR_e	Ryaz-1	Farsund	No Match	150	B
Edna-1	589350	6168535	3081,5	SR_e	Ryaz-1	Farsund	No Match	151	B
Edna-1	589350	6168535	3084,6	SR_e	Ryaz-1	Farsund	No Match	152	B
Edna-1	589350	6168535	3118,1	SR_e	Volg-4	Farsund	No Match	153	B
Edna-1	589350	6168535	3136,4	SR_e	Volg-4	Farsund	No Match	154	B
Edna-1	589350	6168535	3273,6	SR_e	Volg-3	Farsund	No Match	155	B
Edna-1	589350	6168535	3410,7	SR_e	Volg-1	Farsund	No Match	156	B
Edna-1	589350	6168535	3575,3	SR_e	Kimm-3	Farsund	No Match	157	B
Eg-1	560791	6201371	4141,0	SR_e	Ryaz-1	Farsund	No Match	158	B
Eg-1	560791	6201371	4155,9	SR_e	Ryaz-1	Farsund	No Match	159	B
Eg-1	560791	6201371	4312,0	SR_e	Kimm-4	Farsund	No Match	160	B
Eg-1	560791	6201371	4359,9	SR_e	Kimm-3	Farsund	No Match	161	B
Elly-2	582645	6183465	3557,0	SR_e	Volg-3	Farsund	Type 1A	162	B
Elly-2	582645	6183465	3581,4	SR_e	Volg-1	Farsund	Type 1A	163	B
Elly-2	582645	6183465	3630,2	SR_e	Volg-1	Farsund	No Match	164	B
Elly-2	582645	6183465	3682,0	SR_e	Kimm-2	Farsund	Type 1A	165	B
Elly-2	582645	6183465	3874,0	SR_e	Kimm-1	Lola	Type 1B	166	B
Fasan-1	626436	6169817	2759,0	SR_e	Ryaz-1	Farsund	No Match	167	B
Fasan-1	626436	6169817	2840,0	SR_e	Volg-4	Farsund	No Match	168	B
Gert-2	548352	6228420	4017,3	SR_e	Ryaz-1	Farsund	No Match	169	B
Gert-2	548352	6228420	4072,1	SR_e	Volg-3	Farsund	Type 1B	170	B
Gert-2	548352	6228420	4154,4	SR_e	Volg-3	Farsund	Type 1B	171	B
Gert-2	548352	6228420	4236,7	SR_e	Volg-2	Farsund	Type 2	172	B
Gert-2	548352	6228420	4419,6	SR_e	Volg-1	Farsund	Type 1B	173	B
Gert-2	548352	6228420	4556,8	SR_e	Volg-1	Farsund	Type 1B	174	B
Gert-2	548352	6228420	4721,4	SR_e	Kimm-3	Farsund	Type 1B	175	B
Gert-2	548352	6228420	4874,0	SR_e	Kimm-2	Heno	Type 3	176	B
Gert-2	548352	6228420	4890,0	SR_e	Kimm-2	Heno	No Match	177	B
Gulnare-1	589707	6226113	4369,9	SR_e	Ryaz-1	Farsund	Type 1A	178	B
Gwen-2	566509	6219458	4075,2	SR_e	Ryaz-1	Farsund	No Match	179	B
Gwen-2	566509	6219458	4084,3	SR_e	Ryaz-1	Farsund	No Match	180	B
Gwen-2	566509	6219458	4087,4	SR_e	Ryaz-1	Farsund	No Match	181	B
Gwen-2	566509	6219458	4099,6	SR_e	Volg-4	Farsund	No Match	182	B
Gwen-2	566509	6219458	4142,2	SR_e	Volg-2	Farsund	Type 1D	183	B
Gwen-2	566509	6219458	4145,3	SR_e	Volg-1	Farsund	No Match	184	B
Gwen-2	566509	6219458	4148,3	SR_e	Volg-1	Farsund	Type 1D	185	B
Gwen-2	566509	6219458	4151,4	SR_e	Volg-1	Farsund	Type 1D	186	B
Gwen-2	566509	6219458	4157,5	SR_e	Volg-1	Farsund	Type 1D	187	B
Gwen-2	566509	6219458	4163,6	SR_e	Volg-1	Farsund	Type 1D	188	B
Gwen-2	566509	6219458	4169,7	SR_e	Volg-1	Farsund	Type 1C	189	B
Gwen-2	566509	6219458	4175,8	SR_e	Volg-1	Farsund	Type 1D	190	B
Gwen-2	566509	6219458	4181,9	SR_e	Volg-1	Farsund	Type 1D	191	B
Gwen-2	566509	6219458	4188,0	SR_e	Kimm-4	Farsund	Type 1D	192	B
Gwen-2	566509	6219458	4191,0	SR_e	Kimm-4	Farsund	Type 1D	193	B
Gwen-2	566509	6219458	4194,0	SR_e	Kimm-4	Farsund	Type 1D	194	B
Gwen-2	566509	6219458	4200,1	SR_e	Kimm-4	Farsund	Type 1D	195	B
Gwen-2	566509	6219458	4209,3	SR_e	Kimm-4	Farsund	Type 1D	196	B
Gwen-2	566509	6219458	4218,4	SR_e	Kimm-4	Farsund	No Match	197	B
Gwen-2	566509	6219458	4224,5	SR_e	Kimm-3	Farsund	Type 1D	198	B
Gwen-2	566509	6219458	4230,6	SR_e	Kimm-3	Farsund	Type 1D	199	B
Gwen-2	566509	6219458	4358,6	SR_e	Kimm-1	Farsund	No Match	200	B
I-1X	577846	6212796	3380,2	SR_e	Ryaz-1	Farsund	Type 1A	201	B
I-1X	577846	6212796	3483,9	SR_e	Ryaz-1	Farsund	No Match	202	B
I-1X	577846	6212796	3880,1	SR_e	Volg-2	Farsund	No Match	203	B
Iris-1	581199	6219518	3965,1	SR_e	Ryaz-1	Farsund	Type 1B	204	B
Iris-1	581199	6219518	3992,9	SR_e	Ryaz-1	Farsund	Type 1B	205	B
Iris-1	581199	6219518	4038,6	SR_e	Ryaz-1	Farsund	Type 2	206	B
Iris-1	581199	6219518	4084,3	SR_e	Ryaz-1	Farsund	Type 2	207	B
Iris-1	581199	6219518	4221,5	SR_e	Volg-4	Farsund	Type 2	208	B
Iris-1	581199	6219518	4328,2	SR_e	Volg-4	Farsund	Type 1B	209	B
Iris-1	581199	6219518	4450,1	SR_e	Volg-4	Farsund	Type 2	210	B
Jens-1	596639	6175402	2895,6	SR_e	Ryaz-1	Farsund	No Match	211	B
Jens-1	596639	6175402	2895,6	SR_e	Ryaz-1	Farsund	No Match	212	B
Jens-1	596639	6175402	2907,8	SR_e	Ryaz-1	Farsund	No Match	213	B
Jens-1	596639	6175402	2913,9	SR_e	Ryaz-1	Farsund	No Match	214	B
Jens-1	596639	6175402	2926,1	SR_e	Ryaz-1	Farsund	No Match	215	B
Jens-1	596639	6175402	2941,3	SR_e	Volg-4	Farsund	No Match	216	B
Jens-1	596639	6175402	2987,0	SR_e	Volg-4	Farsund	No Match	217	B
Jens-1	596639	6175402	3002,3	SR_e	Volg-4	Farsund	No Match	218	B
Jens-1	596639	6175402	3017,5	SR_e	Volg-3	Farsund	No Match	219	B
Jens-1	596639	6175402	3032,4	SR_e	Volg-3	Farsund	Type 1A	220	B
Jens-1	596639	6175402	3048,0	SR_e	Volg-3	Farsund	Type 1A	221	B

Wellname	utmx	utmy	epth m m	Type	Field/ Seq.	Lithostrat	Oil_Families	index	Matrix
Jens-1	596639	6175402	3413,8	SR_e	Kimm-3	Farsund	Type 1A	222	B
Jens-1	596639	6175402	3474,7	SR_e	Kimm-3	Farsund	Type 1A	223	B
Jens-1	596639	6175402	3596,6	SR_e	Kimm-2	Farsund	Type 1A	224	B
Jens-1	596639	6175402	3611,9	SR_e	Kimm-2	Farsund	Type 1A	225	B
Jens-1	596639	6175402	3886,2	SR_e	Ox-1	Lola	Type 1A	226	B
Jens-1	596639	6175402	4023,4	SR_e	Ox-1	Lola	Type 1A	227	B
Jens-1	596639	6175402	4114,8	SR_e	Ox-1	Lola	Type 1A	228	B
Jens-1	596639	6175402	4175,8	SR_e	Cal-1	Middle Graben	Type 1A	229	B
Jens-1	596639	6175402	4209,3	SR_e	Pliens-1	Fjerritslev	Type 1A	230	B
Jeppe-1	556487	6227123	4401,4	SR_e	Ryaz-1	Farsund	No Match	231	B
Jeppe-1	556487	6227123	4405,0	SR_e	Ryaz-1	Farsund	No Match	232	B
Jeppe-1	556487	6227123	4407,0	SR_e	Ryaz-1	Farsund	No Match	233	B
Jeppe-1	556487	6227123	4407,2	SR_e	Ryaz-1	Farsund	No Match	234	B
Jeppe-1	556487	6227123	4408,1	SR_e	Ryaz-1	Farsund	No Match	235	B
Jeppe-1	556487	6227123	4409,4	SR_e	Ryaz-1	Farsund	No Match	236	B
Jeppe-1	556487	6227123	4410,9	SR_e	Ryaz-1	Farsund	No Match	237	B
Jeppe-1	556487	6227123	4411,1	SR_e	Ryaz-1	Farsund	No Match	238	B
Jeppe-1	556487	6227123	4412,9	SR_e	Ryaz-1	Farsund	No Match	239	B
Jeppe-1	556487	6227123	4414,7	SR_e	Ryaz-1	Farsund	No Match	240	B
Jeppe-1	556487	6227123	4415,5	SR_e	Ryaz-1	Farsund	No Match	241	B
Jeppe-1	556487	6227123	4417,3	SR_e	Ryaz-1	Farsund	No Match	242	B
Jeppe-1	556487	6227123	4417,5	SR_e	Ryaz-1	Farsund	No Match	243	B
Jeppe-1	556487	6227123	4418,7	SR_e	Ryaz-1	Farsund	No Match	244	B
Jeppe-1	556487	6227123	4419,4	SR_e	Ryaz-1	Farsund	No Match	245	B
Karl-1	565202	6239585	4288,5	SR_e	Volg-3	Farsund	No Match	246	B
Karl-1	565202	6239585	4343,4	SR_e	Volg-1	Farsund	Type 1D	247	B
Karl-1	565202	6239585	4370,8	SR_e	Volg-1	Farsund	Type 1D	248	B
Karl-1	565202	6239585	4416,6	SR_e	Kimm-4	Farsund	Type 1C	249	B
Lulu-1	580001	6244144	3246,0	SR_e	Kimm-3	Farsund	No Match	250	B
Lulu-1	580001	6244144	3247,5	SR_e	Kimm-3	Farsund	No Match	251	B
Lulu-1	580001	6244144	3248,3	SR_e	Kimm-3	Farsund	No Match	252	B
Lulu-1	580001	6244144	3249,4	SR_e	Kimm-3	Farsund	No Match	253	B
Lulu-1	580001	6244144	3282,7	SR_e	Kimm-3	Farsund	No Match	254	B
Lulu-1	580001	6244144	3346,7	SR_e	Kimm-2	Farsund	Type 1A	255	B
Lulu-1	580001	6244144	3419,9	SR_e	Kimm-2	Farsund	Type 1A	256	B
Lulu-1	580001	6244144	3465,6	SR_e	Kimm-2	Lola	Type 1B	257	B
Lulu-2	579905	6242411	3505,6	SR_e	Kimm-2	Lola	No Match	258	B
Lulu-2	579905	6242411	3516,0	SR_e	Kimm-2	Lola	No Match	259	B
Lulu-2	579905	6242411	3523,0	SR_e	Kimm-2	Lola	Type 1A	260	B
Lulu-2	579905	6242411	3536,7	SR_e	Kimm-2	Lola	Type 1A	261	B
M-8X	633498	6150238	2734,1	SR_e	Kimm-3	Farsund	Type 1C	262	B
M-8X	633498	6150238	2898,6	SR_e	Kimm-1	Lola	Type 3	263	B
M-8X	633498	6150238	3035,8	SR_e	Ox-1	Lola	Type 3	264	B
M-8X	633498	6150238	3136,4	SR_e	Cal-1	Bryne	No Match	265	B
M-8X	633498	6150238	3255,3	SR_e	Hett-1	Fjerritslev	No Match	266	B
N. Jens-1	597708	6188738	2441,9	SR_e	Ryaz-2	Farsund	No Match	267	B
N. Jens-1	597708	6188738	2963,0	SR_e	Volg-1	Farsund	No Match	268	B
N. Jens-1	597708	6188738	2970,9	SR_e	Volg-1	Farsund	No Match	269	B
N.Jens-1	597708	6188738	2511,6	SR_e	Volg-4	Farsund	No Match	270	B
N.Jens-1	597708	6188738	2529,8	SR_e	Volg-4	Farsund	No Match	271	B
N.Jens-1	597708	6188738	2560,3	SR_e	Volg-4	Farsund	No Match	272	B
N.Jens-1	597708	6188738	2590,8	SR_e	Volg-4	Farsund	No Match	273	B
N.Jens-1	597708	6188738	2621,3	SR_e	Volg-3	Farsund	No Match	274	B
N.Jens-1	597708	6188738	2651,8	SR_e	Volg-3	Farsund	Type 1D	275	B
N.Jens-1	597708	6188738	2682,2	SR_e	Volg-3	Farsund	Type 1D	276	B
N.Jens-1	597708	6188738	2712,7	SR_e	Volg-2	Farsund	Type 1D	277	B
N.Jens-1	597708	6188738	2743,2	SR_e	Volg-2	Farsund	Type 1D	278	B
N.Jens-1	597708	6188738	2773,7	SR_e	Volg-2	Farsund	No Match	279	B
N.Jens-1	597708	6188738	2834,6	SR_e	Volg-2	Farsund	No Match	280	B
N.Jens-1	597708	6188738	2865,1	SR_e	Volg-2	Farsund	No Match	281	B
N.Jens-1	597708	6188738	2895,6	SR_e	Volg-2	Farsund	Type 1D	282	B
N.Jens-1	597708	6188738	2926,1	SR_e	Volg-2	Farsund	No Match	283	B
N.Jens-1	597708	6188738	2987,0	SR_e	Volg-1	Farsund	No Match	284	B
N.Jens-1	597708	6188738	3017,5	SR_e	Volg-1	Farsund	No Match	285	B
N.Jens-1	597708	6188738	3048,0	SR_e	Volg-1	Farsund	No Match	286	B
N.Jens-1	597708	6188738	3078,5	SR_e	Volg-1	Farsund	Type 1D	287	B
N.Jens-1	597708	6188738	3109,0	SR_e	Volg-1	Farsund	No Match	288	B
N.Jens-1	597708	6188738	3139,4	SR_e	Volg-1	Farsund	No Match	289	B
N.Jens-1	597708	6188738	3169,9	SR_e	Volg-1	Farsund	Type 1D	290	B
N.Jens-1	597708	6188738	3200,4	SR_e	Volg-1	Farsund	Type 1D	291	B
N.Jens-1	597708	6188738	3230,9	SR_e	Volg-1	Farsund	Type 1D	292	B
N.Jens-1	597708	6188738	3261,4	SR_e	Volg-1	Farsund	Type 1D	293	B
N.Jens-1	597708	6188738	3291,8	SR_e	Volg-1	Farsund	Type 1D	294	B
N.Jens-1	597708	6188738	3322,3	SR_e	Volg-1	Farsund	Type 1D	295	B

Wellname	utmx	utmy	epth m m	Type	Field/ Seq.	Lithostrat	Oil_Families	index	Matrix
N.Jens-1	597708	6188738	3352,8	SR_e	Kimm-4	Farsund	Type 1D	296	B
N.Jens-1	597708	6188738	3383,3	SR_e	Kimm-4	Farsund	Type 1D	297	B
N.Jens-1	597708	6188738	3413,8	SR_e	Kimm-3	Farsund	Type 1D	298	B
N.Jens-1	597708	6188738	3474,7	SR_e	Kimm-3	Farsund	Type 1D	299	B
N.Jens-1	597708	6188738	3505,2	SR_e	Kimm-3	Farsund	Type 1D	300	B
N.Jens-1	597708	6188738	3535,7	SR_e	Kimm-3	Farsund	Type 1C	301	B
N.Jens-1	597708	6188738	3566,2	SR_e	Kimm-3	Farsund	No Match	302	B
N.Jens-1	597708	6188738	3587,5	SR_e	Kimm-3	Farsund	Type 1D	303	B
N.Jens-1	597708	6188738	3657,6	SR_e	Kimm-3	Farsund	Type 1D	304	B
N.Jens-1	597708	6188738	3779,5	SR_e	Kimm-3	Farsund	Type 1B	305	B
N.Jens-1	597708	6188738	3840,5	SR_e	Kimm-2	Farsund	Type 1B	306	B
N.Jens-1	597708	6188738	3871,0	SR_e	Kimm-2	Farsund	Type 1B	307	B
N.Jens-1	597708	6188738	3901,4	SR_e	Kimm-2	Farsund	Type 1B	308	B
N.Jens-1	597708	6188738	3931,9	SR_e	Kimm-2	Farsund	Type 1B	309	B
N.Jens-1	597708	6188738	3962,4	SR_e	Kimm-2	Farsund	Type 1D	310	B
N.Jens-1	597708	6188738	3992,9	SR_e	Kimm-2	Farsund	Type 1B	311	B
N.Jens-1	597708	6188738	4023,4	SR_e	Kimm-2	Farsund	Type 1B	312	B
N-22A	611261	6159542	3815,3	SR_e	Sin-1	Fjerritslev	Type 1C	313	B
Nora-1	587463	6203677	4029,5	SR_e	Kimm-3	Farsund	Type 2	314	B
Nora-1	587463	6203677	4038,6	SR_e	Kimm-3	Farsund	Type 3	315	B
Nora-1	587463	6203677	4047,7	SR_e	Kimm-3	Farsund	Type 3	316	B
Nora-1	587463	6203677	4066,0	SR_e	Kimm-3	Farsund	Type 2	317	B
Nora-1	587463	6203677	4075,2	SR_e	Kimm-3	Farsund	Type 2	318	B
Nora-1	587463	6203677	4084,3	SR_e	Kimm-3	Farsund	Type 2	319	B
Nora-1	587463	6203677	4111,8	SR_e	Kimm-3	Farsund	Type 2	320	B
Nora-1	587463	6203677	4130,0	SR_e	Kimm-3	Farsund	Type 1B	321	B
Nora-1	587463	6203677	4157,5	SR_e	Kimm-3	Farsund	Type 1B	322	B
Nora-1	587463	6203677	4166,6	SR_e	Kimm-3	Farsund	Type 1B	323	B
Nora-1	587463	6203677	4224,5	SR_e	Kimm-3	Farsund	Type 1B	324	B
Nora-1	587463	6203677	4242,8	SR_e	Kimm-3	Farsund	Type 2	325	B
NW Adda-1	611604	6193764	2885,0	SR_e	Volg-4	Farsund	No Match	326	B
NW-Adda-1	611604	6193764	2848,9	SR_e	Ryaz-1	Farsund	Type 1D	327	B
NW-Adda-1	611604	6193764	2857,4	SR_e	Ryaz-1	Farsund	No Match	328	B
Rita-1X	535424	6223327	3773,4	SR_e	Ryaz-1	Farsund	No Match	329	B
Rita-1X	535424	6223327	3785,6	SR_e	Volg-4	Farsund	No Match	330	B
Rita-1X	535424	6223327	3803,9	SR_e	Volg-4	Farsund	Type 1B	331	B
Rita-1X	535424	6223327	3822,2	SR_e	Volg-4	Farsund	No Match	332	B
Rita-1X	535424	6223327	3822,2	SR_e	Volg-4	Farsund	No Match	333	B
Rita-1X	535424	6223327	3916,2	SR_e	Volg-4	Farsund	Type 1C	334	B
Rita-1X	535424	6223327	3917,6	SR_e	Volg-4	Farsund	Type 1D	335	B
Rita-1X	535424	6223327	3919,4	SR_e	Volg-3	Farsund	Type 1C	336	B
Rita-1X	535424	6223327	4041,6	SR_e	Volg-1	Farsund	Type 1A	337	B
Rita-1X	535424	6223327	4215,4	SR_e	Kimm-4	Farsund	Type 1B	338	B
Rita-1X	535424	6223327	4325,1	SR_e	Kimm-3	Farsund	Type 1B	339	B
Rita-1X	535424	6223327	4474,5	SR_e	Kimm-3	Farsund	Type 3	340	B
SE-Igor-1	642980	6160177	2490,5	SR_e	Volg-2	Farsund	No Match	341	B
SE-Igor-1	642980	6160177	2499,2	SR_e	Volg-2	Farsund	Type 1D	342	B
Skarv-1	588962	6176033	3392,0	SR_e	Ryaz-1	Farsund	No Match	343	B
Skarv-1	588962	6176033	3452,0	SR_e	Volg-4	Farsund	Type 1A	344	B
Skarv-1	588962	6176033	3506,0	SR_e	Volg-3	Farsund	Type 1B	345	B
Skarv-1	588962	6176033	3596,0	SR_e	Kimm-4	Farsund	Type 1A	346	B
Skarv-1	588962	6176033	3641,0	SR_e	Kimm-4	Farsund	Type 1A	347	B
Skarv-1	588962	6176033	3692,0	SR_e	Kimm-2	Farsund	No Match	348	B
Skarv-1	588962	6176033	3713,0	SR_e	Kimm-2	Farsund	No Match	349	B
Skarv-1	588962	6176033	3764,0	SR_e	Kimm-1	Lola	Type 1A	350	B
Skarv-1	588962	6176033	3797,0	SR_e	Kimm-1	Lola	Type 1A	351	B
Skarv-1	588962	6176033	3845,0	SR_e	Sin-1	Fjerritslev	No Match	352	B
Skjold-Flanke-1	619679	6158490	3064,9	SR_e	Volg-2	Farsund	No Match	353	B
Skjold-Flanke-1	619679	6158490	3075,7	SR_e	Volg-1	Farsund	No Match	354	B
Skjold-Flanke-1	619679	6158490	3136,4	SR_e	Kimm-4	Farsund	Type 1D	355	B
Skjold-Flanke-1	619679	6158490	3200,4	SR_e	Kimm-4	Farsund	No Match	356	B
Skjold-Flanke-1	619679	6158490	3383,3	SR_e	Kimm-3	Farsund	No Match	357	B
Skjold-Flanke-1	619679	6158490	3660,6	SR_e	Kimm-2	Farsund	Type 1A	358	B
Skjold-Flanke-1	619679	6158490	4325,1	SR_e	Bat-1	Bryne	Type 1A	359	B
Tordenskjold-1	533860	6199520	3434,6	SR_e	Volg-4	Farsund	No Match	360	B
Tordenskjold-1	533860	6199520	3474,0	SR_e	Volg-3	Farsund	No Match	361	B
Tordenskjold-1	533860	6199520	3537,0	SR_e	Volg-2	Farsund	No Match	362	B
Tordenskjold-1	533860	6199520	3648,0	SR_e	Permian	Permian	No Match	363	B
U-1X	613837	6152161	2551,2	SR_e	Volg-1	Farsund	Type 1D	364	B
U-1X	613837	6152161	2685,3	SR_e	Kimm-3	Farsund	Type 1C	365	B
U-1X	613837	6152161	2852,9	SR_e	Kimm-2	Farsund	Type 1C	366	B
U-1X	613837	6152161	3093,7	SR_e	Ox-1	Lola	Type 3	367	B
U-1X	613837	6152161	3307,1	SR_e	Cal-1	Middle Graben	Type 3	368	B
U-1X	613837	6152161	3413,8	SR_e	Hett-1	Fjerritslev	Type 3	369	B

Wellname	utmx	utmy	epth m m	Type	Field/ Seq.	Lithostrat	Oil_Families	index	Matrix
W. Lulu-1	575686	6244798	3545,8	SR_e	Kimm-1	Lola	Type 3	370	B
W. Lulu-1	575686	6244798	3569,4	SR_e	Cal-1	Lulu	Type 2	371	B
W. Lulu-1	575686	6244798	3569,6	SR_e	Cal-1	Lulu	Type 3	372	B
W. Lulu-1	575686	6244798	3571,5	SR_e	Cal-1	Lulu	Type 3	373	B
W. Lulu-1	575686	6244798	3571,6	SR_e	Cal-1	Lulu	Type 3	374	B
W. Lulu-1	575686	6244798	3571,7	SR_e	Cal-1	Lulu	Type 3	375	B
W. Lulu-2	574427	6243591	3779,8	SR_e	Ox-1	Lola	Type 1B	376	B
W. Lulu-3	574746	6245766	3598,1	SR_e	Ox-1	Lola	Type 3	377	B
Wessel-1	530590	6205876	3031,9	SR_e	Volg-3	Farsund	No Match	378	B
Wessel-1	530590	6205876	3035,0	SR_e	Volg-3	Farsund	No Match	379	B
Wessel-1	530590	6205876	3037,0	SR_e	Volg-3	Farsund	No Match	380	B
Wessel-1	530590	6205876	3040,2	SR_e	Volg-2	Farsund	No Match	381	B
Wessel-1	530590	6205876	3134,7	SR_e	Permian	Permian	No Match	382	B
Wessel-1	530590	6205876	3135,5	SR_e	Permian	Permian	No Match	383	B
Wessel-1	530590	6205876	3136,5	SR_e	Permian	Permian	No Match	384	B
Wessel-1	530590	6205876	3141,0	SR_e	Permian	Permian	No Match	385	B
NJ-1	597707,6	6188737,5	2250,5	Oil_stain	Valdemar	Upper Sola-1	Type 1D	386	C
NJ-1	597707,6	6188737,5	2256,5	Oil_stain	Valdemar	Lower Sola-3	Type 1A	387	C
NJ-1	597707,6	6188737,5	2276,8	Oil_stain	Valdemar	Upper Tuxen-1	Type 1A	388	C
NJ-1	597707,6	6188737,5	2281,3	Oil_stain	Valdemar	Upper Tuxen-1	Type 1A	389	C
NJ-1	597707,6	6188737,5	2282,9	Oil_stain	Valdemar	Upper Tuxen-1	Type 1A	390	C
NJ-1	597707,6	6188737,5	2283,7	Oil_stain	Valdemar	Upper Tuxen-1	Type 1A	391	C
NJ-1	597707,6	6188737,5	2286,3	Oil_stain	Valdemar	Middle Tuxen-2	Type 1A	392	C
NJ-1	597707,6	6188737,5	2302,9	Oil_stain	Valdemar	Middle Tuxen-1	Type 1A	393	C
NJ-1	597707,6	6188737,5	2307,3	Oil_stain	Valdemar	Lower Tuxen-3	Type 1A	394	C
NJ-1	597707,6	6188737,5	2326,7	Oil_stain	Valdemar	Lower Tuxen-1	Type 1D	395	C
V-1	597886,8	6188956	2109,2	Oil_stain	Valdemar	Upper Cretaceous	Type 1D	396	C
V-1H	597841,1	6189359	2528,8	Oil_stain	Valdemar	Middle Tuxen-2	Type 1A	397	C
V-1H	597841,1	6189359	2532,7	Oil_stain	Valdemar	Middle Tuxen-2	Type 1A	398	C
V-1H	597841,1	6189359	2535,0	Oil_stain	Valdemar	Middle Tuxen-2	Type 1D	399	C
V-1H	597771,6	6189627	2824,0	Oil_stain	Valdemar	Upper Tuxen-2	Type 1D	400	C
V-1H	597771,6	6189627	2830,1	Oil_stain	Valdemar	Upper Tuxen-2	Type 1D	401	C
V-1H	597771,6	6189627	2835,5	Oil_stain	Valdemar	Upper Tuxen-2	Type 1A	402	C
V-1H	597686,7	6189956	3143,8	Oil_stain	Valdemar	Upper Tuxen-1	Type 1A	403	C
V-1H	597686,7	6189956	3157,9	Oil_stain	Valdemar	Upper Tuxen-1	Type 1D	404	C
V-1P	597886,8	6188956	2271,1	Oil_stain	Valdemar	Upper Sola-2	Type 1D	405	C
V-1P	597886,8	6188956	2314,5	Oil_stain	Valdemar	Upper Tuxen-1	Type 1A	406	C
V-1P	597886,8	6188956	2318,9	Oil_stain	Valdemar	Upper Tuxen-1	Type 1A	407	C
V-1P	597886,8	6188956	2101,7	Oil_stain	Valdemar	Upper Cretaceous	Type 1D	408	C
V-1P	597886,8	6188956	2317,2	Oil_stain	Valdemar	Upper Tuxen-1	Type 1A	409	C
V-1P	597886,8	6188956	2322,1	Oil_stain	Valdemar	Middle Tuxen-2	Type 1A	410	C
V-1P	597886,8	6188956	2329,9	Oil_stain	Valdemar	Middle Tuxen-2	Type 1A	411	C
V-1P	597886,8	6188956	2341,7	Oil_stain	Valdemar	Middle Tuxen-1	Type 1A	412	C
V-2H	596948,8	6187813	3491,5	Oil_stain	Valdemar	Upper Tuxen-1	Type 1D	413	C
V-2H	596948,8	6187813	3492,6	Oil_stain	Valdemar	Upper Tuxen-1	Type 1D	414	C
V-2H	596948,8	6187813	3494,2	Oil_stain	Valdemar	Upper Tuxen-1	Type 1D	415	C
V-2H	596948,8	6187813	3498,6	Oil_stain	Valdemar	Upper Tuxen-1	Type 1D	416	C
V-2H	596948,8	6187813	3500,5	Oil_stain	Valdemar	Upper Tuxen-1	Type 1D	417	C
V-2H	596948,8	6187813	3503,2	Oil_stain	Valdemar	Upper Tuxen-1	Type 1D	418	C
V-2H	596948,8	6187813	3506,1	Oil_stain	Valdemar	Upper Tuxen-1	Type 1D	419	C
V-2H	596948,8	6187813	3509,4	Oil_stain	Valdemar	Upper Tuxen-1	Type 1D	420	C
V-2H	597081,6	6187961	3291,9	Oil_stain	Valdemar	Lower Tuxen-3	Type 1D	421	C
V-2H	597081,6	6187961	3307,8	Oil_stain	Valdemar	Lower Tuxen-3	Type 1D	422	C
V-2H	596948,8	6187813	3491,1	Oil_stain	Valdemar	Upper Tuxen-1	Type 1D	423	C
V-2H	596948,8	6187813	3500,6	Oil_stain	Valdemar	Upper Tuxen-1	Type 1D	424	C
V-2H	596948,8	6187813	3509,0	Oil_stain	Valdemar	Upper Tuxen-1	Type 1D	425	C
V-2P	597115,5	6187996	2276,1	Oil_stain	Valdemar	Upper Sola-1	Type 1D	426	C
V-2P	597886,5	6188954,5	2278,4	Oil_stain	Valdemar	Upper Sola-1	Type 1D	427	C
V-2P	597886,5	6188954,5	2284,2	Oil_stain	Valdemar	Fischschiefer	Type 1A	428	C
V-2P	597886,5	6188954,5	2310,4	Oil_stain	Valdemar	Upper Tuxen-1	Type 1A	429	C
V-2P	597886,5	6188954,5	2339,5	Oil_stain	Valdemar	Middle Tuxen-1	Type 1A	430	C
V-2P	597886,5	6188954,5	2342,1	Oil_stain	Valdemar	Lower Tuxen-3	Type 1A	431	C
V-3H	597854,4	6188065	2817,2	Oil_stain	Valdemar	Middle Tuxen-1	Type 1D	432	C
V-3H	597854,4	6188065	2818,8	Oil_stain	Valdemar	Middle Tuxen-1	Type 1A	433	C
V-3H	597854,4	6188065	2820,3	Oil_stain	Valdemar	Middle Tuxen-1	Type 1D	434	C
V-3H	597854,4	6188065	2822,9	Oil_stain	Valdemar	Middle Tuxen-1	Type 1D	435	C
V-3H	597860,3	6188012	2844,6	Oil_stain	Valdemar	Middle Tuxen-1	Type 1D	436	C
V-3H	597860,3	6188012	2847,2	Oil_stain	Valdemar	Middle Tuxen-1	Type 1D	437	C
V-3H	597860,3	6188012	2850,3	Oil_stain	Valdemar	Middle Tuxen-1	Type 1D	438	C
V-3H	597860,3	6188012	2851,1	Oil_stain	Valdemar	Middle Tuxen-1	Type 1D	439	C
V-3H	597860,3	6188012	2854,9	Oil_stain	Valdemar	Middle Tuxen-1	Type 1D	440	C
V-3H	597860,3	6188012	2856,3	Oil_stain	Valdemar	Middle Tuxen-1	Type 1D	441	C
V-3H	597860,3	6188012	2858,7	Oil_stain	Valdemar	Middle Tuxen-1	Type 1D	442	C
V-3H	597860,3	6188012	2860,6	Oil_stain	Valdemar	Middle Tuxen-1	Type 1D	443	C

Wellname	utmx	utmy	epth m m	Type	Field/ Seq.	Lithostrat	Oil_Families	index	Matrix
V-4H	597452,6	6188858	2845,0	Oil_stain	Valdemar	Middle Tuxen-2	Type 1A	444	C
V-4H	597452,6	6188858	2847,0	Oil_stain	Valdemar	Middle Tuxen-2	Type 1A	445	C
V-4H	597452,6	6188858	2849,6	Oil_stain	Valdemar	Middle Tuxen-2	Type 1A	446	C
V-4H	597452,6	6188858	2849,6	Oil_stain	Valdemar	Middle Tuxen-2	Type 1A	447	C

SR_e: source rock extract

Appendix B

Wellname	Type	Field/ Seq.	index	Matrix	A_PC-1	A_PC-2	A_PC-3	A*B*C_PC-1	A*B*C_PC-2	A*B*C_PC-3
A-2	Oil_stain	Kraka	1	A	-3,33	-1,57	-1,92	-1,82	0,74	-0,97
A-2	Oil_stain	Kraka	2	A	-3,80	-1,79	-1,85	-2,17	0,99	-0,89
Adda-3	Oil_stain	Adda	3	A	-5,42	-0,15	-2,00	-3,90	-1,36	-0,95
Adda-3	Oil_stain	Adda	4	A	-5,26	-0,38	-2,60	-3,83	-1,46	-1,29
Alma-2	Oil_stain	Alma	5	A	2,79	4,31	-4,31	4,51	-3,84	-3,52
Amalie-1A	Oil_stain	Amalie	6	A	1,69	3,37	1,73	2,66	-1,94	2,48
Anne-3	Oil_stain	Kraka	7	A	-3,14	-0,87	-2,53	-1,58	0,03	-1,38
Anne-3	Oil_stain	Kraka	8	A	-3,13	-0,97	-2,14	-1,54	0,38	-1,15
Anne-3	Oil_stain	Kraka	9	A	-3,42	-1,18	-2,14	-1,76	0,61	-1,06
Bertel-1	Oil_stain	Bertel-1	10	A	7,28	8,09	-3,41	9,49	-4,17	-2,10
Bertel-1	Oil_stain	Bertel-1	11	A	7,16	7,78	-3,75	9,45	-3,99	-2,55
Boje-1A	Oil_stain	Boje area	12	A	-3,85	-1,02	-1,45	-2,21	0,55	-0,36
Boje-1A	Oil_stain	Boje area	13	A	-4,69	-0,80	-2,14	-3,12	-0,20	-0,90
Cecilie-1	Oil_stain	Cecilie	14	A	0,24	-0,60	2,31	1,92	2,21	2,07
Connie-1	Oil_stain	Cecilie	15	A	0,33	-0,64	1,58	1,84	1,91	1,71
T-1X	Oil_stain	Svend	16	A	1,61	0,51	0,71	3,24	1,32	1,14
E-1	Oil_stain	Tyra	17	A	-4,04	-0,47	-3,15	-2,23	-0,11	-1,60
E-2	Oil_stain	Tyra	18	A	-4,61	1,87	0,59	-4,04	-3,98	1,47
E-2	Oil_stain	Tyra	19	A	-5,08	1,59	0,48	-4,51	-3,89	1,46
E-2	Oil_stain	Tyra	20	A	-4,79	2,25	0,86	-4,25	-4,56	1,59
E-2	Oil_stain	Tyra	21	A	-3,22	-1,11	-0,40	-1,90	0,43	0,17
E-2	Oil_stain	Tyra	22	A	-3,12	-1,58	-0,23	-1,75	0,96	0,15
E-8X	Oil_stain	Tyra	23	A	-2,68	0,09	0,17	-1,50	-0,70	0,59
Elin-1	Oil_stain	Elin-1	24	A	0,24	-0,18	2,83	1,31	1,18	3,01
Elly-1	Oil_stain	Elly	25	A	1,96	2,76	2,45	2,55	-2,62	2,09
Elly-1	Oil_stain	Elly	26	A	1,54	3,69	2,91	1,88	-3,46	3,05
Elna-1	Oil_stain	Elna-1	27	A	1,19	2,31	0,26	2,11	-2,17	0,65
E-Rosa-1	Oil_stain	Dagmar	28	A	0,87	0,46	-0,86	2,27	0,27	-0,59
E-Rosa-1	Oil_stain	Dagmar	29	A	1,17	0,12	-1,72	2,67	0,53	-1,13
E-Rosa-2	Oil_stain	Dagmar	30	A	2,12	-0,19	-1,14	3,74	1,54	-0,87
E-Rosa-2	Oil_stain	Dagmar	31	A	1,99	-0,16	-0,74	3,65	1,86	-0,47
E-Rosa-2	Oil_stain	Dagmar	32	A	1,28	-0,20	-0,79	2,85	1,37	-0,56
Gert-1	Oil_stain	Freja	33	A	4,81	6,53	-3,40	6,43	-5,17	-2,20
Gert-1	Oil_stain	Freja	34	A	5,32	6,72	-2,73	6,80	-5,21	-1,88
H-1	Oil_stain	Roar	35	A	-1,32	-1,48	0,19	0,34	1,94	0,53
H-1	Oil_stain	Roar	36	A	-1,25	-1,25	0,11	0,34	1,60	0,61
H-1	Oil_stain	Roar	37	A	-2,19	1,72	1,94	-1,72	-2,91	2,43
H-1	Oil_stain	Roar	38	A	-3,39	3,44	3,71	-2,89	-5,22	3,25
I-1X	Oil_stain	South Arne	39	A	-0,73	-0,82	1,47	0,66	1,41	1,65
Jens-1	Oil_stain	Jens-1	40	A	2,53	3,47	0,54	3,87	-1,62	1,20
Jens-1	Oil_stain	Jens-1	41	A	2,88	3,47	0,39	4,09	-1,69	1,21
Lone-1	Oil_stain	Lone-1	42	A	0,94	-1,01	0,17	2,24	1,78	0,11
Lone-1	Oil_stain	Lone-1	43	A	0,88	-0,82	0,22	2,08	1,19	0,04
Lulita-1	Oil_stain	Lulita	44	A	3,13	3,24	1,12	3,97	-3,03	0,87
Lulita-2	Oil_stain	Lulita	45	A	3,28	2,77	0,76	3,88	-3,05	0,72
Lulita-2	Oil_stain	Lulita	46	A	3,60	3,06	1,72	4,16	-2,84	1,38
M. Rosa-2	Oil_stain	Rolf	47	A	2,77	0,18	-0,44	4,18	1,29	-0,12
M. Rosa-2	Oil_stain	Rolf	48	A	2,82	-0,03	-0,42	4,30	1,47	-0,20
M-1	Oil_stain	Dan	49	A	-3,84	-2,23	-1,53	-2,21	1,55	-0,71
M-1	Oil_stain	Dan	50	A	-4,26	-1,90	-1,74	-2,71	1,09	-0,60
M-2	Oil_stain	Dan	51	A	-3,58	-2,14	-1,19	-1,95	1,44	-0,62
Mona-1	Oil_stain	Mona-1	52	A	2,11	-1,86	0,70			
N-1	Oil_stain	Gorm	53	A	-4,04	-2,03	-1,65	-2,36	1,38	-0,72
N-1	Oil_stain	Gorm	54	A	-2,63	-1,76	-1,67	-1,03	1,51	-0,71
N-1	Oil_stain	Gorm	55	A	-2,60	-1,81	-1,51	-0,93	1,62	-0,70
Nana-1X	Oil_stain	Halfdan	56	A	-3,58	-1,70	-0,83	-2,08	1,14	-0,03
Nana-1X	Oil_stain	Halfdan	57	A	-4,04	-1,45	-1,25	-2,44	0,67	-0,35
Nini-1A	Oil_stain	Nini	58	A	-1,49	-1,44	-0,71	0,38	2,23	-0,22
Nini-2	Oil_stain	Nini	59	A	-2,26	-0,02	-2,61	-0,69	-0,26	-1,33
Nini-2	Oil_stain	Nini	60	A	-2,22	-0,05	-2,46	-0,60	-0,19	-1,42
Nini-3	Oil_stain	Nini	61	A	-1,19	-1,19	0,01	0,62	2,02	0,29
North Jens-2	Oil_stain	Valdemar	62	A	-3,15	-1,50	-0,32	-1,74	1,22	0,42
North Jens-2	Oil_stain	Valdemar	63	A	-1,60	-0,96	1,07	-0,32	1,29	1,63
North Jens-2	Oil_stain	Valdemar	64	A	-2,73	-1,09	-0,05	-1,32	1,01	0,75
Olaf-1	Oil_stain	Olaf-1	65	A	3,28	-0,19	1,85	5,18	3,23	1,65
Otto-1	Oil_stain	Svend	66	A	0,79	0,07	1,53	2,14	1,02	1,61
Ravn-1	Oil_stain	Ravn	67	A	1,32	2,77	1,04	2,14	-1,87	2,23
Ravn-1	Oil_stain	Ravn	68	A	1,09	3,27	1,34	1,86	-2,25	2,54
Ravn-1	Oil_stain	Ravn	69	A	1,23	3,04	1,05	1,96	-2,32	2,20
Regnar-3	Oil_stain	Regnar	70	A	-3,85	-1,70	-2,92	-2,13	0,97	-1,79
Rigs-1	Oil_stain	South Arne	71	A	0,49	-0,12	2,18	1,61	0,78	2,15
Rigs-2A	Oil_stain	South Arne	72	A	0,11	0,18	1,71	1,36	0,55	1,95
Rita-1X oil	Oil_stain	Rita-1	73	A	9,07	4,64	-8,26	11,42	-1,86	-5,72
Roar 7B	Oil_stain	Roar	74	A	-4,10	1,75	0,93	-3,39	-3,33	1,74
Roar-3C	Oil_stain	Roar	75	A	-2,50	3,28	3,65	-2,26	-4,48	3,54
Roar-3C	Oil_stain	Roar	76	A	-2,22	2,53	2,20	-1,66	-3,54	2,53

Wellname	Type	Field/ Seq.	index	Matrix	A_PC-1	A_PC-2	A_PC-3	A*B*C_PC-1	A*B*C_PC-2	A*B*C_PC-3
SA-1	Oil_stain	South Arne	77	A	-0,53	-0,46	1,31	0,76	1,02	1,76
SA-12	Oil_stain	South Arne	78	A	0,23	-0,25	2,00	1,56	1,15	1,95
SA-14	Oil_stain	South Arne	79	A	0,96	0,30	2,06	2,22	1,03	2,27
SA-16	Oil_stain	South Arne	80	A	0,28	-0,04	2,62	1,46	0,97	2,54
SA-2	Oil_stain	South Arne	81	A	0,29	-0,01	1,57	1,56	0,97	1,96
SA-3	Oil_stain	South Arne	82	A	0,32	-0,02	1,86	1,53	0,80	2,14
SA-4	Oil_stain	South Arne	83	A	0,35	-0,08	2,06	1,68	1,17	2,19
SA-5	Oil_stain	South Arne	84	A	0,12	-0,23	2,03	1,45	1,24	2,21
SA-7	Oil_stain	South Arne	85	A	-0,41	-0,69	1,53	0,97	1,31	1,59
SA-9	Oil_stain	South Arne	86	A	-0,30	-0,99	1,26	1,06	1,60	1,38
Saxo-1	Oil_stain	Saxo	87	A	10,38	-15,65	-1,67			
Saxo-1	Oil_stain	Saxo	88	A	6,05	-11,31	-2,87			
Siri-1	Oil_stain	Siri	89	A	-0,34	-0,85	0,93	1,12	1,60	1,24
Siri-1	Oil_stain	Siri	90	A	-0,26	-0,58	1,10	1,09	1,32	1,44
Siri-3A	Oil_stain	Siri	91	A	-0,35	-0,91	0,11	1,20	1,78	0,65
Skjold Flanke-4A	Oil_stain	Skold Flanke-4	92	A	-3,79	-1,84	-1,73	-2,18	1,17	-0,79
Tabita-1	Oil_stain	Tabita	93	A	-0,23	0,02	1,19	1,11	0,77	1,58
Wessel-1	Oil_stain	Wessel	94	A	5,63	-6,16	1,77			
Wessel-1	Oil_stain	Wessel	95	A	2,30	-3,58	2,61			
Wessel-1	Oil_stain	Wessel	96	A	7,91	-8,06	1,74			
Wessel-1	Oil_stain	Wessel	97	A	7,78	-8,08	1,50			
West Lulu-1	Oil_stain	Harald	98	A	3,28	4,48	2,17	3,35	-6,21	0,99
West Lulu-3	Oil_stain	Harald	99	A	2,79	4,08	1,39	3,09	-5,68	0,60
Adda-1	SR_e	Ryaz-1	100	B						
Adda-1	SR_e	Ryaz-1	101	B						
Adda-1	SR_e	Ryaz-1	102	B						
Adda-1	SR_e	Ryaz-1	103	B						
Adda-1	SR_e	Volg-4	104	B						
Adda-1	SR_e	Volg-4	105	B						
Adda-1	SR_e	Volg-3	106	B						
Adda-1	SR_e	Volg-3	107	B						
Alma-1X	SR_e	Ryaz-1	108	B						
Alma-1X	SR_e	Volg-2	109	B						
Alma-1X	SR_e	Kimm-3	110	B						
Alma-1X	SR_e	Kimm-3	111	B				-5,09	-1,14	-2,25
Alma-1X	SR_e	Ox-1	112	B				-1,89	-5,79	-1,45
Alma-1X	SR_e	Bat-1	113	B				-0,11	-3,54	-0,14
Alma-1X	SR_e	Bat-1	114	B				4,31	-3,14	-2,60
Alma-1X	SR_e	Baj-1	115	B				-0,25	-3,97	-1,78
Anne-3A	SR_e	Volg-4	116	B						
Anne-3A	SR_e	Kimm-3	117	B						
Bo-1	SR_e	Ryaz-1	118	B						
Bo-1	SR_e	Ryaz-1	119	B						
Bo-1	SR_e	Ryaz-1	120	B						
Bo-1	SR_e	Volg-4	121	B						
Bo-1	SR_e	Volg-4	122	B						
Bo-1	SR_e	Volg-4	123	B				-9,67	-0,92	-6,84
Boje-1	SR_e	Ryaz-1	124	B						
Cleo-1	SR_e	Kimm-2	125	B				-7,48	-5,40	-0,17
Cleo-1	SR_e	Kimm-2	126	B				-2,84	-3,36	-0,55
Cleo-1	SR_e	Ox-1	127	B						
Cleo-1	SR_e	Cal-1	128	B						
Deep Adda-1	SR_e	Ryaz-1	129	B						
Deep-Adda-1	SR_e	Volg-4	130	B				-3,53	-1,32	-5,03
Deep-Adda-1	SR_e	Volg-3	131	B				-3,67	-1,04	-5,10
Deep-Adda-1	SR_e	Volg-2	132	B				-3,64	-1,77	-3,38
Diamant-1	SR_e	Volg-4	133	B						
Diamant-1	SR_e	Volg-3	134	B				0,92	0,05	0,17
Diamant-1	SR_e	Volg-3	135	B						
Diamant-1	SR_e	Volg-3	136	B						
Diamant-1	SR_e	Volg-3	137	B						
Diamant-1	SR_e	Volg-3	138	B						
Diamant-1	SR_e	Volg-1	139	B						
Diamant-1	SR_e	Volg-1	140	B						
E-1X	SR_e	Ryaz-1	141	B						
E-1X	SR_e	Ryaz-1	142	B						
E-1X	SR_e	Ryaz-1	143	B						
E-1X	SR_e	Ryaz-1	144	B						
E-1X	SR_e	Ryaz-1	145	B						
E-1X	SR_e	Ryaz-1	146	B						
E-1X	SR_e	Volg-4	147	B						
E-1X	SR_e	Volg-4	148	B						
Edna-1	SR_e	Ryaz-2	149	B				1,58	1,71	-0,30
Edna-1	SR_e	Ryaz-1	150	B						
Edna-1	SR_e	Ryaz-1	151	B						
Edna-1	SR_e	Ryaz-1	152	B						
Edna-1	SR_e	Volg-4	153	B						

Wellname	Type	Field/ Seq.	index	Matrix	A_PC-1	A_PC-2	A_PC-3	A*B*C_PC-1	A*B*C_PC-2	A*B*C_PC-3
Edna-1	SR_e	Volg-4	154	B						
Edna-1	SR_e	Volg-3	155	B						
Edna-1	SR_e	Volg-1	156	B						
Edna-1	SR_e	Kimm-3	157	B						
Eg-1	SR_e	Ryaz-1	158	B						
Eg-1	SR_e	Ryaz-1	159	B						
Eg-1	SR_e	Kimm-4	160	B						
Eg-1	SR_e	Kimm-3	161	B						
Elly-2	SR_e	Volg-3	162	B				1,35	1,22	1,21
Elly-2	SR_e	Volg-1	163	B				3,21	2,23	1,50
Elly-2	SR_e	Volg-1	164	B						
Elly-2	SR_e	Kimm-2	165	B				3,70	1,77	2,50
Elly-2	SR_e	Kimm-1	166	B				-0,06	-1,08	3,04
Fasan-1	SR_e	Ryaz-1	167	B						
Fasan-1	SR_e	Volg-4	168	B						
Gert-2	SR_e	Ryaz-1	169	B						
Gert-2	SR_e	Volg-3	170	B				-7,81	-1,52	0,35
Gert-2	SR_e	Volg-3	171	B				-7,84	-1,13	1,04
Gert-2	SR_e	Volg-2	172	B				-8,20	-4,19	1,99
Gert-2	SR_e	Volg-1	173	B				-5,50	-0,38	1,01
Gert-2	SR_e	Volg-1	174	B				-3,31	-0,10	0,15
Gert-2	SR_e	Kimm-3	175	B				1,19	-0,70	0,46
Gert-2	SR_e	Kimm-2	176	B				4,92	-3,99	-3,11
Gert-2	SR_e	Kimm-2	177	B						
Gulnare-1	SR_e	Ryaz-1	178	B				2,03	0,01	1,63
Gwen-2	SR_e	Ryaz-1	179	B						
Gwen-2	SR_e	Ryaz-1	180	B						
Gwen-2	SR_e	Ryaz-1	181	B						
Gwen-2	SR_e	Volg-4	182	B						
Gwen-2	SR_e	Volg-2	183	B				10,60	2,25	-1,98
Gwen-2	SR_e	Volg-1	184	B						
Gwen-2	SR_e	Volg-1	185	B				10,62	2,31	-1,93
Gwen-2	SR_e	Volg-1	186	B				9,03	1,24	-0,86
Gwen-2	SR_e	Volg-1	187	B				9,91	0,26	-2,48
Gwen-2	SR_e	Volg-1	188	B				10,50	1,51	-1,64
Gwen-2	SR_e	Volg-1	189	B				7,99	-0,15	-0,14
Gwen-2	SR_e	Volg-1	190	B				10,16	1,60	-1,88
Gwen-2	SR_e	Volg-1	191	B				9,74	0,97	-1,98
Gwen-2	SR_e	Kimm-4	192	B				10,31	0,88	-2,14
Gwen-2	SR_e	Kimm-4	193	B				11,02	1,59	-2,53
Gwen-2	SR_e	Kimm-4	194	B				10,81	1,98	-2,08
Gwen-2	SR_e	Kimm-4	195	B				9,99	0,37	-1,16
Gwen-2	SR_e	Kimm-4	196	B				8,72	0,42	-0,65
Gwen-2	SR_e	Kimm-4	197	B						
Gwen-2	SR_e	Kimm-3	198	B				9,27	0,28	-2,22
Gwen-2	SR_e	Kimm-3	199	B				10,46	1,84	-2,08
Gwen-2	SR_e	Kimm-1	200	B						
I-1X	SR_e	Ryaz-1	201	B				1,91	2,94	3,24
I-1X	SR_e	Ryaz-1	202	B						
I-1X	SR_e	Volg-2	203	B						
Iris-1	SR_e	Ryaz-1	204	B				-1,42	-1,42	3,54
Iris-1	SR_e	Ryaz-1	205	B				-0,42	-0,72	3,37
Iris-1	SR_e	Ryaz-1	206	B				-1,94	-2,04	4,02
Iris-1	SR_e	Ryaz-1	207	B				-1,68	-1,93	3,26
Iris-1	SR_e	Volg-4	208	B				-0,65	-2,75	3,33
Iris-1	SR_e	Volg-4	209	B				0,04	-0,04	2,25
Iris-1	SR_e	Volg-4	210	B				-1,70	-2,88	0,22
Jens-1	SR_e	Ryaz-1	211	B						
Jens-1	SR_e	Ryaz-1	212	B						
Jens-1	SR_e	Ryaz-1	213	B						
Jens-1	SR_e	Ryaz-1	214	B						
Jens-1	SR_e	Ryaz-1	215	B						
Jens-1	SR_e	Volg-4	216	B						
Jens-1	SR_e	Volg-4	217	B						
Jens-1	SR_e	Volg-4	218	B						
Jens-1	SR_e	Volg-3	219	B						
Jens-1	SR_e	Volg-3	220	B				-6,28	1,57	0,26
Jens-1	SR_e	Volg-3	221	B				-1,76	2,58	0,07
Jens-1	SR_e	Kimm-3	222	B				0,04	0,93	1,69
Jens-1	SR_e	Kimm-3	223	B				-0,24	0,70	1,79
Jens-1	SR_e	Kimm-2	224	B				0,21	0,72	1,83
Jens-1	SR_e	Kimm-2	225	B				0,82	0,36	1,65
Jens-1	SR_e	Ox-1	226	B				0,83	0,47	2,02
Jens-1	SR_e	Ox-1	227	B				-0,71	0,75	0,91
Jens-1	SR_e	Ox-1	228	B				0,48	1,36	1,57
Jens-1	SR_e	Cal-1	229	B				1,14	1,71	1,28
Jens-1	SR_e	Pliens-1	230	B				-1,22	0,35	1,35

Wellname	Type	Field/ Seq.	index	Matrix	A_PC-1	A_PC-2	A_PC-3	A*B*C_PC-1	A*B*C_PC-2	A*B*C_PC-3
Jeppe-1	SR_e	Ryaz-1	231	B						
Jeppe-1	SR_e	Ryaz-1	232	B						
Jeppe-1	SR_e	Ryaz-1	233	B						
Jeppe-1	SR_e	Ryaz-1	234	B						
Jeppe-1	SR_e	Ryaz-1	235	B						
Jeppe-1	SR_e	Ryaz-1	236	B						
Jeppe-1	SR_e	Ryaz-1	237	B						
Jeppe-1	SR_e	Ryaz-1	238	B						
Jeppe-1	SR_e	Ryaz-1	239	B						
Jeppe-1	SR_e	Ryaz-1	240	B						
Jeppe-1	SR_e	Ryaz-1	241	B						
Jeppe-1	SR_e	Ryaz-1	242	B						
Jeppe-1	SR_e	Ryaz-1	243	B						
Jeppe-1	SR_e	Ryaz-1	244	B						
Jeppe-1	SR_e	Ryaz-1	245	B						
Karl-1	SR_e	Volg-3	246	B						
Karl-1	SR_e	Volg-1	247	B				8,37	1,30	-1,33
Karl-1	SR_e	Volg-1	248	B				6,00	0,09	-0,31
Karl-1	SR_e	Kimm-4	249	B				6,31	-0,35	-1,04
Lulu-1	SR_e	Kimm-3	250	B						
Lulu-1	SR_e	Kimm-3	251	B						
Lulu-1	SR_e	Kimm-3	252	B						
Lulu-1	SR_e	Kimm-3	253	B						
Lulu-1	SR_e	Kimm-3	254	B						
Lulu-1	SR_e	Kimm-2	255	B				-0,12	0,85	0,04
Lulu-1	SR_e	Kimm-2	256	B				2,26	0,79	0,47
Lulu-1	SR_e	Kimm-2	257	B				1,65	-0,48	1,03
Lulu-2	SR_e	Kimm-2	258	B						
Lulu-2	SR_e	Kimm-2	259	B						
Lulu-2	SR_e	Kimm-2	260	B				4,99	0,36	0,91
Lulu-2	SR_e	Kimm-2	261	B				5,94	1,19	0,32
M-8X	SR_e	Kimm-3	262	B				-4,26	-0,29	-2,82
M-8X	SR_e	Kimm-1	263	B				-3,34	-4,16	-3,06
M-8X	SR_e	Ox-1	264	B				-2,16	-4,04	-2,30
M-8X	SR_e	Cal-1	265	B						
M-8X	SR_e	Hett-1	266	B						
N. Jens-1	SR_e	Ryaz-2	267	B						
N. Jens-1	SR_e	Volg-1	268	B						
N. Jens-1	SR_e	Volg-1	269	B						
N.Jens-1	SR_e	Volg-4	270	B						
N.Jens-1	SR_e	Volg-4	271	B						
N.Jens-1	SR_e	Volg-4	272	B						
N.Jens-1	SR_e	Volg-4	273	B						
N.Jens-1	SR_e	Volg-3	274	B						
N.Jens-1	SR_e	Volg-3	275	B				-5,40	2,10	-3,47
N.Jens-1	SR_e	Volg-3	276	B				-4,99	2,22	-3,09
N.Jens-1	SR_e	Volg-2	277	B				-4,50	1,88	-3,41
N.Jens-1	SR_e	Volg-2	278	B				-4,24	2,22	-2,70
N.Jens-1	SR_e	Volg-2	279	B						
N.Jens-1	SR_e	Volg-2	280	B						
N.Jens-1	SR_e	Volg-2	281	B						
N.Jens-1	SR_e	Volg-2	282	B				-5,82	1,06	-3,91
N.Jens-1	SR_e	Volg-2	283	B						
N.Jens-1	SR_e	Volg-1	284	B						
N.Jens-1	SR_e	Volg-1	285	B						
N.Jens-1	SR_e	Volg-1	286	B						
N.Jens-1	SR_e	Volg-1	287	B				-4,50	2,12	-2,78
N.Jens-1	SR_e	Volg-1	288	B						
N.Jens-1	SR_e	Volg-1	289	B						
N.Jens-1	SR_e	Volg-1	290	B				-5,27	1,72	-3,10
N.Jens-1	SR_e	Volg-1	291	B				-5,33	1,38	-3,54
N.Jens-1	SR_e	Volg-1	292	B				-5,17	0,92	-3,08
N.Jens-1	SR_e	Volg-1	293	B				-4,91	0,90	-2,69
N.Jens-1	SR_e	Volg-1	294	B				-5,46	1,47	-2,97
N.Jens-1	SR_e	Volg-1	295	B				-5,65	1,61	-3,46
N.Jens-1	SR_e	Kimm-4	296	B				-4,90	1,65	-3,07
N.Jens-1	SR_e	Kimm-4	297	B				-5,21	1,81	-3,21
N.Jens-1	SR_e	Kimm-3	298	B				-4,65	1,84	-2,80
N.Jens-1	SR_e	Kimm-3	299	B				-5,03	1,91	-2,80
N.Jens-1	SR_e	Kimm-3	300	B				-4,64	1,06	-2,69
N.Jens-1	SR_e	Kimm-3	301	B				-2,65	-1,44	-1,08
N.Jens-1	SR_e	Kimm-3	302	B						
N.Jens-1	SR_e	Kimm-3	303	B				-2,67	1,15	-0,52
N.Jens-1	SR_e	Kimm-3	304	B				-2,19	0,91	-0,70
N.Jens-1	SR_e	Kimm-3	305	B				0,12	-0,96	2,14
N.Jens-1	SR_e	Kimm-2	306	B				0,96	-0,86	2,40
N.Jens-1	SR_e	Kimm-2	307	B				0,71	-1,12	1,92

Wellname	Type	Field/ Seq.	index	Matrix	A_PC-1	A_PC-2	A_PC-3	A*B*C_PC-1	A*B*C_PC-2	A*B*C_PC-3
N.Jens-1	SR_e	Kimm-2	308	B				1,93	-1,05	3,29
N.Jens-1	SR_e	Kimm-2	309	B				2,01	-0,74	2,93
N.Jens-1	SR_e	Kimm-2	310	B				-4,93	1,85	-3,25
N.Jens-1	SR_e	Kimm-2	311	B				1,34	-1,32	3,74
N.Jens-1	SR_e	Kimm-2	312	B				1,24	-1,33	3,66
N-22A	SR_e	Sin-1	313	B				-0,91	-1,05	-2,13
Nora-1	SR_e	Kimm-3	314	B				-2,72	-2,08	0,34
Nora-1	SR_e	Kimm-3	315	B				-3,56	-2,97	-0,01
Nora-1	SR_e	Kimm-3	316	B				-2,96	-2,27	-0,44
Nora-1	SR_e	Kimm-3	317	B				-5,02	-3,40	0,91
Nora-1	SR_e	Kimm-3	318	B				-6,47	-3,93	1,60
Nora-1	SR_e	Kimm-3	319	B				-6,97	-3,68	2,11
Nora-1	SR_e	Kimm-3	320	B				-4,17	-2,28	1,52
Nora-1	SR_e	Kimm-3	321	B				-3,08	-1,12	1,26
Nora-1	SR_e	Kimm-3	322	B				-2,53	-1,38	1,41
Nora-1	SR_e	Kimm-3	323	B				-3,74	-0,23	3,48
Nora-1	SR_e	Kimm-3	324	B				-3,16	-1,74	1,45
Nora-1	SR_e	Kimm-3	325	B				-3,58	-2,37	1,38
NW Adda-1	SR_e	Volg-4	326	B						
NW-Adda-1	SR_e	Ryaz-1	327	B				-3,89	2,03	-1,86
NW-Adda-1	SR_e	Ryaz-1	328	B						
Rita-1X	SR_e	Ryaz-1	329	B						
Rita-1X	SR_e	Volg-4	330	B						
Rita-1X	SR_e	Volg-4	331	B				-5,22	-0,01	0,96
Rita-1X	SR_e	Volg-4	332	B						
Rita-1X	SR_e	Volg-4	333	B						
Rita-1X	SR_e	Volg-4	334	B				0,30	-1,40	-1,62
Rita-1X	SR_e	Volg-4	335	B				-0,22	0,57	-1,76
Rita-1X	SR_e	Volg-3	336	B				-0,10	-1,05	-2,11
Rita-1X	SR_e	Volg-1	337	B				1,33	0,37	1,38
Rita-1X	SR_e	Kimm-4	338	B				3,97	-1,21	0,51
Rita-1X	SR_e	Kimm-3	339	B				5,48	-1,32	0,05
Rita-1X	SR_e	Kimm-3	340	B				12,38	-5,78	-9,66
SE-Igor-1	SR_e	Volg-2	341	B						
SE-Igor-1	SR_e	Volg-2	342	B				-0,64	1,80	-1,21
Skarv-1	SR_e	Ryaz-1	343	B						
Skarv-1	SR_e	Volg-4	344	B				2,93	2,41	1,23
Skarv-1	SR_e	Volg-3	345	B				1,48	-0,67	2,52
Skarv-1	SR_e	Kimm-4	346	B				3,08	0,86	0,39
Skarv-1	SR_e	Kimm-4	347	B				3,46	2,35	1,56
Skarv-1	SR_e	Kimm-2	348	B						
Skarv-1	SR_e	Kimm-2	349	B						
Skarv-1	SR_e	Kimm-1	350	B				3,80	1,35	1,75
Skarv-1	SR_e	Kimm-1	351	B				4,25	2,07	1,31
Skarv-1	SR_e	Sin-1	352	B						
Skjold-Flanke-1	SR_e	Volg-2	353	B						
Skjold-Flanke-1	SR_e	Volg-1	354	B						
Skjold-Flanke-1	SR_e	Kimm-4	355	B				-0,20	2,16	-0,10
Skjold-Flanke-1	SR_e	Kimm-4	356	B						
Skjold-Flanke-1	SR_e	Kimm-3	357	B						
Skjold-Flanke-1	SR_e	Kimm-2	358	B				-0,14	1,93	0,24
Skjold-Flanke-1	SR_e	Bat-1	359	B				0,26	0,36	0,84
Tordenskjold-1	SR_e	Volg-4	360	B						
Tordenskjold-1	SR_e	Volg-3	361	B						
Tordenskjold-1	SR_e	Volg-2	362	B						
Tordenskjold-1	SR_e	Permian	363	B						
U-1X	SR_e	Volg-1	364	B				-4,83	2,42	-3,04
U-1X	SR_e	Kimm-3	365	B				-5,39	-0,36	-2,75
U-1X	SR_e	Kimm-2	366	B				-4,89	-1,48	-2,72
U-1X	SR_e	Ox-1	367	B				-4,01	-3,39	-0,93
U-1X	SR_e	Cal-1	368	B				-2,92	-5,20	-0,01
U-1X	SR_e	Hett-1	369	B				-2,23	-5,31	-0,14
W. Lulu-1	SR_e	Kimm-1	370	B				0,98	-6,87	-1,98
W. Lulu-1	SR_e	Cal-1	371	B				0,52	-6,06	0,09
W. Lulu-1	SR_e	Cal-1	372	B				1,05	-5,87	-0,09
W. Lulu-1	SR_e	Cal-1	373	B				0,77	-6,14	-0,17
W. Lulu-1	SR_e	Cal-1	374	B				1,03	-5,76	-0,50
W. Lulu-1	SR_e	Cal-1	375	B				1,23	-6,04	-0,23
W. Lulu-2	SR_e	Ox-1	376	B				6,42	-0,83	0,00
W. Lulu-3	SR_e	Ox-1	377	B				1,76	-5,62	-2,60
Wessel-1	SR_e	Volg-3	378	B						
Wessel-1	SR_e	Volg-3	379	B						
Wessel-1	SR_e	Volg-3	380	B						
Wessel-1	SR_e	Volg-2	381	B						
Wessel-1	SR_e	Permian	382	B						
Wessel-1	SR_e	Permian	383	B						
Wessel-1	SR_e	Permian	384	B						

Wellname	Type	Field/ Seq.	index	Matrix	A_PC-1	A_PC-2	A_PC-3	A*B*C_PC-1	A*B*C_PC-2	A*B*C_PC-3
Wessel-1	SR_e	Permian	385	B						
NJ-1	Oil_stain	Valdemar	386	C				-1,05	2,72	-0,51
NJ-1	Oil_stain	Valdemar	387	C				-1,41	1,45	0,89
NJ-1	Oil_stain	Valdemar	388	C				0,17	2,42	1,21
NJ-1	Oil_stain	Valdemar	389	C				-0,29	1,98	1,53
NJ-1	Oil_stain	Valdemar	390	C				0,15	2,52	1,35
NJ-1	Oil_stain	Valdemar	391	C				-0,43	1,62	1,11
NJ-1	Oil_stain	Valdemar	392	C				-0,33	1,75	1,24
NJ-1	Oil_stain	Valdemar	393	C				-0,31	1,74	1,16
NJ-1	Oil_stain	Valdemar	394	C				-0,99	1,77	0,95
NJ-1	Oil_stain	Valdemar	395	C				-0,20	3,43	-0,05
V-1	Oil_stain	Valdemar	396	C				-0,99	2,69	-0,02
V-1H	Oil_stain	Valdemar	397	C				-1,17	1,31	0,07
V-1H	Oil_stain	Valdemar	398	C				-1,54	0,90	0,21
V-1H	Oil_stain	Valdemar	399	C				-0,79	1,85	-0,05
V-1H	Oil_stain	Valdemar	400	C				-0,06	3,05	0,00
V-1H	Oil_stain	Valdemar	401	C				-1,02	1,92	-0,14
V-1H	Oil_stain	Valdemar	402	C				-2,36	0,78	0,27
V-1H	Oil_stain	Valdemar	403	C				-0,90	1,18	0,53
V-1H	Oil_stain	Valdemar	404	C				-1,49	1,14	-0,27
V-1P	Oil_stain	Valdemar	405	C				-1,44	2,52	-0,68
V-1P	Oil_stain	Valdemar	406	C				0,19	1,96	1,44
V-1P	Oil_stain	Valdemar	407	C				0,12	1,84	0,94
V-1P	Oil_stain	Valdemar	408	C				-1,03	2,59	-0,33
V-1P	Oil_stain	Valdemar	409	C				-0,66	0,82	1,32
V-1P	Oil_stain	Valdemar	410	C				-0,97	0,53	0,91
V-1P	Oil_stain	Valdemar	411	C				-0,89	1,15	0,41
V-1P	Oil_stain	Valdemar	412	C				-1,12	1,45	0,21
V-2H	Oil_stain	Valdemar	413	C				-2,05	1,41	-0,13
V-2H	Oil_stain	Valdemar	414	C				-1,69	1,63	-0,46
V-2H	Oil_stain	Valdemar	415	C				-1,55	1,96	-0,60
V-2H	Oil_stain	Valdemar	416	C				-2,07	1,31	-0,25
V-2H	Oil_stain	Valdemar	417	C				-2,00	1,49	-0,18
V-2H	Oil_stain	Valdemar	418	C				-1,71	1,82	-0,34
V-2H	Oil_stain	Valdemar	419	C				-2,04	1,31	-0,03
V-2H	Oil_stain	Valdemar	420	C				-2,34	0,93	-0,11
V-2H	Oil_stain	Valdemar	421	C				-2,11	1,90	-0,63
V-2H	Oil_stain	Valdemar	422	C				-1,41	2,60	-0,50
V-2H	Oil_stain	Valdemar	423	C				-1,37	2,33	-0,85
V-2H	Oil_stain	Valdemar	424	C				-1,46	2,09	-0,51
V-2H	Oil_stain	Valdemar	425	C				-1,27	2,36	-0,59
V-2P	Oil_stain	Valdemar	426	C				-1,39	2,17	-0,13
V-2P	Oil_stain	Valdemar	427	C				-1,39	1,88	-0,57
V-2P	Oil_stain	Valdemar	428	C				-1,56	1,28	0,29
V-2P	Oil_stain	Valdemar	429	C				-0,20	1,87	1,68
V-2P	Oil_stain	Valdemar	430	C				-0,84	1,41	1,27
V-2P	Oil_stain	Valdemar	431	C				-0,67	1,92	0,70
V-3H	Oil_stain	Valdemar	432	C				-2,46	1,40	-0,32
V-3H	Oil_stain	Valdemar	433	C				-2,43	1,77	0,02
V-3H	Oil_stain	Valdemar	434	C				-2,17	2,09	-0,23
V-3H	Oil_stain	Valdemar	435	C				-2,44	1,90	-0,16
V-3H	Oil_stain	Valdemar	436	C				-2,25	2,01	-0,07
V-3H	Oil_stain	Valdemar	437	C				-2,60	1,82	-0,14
V-3H	Oil_stain	Valdemar	438	C				-2,15	1,95	-0,32
V-3H	Oil_stain	Valdemar	439	C				-2,51	1,56	-0,20
V-3H	Oil_stain	Valdemar	440	C				-2,03	2,12	-0,32
V-3H	Oil_stain	Valdemar	441	C				-2,49	1,57	-0,39
V-3H	Oil_stain	Valdemar	442	C				-2,49	2,07	-0,02
V-3H	Oil_stain	Valdemar	443	C				-1,95	2,30	-0,72
V-4H	Oil_stain	Valdemar	444	C				0,57	2,44	1,73
V-4H	Oil_stain	Valdemar	445	C				0,49	1,80	1,47
V-4H	Oil_stain	Valdemar	446	C				-0,15	1,32	1,83
V-4H	Oil_stain	Valdemar	447	C				0,65	2,59	1,86

Oil_stain: Oils and stains; SR_e: source rock extract